Geometrical Derivatives of Energy Surfaces and Spectroscopic Properties of Open Shell Molecules and Molecular Excited States : A Coupled Cluster Investigation

Thesis submitted to the

University of Pune

For the degree of

Doctor of Philosophy

in

Chemistry

by

Achintya Kumar Dutta

Physical Chemistry Division
CSIR-National Chemical Laboratory
Pune 411008
India

Dr. Sourav Pal
(Research Guide)

Dr. Nayana Vaval
(Research Co-guide)

July 2014

CERTIFICATE

This is to certify that the work presented in this thesis entitled, "**Geometrical Derivatives of Energy Surfaces and Spectroscopic Properties of Open Shell Molecules and Molecular Excited States :A Coupled Cluster Investigation**" by **Mr. Achintya Kumar Dutta**, for the degree of **Doctor of Philosophy**, was carried out by the candidate under my supervision in the Physical Chemistry Division, CSIR-National Chemical Laboratory, Pune-411008, India. Any material that has been obtained from other sources has been duly acknowledged in the thesis.

Date:

Place: Pune

Dr. Sourav Pal

(Research Guide)

Physical Chemistry Division

CSIR-National Chemical Laboratory

Pune-411008, India

DECLARATION

I, Mr. Achintya Kumar Dutta, hereby declare that the work incorporated in the thesis entiled "**Geometrical Derivatives of Energy Surfaces and Spectroscopic Properties of Open Shell Molecules and Molecular Excited States :A Coupled Cluster Investigation**" submitted by me to **University of Pune** for the degree of **Doctor of Philosophy** is original and has not been submitted to this or other University or Institution for the award of Degree or Diploma. Such material, as has been obtained from other sources has been duly acknowledged.

Date:

Place: Pune

Achintya Kumar Dutta

To my Dad, the finest man I have seen

Acknowledgements

"It was the best of times, it was the worst of times, it was the age of wisdom, it was the age of foolishness, it was the epoch of belief, it was the epoch of incredulity, it was the season of Light, it was the season of Darkness, it was the spring of hope, it was the winter of despair, we had everything before us, we had nothing before us, we were all going direct to Heaven, we were all going direct the other way – in short, the period was so far like the present period, that some of its noisiest authorities insisted on its being received, for good or for evil, in the superlative degree of comparison only."

Charles Dickens, A Tale of Two Cities

It is my great pleasure to present my research work in the form of this Ph. D thesis. The journey has been interesting, bumpy at times, partly because of the unknown paths, and mainly due to the weaknesses, inherent to this human birth. Although, the road was not smooth, it was never lonely. I want to take this opportunity to express my gratitude towards the persons, who has accompanied me to reach my destination.

First, I want to acknowledge my guide Dr. Sourav Pal, for giving me the opportunity to work under him. It has been a great learning experience both professionally and personally. He has been an excellent teacher and great mentor. I have sensed his great power to motivate the student when he is down and cut him off when he

is jumping with excitement. His personality, down to earth attitude, and his unique sense of humor has played a great deal in transforming my character during this journey from boyhood to manhood and going to keep an everlasting imprint in my life.

I specially want to thank Dr. Nayana Vaval, my co-guide, for her advice, encouragement, and help throughout my Ph. D time. She always has the grace to treat me as a lab met, rather than her student. The real education makes a person simple and humble, and she is one of the prime examples of that. I would have prayed to god to make me as humble and simple as her, but I think that is beyond the power of the "ALMIGHTY" and I find yet another reason not to believe in him.

I want to acknowledge Dr. Debashree Ghosh, "my nearest neighbor boss", for her help, guidance, and innovative ideas. She is the one who has me introduced to C++ and qchem, more over to the concept what hard work means.

I am extremely grateful to Dr. Prasant U Manohar, my senior and collaborator. He is patient, diligent, and organized, just opposite of everything that defines me. Therefore, our collaboration has always remained intense, but fruitful.

I want to acknowledge Dr. Kumar Vanka, Dr. Neelanjan Sengupta, Dr. Sudip Roy, Dr. Suman Chakraborty, Dr. Kavita Joshi and Dr. Durba Sengupta for their kind help and advice.

I thank my lab seniors Dr. Arijit Bag, Dr. Subrata Banik, Dr. Lalitha Ravichandan, Dr. Himadri Day. Dr. Sapna Shedge and Dr. Sumantra Bhattachraya for making life comfortable in the initial difficult phase. My association with Sumantra da has been the source of fountain of memories. I am never going to forget our bike trips, roof top parties,

many triumphs and some disasters, but all enjoyed together. May be we have been brothers in some previous incarnation. Damn It! Who has seen the previous birth? We are brothers in this life only. I want to acknowledge all my labmates Susanta, Debarati Di, Turbasu, Sayali, Manzoor, Sudip, Aryya, Himadri, Deepti Di, Gupta Ji, Mudit, Deepak, Kamalika, Anagha, Saba, Vidhika, Madhulita, Ashis, Mritunjay, Prathith, Amrita, Shantanu, Sneha, Jaya, Nisha, Manoj, Jugal, Yuvraj, Subrashis and Tamal for creating a nice working environment in the lab. I will always cherish the fun time in our year end lab trips and New Year parties.

My stay on this campus has been pleasant with the association of all the research scholars at CSIR NCL. I am thankful to Partha da, Mrinmoy, Tamosh da, Arpan, Kanak, Anjan, Saikat da, Pravat, Jayasis da, Pati da, Krisanu da, Animesh da, Binay da Shyam da, Sajal da, Munmun, Subha Di, Tanaya, Jhumur, Anupam da, Abhik, Souvik, Doss, Prithvi, Sujit da, Debasis da, Subhadip da, Garai da, Basab da, Prathit, Chandan Da (Dey), Chandan da (Choudhury), Nivedita di, Amrita, Swagata, Chakadola, Krunal, Chinmay, Jitu, Kaushalendra, Kiran, Deepak bhaiya, Prabhakar, Pankaj, Wahid, Saleem, Gouri Di, Majid, Devraj, Manoj (Sharma), Brijesh, Anand bhaiya, Lakshmi, Ashok, Anjani, Kailash, Sujit, and Atul.

I would also like to thank my all juniors Anup, Soumen (Das), Saibal, Sudip, Shantanu, Prasenjit, Atanu, Santu, Somen (Dey), Atreyee, Arunava, Shantigopal, Hridesh, Manik, Soumyojyoti, Tapas, Bappa, Santanu, Manik, Suman, Chyanika, Jagadish and Ramkrishna.

I take this opportunity to thank my schoolmates Rana, Niladri and Saikat and university mates Hemanta, Bichitra, Damodar and Kanchan da. My university roommate Sudip will always have a special place in my life. Special thanks should be extended to my past GJ roommate Dr. Bhuban Panda and present roommate Raju Nanda for tolerating me. I want to express my gratitude towards my first chemistry teacher Rajib Kesh and my university teachers Dr. Pranab Sarkar and Dr. Bidhan Bag for motivating me towards this fascinating world of research. I am going to miss my Golden Jubilee hostel. Especially, the table gossips in the mess hall and my "bawal" group Members.

Of course, many names were left in the process, some by mistake and some by deliberation! It does not necessarily mean that their contribution were less in shaping my life during this time. Let, the pages of my heart be reserved for etching their names.

I find it difficult to express my gratitude towards my parents "Chandra Sekhar Dutta" and "Anita Dutta" for their love, support, and sacrifice. I want to acknowledge my sister "Moumi" for her love and care. I will always indebt to my Meshomoshai "Dilip Kesh", My Mashi "Jotshna Kesh" and my brother "Dinabandhu" for their love and support. I take this opportunity to pay tribute to the memories of my grandmother late "Narayani Dutta" and my Jethu late "Shashanka Sekhar Dutta". Finally, it is the journey that has been more enjoyable then the destination itself.

Achintya Kumar Dutta

Table of Contents

List of Tables

List of Figure

List of abbreviations

AO	Atomic orbital
BO	Born-Oppenheimer
BOA	Born-Oppenheimer Approximation
BWPT	Brillouin-Weigner Perturbation Theory
CAS	Complete Active Space
CASSCF	Complete Active Space Self Consistent Field
CBH	Campbell-Baker-Hausdroff
CC	Coupled Cluster
CCSD	Coupled Cluster truncated at Singles Doubles Excitation
CCSD(T)	Coupled Cluster truncated at Singles Doubles Excitation with inclusion of partial Triples
CCSDT	Coupled Cluster truncated at Singles, Doubles, Triples excitation
CCSDTQ	Coupled Cluster truncated at Singles, Doubles, Triples and Quadruple excitation
CEPA	Coupled Electron Pair Approximation
CPMET	Coupled-Pair Many-Electron Theory
CI	Configuration Interaction
CISD	Configuration Interaction truncated at Singles

	Doubles excitation
DFT	Density Functional Theory
EA	Electron Affinity
ECC	Extended Coupled Cluster
EE	Excitation Energy
EOM-CC	Equations-of-Motion Coupled Cluster
FCI	Full Configuration Interaction
FSMRCC	Fock Space Multi-reference Coupled Cluster
HF	Hartree-Fock
HSMRCC	Hilbert Space Multi Reference Coupled Cluster
ICC	Internally Contracted Configurations
ic-MRCC	Internally Contracted Multi reference coupled cluster
IH	Intermediate Hamiltonian
IMS	Incomplete model space
IP	Ionization Potential
MCSCF	Multi Configuration Self Consistent Field
MBPT	Many Body Perturbation Theory
Mk-MRCC	Mukherjee Multi Reference Coupled Cluster
MP2	Møller-Plesset second order Perturbation
MRCC	Multi Reference Coupled Cluster
MRCI	Multi Reference Configuration Interaction
MRCISD	Multi Reference Configuration Interaction truncated

	at Singles Doubles excitation
MRPT	Multi Reference Multi Reference
QDPT	Quasi-Degenerate Perturbation Theory
RHF	Restricted Hartree-Fock
ROHF	Restricted Open Shell Hartree-Fock
RSPT	Rayleigh-Schrödinger Perturbation Theory
SAC-CI	Symmetry Adopted Cluster Configuration
	Interaction
SCF	Self Consistent Field
SEC	Subsystem Embedding Condition
SES	Smooth Exterior Scaling
SRCC	Single Reference Coupled Cluster
SSMRCC	State Specific Multi Reference Coupled Cluster
STEOM-CC	Similarity Transformed Equation-Of-Motion
	Coupled Cluster
SUMRCC	State universal Multi Reference Coupled Cluster
UCC	Unitary Coupled Cluster
UHF	Unrestricted Hartree-Fock
VUMRCC	Valence Universal Multi reference Coupled Cluster
XCC	Expectation value Coupled Cluster

List of publications

1. **Achintya Kumar Dutta**, Nayana Vaval, and Sourav Pal. "NO x Catalyzed Pathway of Stratospheric Ozone Depletion: A Coupled Cluster Investigation." *Journal of Chemical Theory and Computation,* 8.6 (2012): 1895-1901.
2. Sayali P. Joshi, **Achintya Kumar Dutta**, Sourav Pal, and Nayana Vaval. "Extended coupled cluster for Raman and Infrared spectra of small molecules." *Chemical Physics,* 403(2012):25-32.
3. Sangram S. Kale, Amol S. Kotmale, **Achintya Kumar Dutta**, Sourav Pal, P. R. Rajamohanan, and Gangadhar J. Sanjayan. "Conformational modulation of Ant–Pro oligomers using chirality alteration of proline residues." *Organic & Biomolecular Chemistry* , 10(42) (2012): 8426-8433.
4. Subhash P. Chavan, Sumanta Garai, **Achintya Kumar Dutta**, and Sourav Pal. "Friedel–Crafts Acylation Reactions Using Esters." *European Journal of Organic Chemistry,* 35 (2012): 6841-6845.
5. **Achintya Kumar Dutta**, Nayana Vaval, and Sourav Pal. ″ Performance of the EOMIP-CCSD (2) method for determining the structure and properties of doublet radicals: A benchmark investigation " *Journal of Chemical Theory and Computation,* 9.10 (2013): 4313-4331.
6. **Achintya Kumar Dutta**, Sourav Pal and Debashree Gosh " Perturbative approximations to single and double spin flip equation of motion coupled cluster singles doubles methods*" The Journal of Chemical Physics,* 139 (12), (2013):124116.
7. M Pandey, PS Chowdhury, **Achintya Kumar Dutta,** P Kumar, S Pal" A highly concise and practical route to clavaminols, sphinganine and (+)-spisulosine via indium mediated allylation of α-hydrazino aldehyde and a theoretical insight into the stereochemical aspects of the reaction" *RSC Advances,* 35, (2013) :15442-15448.

8. **Achintya Kumar Dutta**, Manzoor Dar .Nayana Vaval, and Sourav Pal. "Structure, Stability and Properties of Trans Peroxo Nitrate Radical: The Importance of Non-dynamic Correlation " *The Journal of Physical Chemistry A,* 118 (8), (2014) :1350.
9. **Achintya Kumar Dutta**, P. U. Manohar, Nayana Vaval, and Sourav Pal. *"*Ground State of Naphthyl cation : Singlet or Triplet" *The Journal of chemical physics,* 140,(2014)114312.
10. **Achintya Kumar Dutta**, Jitendra Gupta, Himadi Pathak Nayana Vaval, and Sourav Pal. *"*Partitioned EOMEA-CCSD(2): An Efficient N^5 Scaling Method for Calculation of Electron Affinities" *Journal of Chemical Theory and Computation,* 10.5(2014): 1923-1933
11. **Achintya Kumar Dutta** and Sumantra Bhattacharya. *"*Excited State Geometry Optimization Using Fock Space Multi-Reference Coupled Cluster Method *" Mol Phys* (2014) (DOI**:** 10.1080/00268976.2014.915997)
12. **Achintya Kumar Dutta**, Jitendra Gupta, Nayana Vaval, and Sourav Pal. " Intermediate Hamiltonian Fock Space Multi-reference Coupled Cluster Approach to Core Excitation Spectra" (Under revision in *Journal of Chemical Theory and Computation*)
13. **Achintya Kumar Dutta**, Turbashu Sengupta, Nayana Vaval, and Sourav Pal. " Electron attachment to DNA and RNA nucleo-bases: an EOMCC investigation*"* (Under revision in *The Journal of physical chemistry A*)
14. **Achintya Kumar Dutta**, Nayana Vaval, and Sourav Pal. " A new approach to perturbative triples correction in (0,1) sector of FSMRCC*"* (To be communicated to *The Journal of Chemistry Physics*)
15. **Achintya Kumar Dutta**, Nayana Vaval, and Sourav Pal." Similarity Transformed Equation of Motion Coupled Cluster Method : A Near Black Box Approach to Core Excitation Spectra" (To be communicated to *Journal of Chemical Theory and Computation*)

16. **Achintya Kumar Dutta**, Nayana Vaval, and Sourav Pal. “How good is the EOMIP-CCSD(2) approximation for calculation of ionization potential ? “ (Manuscript in preparation)
17. **Achintya Kumar Dutta**, Nayana Vaval, and Sourav Pal. “EOMIP-CCSD(2)*: A new method for calculation of Ionization Potential “ (Manuscript in preparation)

Abstract

In this thesis, we shall mainly focus on the study of structure and properties of radicals and molecular excited states. This work will involve the application of existing coupled cluster methods, as well as, development of new approximations having lower computational cost.

The state-of-the-art single-reference coupled cluster (SRCC) [1-2] theory is one of the most accurate and widely used electronic structure methods for studying ground state structure [3-5], properties [6] and spectroscopy [7-9] of closed-shell molecules around equilibrium geometry. Apart from a high-level treatment of dynamic electron-correlation, the most attractive feature of SRCC method is that it is size-extensive [2] and separates correctly, even at the truncated level, provided the reference state is also size-consistent, which is not true for truncated configuration interaction (CI) methods [10].

The SRCC theory, however, fails to properly describe the electron correlation, when multiple determinants become equally important for the zeroth order description of the wave function. In general, for quasi-degenerate situations, such as potential energy surfaces, bond-breaking or making regions, open shell systems and low-lying excited states of molecules, where multiple determinants become equally important, the use of multi-reference coupled cluster method becomes necessary.

The MRCC theories can be divided into two classes. The first is single root MRCC methods i.e. state specific MRCC [11-16]. The second class constitutes multi-root description through effective Hamiltonian approach. We shall focus on the second class. Diagonalizing the effective Hamiltonian within the model space, we get multiple roots simultaneously [17]. There are two basic classes of effective Hamiltonian based MRCC theories, *viz*, the state-universal MRCC (SUMRCC) or Hilbert space multi reference coupled cluster (HSMRCC) method [18-19] and the valence-universal MRCC

(VUMRCC) or Fock space multi reference coupled cluster (FSMRCC) method [20-23]. Both the approaches differ in the way the dynamic correlation is introduced and hence are suitable for different types of situations. HSMRCC is suitable for studying potential energy surface. On the other hand, FSMRCC is suitable for the calculation of difference of energies like ionization potential [24], electron affinity and excitation energy [21,23,25]. In this thesis, we have used FSMRCC for our study.

In parallel to the MRCC approaches, the equation of motion coupled cluster (EOM-CC) method [26-29] is known for incorporating a balanced description of both dynamic and non-dynamic correlation within the frame work of single-reference coupled cluster method and presents a black box approach for the accurate calculation of energy [29-30], structure [31-33] and properties [34] of open shell molecules and molecular excited states. For principal peaks in electron affinity and ionization problem, the EOM-CC method is equivalent [35] to (1,0) and (0,1) sectors of FSMRCC. However, the equivalence breaks down in high sectors.

The EOM-CC or FSMRCC method, even in the singles and doubles approximation, has the prohibitively high N^6 scaling and large storage requirements, which restrict its application beyond ten atoms, in a moderate basis set. Thus, it is highly desirable to develop methods, similar in spirit with the standard EOM-CCSD or FSMRCCSD method, but with lower computational scaling and smaller storage requirements. The thesis is organized as follows:

First chapter: A general introduction is proposed leading to the subject matter of the thesis. Here, a brief overview of some of the basic concepts and developments in single-reference coupled cluster theories are presented. The source of the problem in single-reference methods for theoretical treatment of high-energy radicals and excited states are discussed. The necessity of multi-reference treatments to these problematic cases is also highlighted. We introduce the theory of equation of motion coupled cluster

method as an alternative single-reference approach to multi-reference situations. We conclude the first chapter with the objectives and scope of the thesis.

Second chapter: The second chapter deals with the study of NO_x catalyzed pathway of stratospheric ozone depletion, using highly accurate coupled cluster methods. These catalytic reactions represent a great challenge to the state-of-the-art *ab initio* methods, while their mechanisms remain unclear to both experimentalists and theoreticians. In this work, we have used the so-called "gold standard of quantum chemistry," the CCSD(T) method, to identify the saddle points on NO_x based reaction pathways of ozone hole formation. Energies of the saddle points are calculated using the multi reference variants of coupled cluster methods. The calculated activation energies and rate constants show good agreement with available experimental results. Tropospheric precursors to stratospheric NO_x radicals have been identified, and their potential importance in stratospheric chemistry has been discussed. Our calculations resolve previous conflicts between *ab initio* and experimental results for a trans nitro peroxide intermediate, in the NO_x catalyzed pathway of ozone depletion.

Third Chapter: In this chapter, we report a comparative single-reference and multi reference coupled-cluster investigation on the structure, potential energy surface, and IR spectroscopic properties of the trans peroxo nitrate radical, one of the key intermediates in stratospheric NO_X chemistry. The previous single-reference *ab-initio* studies predicted an unbound structure for the trans peroxo nitrate radical. However, our Fock space multi reference coupled cluster calculation confirms a bound structure for the trans peroxo nitrate radical, in accordance with the experimental results reported earlier. Further, the analysis of the potential energy surface in FSMRCC method indicates a well-behaved minimum, contrary to the shallow minima predicted by the single-reference coupled cluster method. The harmonic force field analysis, of various possible isomers of peroxo nitrate also reveals that only the trans structure leads to the experimentally observed IR peak at 1840 cm^{-1}. The present study highlights the critical importance of non-dynamic

correlation in predicting the structure and properties of high-energy stratospheric NO_x radicals.

Fourth Chapter: In this chapter, we present a benchmark study on the performance of the EOMIP-CCSD(2) method for computation of structure and properties of doublet radicals. The EOMIP-CCSD(2) method is a second-order approximation to the standard EOMIP-CCSD method. By retaining the black box nature of the standard EOMIP-CCSD method and adding favorable N^5 scaling, the EOMIP-CCSD(2) method can become the method of choice for predicting the structure and spectroscopic properties of large doublet radicals. The EOMIP-CCSD(2) method overcomes the typical problems associated with the standard single-reference *ab-initio* treatment of doublet radicals. We compare our results for geometries and harmonic vibrational frequencies with those obtained using the standard EOMIP-CCSD method, as well as unrestricted Hartree–Fock (UHF)- and restricted open-shell Hartree–Fock (ROHF)-based single-reference coupled cluster and second order many-body perturbation theory (MBPT(2)) methods. The effect of the basis set on the quality of the results has been studied using a hierarchy of Dunning's correlation-consistent aug-cc-pVXZ (X = D, T, Q) basis sets. Numerical results show that the EOMIP-CCSD(2) method, despite its N^5 scaling, gives better agreement with experimental results, compared to the UHF- and ROHF-based MBPT(2), as well as the single-reference coupled cluster methods.

Fifth Chapter: In this chapter, we present an N^5 scaling modification to the standard EOMEA-CCSD method, based on the matrix partitioning technique and perturbative approximations. The method has lower computational scaling and smaller storage requirements than the standard EOMEA-CCSD method and, therefore, can be used to calculate electron affinities of large molecules and clusters. The performance and capabilities of the new method have been benchmarked with the standard EOMEA-CCSD method, for a test set of 20 small molecules, and the average absolute deviation is only 0.03 eV. The method is further used to investigate electron affinities of DNA and

RNA nucleobases, and the results are in excellent agreement with the experimental values.

Sixth Chapter: Spin flip equation of motion coupled cluster (EOM-SF-CC) can correctly treat situations involving electronic degeneracies or near degeneracies, e.g., bond breaking, di- and tri-radicals, etc. However, for large systems EOM-SF-CC (even in single and double excitations) is computationally prohibitively expensive. Therefore, earlier approximations to EOM-SF-CC methods such as spin flip configuration interaction singles with perturbative doubles (SF-CIS(D)) have been proposed. In this chapter, we present a new perturbative approximation to EOM-SF-CC, which has been found to be more accurate than SF-CIS(D). The capabilities, advantages, and timings of the new approach have been demonstrated considering the singlet-triplet gaps in di- and tri-radicals as well as bond breaking examples. The method is extended to double spin flip EOM-CC, and its capabilities have been tested. We have shown that the second order approximation to single and double spin flip EOM-CC can generate very accurate potential energy surface and their geometrical derivatives.

Seventh Chapter: In this chapter, we present a benchmark investigation on the performance of EOMIP-CCSD(2) method for calculation of ionization potential. The calculated ionization potential (IP) values are found to be significantly overestimated compared to that obtained in the standard EOMIP-CCSD method. However, the EOMIP-CCSD(2) method correctly reproduces the basis set convergence behavior of standard EOMIP-CCSD method, and a small basis set EOMIP-CCSD calculation, extrapolated with large basis set EOMIP-CCSD(2) results can correct the errors of the original EOMIP-CCSD(2) approximation to a large extend. However, the method gives inferior performance for the cases where relaxation effect plays an important role.

Eighth Chapter: In this chapter, we present a new approximation to the standard EOMIP-CCSD method. The new method (EOMIP-CCSD(2)*) scales as non-iterative N^6

and has significantly low storage requirement. The problem of over estimation of ionization potential in EOMIP-CCSD(2) approximation is corrected in this new method and the EOMIP-CCSD(2)* method gives excellent agreement with experimental values. It also gives very good with the experiment for bond-length and IR frequencies and produces value comparable to CCSD(T), in significantly less computational cost. The EOMIP-CCSD(2)* approximation works even for core-ionization and satellite IP, where the previous EOMIP-CCSD(2) approximation drastically fails.

References:

1. Cizek, J., On the Correlation Problem in Atomic and Molecular Systems. Calculation of Wavefunction Components in Ursell-Type Expansion Using Quantum-Field Theoretical Methods. *J. Chem. Phys.* **1966,** *45*, 4256-4266.
2. Bartlett, R. J., MANY-BODY PERTURBATION-THEORY AND COUPLED CLUSTER THEORY FOR ELECTRON CORRELATION IN MOLECULES. *Annu. Rev. Phys. Chem.* **1981,** *32*, 359-401.
3. Adamowicz, L.; Laidig, W. D.; Bartlett, R. J., Analytical gradients for the coupled-cluster method. *Int. J. Quant. Chem.* **1984,** *26*, 245-254.
4. Salter, E. A.; Trucks, G. W.; Bartlett, R. J., Analytic energy derivatives in many-body methods. I. First derivatives. *J. Chem. Phys.* **1989,** *90*, 1752-1766.
5. Scheiner, A. C.; Scuseria, G. E.; Rice, J. E.; Lee, T. J.; Schaefer III, H. F., Analytic evaluation of energy gradients for the single and double excitation coupled cluster (CCSD) wave function: Theory and application. *J. Chem. Phys.* **1987,** *87*, 5361-5373.
6. Monkhorst, H. J., Calculation of properties with the coupled-cluster method. *Int. J. Quant. Chem.* **1977,** *12*, 421-432.
7. Besler, B. H.; Scuseria, G. E.; Scheiner, A. C.; Schaefer III, H. F., A systematic theoretical study of harmonic vibrational frequencies: The single and double excitation coupled cluster (CCSD) method. *J. Chem. Phys.* **1988,** *89*, 360-366.
8. Koch, H.; Jensen, H. J. A.; Jorgensen, P.; Helgaker, T.; Scuseria, G. E.; Schaefer III, H. F., Coupled cluster energy derivatives. Analytic Hessian for the closed-shell coupled cluster singles and doubles wave function: Theory and applications. *J. Chem. Phys.* **1990,** *92*, 4924-4940.
9. Salter, E. A.; Bartlett, R. J., Analytic energy derivatives in many-body methods. II. Second derivatives. *J. Chem. Phys.* **1989,** *90*, 1767-1773.
10. Shavitt, I., The method of configuration interaction. In *Methods of electronic structure theory*, III, H. F. S., Ed. Springer: New York, 1977; pp 189-275.

11. Hanrath, M., Higher excitations for an exponential multireference wavefunction Ansatz and single-reference based multireference coupled cluster Ansatz: Application to model systems H_4, P_4, and BeH_2. *J. Chem. Phys.* **2008,** *128*, 154118-10.

12. Hanrath, M., An exponential multireference wave-function Ansatz. *J. Chem. Phys.* **2005,** *123*, 084102-12.

13. Evangelista, F. A.; Simmonett, A. C.; Allen, W. D.; Schaefer, H. F.; Iii; Gauss, J., Triple excitations in state-specific multireference coupled cluster theory: Application of Mk-MRCCSDT and Mk-MRCCSDT-n methods to model systems. *J. Chem. Phys.* **2008,** *128*, 124104-13.

14. Evangelista, F. A.; Allen, W. D.; Schaefer, H. F.; Iii, Coupling term derivation and general implementation of state-specific multireference coupled cluster theories. *J. Chem. Phys.* **2007,** *127*, 024102-17.

15. Chattopadhyay, S.; Sinha Mahapatra, U.; Datta, B.; Mukherjee, D., State-specific multi-reference coupled electron-pair approximation like methods: formulation and molecular applications. *Chem. Phys. Lett.* **2002,** *357*, 426-433.

16. Masik, J.; Hubac, I., Multireference Brillouin-Wigner Coupled-Cluster Theory. Single-root approach. *Advances in quantum chemistry* **1998,** *31*, 75-104.

17. Hurtubise, V.; Freed, K. F., The algebra of effective hamiltonians and operators: Exact operators. *Advances in chemical physics* **1993,** *83*, 465-465.

18. Balkova, A.; Kucharski, S. A.; Meissner, L.; Bartlett, R. J., The multireference coupled-cluster method in Hilbert space: An incomplete model space application to the LiH molecule. *J. Chem. Phys.* **1991,** *95*, 4311-4316.

19. Balkova, A.; Bartlett, R. J., A multireference coupled-cluster study of the ground state and lowest excited states of cyclobutadiene. *J. Chem. Phys.* **1994,** *101*, 8972-8987.

20. Mukherjee, D.; Pal, S., Use of Cluster Expansion Methods in the Open-Shell Correlation Problem. In *Advances in Quantum Chemistry*, Per-Olov, L., Ed. Academic Press: 1989; Vol. Volume 20, pp 291-373.

21. Pal, S.; Rittby, M.; Bartlett, R. J.; Sinha, D.; Mukherjee, D., Molecular applications of multireference coupled-cluster methods using an incomplete model space: Direct calculation of excitation energies. *J. Chem. Phys.* **1988,** *88*, 4357-4366.

22. Pal, S., Fock space multi-reference coupled-cluster method for energies and energy derivatives. *Mol. Phys.* **2010,** *108*, 3033-3042.

23. Kaldor, U.; Haque, A., Open-shell coupled-cluster method: Direct calculation of excitation energies. *Chem. Phys. Lett.* **1986,** *128*, 45-48.

24. Vaval, N.; Ghose, K. B.; Pal, S.; Mukherjee, D., Fock-space multireference coupled-cluster theory. fourth-order corrections to the ionization potential. *Chem. Phys. Lett.* **1993,** *209*, 292-298.

25. Vaval, N.; Pal, S.; Mukherjee, D., Fock space multireference coupled cluster theory: noniterative inclusion of triples for excitation energies. *Theor. Chem. Acc.* **1998,** *99*, 100-105.

26. Nooijen, M.; Bartlett, R. J., Equation of motion coupled cluster method for electron attachment. *J. Chem. Phys.* **1995,** *102*, 3629-3647.

27. Sekino, H.; Bartlett, R. J., A linear response, coupled-cluster theory for excitation energy. *International Journal of Quantum Chemistry* **1984,** *26*, 255-265.

28. Krylov, A. I., Size-consistent wave functions for bond-breaking: the equation-of-motion spin-flip model. *Chem. Phys. Lett.* **2001,** *338*, 375-384.

29. Stanton, J. F.; Bartlett, R. J., The equation of motion coupled-cluster method. A systematic biorthogonal approach to molecular excitation energies, transition probabilities, and excited state properties. *J. Chem. Phys.* **1993,** *98*, 7029-7039.

30. Kowalski, K.; Piecuch, P., The active-space equation-of-motion coupled-cluster methods for excited electronic states: Full EOMCCSDt. *J. Chem. Phys.* **2001,** *115*, 643-651.

31. Stanton, J. F.; Gauss, J., Analytic energy derivatives for ionized states described by the equation-of-motion coupled cluster method. *J. Chem. Phys.* **1994,** *101*, 8938-8944.

32. Levchenko, S. V.; Wang, T.; Krylov, A. I., Analytic gradients for the spin-conserving and spin-flipping equation-of-motion coupled-cluster models with single and double substitutions. *J. Chem. Phys.* **2005,** *122*, 224106-11.

33. Stanton, J. F., Many-body methods for excited state potential energy surfaces. I. General theory of energy gradients for the equation-of-motion coupled-cluster method. *J. Chem. Phys.* **1993,** *99*, 8840-8847.

34. Kállay, M.; Gauss, J., Calculation of excited-state properties using general coupled-cluster and configuration-interaction models. *J. Chem. Phys.* **2004,** *121*, 9257-9269.

35. Musial, M.; Bartlett, R. J., Multireference Fock-space coupled-cluster and equation-of-motion coupled-cluster theories: The detailed interconnections. *J. Chem. Phys.* **2008,** *129*, 134105-12.

Chapter 1
Introduction

"It is the goal that makes the difference"

Warner von Braun

A general introduction is proposed leading to the subject matter of the thesis. Here, a brief overview of some of the basic concepts and developments in single-reference coupled cluster theories are presented. The source of the problem in single-reference methods for theoretical treatment of high-energy radicals and excited states are discussed. The necessity of multi-reference treatments to these problematic cases is also highlighted. We introduce the theory of equation of motion coupled cluster method as an alternative single-reference approach to multi-reference situations. We conclude the first chapter with the objectives and scope of the thesis.

1.1 Introduction

Recent years have seen spectacular developments, in the field of many-body methods and their role in incorporating electron correlation, both conceptually and computationally. The importance of many body methods has been highlighted several times in the literature [1-9]. The methods have gained special attention because they satisfy size-consistency and size-extensivity, which has been realized as an important criteria in model theoretical chemistry. There are still several new and emerging challenges in the development and application of many body theories to chemical problems. This thesis will deal with some these challenges, within the framework of so-called coupled cluster methods, to describe the spectroscopic energies, structures and properties of quasi-degenerate states. The aim of thesis is to present a critical study on the application of existing methods to the quasi-degenerate states of atoms and molecules, as well as, development of new low cost approximation, which could be the forebearer of meaningful application to realistic chemical systems.

In this chapter, we will present a brief review of the background material and specifically, the current status of developments in coupled cluster method in the area of energy, structure, and spectroscopic properties. This will help the presentation of the study from second chapter onwards.

1.2 Atomic and Molecular Structure Theory: A Quantum Mechanical Approach

The delicate balance of interactions between positively charged nuclei and negatively charged electrons leads to stable the Atomic and molecular systems. The electronic

structure of atoms and molecules are described by quantum mechanical bound states and can be studied by solving time-independent Schrödinger wave equation[8].

$$\hat{H}\Psi = E\Psi \tag{1.1}$$

Where, H is the Hamiltonian operator for the total energy of the system. The total energy is the sum of, kinetic energy of its constituent particles, the potential energy due to attractive and repulsive interactions amongst the particles and the energy due to interaction of the system with the surroundings. Now, the interaction of the system with surroundings may be quite complicated and can include the effect of external electric field, magnetic field, geometrical distortion, etc. In the absence of external perturbations, the kinetic energy of the system can be divided into two parts, namely, nuclear and electronic kinetic energies. The potential energy has three parts: nuclear-electron attraction energy, electron-electron repulsion energy and the nuclear-nuclear repulsion energy. For a system consist of M nuclei and N electrons, Hamiltonian operator can be written as [8],

$$H = -\frac{1}{2}\sum_{A=1}^{M}\frac{1}{M_A}\nabla_A^2 - \frac{1}{2}\sum_{i=1}^{N}\nabla_i^2 - \sum_{i=1}^{N}\sum_{A=1}^{M}\frac{Z_A}{\|r_i - R_A\|} + \sum_{\substack{i,j \\ i<j}}^{N}\frac{1}{\|r_i - r_j\|} + \sum_{\substack{A,B \\ A<B}}^{N}\frac{Z_A Z_B}{\|R_A - R_B\|} \tag{1.2}$$

In the above equation, R_A and r_i are the spatial coordinates of A^{th} nuclei and i^{th} electron respectively. The N-electron wave function is a complicated function of spatial coordinates of nuclei and space-spin coordinates of electrons, and can be written as $\Psi(R_1,...,R_M,x_1,...,x_N)$. According to Pauli's exclusion principle, the wave function of a system must be anti-symmetric with respect to the exchange of space-spin coordinates of any two electrons and can be expressed as,

$$\Psi(x_1,....x_i....x_j,...,x_N) = -\Psi(x_1,....x_j.....x_i,...,x_N) \tag{1.3}$$

The most convenient way to impose the condition of anti-symmetry on wave function is to express it as a determinant of N-spin orbitals or linear combination of determinants.

One can obtain a complete set of N-electron determinants and therefore, the exact wave function of N-electron system, provided the chosen orbitals form a complete set.

1.3 Born-Oppenheimer Approximation and Electronic Hamiltonian

It is extremely difficult to solve the eigen value problem of Equation (1.1) using full the Hamiltonian, as given by Equation (1.2), even for small systems. Since nuclei are much heavier than electrons, during the electronic motion, the nuclear framework remains virtually static. Therefore, one can separate the nuclear motion from the electronic motion to a good approximation. This is generally known as Born-Oppenheimer approximation (BOA). Under the Born-Oppenheimer approximation, kinetic energy of nuclei vanishes and the nuclear-nuclear repulsion energy becomes constant. Addition of any constant to an operator does not change the Eigen functions but simply adds to the eigen values. Hence, as a consequence of BOA, problem of total Hamiltonian eigen value can be reduced as a problem of electronic Hamiltonian only, which can be written as,

$$H_{el} = -\frac{1}{2}\sum_{i=1}^{N}\nabla_i^2 - \sum_{i=1}^{N}\sum_{A=1}^{M}\frac{Z_A}{\|r_i - R_A\|} + \sum_{\substack{i,j \\ i<j}}^{N}\frac{1}{\|r_i - r_j\|} \tag{1.4}$$

1.4 Hartree-Fock Theory

The exact solution of the electronic Hamiltonian is not possible for an interacting N electronic system. However, the best possible solution within the framework of independent particle model can be obtained by spherical averaging of inter-electronic interactions. This is known as the Hartree-Fock method [8, 10-12]. It is based on the

approximation that the ground state of closed shell atoms and molecules can be described by a single determinant configuration.

$$\Phi_0(x_1, x_2, ..., x_N) = \frac{1}{\sqrt{N!}} \begin{vmatrix} \chi_1(x_1) & \chi_1(x_2) ..... \chi_1(x_N) \\ \chi_2(x_1) & \chi_2(x_2) ..... \chi_2(x_N) \\ .. & .. & .. \\ \chi_N(x_1) & \chi_N(x_2) ..... \chi_N(x_N) \end{vmatrix} \tag{1.5}$$

Electrons are assumed to be independent of each other, and each electrons move in a spherically averaged inter-electronic repulsion potential due to other (N-1) electrons. According to the variation principle, the best possible wave function of the form given by Equation (1.5) is the one, which provides the minimum energy.

$$E_0 = \langle \Phi_0 | H_{el} | \Phi_0 \rangle \tag{1.6}$$

Variational optimization of wave function is performed with the choice of orthonormal spin orbitals, which leads to integro-differential equations known as Hartree-Fock equation. Hartree-Fock equation has to be solved in an iterative manner.

$$f(x)\chi_a(x) = \varepsilon_a \chi_a(x) \tag{1.7}$$

$$\begin{aligned} f(x) &= T_e + V_{ne} + V_{HF}(x) \\ &= -\frac{1}{2}\nabla^2 - \sum_{A=1}^{M} \frac{Z_A}{\|r - R_A\|} + V_{HF} \end{aligned} \tag{1.8}$$

$$V_{HF}(x) = \sum_{j=1}^{N} J_j(x) + \sum_{j=1}^{N} K_j(x) \tag{1.9}$$

$$J_j(x)\chi_i(x) = \int dx' \frac{\chi_j^*(x')\chi_j(x')}{|x - x'|}\chi_i(x) \tag{1.10}$$

$$K_j(x)\chi_i(x) = \int dx' \frac{\chi_j^*(x')\chi_i(x')}{|x-x'|}\chi_j(x) \tag{1.11}$$

Here, the $f(x)$ is the Fock operator which is an effective one electron operator. The operator $v_{HF}(x)$ is average potential experienced by an electron due to all other electrons. It includes the average Coulomb interaction $J_j(x)$ and exchange interaction $K_j(x)$. The exchange potential is the consequence of the anti-symmetric nature of wave function.

For atoms, the HF equations can be exactly solved as integro-differential equation. However, for molecules, the explicit integration of the two electron interaction term is difficult as the orbitals involved are centered at different nuclei. To overcome this problem, Roothan [13, 14] introduced the idea of basis set expansion. For closed shell systems, the spin orbitals with opposite spin functions are paired up, and the problem can be simplified by using only spatial orbitals after spin integration. This method is known as restricted HF (RHF). The open shell systems also have most of the electrons paired up and can be solved by a Restricted Open-shell HF (ROHF) method. HF equations can also be solved using explicit spin orbital's, which is called Unrestricted HF (UHF). The RHF determinant is a pure eigen function of the total spin square operator ($\hat{S}^2$), while linear combination of suitably chosen ROHF determinants can be adapted to be the eigen function of the spin square operator. However, UHF determinant is neither an eigen function nor it can be spin adapted in general.

It is well known [1] that the HF wave function takes care of the correlation of electrons with parallel spin (Fermi hole), but cannot prevent two electrons of opposite spin to occupy the same space (coulomb hole). This can be taken care by higher-level beyond HF theories, which includes electron correlation. The correlation energy as defined by Löwdin [1] is the difference between the Hartree-Fock limit energy, obtained in a complete basis set, and the exact solution of the non-relativistic Schrödinger equation. However, one can define the correlation energy analogously in a finite basis. Usually the correlation energy is very small compared to the total energy of the system. Nevertheless,

in many cases, we deal with the small energy differences like binding energy, ionization potentials, electron affinities, etc, which are sensitive to correlation effects. For the difference energies, it is also necessary to treat the correlation in a consistent and balanced manner for both the states. Apart from the accuracy and balanced treatment of the calculated quantities, another important aspect is that the energies and molecular properties must be obtained in a size-extensive way, i.e they must scale correctly with the number of particles. This also ensures that the quantities of interest separate correctly. Restricted HF approximation becomes progressively worse in the separation limit, where the separating fragments are open shell systems, resulting in grossly distorted values at this limit. However, this may be corrected in the independent particle model itself using the unrestricted HF method.

Various schemes have emerged to go beyond the independent particle model, starting from multi-configurational SCF [5] to sophisticated methods, which includes electron correlation effects like configuration interaction [15] , many body perturbation theory [16] and coupled cluster method [17-21]. All these methods lead to the lowering of the energy of a specific state, in particular the ground state of the system. Before, we proceed further, in the following section, we state the basic criteria that all the correlation methods must satisfy.

1.5 Basic Criteria for An Ideal Electron Correlation Theory

All the correlation methods should satisfy some basic conditions at all the stages so that it might be considered as a theoretical model for electronic calculations. These criteria, as proposed by Pople *et. al.* [22] and Bartlett [23], can be briefly discussed as follows.

1. The method should be independent of certain choices of configurations and symmetry and should be applicable on a wide range of molecular systems.
2. The method should be invariant with respect to. unitary transformations.
3. The method should be size-consistent i.e. the energy obtained through a method for the composite system is equal to the summation of energies obtained through the same method for its constituent subsystems, at the non interacting limit.
4. The method should be size-extensive, which means that the energy of a strongly interacting many electron system for a given nuclear framework should approximately be proportional to the number of electrons.
5. The method should be computationally efficient as well as cost-effective, in order to extend its applicability to molecular systems of chemist's interest.
6. The method should be applicable for open shell systems and excited states.

Among these, size-consistency and size-extensivity are the most important criteria as, the efficiency and accuracy of the method are determined by these two factors.

1.6 Size-consistency and Size-extensivity

As defined by Pople and co-workers [22] and Bartlett [23], size-consistency of a method refers to its behavior when it is applied to a collection of N non-interacting monomers. A method is termed size-consistent, if the energy obtained in its application to this collection of monomers is N times the energy obtained in its separate application to the monomer. In other words, when a size-consistent method is applied to a molecule AB dissociating into two fragments A and B, the energy of the molecule calculated at the dissociating limit (or infinite separation limit) is equal to the sum of energies of both fragments calculated by separately applying the method to individual fragments.

$$E_{method}(AB) = E_{method}(A) + E_{method}(B) \tag{1.12}$$

In addition, the size-consistency of a method ensures that it also predicts a qualitatively correct dissociation curve. Clearly, size-consistency is a desirable feature for any approximate method.

Size-extensivity, a concept related to size-consistency, refers to mathematical scaling of the energy with the number of electrons [24, 25]. A method is size-extensive if the energy a many-electron system calculated with the method, even in the presence of interactions, is approximately proportional to the number of electrons N and becomes exact as $N \rightarrow \infty$. In other words, the energy and the error in energy should increase in proportion with the size of the system. Size-extensivity is especially important for methods of electron correlation. If a method is not size-extensive, the error in correlation energy shows either sub-linear or super-linear dependence on the number of electrons (or equivalently the size of the system). In the former case, fraction of the exact correlation energy recovered per electron decreases as the size of the system increases eventually leading to zero correlation energy in the limit $N \rightarrow \infty$. In the latter case, the same fraction increases with the system size, leading to prediction of infinite correlation energy per electron as $N \rightarrow \infty$. Therefore, all non-size-extensive methods show progressively unphysical behavior as size of the system increases. Size-extensive methods are considered to be particularly appropriate for large systems, as they strive to recover a roughly constant fraction of exact correlation energy with increasing system size.

Another related concept that is useful in discussion on size-consistency and size-extensivity is separability. As discussed by Primas [26], separability is related to the behavior of certain quantities of a system composed of two sub-systems interacting with each other in the limit of vanishing interaction strength [25, 26]. An additively separable quantity of the system, as the interaction vanishes, should be the sum of the same quantity for the individual sub-systems. Similarly, a multiplicatively separable quantity should be the product of the same quantity for the individual systems. For example, the

total energy of many-electron systems is an additively separable quantity. Similarly, wave function is multiplicatively separable. Clearly, separability condition is the generalization of the size-consistency condition on energy, with respect to an arbitrary division of the system into sub-systems.

1.7 Different Correlated Methods

A critical and broad survey of several correlated methods points to three popular techniques for the proper treatment of correlation effects: a) the linear variation based configuration interaction, b) many-body perturbation method and c) coupled cluster approach. Approximate versions of these methods such as truncated CI, and the coupled electron pair approximation, finite order MBPT and approximate versions coupled cluster method have been used in many cases for one reason or the other. Each of these has strengths and weakness, relating to problems either implementational or intrinsic problems like loss of size-extensivity, as is in the case in truncated CI. We will discuss these at appropriate places of this chapter.

1.8 Configuration Interaction Method

CI is conceptually the simplest and the most traditional method, where the wave function is expressed as a linear combination of Slater determinants, and the coefficients are determined by a linear variation method. CI wave function is given by,

$$\Psi = \Phi_0 + \sum_{i,a} C_i^a \Phi_i^a + \sum_{\substack{i<j \\ a<b}} C_{ij}^{ab} \Phi_{ij}^{ab} + ... \qquad (1.13)$$

Where, Φ_0 is the Hartree-Fock determinant and Φ_i^a and Φ_{ij}^{ab} are the singly and doubly excited determinants, respectively. Here (i, j, ..) and (a, b, …) denote the occupied and unoccupied orbitals, respectively, in the reference (HF) determinant. Furthermore, the intermediate normalization convention $\langle \Phi_0 | \Psi \rangle = 1$ has been used.

CI, being a variational method, gives variational upper bound. While this is of some advantage in the calculation of energy for a particular state, it is not so for the case of difference energies. In fact, it is more important to calculate these difference energies in a direct manner. Some of the methods like coupled cluster linear response, equation of motion coupled cluster method and quasi-degenerate perturbation theory are able to calculate these difference energies directly rather than the difference of energy obtained in two separate calculations. The common correlation energies of the two states are automatically cancelled. The many body methods that are routinely used are mostly non-variational and it has been shown that the results obtained using these methods usually differ from the rigorous variational bounds only in fifth or higher orders perturbation [23]. Hence, at least for cases where such higher-order corrections are not important, MBPT/CCM methods used may be called as quasi-variational.

When all possible determinants in a given one particle basis are included in the wave function, the method is called as full CI (FCI). This produces exact results in a given basis set. Since, FCI is not feasible even for the small and medium-size molecules in some meaningful basis; we require approximations like truncating the expansions in a CI wave function. Truncating the CI space only up to singly and doubly excited determinants along with the reference HF determinant leads to CISD approximation. Use of linear variation method to determine the expansion coefficients leads to eigen value problem for the Hamiltonian matrix defined over all the determinants present in approximate CI wave function. Matrix elements of the Hamiltonian between any two determinants can be evaluated using Slater-Condon rules [8]. Lowest eigen value and eigenvector of the CI Hamiltonian matrix corresponds to the ground state and rest of the

eigen values, and eigenvectors correspond to different excited states. It is well known that any approximate or truncated form of CI is not generally size-extensive and does not separate into appropriate fragments.

The origin of the lack of size-extensivity of truncated CI is related to its inability to account for the dynamic correlation effects in a proper manner. Sinanoglu [27] has shown, in the context of pair correlation theory, that simultaneous but independent doubly excited processes are also important. This leads to quadruply, hextuply etc. configurations with amplitudes as appropriate products of doubly excited amplitudes. Similar physical effects take place involving higher excited determinants. Any truncation based on a fixed degree of excitations cannot account for such effects and thus truncated CI suffers from lack of size-extensivity.

1.9 Many body Perturbation Theory

Many body perturbation theory (MBPT) [28-33] offers an alternative procedure for systematic incorporation of dynamic correlation effects and producing energy in a size-extensive manner, at each order of the theory. In this approach, the exact Hamiltonian is partitioned into two parts, a zeroth order part (H_o) whose solutions are usually known and a perturbation part (V), assumed to be very small compared to the zeroth order part. There are two different perturbation series one based on Rayleigh Schrödinger (RSPT) [28, 29, 31] and another based on Brillouin Wigner perturbation theory (BWPT) [31]. In both the perturbation series, the wave function is expressed as a power series around the solution of the zeroth order Hamiltonian. Correction to the wave function at each order is written in terms of the eigen-functions of H_o. In Brillouin Wigner theory, the energy expression depends on the energy itself and so, an iterative procedure has to be adapted for getting the energy. Each successive iteration produces energy at higher order, which

is not size-extensive. Hence, BWPT is seldom used to obtain the correlation energy. The properties of RSPT, however, depend upon the exact scheme utilized for its solution. Depending on the partitioning of the Hamiltonian, there exist two different variants of RSPT: Moller-Plesset (MP) and Epstien-Nesbet perturbation theory. The use of Fock operator as H_0 leads to MP partitioning. It can be shown that MP partitioning in a RSPT framework leads to a perturbation series, which scales correctly with the number of electrons (N). This size extensive series is known as MBPT series. Brueckner [34] first observed this scaling property for infinite nuclear separation. The terms proportional to the square or higher power of N, cancel among each other at every order. However, he could not prove it for higher orders. Goldstone [35] devised a diagrammatic approach to show that the terms, which have incorrect scaling can be represented by unlinked diagrams. He proved that such unlinked diagrams cancel among themselves at each orders of perturbation. This is the famous linked diagrams theorem. Kelly [36] applied the diagrammatic approach to atoms. Finite order MBPT has been extensively used for the correlation energies of atoms and molecules. In MBPT, we construct the zeroth order Hamiltonian as the sum of Fock operators and the perturbation (V) is the full electron-electron repulsion $1/r_{ij}$ term without the spherical average part, which is included in the definition of H_0.

Now a days, the accuracy of any many-body method can be measured in terms of the perturbation order. Thus, MBPT offers a very efficient tool for calibrating the accuracy of energy as well as wave function. The MP based RSPT is now commonly used for correlated calculations of atoms and molecules. The acronyms MP2, MP4, MBPT (n), etc. have become very popular because of the accuracy and relative simplicity of the method.

One the other hand, if the diagonal part of the Hamiltonian [7] is used as H_0, it is called Epstein-Nesbet (EN) partitioning and leads to a perturbation expansion in which the denominator contains the difference of diagonal matrix elements of the full Hamiltonian

H_{00}-H_{ii}. In this case, H_0 is not a one-electron operator, and perturbation expansions can also be obtained as a result of infinite-order summation of certain classes of terms in MP series. Although unlike the MP choice, the EN expansion is not invariant under orbital rotations.

Even though the MBPT gives size-extensive results at each order, the slow convergence of the perturbation series is well known. To avoid the convergence problem, non-perturbative methods are more desirable.

In the subsequent sections, we discuss some methods, which are neither strictly perturbative nor strictly variational and they transcend both perturbative and variational types.

1.10 Independent Pair Approximation

Interaction between the pair plays the central role in correlation methods. Pauli's exclusion principle and the two-particle nature of the Hamiltonian ensure that the electron pair theories serve a good approximation for the N electron atomic and molecular problem. The pair theories in its simplest form consider only one electron pair at a time. Thus, an N electron problem is conveniently simplifies to $N(N-1)/2$ electron pairs. The interactions among the pairs are neglected. The total correlation energy can be represented as the sum of the pair contributions, which are obtained independently by solving the effective two electron equations. This decoupling of pairs is known as the independent electron pair approximation (IEPA). It was developed by Sinanoglu [27, 37], and Nesbet [38] independently. Sinanoglu used partial variation method for its derivation and called his version coupled pair many electron theory, while, Nesbit called his theory as Bethe-Goldstone theory. Freed [39] and Robb [40] have extensively reviewed the

relation between the IEPA and perturbation theories. The IEPA wave function for the pair ij may be written as,

$$\left|\Psi_{ij}\right\rangle = \left|\Phi_0\right\rangle + \sum_{a<b} C_{ij}^{ab} \left|\Phi_{ij}^{ab}\right\rangle \tag{1.14}$$

Where, i, j are the occupied orbitals and a, b are the unoccupied (virtual) orbitals in the Hartree-Fock determinant. Linear variation method can be used to calculate the energy E_{ij} , which is a sum of Hartree-Fock energy and the pair correlation energy corresponding to the pair ij.

$$E_{ij} = E_0 + e_{ij}^{IEPA} \tag{1.15}$$

The total correlation energy in IEPA approximation is defined as,

$$E_{corr}^{IEPA} = \sum_{i<j} e_{ij}^{IEPA} \tag{1.16}$$

For an extensive review of the pair theories see references [41] and [42]. However, some important features of the pair theories are presented here. Although the correlation energy for each pair is obtained through linear variation, the sum is not the upper bound to the exact correlation energy. Computationally, IEPA is equivalent to doing DCI for each pair separately, and hence it is called “pair-at-a-time” CI. It might look that IEPA is an approximation to DCI, but is actually not. Rather, it may be viewed as an approximation to FCI. While, DCI is not size-extensive, IEPA gives size-extensive results. The major disadvantage IEPA, though, is that it is not invariant to unitary transformation.

1.11 Coupled Electron Pair Approximation

IEPA is based on two approximations: (a) neglect of pair coupling terms and (b) assumption that the nonlinear terms cancel with part of the energy terms. The first

approximation is cruder. W. Meyer [43] proposed a series of schemes, which considered the coupling between the pairs. These are known as various versions of coupled electron pair approximations (CEPA) [41, 42, 44, 45]. Some of them give size-extensive results. CEPA takes care of the pair interaction terms which are neglected in IEPA. However, it neglects most of the non-linear terms, which are included in what is known as CCM, to be discussed in details below. Thus, CEPA is between IEPA and CCM. While, CEPA has some origin in the variational CI type method, these can also be derived in a non-variational manner. In fact, they are known to have a similarity with not only the approximate versions of CI, but also non-perturbative, non-variational CCM. We will discuss some of these connections in the course of this chapter.

1.12 Coupled Cluster Method

The coupled cluster method(CCM) of electron correlation has its conceptual origin in the pair theories of Sinanoglu [27, 37] and Nesbet [38]. In electronic structure theory, Cizek and Paldus [46-48] introduced the coupled cluster theory, in its present standard form. In CCM, the wave function can be described to be formed by the action of an exponential wave operator acting on a suitable reference function, which is generally, but not necessarily, a Hartree-Fock determinant.

$$\left|\Psi_{cc}\right\rangle = e^{T}\left|\Phi_{0}\right\rangle \tag{1.17}$$

Generally, the intermediate normalization is employed for the wave function, and T is known as the cluster operator. The cluster operators are expressed as a sum of electron-excitation operators, *viz*, one-electron, two-electron, etc.

$$T = T_1 + T_2 + T_3 + ... + T_N \tag{1.18}$$

With the form,

$$
\begin{aligned}
T_1 &= \sum_{i,a} t_i^a a_a^\dagger a_i \\
T_2 &= \sum_{\substack{i>j \\ a>b}} t_{ij}^{ab} a_a^\dagger a_b^\dagger a_j a_i \\
&\cdots\cdots\cdots\cdots \\
T_N &= \sum_{\substack{i>j>k.... \\ a>b>c....}} t_{ijk..}^{abc..} a_a^\dagger a_b^\dagger a_c^\dagger a_k a_j a_i
\end{aligned}
\tag{1.19}
$$

An N-body cluster operator, T_N acting on a vacuum $|\Phi_0\rangle$ produces N-tuply hole-particle excited determinant. The cluster operators commute with each other.

Since in the Equation (1.17) only one single determinant has been used as a reference function, this method is known as single reference coupled cluster method (SRCC). Since in the limit of all possible excitations, i.e. N equals to the total no of electrons, CC theory must be equal to full CI, we can express the relationship between CI and CC coefficients as,

$$
\begin{aligned}
C_1 &= T \\
C_2 &= T_2 + \frac{1}{2!}T_1^2 \\
C_3 &= T_3 + T_1 T_2 + \frac{1}{3!}T_1^3 \\
C_4 &= T_4 + T_1 T_3 + \frac{1}{2!}T_2^2 + \frac{1}{4!}T_1^4
\end{aligned}
\tag{1.20}
$$

The coupled cluster equations are generally solved by method of projection. Substituting Equation (1.17) into Schrödinger equation with normal ordered Hamiltonian leads to:

$$
H_N e^T |\Phi_0\rangle = \varepsilon_{corr} e^T |\Phi_0\rangle \tag{1.21}
$$

Projecting from left of Equation (1.21) by $|\Phi_0\rangle$, we get the equation for the correlation energy.

$$\left\langle \Phi_0 \middle| H_N e^T \middle| \Phi_0 \right\rangle = \varepsilon_{corr} \left\langle \Phi_0 \middle| e^T \middle| \Phi_0 \right\rangle \tag{1.22}$$

Expanding the right hand side of Equation (1.22), only the term, which does not contain T due to normalization condition, survives. Hence, the Equation (1.22) can be written as

$$\left\langle \Phi_0 \middle| H_N e^T \middle| \Phi_0 \right\rangle = \varepsilon_{corr} \tag{1.23}$$

The cluster amplitudes corresponding to any particular excitation can be obtained by left multiplying Equation (1.21) by that particular excited determinant. For example, T_2 can be obtained from

$$\left\langle \Phi_{ij\ldots}^{ab\ldots} \middle| H_N e^T \middle| \Phi_0 \right\rangle = \varepsilon_{corr} \left\langle \Phi_{ij\ldots}^{ab\ldots} \middle| e^T \middle| \Phi_0 \right\rangle \tag{1.24}$$

Both the left and right side of Equation (1.24) have connected as well as disconnected terms. However, the presence of e^T term ensures the mutual cancellation of unlinked terms from both sides of the Equation (1.24). The disconnected terms of the Equation (1.24) for double excitations can occur as a product of connected single excitation terms $\left\langle \Phi_i^a \middle| H_N e^T \middle| \Phi_0 \right\rangle_{open,connected}$ with singly excited cluster amplitude $\left(t_j^b\right)$ disappears from final equations. In the same way, only the connected, open terms survive in Equation (1.24), leading to completely connected CC equations. Thus, Equation (1.23) and (1.24) can be written as,

$$\varepsilon_{corr} = \left\langle \Phi_0 \middle| H_N e^T \middle| \Phi_0 \right\rangle_{closed,connected} \tag{1.25}$$

$$\left\langle \Phi_{ij\ldots}^{ab\ldots} \middle| H_N e^T \middle| \Phi_0 \right\rangle_{open,linked} = 0 \tag{1.26}$$

Because of commutation relation, there is no contraction between the cluster operators. This means that in CC diagrams, each cluster operator in the diagram should be connected with Hamiltonian vertex and not with each other. Due to two particle nature of the Hamiltonian operator, it can have a maximum four number of contractions with cluster operators. Therefore, the CC equations are algebraic non-linear equations in

unknown cluster amplitudes and are at most of quartic power. On the other hand from Equation (1.25), the correlation energy contains only one-body and two-body cluster operators, which are coupled to higher-body cluster operators through Equation (1.26).

The above CC equations can be derived in an alternative way by pre-multiplying Equation (1.21) by e^{-T} as,

$$e^{-T}H_N e^{T}\left|\Phi_0\right\rangle = \varepsilon_{corr}\left|\Phi_0\right\rangle \tag{1.27}$$

Thus, Equation (1.27) can be viewed as an eigen value equation for the similarity transformed Hamiltonian, $\bar{H} = e^{-T}H_N e^{T}$. As, the similarity transformation of the Hamiltonian does not change its eigen values, Eqs. (1.25) and (1.26) can be derived by following the same procedure, and we get the following set of equations.

$$\varepsilon_{corr} = \left\langle\Phi_0\right|e^{-T}H_N e^{T}\left|\Phi_0\right\rangle \tag{1.28}$$

$$\left\langle\Phi_{ij....}^{ab....}\right|e^{-T}H_N e^{T}\left|\Phi_0\right\rangle = 0 \tag{1.29}$$

Using Campbell-Baker-Hausdroff (CBH) formula, $e^{-T}H_N e^{T}$ can be expanded as,

$$\bar{H} = e^{-T}H_N e^{T} = H_N + \left[H_N, T\right] + \frac{1}{2!}\left[\left[H_N, T\right], T\right] + \frac{1}{3!}\left[\left[\left[H_N, T\right], T\right], T\right] + \frac{1}{4!}\left[\left[\left[\left[H_N, T\right], T\right], T\right], T\right] + ... \tag{1.30}$$

Due to the two-body nature of H_N and commutative nature of the cluster operators, this series can be shown to be terminated after four-fold commutations. The connected nature of correlation energy and cluster amplitudes is explicitly revealed by the presence of commutators Equation (1.30). With H_N being connected, its commutation with cluster operators generates only connected terms. This eventually leads to a completely connected series.

The Equation (1.26) leads to a set of coupled nonlinear equations, which are generally solved iteratively to obtain the cluster amplitudes. Perturbation analysis of the iterative procedure shows that at every iteration, the functional gains corrections from various orders of perturbations. After the self-consistency and numerical accuracy is attained, the correlation energy is obtained using Equation (1.25). If the T contains all possible excitation operators, i.e. up to T_N for N-electron system, then the method is called full CC (FCC), which is equivalent to FCI. Obviously, the numbers of cluster operators are same as CI operators. However, for practical applications, one needs to truncate at finite order. The most commonly used truncation is to define $T = T_1 + T_2$ leading to singles and doubles (SD) approximation [49, 50]. Unlike truncated CI, CC method continues to be size-consistent, for all orders of truncation. This is because of the exponential nature of the wave operator, which includes higher excitations through the products of T_1 and T_2. The CCSD ansatz can be further improved by perturbative or complete inclusion of triples (partial and full) [51, 52], quadruple (CCSDT(Q) and CCSDTQ)[53], etc. These ansatz improves the results towards the exactness.

1.13 Alternate Single-Reference CC Approaches

The standard coupled cluster method just discussed is also known as normal coupled cluster method. The normal coupled cluster (NCC) or single-reference coupled cluster (SRCC) method is neither variational, nor perturbative. Due to its non-variational nature, it seems to be computationally unattractive for energy derivatives. An alternate way is to cast the coupled cluster equation in a variational framework. The direct advantage of casting the CC equations variationally is that, it fulfills the Hellmann-Feynman theorem and (2n+1) rule. This makes the method attractive for higher-order energy derivatives. Expectation value CC (XCC) [54-56], unitary CC (UCC) [41, 57] and extended CC (ECC) [58-60] are among the methods used in stationary or variational CC theory.

However, in the present thesis, we stick to the use of coupled cluster method, in its traditional non-variational form.

Although single-reference coupled cluster method is extremely successful in theoretical treatment of closed shell molecules, its performance deteriorates in case of the open shell molecule. In the next section, we will try to investigate the cause behind the failures of single-reference coupled cluster methods for the open shell molecules.

1.14 Problems Associated With the Quantum Mechanical Treatment of Open-shell Molecules

Theoretical treatment of open shell molecules is often difficult. For these systems, the single-determinant description often provides an inadequate starting point. Several types of problems arise that are infrequent or never encountered in treating closed-shell molecules [61]. These include spin contamination [62] and the phenomenon usually called ‘‘symmetry breaking’’ in the reference function [63], instability and near-singularity of the HF-SCF solutions [64, 65], strong (non-dynamical) electron correlation effects, and adiabatic potential energy surfaces that exhibit many complicated features such as loci of conical intersections and avoided crossings.

While it is now possible to ‘‘push a button’’ and obtain highly accurate results for a closed-shell system, the same is not possible and perhaps never will be possible for open shell systems. Each system presents its own unique set of problems and requires careful attention. The selection of a technique can involve a nontrivial analysis, and experience, as well as, expertise is required for making a judicious choice [61].

In spite of the intrinsic challenge posed by theoretical treatment of open-shell systems, there exists a considerable amount of motivation for their accurate study. First, the highly

reactive nature of radicals often makes their study in the laboratory extraordinarily difficult, sometimes impossible, and the presence of several low-lying excited states tends to make their electronic spectroscopy complicated. In fact, the assistance of quantum chemistry is essential to properly interpret many experimental studies of these systems. The open-shell molecules are important in the areas that include atmospheric chemistry, interstellar chemistry, and theories of the origin of life. In recent times, there has been a lot of interest in the chemistry of radical cations and anions, because of the involvement of these species in a wide variety of organic and biological reactions, radiation chemistry, and single electron transfer processes [66, 67]. Due to their transient nature and other problems associated with the experimental studies, the *ab-initio* methods can play a vital role in unraveling their properties and, therefore, a proper understanding of the important issues associated with theoretical study of open shell molecules is absolutely necessary. In the next subsection, we are going to take a brief glance at the problems associated with the *ab-initio* treatment of open shell molecules.

1.14.1 Spin Contamination

Calculation of molecular orbitals for most of the closed shell molecules is often straightforward. It provides a solution that obeys some of the symmetry property satisfied by the exact wave function. To be precise, the density calculated from the Slater determinant comprising the molecular orbitals transforms according to the total symmetric representation of the molecular point group, and the wave function is an eigen function of the spin-squared (S^2) operator with eigen value zero. The dominant part of the correlation energy for the closed shell molecules comes from the so-called "dynamical" part. Therefore, the mathematical structure of the exact wave function (written in the FCI expansion) is dominated by the reference Slater determinant, along with small but important contributions from higher excited determinants.

However, the situation is altogether different in case of Open-shell molecules, where most of the problems associated with their theoretical description is connected with the choice of the starting point for higher-level calculations. In the HF method, the Fock operator is itself a function of its solution, and becomes diagonal at convergence. Hence, unlike the eigen functions of the Hamiltonian, the Slater determinants made up of molecular orbitals, obtained by a SCF calculation, do not necessarily obey spin and symmetry properties of the exact wave function. Multiple solutions can be obtained by relaxing constraints on the molecular orbital solutions. Therefore, lower SCF energies often can be obtained, at the expense of violating fundamental symmetry properties.

The most well-known problem associated with HF-SCF solutions for the radicals is known as ‘‘spin contamination’’ [62] and occurs when one uses the unrestricted Hartree–Fock (UHF) approximation [68]. It utilizes distinct sets of molecular orbitals for electrons of different spin. Unlike the case of ROHF, where a radical is described by a set of doubly occupied orbitals and then one half-filled orbital for each unpaired electron, all of the orbitals in the UHF calculation are singly occupied. The result is that the wave function is no longer an eigen function of the S^2 operator with eigen value $S(S+1)$. If resolved into eigen functions of particular spin states, the UHF wave function contains components of the appropriate spin multiplicity $(2S+1)$ plus ‘‘contamination’’ from those with higher levels of spin multiplicity. For example, the UHF description of a doublet contains doublet, quartet, sextet, and so on, components, while that of a triplet is contaminated by pentet, septet, and so on, contributions.

To avoid spin contamination, another type of reference function can be used, specifically that of the restricted open-shell Hartree–Fock (ROHF) type [69, 70]. In ROHF, maximum double occupancy of spatial orbitals is enforced, and the resulting Slater determinant solution is an eigen function of the S^2 operator.

However, it has been shown by Stanton and Gauss [61] that at the coupled cluster level, the spin contamination is negligible, even if the reference UHF wave-function is heavily

spin contaminated, and the results are comparable to the corresponding ROHF based CC results. Moreover, most implementations of open-shell MP and CC theories based on an ROHF determinant do not give results that are free from spin contamination [71]. The most common realizations of ROHF-based MP and CC theories are carried out in a spin orbital basis, and the correlation treatment introduces a small amount of spin contamination.

While the discussion in the above paragraph is intended to convey that the spin contamination does not represent a major problem in CC calculations [72], it is not always possible to carry out CC treatments for larger molecules. In that cases, the issue of reference function will become important if the treatment of correlation is omitted or simply restricted to the MBPT(2) model. At first glance, one might think that ROHF would be the preferred choice, since it is ‘‘closer’’ (in the sense of spin properties) to the exact wave function. However,, ROHF methods suffer from another problem (usually termed symmetry breaking but in a way represents a more general and notorious phenomenon than the name indicates) that involves the way SCF orbitals respond to various perturbations. This issue is dealt in the next section.

1.14.2 Response of Molecular Orbitals And The Issue of " Symmetry Breaking ’’

The second order change in total SCF energy with respect to any external perturbation χ can be written as

$$\frac{\partial^2 E}{\partial\chi\partial\lambda} = \langle\psi|\frac{\partial^2 H}{\partial\chi\partial\lambda}|\psi\rangle + 2\sum_k \frac{\langle\psi|\frac{\partial H}{\partial\chi}|\psi_k\rangle\langle\psi_k|\frac{\partial H}{\partial\lambda}|\psi\rangle}{E - E_k} \tag{1.31}$$

The contribution from the first term depends upon the second-order behavior of the Hamiltonian operator and the unperturbed reference state wave function, while the

second term (which will be referred to as the ‘‘relaxation contribution’’ or ‘‘relaxation term’’ in the rest of the discussions) depends on the derivative of the wave function.

At the HF level of theory, the wave function is a single Slater determinant consists of molecular orbitals. Generally, these are obtained by linear combinations of atom-centered basis functions, and these ‘‘MO coefficients’’ are obtained by the self-consistent field procedure. The first-order change to the wave function is, therefore, governed by the first-order change in the MO coefficients. The derivatives of the MO coefficients are

$$\frac{\partial c_{\mu p}}{\partial \chi} = \sum_{q} U_{pq}^{\lambda} c_{\mu q} \tag{1.32}$$

where CPHF coefficients U_{ai}^{χ}, U_{ij}^{χ} and U_{ab}^{χ} can be written as

$$U_{ai}^{\chi} = \sum_{bj} \left(A^{-1}\right)_{ai,bj} b_{bj}^{\chi} \tag{1.33}$$

$$U_{ij}^{\chi} = -\frac{1}{2} S_{ij}^{\chi} \tag{1.34}$$

$$U_{ab}^{\chi} = -\frac{1}{2} S_{ab}^{\chi} \tag{1.35}$$

Where the perturbation-dependent b^{χ} represents the changes in the Hamiltonian and orthogonality constraint with the perturbation, S^{χ} is the derivative of the atomic orbital overlap matrix transformed into the molecular orbital representation, and the elements of the matrix A is given by

$$A_{ai,bj} = \left(\varepsilon_i - \varepsilon_a\right)\delta_{ij}\delta_{ab} + \left\langle ai \middle|\middle| bj \right\rangle \pm \left\langle ab \middle|\middle| ij \right\rangle \tag{1.36}$$

Where, the SCF eigen values are denoted by ε_a and δ_{pq} is the usual Kronecker delta. Obviously, the difference between occupied and virtual SCF eigen values offers only a crude approximation to the excitation energies found in the denominator of Equation (1.31), and these can never become degenerate in practice. However, since *A* is not a

diagonal matrix, the conditions under which it becomes singular are not associated with degeneracy in SCF eigen values. Rather, the quantities that play the role of excitation energies in determining the response of the molecular wave function are the eigen values of *A*. There remains an ambiguity about the sign of the third term in Equation (1.36). If the perturbation under consideration is real, the appropriate sign is plus. If, however, the perturbation is a formally imaginary quantity (such as a magnetic field), the sign changes to be negative. Now, for any arbitrary perturbation χ, which is simply a rotation that mixes occupied and virtual orbitals, and If the molecular orbitals satisfy the SCF equations, the first-order change in energy vanishes. In second order, the change is

$$\frac{\partial^2 E}{\partial \chi^2} - 2\sum_k \frac{\langle \psi | \frac{\partial H}{\partial \chi} | \psi_k \rangle \langle \psi_k | \frac{\partial H}{\partial \chi} | \psi \rangle}{E - E_k} \tag{1.37}$$

Where, the sum is taken for convenience over the diagonal representation of orbital rotations described by *A,* and the denominators are the corresponding eigen values. Now, the presence of a single negative eigen value means that it is possible to obtain a lower-energy solution by an appropriate rotation of the molecular orbitals. Now, when these negative eigen values occur, it is assumed that one has a so-called Hartree-Fock instability. If the associated orbital rotation is not totally symmetric, there exists a lower-lying solution to the SCF equations in which the symmetry properties of the overall wave function are corrupted. However, there are cases where the orbital rotation is totally symmetric; although very rare, when present, there is a lower-energy solution that maintains the same spatial symmetry properties as $|\psi_0\rangle$.

The force constants and other second-order properties calculated for molecules at the SCF level contain terms that are roughly correspond to the two contributions in Eq (1.31), except the fact that it is the eigen values of A, rather than true excitation energies, which determine the magnitude of the relaxation term. If none of the eigen values of *A* are too small in magnitude, then the presence of an SCF instability does not have disastrous

consequences for the results. Therefore, it is not the presence of wave-function instabilities that poses problems for the calculation of molecular properties, but rather the presence of near-instabilities [61]. It is entirely possible to obtain quite satisfactory results with a highly unstable SCF solution, and also at the same time to obtain completely absurd results with a stable solution. The important issue is the magnitude of the smallest eigen value of the A matrix, irrespective of the sign [73].

Surprising things can occur when electron correlation is included [74]. In any correlation method, short of a FCI treatment, the total energy is dependent upon the choice of orbitals. Therefore, the properties calculated as second derivatives also involve contributions from the relaxation of the molecular orbitals. For methods like CC theory, which show relatively strong invariance of the total energy to the orbital changes, the effects are rather minimal and tend to be conspicuous if and only if the orbital relaxation is very strong. Specifically, the problems happen in regions of the potential energy surface where eigen values of *A* are very small in magnitude.

Another problem is that the sign of anomalous property values calculated at correlated levels does not give any information about the sign of the corresponding small *A* matrix eigen value. As the total energy is not stationary with respect to orbital rotations, it is possible to show [74] that the properties blow up quadratically with the reciprocal eigen value rather, than linearly. Therefore, if the magnitude of a second-order property is plotted as a function of a geometrical coordinate, it will blow up to plus or minus infinity on both sides of the point, where A is precisely singular. For methods that are highly sensitive to orbital choice (perturbation theory, especially the popular MBPT(2) variant), the presence of the singularity can cause serious problems for the calculation of second-order properties even far from where they actually diverge. As mentioned by Stanton and Gauss [71] in their excellent review article, that the total energy that corresponds to a symmetry-broken reference function is generally higher than that calculated from the symmetry-constrained function, exactly the opposite of the relative SCF energy ordering,

and therefore, properties typically diverge to large positive values on both sides of the singularity.

There can be ‘symmetry-breaking’’ effects in molecules, even, where there is no symmetry and the same fundamental problem that causes the instability does not lead to a wave function having lower symmetry. Essentially, the reason behind the fact that the SCF calculations often give symmetry-broken solutions at lower energies than constrained solutions is that in many symmetric open-shell molecules (NO_2, LiO_2, and others) the broken symmetry solution allows the unpaired electron spin to be almost entirely located on a single atomic center [63]. This increases the exchange contribution to the energy and, therefore, decreases the total energy. However, the similar unphysical localization phenomenon can also occur in molecules where the localization does not break the framework molecular symmetry. This is a major problem in calculations on open-shell molecules. If one has appropriate elements of symmetry, then unphysical solutions can be avoided by enforcing the symmetry constraints on the wave function. Even when the constraints are not enforced, problems with the reference function are easily identifiable from the markers like nonzero dipole moments along directions where the exact value must vanish by symmetry, unsymmetrical spin densities, and so on. However, the issue is more treacherous in lower-symmetry species where localization does not break the framework’s molecular symmetry. In that cases, UHF and ROHF solutions can be quite unphysical. However, it is considerably more difficult to diagnosis the problem, especially with ROHF, since it is necessarily an eigen function of the S^2 operator and might be impossible to prevent. Therefore, the term ‘‘symmetry-breaking’’ applies to a larger class of problems than just those to which the name literally applies [61].

1.14.3 The Pseudo-Jahn-Teller Effect

In the previous section, strongly changing wave functions and abnormally large relaxation contributions to molecular second-order properties were discussed. However, these effects can also occur in other circumstances, namely where the spectrum of the exact electronic Hamiltonian has a quasi-degeneracy. The so called "artificial'' and ''real'' effects should be distinguished in the sense that the former are those arising from problems associated with the reference function, while the ''real'' effects are those due to true nearby states. When there is a strong coupling with a nearby state, force constants can be profoundly affected, and otherwise symmetric molecules assume non-rigid behavior and might even adopt equilibrium geometries with lower symmetry [75, 76]. This is known as a second-order or pseudo-Jahn-Teller (PJT) effect [77]. It is an important topic in the study of open-shell molecules, electron transfer, and a number of other issues in physical chemistry.

The SCF calculations cannot account for these effects unless by sheer chance eigen values of the *A* matrix are close to the exact excitation energies, that they vanish where there is a true degeneracy of states. It is interesting to note the behavior of the perturbation theories. The MBPT(2) and its higher-order derivatives are intrinsically unable to describe this behavior irrespective of order the perturbation used [78, 79]. The reason lies in the fact that the only additional parameters that come into play in the MBPT wave-function expansion are those associated with denominators formed from differences of orbital energies. In practice, these never vanish, and the only poles that occur in property calculations are those that are already found at the SCF level of theory. The exact poles, which reflect the true spectrum of the Hamiltonian, can never be observed in calculations based on perturbation theory, and one can formulate a rather persuasive argument that the SCF may be superior to MBPT for studying PJT effects. At the very least, poles that occur at the SCF level are of the proper first-order behavior, even though the energy differences on which the properties depend on are clearly only crude approximations to the excitation energies. However, the high sensitivity of the

MBPT(2) energy to orbital rotations and the second-order nature of instability poles at correlated methods generally mean that the domain of nuclear configuration space affected by the singularity will be much larger than at the SCF level. Accordingly, the chance of obtaining an anomalous result is greater

Coupled cluster calculations represent a qualitative improvement over perturbation theory in treating PJT effects. The principal difference between CC and MBPT in this context is that the CC wave function involves an additional nontrivial set of parameters, specifically the T amplitudes. It can be shown [78] that force constants in CC theory can be written as

$$\begin{aligned}\frac{\partial^2 E}{\partial \chi^2} &= \langle \psi_{CC}^{\not 0} | \frac{\partial^2 H}{\partial \chi^2} | \psi_{CC} \rangle \\ &-2\sum_k \frac{\langle \psi_{CC}^{\not 0} | \frac{\partial H}{\partial \chi} | \psi_{EOM}^k \rangle \langle \psi_{EOM}^{\not k} | \frac{\partial H}{\partial \chi} | \psi_{CC} \rangle}{E_k - E} \\ &+\langle 0 | L\bar{H} | q \rangle \langle q | \frac{\partial T}{\partial \chi} \frac{\partial T}{\partial \chi} | 0 \rangle\end{aligned} \tag{1.38}$$

In the equation above, the symbol q designates determinants that lie outside the principal projection space used in the CC equations (Equation 1.29) —that is, triples, quadruples, and so on, for CCSD. It should be noted that the first two terms strongly resemble those in the exact expression (Equation 1.31). In fact, to the extent that the right and left CC wave functions approximate the exact wave function, and its Hermitian conjugate and that the excited states of the system are represented by the EOM approximation, these terms correspond precisely to the exact quantum-mechanical result. However, there is an additional term, which spoils the fundamental description of PJT effects within coupled-cluster theory and needs special attention.

This last term in equation, which vanishes in the FCI limit, depends quadratically on the derivative of the T amplitudes, which in turn diverge when another state in the EOM-CC spectrum becomes degenerate with the state of interest. Hence, the force constant blows

up quadratically in the immediate vicinity of the state crossing, which sometimes may lead to disastrous results. Moreover, as the direction of the second-order contribution is given by $\langle 0|L\bar{H}|q\rangle$ and it may go in both directions. Fortunately, the residue of the second-order contribution can be shown to vanish in the limit of a pure single excitation process [78]. Since most excited states of interest are dominated largely by single excitation character, the region of the potential surface strongly affected by the second term is small. The relaxation term that depends on the EOM excited states, however, has an appropriate magnitude and sign. So, standard CC methods represent a qualitative improvement over MBPT. Therefore, at distances relatively far from the crossing, the sign and magnitude of the relaxation effect on the force constant (or other second-order properties) is generally fairly accurate. In this context, it should be emphasized [61] that the equilibrium geometry of most open-shell molecules is generally not close to adiabatic surface crossings, even though they might experience a PJT effect that is not negligible. In these cases, SRCC methods can provide reliable results, as seen in a number of examples in the literature [80, 81]. However, in the vicinity of qausi-degenerate surfaces SRCC methods show drastic failure, which becomes difficult to rectify within the framework of single-reference CC.

1.15 Need for A Multi-reference Description

The most obvious way to avoid the above-mentioned problems associated with the single-reference treatment of open shell molecules, is to go for a multi-reference description of the wave function. The starting wave function for a multi-reference method is given by the determinantal expansion

$$|\psi\rangle = \sum_i C_i |\phi_i\rangle \tag{1.39}$$

where, the coefficients C_i and the orbitals in ϕ_i are simultaneously optimized [82]. If the sum is carried over the full space of n electron determinants, the method is equivalent to FCI, but for practical applications, one need to truncate at finite order. In general, the ‘‘most important’’ configurations must be included in the expansion, the identification of which is usually not obvious a priori and is the source of ambiguity in all multi-reference *ab-initio* methods. The orbitals are generally partitioned into active and inactive spaces, the former including either the entire valence region or some appropriately chosen subset and the corresponding virtual levels. Determinants representing all possible occupation schemes within this active space are then included in the equation. (1.39). Such calculations go by various names, including fully optimized reaction space and complete active space self-consistent field (FORS-SCF [83] and CASSCF [84]) method. These are special cases of the multi-configurational SCF (MCSCF), a label that can be applied to any calculation that uses a fully optimized wave function of the form given by equation. (1.39). The plus point of MCSCF calculations is that they are well-suited to handle cases in which more than one configuration makes a substantial contribution to the wave function. The nature of the wave-function parameterization guarantees a balanced treatment of these determinants, unlike single-determinant CI, PT, and CC methods in which an inherent bias exists toward a specific determinant. Despite an effective treatment of non-dynamical electron correlation, MCSCF calculations carried out in feasible active spaces do not produce quantitatively reliable results. The reason for this is the neglect of dynamical electron correlation involving the inactive occupied and virtual orbitals. Qualitatively, the effects of anti-bonding orbitals are typically exaggerated in MCSCF calculations, with the result that force constants are usually too small and bond lengths too long. A variety of methods has been described in the literature as a tool for including the residual correlation effects. Most straightforward of these is CI, in which these effects are treated by matrix diagonalization. If used in conjunction with large active spaces, these ‘‘MRCI’’ calculations are extremely accurate [85] and are even used to generate benchmark values for calibrating the performance of other methods. However, a sufficiently large basis set and active space needed for reasonable results hike

the computational cost to an unmanageable value. The cost of MRCI calculations (like MCSCF itself) increases exponentially with the size of the system, which limits its applicability beyond small molecules. Another serious limitation to all MRCI calculations is that they suffer from a size-consistency error. However, this can be treated by *ad hoc* corrections or, preferably, in a self-consistent fashion by methods such as ‘‘averaged coupled pair functional’’ (MR-ACPF) [86] or ‘‘approximate quadratic coupled cluster ’’ (MR-AQCC) [87]. While the domain of applicability is limited due to their expensive nature, highly accurate results can be achieved in these calculations.

Another way of including the residual correlation effects beyond the MCSCF level is by means of perturbation theory. Indeed, if the size of the active space is large, it follows that the amount of correlation not already treated in zeroth order is small, and it is sensible to appeal to perturbation theory. Several variants of second-order perturbation theory have been reported in the literature [88], however, the most popular is the CASPT2 method [89]. Many of the applications of CASPT2 have focused on excited states of closed-shell molecules and bi-radical systems that are of considerable interest in organic chemistry. Although, CASPT2 is not a size-consistent method [90], but the practical importance of this shortcoming is not very clear at this time. However, in applications to large molecules that necessarily involve small active spaces, the suitability of using second-order perturbation theory to treat residual correlation effects is called into question. Hence, the advantages of CASPT2 relative to a more elaborate treatment based on MRCI are vastly reduced in these cases.

The most systematic way to include a balanced description of dynamic and non-dynamic correlation is through multi-reference coupled cluster methods. The next subsection gives a brief overview of it.

1.16 Multi-reference Coupled Cluster Method

In contrast to the SRCC theory, which mainly evolved from its correspondence with the single-reference MBPT, the evolution of multi-reference coupled-cluster (MRCC) theories has been more or less independent of the underlying perturbative structure. An MRCC theory is obtained by finding an exponentially parameterized ansatz for the wave-operator Ω , and formulating a scheme for unambiguous determination of these parameters. The motivation for an exponential parameterization comes from the possibility of obtaining size-extensive results, along with the usual high accuracy stemming from partial infinite-order summation nature of CC theory.

Unlike in SRCC methods, where there is only one way to parameterize, several possibilities open up for the multi-reference case. However, they can be classified into two broad categories: the first one describes a specific root, known as the state-specific MRCC and other is the multi root description by effective Hamiltonian approach.

Various approaches are available for describing the state-specific MRCC ansatz, such as Brillouin-Wigner (BW) MRCC ansatz [91, 92], the state-specific ansatz suggested by Mukherjee and co-workers (MK-MRCC) [93-95], exponential multi-reference wave function ansatz (MRexpT) [94-97] and internally contracted multi-reference coupled cluster ansatz (ic-MRCC) [64,98].

On the other hand, effective Hamiltonian based theories are subdivided into two basic subclasses: Hilbert space (HS) approach and Fock Space (FS) approach. In both the approaches, energies are obtained by diagonalization of the effective Hamiltonian defined within a pre-chosen model space, and both approaches are fully size extensive. The HS-MRCC approach [99, 100] uses a state universal operator with different cluster operators for each determinants in the model space. The FS-MRCC approach, on the other hand, uses common vacuum and a valence universal wave operator, which correlates model space with the virtual space. The HSMRCC method is more suitable for the calculation of potential energy surface. On the other hand, the FSMRCC method is more suitable for

direct difference of energy calculation such as ionization potential, electron affinity, and excitation energies. In this thesis, we are mainly going to focus on FSMRCC.

1.17 Effective Hamiltonian Formulation of FSMRCC Theory

The FSMRCC is based on the concept [101,102] of a common vacuum, which is generally, but not necessarily, an N electron closed shell Hartree-Fock determinant. The holes and the particles are defined with respect to this common vacuum. These holes and particles are further classified into active and inactive ones. The model space is then constructed by a linear combination of suitably chosen (based on energetic criteria) active configurations. Thus, a model space for a (p,h) valence Fock space, which includes h active hole and p active particle, can be written as

$$\left|\psi_{(\mathrm{O})\mu}^{(p,h)}\right\rangle = \sum_{i} C_{i\mu}^{(p,h)} \left|\phi_{i}^{(p,h)}\right\rangle \tag{1.40}$$

The principal idea of effective Hamiltonian theory is to extract some selective eigen values of Hamiltonian from the whole eigen value spectrum. To fulfill the purpose, the configuration space is partitioned into model space and orthogonal space. When all possible resulting configurations, generated by distributing the valance electrons among all the valance orbitals in all possible ways are included in the model space, it is referred to as complete model space (CMS). An incomplete model space (IMS) results when only a subset of these configurations is included. The projection operator for model space is defined as

$$P_{M}^{(p,h)} = \sum_{i} \left|\Phi_{i}^{(p,h)}\right\rangle \left\langle\Phi_{i}^{(p.h)}\right| \tag{1.41}$$

The projection operator in the orthogonal space, i.e. the virtual space, is defined as

$$Q_M = 1 - P_M \tag{1.42}$$

The diagonalization of the effective Hamiltonian takes care of the non-dynamic correlation coming from the interactions of the model space configurations. Whereas, the dynamic correlation arises due to the interactions of the model-space configurations with the virtual space configurations. This interaction is introduced through valence universal wave operator Ω, which is parameterized such that it generates the exact wave function by acting on the model space. To generate the exact states for the (p,h) valence system, the wave operator must be able to generate all the valid excitations from the model space. The valence universal wave operator Ω has the form

$$\Omega = \left\{ e^{\mathcal{S}^{(p,h)}} \right\} \tag{1.43}$$

Where, the curly braces indicate normal ordering of the cluster operators, and $\mathcal{S}^{(p,h)}$ is defined as following

$$\mathcal{S}^{(p,h)} = \sum_{k=0}^{p} \sum_{l=0}^{h} \hat{S}^{(k,l)} \tag{1.44}$$

The cluster operator $\mathcal{S}^{(k,l)}$ is capable of destroying exactly k active particles and l active holes, in addition to creation of holes and particles. The $\mathcal{S}^{(p,h)}$ subsumes all lower sector Fock space $\mathcal{S}^{(k,l)}$ operators. The $\mathcal{S}^{(0,0)}$ is equivalent to standard single-reference coupled cluster amplitudes.

The Schrödinger equation for the manifold of quasi-degenerate states can be written as

$$\hat{H} \left| \Psi_i^{(p,h)} \right\rangle = E_i \left| \Psi_i^{(p,h)} \right\rangle \tag{1.45}$$

The correlated μ^{th} wave function in MRCC formalism can be written as

$$\left|\Psi_{\mu}^{(p,h)}\right\rangle = \Omega\left|\Psi_{(0)\mu}^{(p,h)}\right\rangle \tag{1.46}$$

From the equation (1.40) we get

$$\hat{H}\Omega\left(\sum_i C_{i\mu}^{(p,h)}\phi_i^{(p,h)}\right) = E_\mu\Omega\left(\sum_i C_{i\mu}^{(p,h)}\phi_i^{(p,h)}\right) \tag{1.47}$$

The effective Hamiltonian for (p,h) valence system can be defined as

$$\sum_j\left(\hat{H}_{eff}^{(p,h)}\right)_{ij} C_{j\mu} = E_\mu C_{i\mu} \tag{1.48}$$

where

$$\left(\hat{H}_{eff}^{(p,h)}\right)_{ij} = \left\langle\phi_i^{(p,h)}\left|\Omega^{-1}\hat{H}\Omega\right|\phi_j^{(p,h)}\right\rangle \tag{1.49}$$

Equation (1.49) can be written as

$$\hat{H}_{eff} = P_M^{(p,h)}\Omega^{-1}\hat{H}\Omega P_M^{(p,h)} \tag{1.50}$$

However, the Ω^{-1} may not be well defined in all the cases [102]. Therefore, the above definition of effective Hamiltonian is seldom used. Instead, the Bloch-Lindgren approach is generally used for solving the equations. The Bloch equation is just a modified form of Schrödinger equation.

$$\hat{H}\Omega P_M = \Omega\hat{H}_{eff}P_M \tag{1.51}$$

The Bloch-Lindgren approach eliminates the requirement of Ω^{-1} for the solution of effective Hamiltonian.

The Bloch projection approach to solve the equation involves left projection of equation (1.51) with P and Q, leading to

$$P_M^{(k,l)}\left[\hat{H}\Omega - \Omega\hat{H}_{eff}\right]P_M^{(k,l)} = 0 \tag{1.52}$$

$$Q_M^{(k,l)}\left[\hat{H}\Omega - \Omega\hat{H}_{eff}\right]P_M^{(k,l)} = 0 \tag{1.53}$$

$;\forall k = 0,.....p; l = 0,.....h$

To solve the equations, an additional normalization is imposed through parameterization of Ω. In case of CMS, this is generally performed by imposing the intermediate normalization condition $P_M \Omega P_M = P_M$. However, the situation is little bit different in case of incomplete model space. Mukherjee[103] has shown that in case of incomplete model space, the valence universality of the wave operator is sufficient to guarantee linked-cluster theorem; however, one need to relax the intermediate normalization. Pal *et. al* [104] have shown that for the special case of quasi-complete model space in (1,1) sector, the intermediate normalization can be used without any loss of generality.

In general, the equations for Ω and H_{eff} are coupled to each other through Equation. (1.52) and (1.53) and H_{eff} cannot be expressed explicitly in terms of Ω. However, when intermediate normalization is imposed, H_{eff} can directly be written as a function of Ω. In this case, the equation (1.52) can be written as

$$P_M^{(p,h)}\hat{H}\Omega P_M^{(p,h)} = P_M^{(p,h)}\hat{H}_{eff}^{(p,h)}P_M^{(p,h)} \tag{1.54}$$

After solving the equations for Ω and H_{eff}, The diagonalization of the effective Hamiltonian within the P space gives the energies of the corresponding states and the left and the right eigen vectors.

$$\hat{H}_{eff}^{(p,h)}C^{(p,h)} = C^{(p,h)}E \tag{1.55}$$

$$\tilde{C}^{(p,h)}\hat{H}_{eff}^{(p,h)} = E\tilde{C}^{(p,h)} \tag{1.56}$$

$$\tilde{C}^{(p,h)}C^{(p,h)} = C^{(p,h)}\tilde{C}^{(p,h)} = 1 \tag{1.57}$$

The contractions amongst different cluster operators within the exponential are avoided due to the normal ordering, leading to partial hierarchical decoupling of cluster equations, i.e. ones the amplitude equations of a particular sector of Fock space is solved, it appears as a known parameter in the equations for the higher sectors of Fock space. This is commonly referred to as sub-system embedding condition (SEC). The lower valence cluster equations are decoupled from the higher valence cluster equations, because of the SEC. Hence, the Bloch equations are solved progressively from the lowest valence (0, 0) sector upwards up to (p, h) valence sector.

1.18 Intermediate Hamiltonian Formulation of FSMRCC Theory

In this thesis, we follow the approach used by Meissener [105] to describe the intermediate Hamiltonian formulation of FSMRCC. The H_{eff} is defined in the P space, with a dimension much smaller (say m) than the actual Hamiltonian. The diagonalization of the effective Hamiltonian produces m eigenvalues, which are equal to a subset of the eigen values of the exact Hamiltonian $\hat{H}$. When the model space configurations (P) are not energetically well separated from those of complementary space (Q) that results in a very small or negative energy denominator in the iterative solution procedure leading to divergence or severe convergence problem. It is known as intruder state problem and is a common difficulty associated with all multi-root theories. They are particularly common in complete model space treatments because such spaces include high-energy multiple excitation model spaces, which contribute very little to the wave functions, but required for the completeness of the model space.

The intermediate Hamiltonian (IH) approach overcomes the intruder state problem by introducing a buffer space between the model space and rest of the Q space. Basically, in the IH formulation, the configuration space is divided into three subspaces, namely, main,

intermediate, and outer space (see Figure 1.1) with the projection operators P_M, P_I, and Q_0, respectively [7, 106]. The main space of IH formulation is the same as the model space of effective Hamiltonian theory, while the intermediate space (P_I) has been obtained from a subpart of the complementary space (Q_M) of the effective Hamiltonian theory, by further dividing it into two parts: the intermediate space and the outer space. The diagonalization of the intermediate Hamiltonian provides the eigen values, a subset of which corresponds to those obtained through effective Hamiltonian theory. The remaining eigen values are essentially arbitrary.

Because of the arbitrariness of the extra solution by IH approach, the intermediate Hamiltonian and its determining equations are not unique.

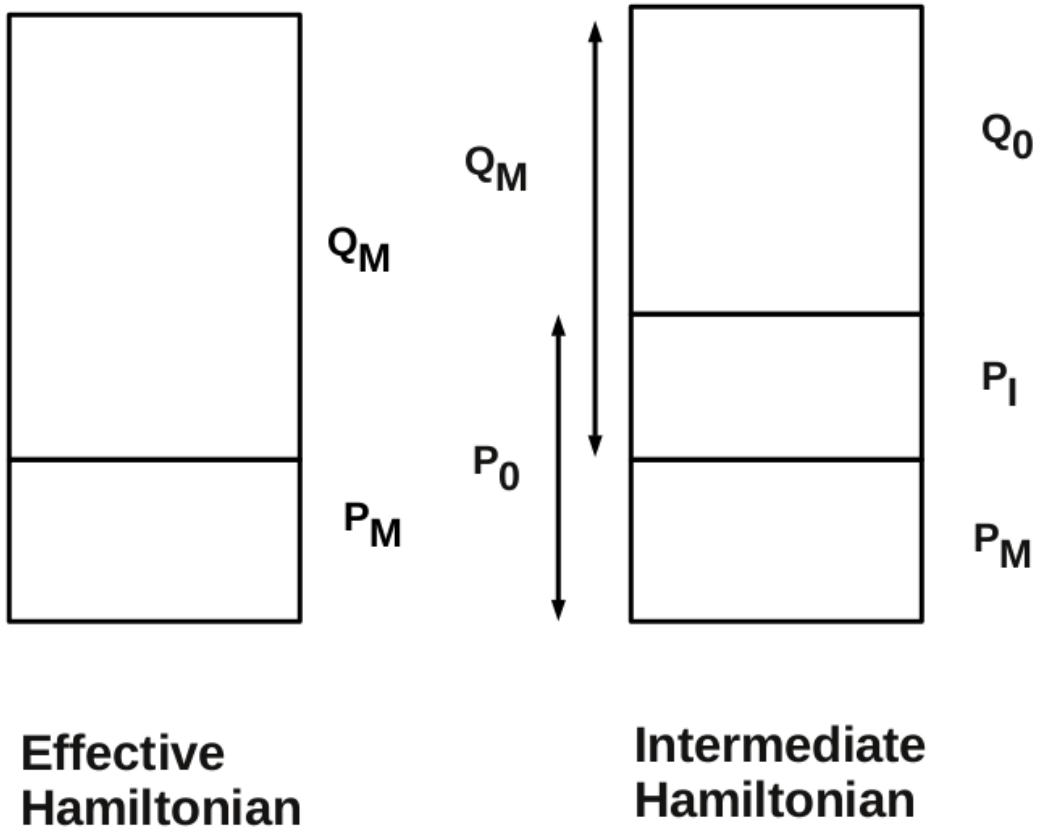

Figure 1.1 : Model space of effective and intermediate Hamiltonian

Different variants of intermediate Hamiltonian approach, employing different auxiliary condition for the definition of intermediate Hamiltonian [105, 107, 108] have been proposed and applied in the context of FSMRCC. The similarity transformation approach[105] by Meissner is particularly convenient among them. In this formulation, the final working equation of FSMRCC can be rewritten a

$$P_I^{(p,h)}\left(\bar{H}\left\{e^{-S}\right\}-\left\{e^{-S}\right\}H_{eff}^{(p,h)}\right)P_M^{(p,h)} \tag{1.58}$$

$$\hat{H}_{eff}^{(p,h)}=P_M^{(p,h)}\bar{H}\left\{e^{S}\right\}P_M^{(p,h)} \tag{1.59}$$

Let us define a new operator

$$\hat{X}=\left\{e^{S}-1\right\}P_M \tag{1.60}$$

For, which

$$\hat{X}=Q_M\hat{X}P_M \tag{1.61}$$

and

$$\hat{X}^2=0 \tag{1.62}$$

Now, equation (1.58) and (1.59) can be written in terms of $\hat{X}$ as

$$P_I^{(p,h)}\left(1-\hat{X}\right)\bar{H}\left(1+X\right)P_M^{(p,h)}=0 \tag{1.63}$$

$$P_M^{(p,h)}\left(1-\hat{X}\right)\bar{H}\left(1+\hat{X}\right)P_M^{(p,h)}=\hat{H}_{eff}^{(p,h)} \tag{1.64}$$

Equation (1.63) is a quadratic equation in $\hat{X}$, therefore, has multiple solutions. This procedure also suffers from the convergence difficulties caused by the intruder state problem. In the IH formulation, these difficulties can be averted, by splitting the similarity transformation described in equation (1.63), as follows

$$\left(1-\hat{X}\right)\bar{H}\left(1+\hat{X}\right)=\left(1-\hat{Z}\right)\left(1-\hat{Y}\right)\bar{H}\left(1+\hat{Z}\right)\left(1+\hat{Y}\right) \tag{1.65}$$

Where

$$\hat{X}=\hat{Y}+\hat{Z} \tag{1.66}$$

$$\begin{aligned}&\hat{Y}=Q_0\hat{X}P_M,\\&\hat{Z}=P_I\hat{X}P_M\end{aligned} \tag{1.67}$$

and

$$P_0=P_M+P_I \tag{1.68}$$

$$Q_M=P_I+Q_0 \tag{1.69}$$

From the definition of $\hat{X}$, $\hat{Y}$ and $\hat{Z}$

$$\begin{aligned}&\left(1-\hat{X}\right)=\left(1+\hat{X}\right)^{-1},\\&\left(1-\hat{Y}\right)=\left(1+\hat{Y}\right)^{-1}\\&and\\&\left(1-\hat{Z}\right)=\left(1+\hat{Z}\right)^{-1}\end{aligned} \tag{1.70}$$

From the above relation, it is clear that if the equation (1.63) is satisfied, then the m number of roots can be extracted equivalently both from diagonalization of $\left(1-\hat{X}\right)\bar{H}\left(1+\hat{X}\right)$ or $\left(1-\hat{Y}\right)\bar{H}\left(1+\hat{Y}\right)$ operator within the P_0 to P_0 space, as both operators are related to each other by a similarity transformation with respect to a third operator (1+Z).

Now the intermediate Hamiltonian is defined as,

$$\hat{H}_I^{(p,h)}=P_0^{(p,h)}\left(1-Y\right)\bar{H}\left(1+Y\right)P_0^{(p,h)} \tag{1.71}$$

As, P_M , P_I and Q_0 are projection operators of mutually orthogonal spaces, the intermediate Hamiltonian in equation (1.71) can be expressed as

$$\hat{H}_I^{(p,h)} = P_0^{(p,h)} \bar{H} \left(1 + \hat{Y}\right) P_0^{(p,h)} = P_0^{(p,h)} \bar{H} P_0^{(p,h)} + P_0^{(p,h)} \bar{H} \hat{Y} P_M^{(p,h)} \tag{1.72}$$

Now, for solving the above equation, we assume that equations for (0,0) sector, which is essentially the standard closed shell single-reference cluster equations, have already been solved.

Now, for (1,0) and (0,1) sectors of Fock space

$$\begin{aligned} Y^{(0,1)} &= Y^{(1,0)} = 0 \\ Y^{(1,0)} &= Y^{(1,0)} = 0 \\ X^{(1,0)} &= Z^{(1,0)} = S^{(1,0)} \end{aligned} \tag{1.73}$$

For, (1,1) sector of Fock space

$$X^{(1,1)} = Y^{(1,1)} + Z^{(1,1)} \tag{1.74}$$

$$Y^{(1,1)} = Q_0^{(1,1)} \left\{ S_2^{(0,1)} + S_2^{(1,0)} + S_1^{(0,1)} S_2^{(1,0)} + S_1^{(1,0)} S_2^{(0,1)} + S_2^{(0,1)} S_2^{(1,0)} \right\} P_M^{(1,1)} \tag{1.75}$$

and

$$Z^{(1,1)} = P_I^{(1,1)} \left\{ S_1^{(0,1)} + S_1^{(1,0)} + S_1^{(0,1)} S_1^{(1,0)} + S_2^{(1,1)} \right\} P_M^{(1,1)} \tag{1.76}$$

The intermediate Hamiltonian for (0,1) and (1,0) sector can be written as

$$H_I^{(0,1)} = P_0^{(0,1)} \bar{H} P_0^{(0,1)} \tag{1.77}$$

and

$$H_I^{(1,0)} = P_0^{(1,0)} \bar{H} P_0^{(1,0)} \tag{1.78}$$

Now the eigen value problem for (0,1) and (1,0) sector can be solved by diagonalization of $\bar{H}$ within the space spanned by 1h, 2h1p and 1p, 2p1h determinants, respectively. Hence, the IHFSCC approach for one valence problem is independent of choice of active space and becomes identical with IP/EA-EOMCC approach [109, 110] However, for the solution of higher sectors, the cluster amplitudes for (0,1) and (1,0) are explicitly required. Therefore, it becomes essential to define the model space by choosing a subset of total no of holes and particles as active, which is generally, but not necessarily near the Fermi level.

The cluster amplitudes for the one valence sector can be obtained [105, 107] by imposing the intermediate normalization condition on the selectively chosen eigen vectors corresponding to active holes and particles.

Now the intermediate Hamiltonian for (1,1) sector is defined as

$$H_I^{(1,1)} = P_0^{(1,1)} \bar{H} P_0^{(1,1)} + P_0^{(1,1)} \bar{H} Y^{(1,1)} P_M^{(1,1)} \tag{1.79}$$

From the equation (1.79), it can be seen that the intermediate Hamiltonian for the (1,1) sector of Fock space can be constructed by the matrix representation of H_I within 1h1p space. As the expression for $Y^{(1,1)}$ does not contain $S^{(1,1)}$, the solution of the eigen value problem for (1,1) sector in IH framework, only requires the knowledge of lower sector amplitudes. However, $S^{(1,1)}$ can be determined by putting the intermediate normalization on the selectively chosen eigen vectors, analogous to that in one valence problem. Very recently Pal and coworkers [109] have extended the idea for calculation of properties in (1,1) sector, within the IH framework.

In this IH formulation of FSMRCC, the equations are not solved in a coupled iterative manner. Rather, the eigenvalue problem is solved through diagonalization procedure. This leads to easier convergence, even with a large active space, which not only helps one to obtain more no of states, but also systematically improves the correlation effects in case of (1,1) sector.

However, the active space dependency of results beyond one valence problem keeps IH-FSMCC short of a complete "black box" method. Although, some markers like "percentage active component" is available as a diagnosis for the quality of the chosen active space, it still requires substantial involvement from the part of the user. On the other hand, the equation of motion coupled cluster provides a "black box" way to approach different sectors of Fock within the frame work of single-reference coupled cluster method.

1.19 Equation of Motion Coupled Cluster Method

The equation of motion coupled cluster (EOM-CC) method [110] is a single-reference approach, where the excited state wave function is generated by the action of a linear CI like operator on the correlated reference state wave function.

The Schrödinger equation for the reference state and the exited state (can be electron attached or ionized state also) can be described by

$$\hat{H}\Psi_0 = E_0\Psi_0 \tag{1.80}$$

$$\hat{H}\Psi_k = E_k\Psi_k \tag{1.81}$$

The excited state wave function Ψ_k is related to the reference state wave function by

$$\Psi_k = \hat{\Omega}_k\Psi_0 \tag{1.82}$$

Left multiplying equation 1.80 with $\hat{\Omega}_k$ and subtracting from equation 1.81, we get

$$\left[\hat{H},\hat{\Omega}\right]\Psi_0 = \omega_k\Omega_k\Psi_0 \tag{1.83}$$

Where $\omega_k = E_k - E_0$

The form of Ω_k defines the particular EOM method corresponding to the target state.

For Ionization problem

$$\Omega_k^{IP} = \sum_i R_i(k) i + \sum_{i>j,a} R_{ij}^a(k) \hat{a}^\dagger \hat{j}\hat{i} + ... \tag{1.84}$$

For electron affinity problem

$$\Omega_k^{EA} = \sum_a R^a(k) \hat{a}^\dagger + \sum_{a>b,j} R_j^{ba}(k) \hat{b}^\dagger \hat{j} \hat{a}^\dagger + ... \tag{1.85}$$

For excitation energy problem

$$\Omega_k^{EE} = R_0(k) + \sum_{i,a} R_i^a(k) \hat{a}^\dagger i + \sum_{a>b,i>j} R_{ij}^{ab}(k) \hat{a}^\dagger \hat{b}^\dagger ij + ... \tag{1.86}$$

Now, this is a general EOM framework. The coupled cluster theory is introduced by generating the correlated wave function by action of an exponential operator on a Slater determinant, which is generally, but not necessarily a Hartree-Fock determinant.

$$\Psi_0 = e^{\hat{T}} \left| \Phi_0 \right\rangle \tag{1.87}$$

Where, $\hat{T} = \hat{T}_1 + \hat{T}_2 + ...$ and $\hat{T}_1 = \sum_{ia} t_i^a \left\{ a_a^\dagger a_i \right\}$, $\hat{T}_2 = \frac{1}{4} \sum_{ijab} t_{ij}^{ab} \left\{ a_a^\dagger a_b^\dagger a_j a_i \right\}$ .....

Since, $\hat{\Omega}$ and $\hat{T}$ commute among themselves, we can write equation 1.83 as

$$\left[\bar{H}, \hat{\Omega} \right] \Phi_0 = \left(\bar{H} \hat{\Omega} \right)_c = \omega_k \hat{\Omega}_k \Phi_0 \tag{1.88}$$

Where, $\bar{H} = e^{-\hat{T}} H e^{\hat{T}}$, and c denotes the connectedness of $\bar{H}$ and $\hat{\Omega}$

Since $\bar{H}$ is non Hermitian, there exist different right (R) and left (L) eigenvectors which are biorthogonal and can be normalized to satisfy

$$L_k R_l = \delta_{kl} \tag{1.89}$$

The EOMCC approach has been extensively used to calculate energy [110, 111], structure [80, 112, 113] and properties [114] of radicals and excited states.

1.20 The Equivalence of Fock Space Multi-reference Coupled Cluster Method and Equation of Motions Coupled Cluster Method for One Valence Problem

It is possible to show that for IP and EA problem, the EOM-CC method is equivalent to (0,1) and (1,0) sector of Fock space [7]. Let consider an ionized state dominated by removal of an electron from hole state. The EOM-IP-CC ansatz for this state

$$\left|\psi_k\right\rangle = \Omega_k e^{\hat{T}} \left|\phi_0\right\rangle \tag{1.90}$$

and Ω_k has the form as given by equation (1.84) . The equation (1.90) takes advantage of the commutation of $\hat{T}$ and Ω_k .

In case of FSMRCC, the ansatz is

$$\left|\psi_k\right\rangle = \left\{e^{\hat{S}^{(0,1)}}\right\}\left|\phi_k\right\rangle = \left(1+\hat{S}^{(0,1)}\right)\left|\phi_k\right\rangle \tag{1.91}$$

Where, $\left|\phi_k\right\rangle = \hat{k}\left|\phi_0\right\rangle$ is one-vacant-hole-state model determinant and the effective Hamiltonian matrix is

$$H_{eff}^{(0,1)} = \left\langle \psi^{(0,1)} \middle| \hat{H}_{eff} \middle| \psi^{(0,1)} \right\rangle = \left\langle \psi^{(0,1)} \middle| \hat{H}\left(1+\hat{S}^{(0,1)}\right) \middle| \psi^{(0,1)} \right\rangle \tag{1.92}$$

Now, because $\left(\hat{S}^{(0,1)}\right)^2 \hat{P}^{(0,1)} = 0$, $\left|\phi^{(0,1)}\right\rangle$ a row vector of the one-vacant-active-hole determinant and $\left\langle\phi^{(0,1)}\right|$ is its adjoint column vector. The main difference between the matrix (1.92) and the IP-EOM-CCSD matrix implicit in (1.88) is that the latter has a dimension of one-hole single and double excitations while the former has the smaller dimension n_h of just the one-vacant-active-hole determinants. Thus we expect to have a matrix partitioning relating the two matrices.

Now

$$\langle \phi_i | R_i \hat{i} | \phi_0 \rangle = R_i \tag{1.93}$$

$$\langle \phi_{ij}^a | R_{ij}^a \{ \hat{a}^\dagger \hat{j} \hat{i} \} | \phi_0 \rangle = R_{ij}^a \tag{1.94}$$

Now, using Lowdin's partitioning technique, the EOMIP-CCSD for kth hole state can be written as

$$\begin{pmatrix} \langle \phi^{(0,1)} | H | \phi^{(0,1)} \rangle & \langle \phi^{(0,1)} | H | \phi^{(1,2)} \rangle \\ \langle \phi^{(1,2)} | H | \phi^{(0,1)} \rangle & \langle \phi^{(1,2)} | H | \phi^{(1,2)} \rangle \end{pmatrix}_C \begin{pmatrix} R^{(0,1)} \\ R^{(1,2)} \end{pmatrix} = \begin{pmatrix} R^{(0,1)} \\ R^{(1,2)} \end{pmatrix} \omega_k \tag{1.95}$$

Where, ω_k is the ionization energy of hole state k. Normally, if we use sector designators such as (0, 1) and (1, 2) in EOM-CC, then they would refer to all orbitals since there is no separation between active and inactive orbitals in this model. Specifically, $|\phi^{(0,1)}\rangle$ and $|\phi^{(1,2)}\rangle$ are row vectors consisting of all determinants of types ϕ_i and ϕ_{ij}^a, respectively; to bring out the analogy between EOM-CC and FSMRCC, we may designate a subset of orbitals as active and restrict the sector definitions to this subset. Also, $R^{(1,0)}$ and $R^{(1,2)}$ are column vectors consisting of elements of types R_i and R_{ij}^a, respectively.

Separating, the equation for R_k gives

$$\sum_i \langle \phi_k | H | \phi_i \rangle R_i + \sum_{ija} \langle \phi_k | H | \phi_{ij}^a \rangle R_{ij}^a = R_k \omega_k \tag{1.96}$$

Multiplying on the right by R_k^{-1}, we have

$$\langle \phi_k | H | \phi_k \rangle + \sum_{i \neq k} \langle \phi_k | H | \phi_i \rangle R_i R_k^{-1} + \sum_{ija} \langle \phi_k | H | \phi_{ij}^a \rangle R_{ij}^a R_k^{-1} = \omega_k \tag{1.97}$$

For the remaining equations, we define the vectors

$$\left|\phi\right\rangle = \left|\phi^{(0,1)\prime}\phi^{(1,2)}\right\rangle \tag{1.98}$$

$$R = \begin{pmatrix} R^{(0,1)'} \\ R^{(1,2)} \end{pmatrix} \tag{1.99}$$

and the adjoint column vector $\langle\phi|$.

The prime on (0, 1) indicates the omission of ϕ_k and R_k . These equations now take the form

$$\langle\phi|H|\phi_k\rangle + \langle\phi|H|\phi\rangle R R_k^{-1} = R\omega_k R_k^{-1} \tag{2.00}$$

From equation (1.92) , however,

$$\langle\phi_k|H_{eff}|\phi_k\rangle = \langle\phi_k|H\left(1+\hat{S}^{(0,1)}\right)|\phi_k\rangle \tag{2.01}$$

Identifying $\langle\phi_k|\hat{H}_{eff}|\phi_k\rangle$ with ω_k (which it equals when H_{eff} is diagonalized) and $\hat{S}^{(0,1)}$ with $\langle\phi|\hat{S}^{(0,1)}\left|\phi^{(0,1)}\right\rangle = R R_k^{-1}$, we regain the FSMRCC H_{eff}. Further, the FSMRCC equation becomes

$$\langle\phi|H\left|\phi^{(0,1)}\right\rangle + \left(\hat{S}^{(0,1)} - \hat{S}^{(0,1)}H_{eff}\right) = 0 \tag{2.02}$$

With minor medications we can identify any number of orbitals as active, treating active hole states similarly to state m. It does not matter which orbitals are actually active. Each principal ionization potential for any orbital in IP-EOM-CC can be obtained and, unlike a true multi-reference theory, expanding the number of active orbitals does not provide any better an approximation [7].

Similarly, it can be shown that for principal peak EOMEA-CC is equivalent to (1,0) sector of Fock space.

In an alternative viewpoint, it can be said that EOMCC for IP and EA problem is the FSMRCC in the intermediate Hamiltonian formulation. For the rest of the thesis, we are going to use EOMCC and FSMRCC interchangeably for one valence problem of Fock space.

1.21 Scope and Objective of The Thesis

As mentioned earlier, the standard SRCC method shows drastic failures for high-energy open shell molecules, whereas, MRCC and EOMCC methods provide an efficient way to overcome the problem. In this thesis, we have studied the high-energy radical reactions prevailing in the stratosphere using FSMRCC and EOMCC methods. However, the standard EOMCC, as well as FSMRCC methods, in singles and doubles approximation scales as N^6 and has a very high storage requirement that prohibits its use beyond small molecules. Therefore, as a part of this thesis, we have also tried to develop approximations to EOMCC with smaller storage requirement and lower scaling. These methods can be applied to larger systems, without sacrificing much on its accuracy.

The present thesis is organized as follows. In chapter 2, we have investigated the NO_x catalyzed pathway of stratospheric ozone depletion, using the coupled cluster method. In chapter 3, we have discussed the potential stability of peroxo nitrate radical. In chapter 4, the suitability of EOMIP-CCSD(2) approximation for studying geometry and IR frequencies of problematic doublet radicals has been investigated. In chapter 5, we have presented a new N^5 scaling and low storage requiring method for studying electron affinity, within the framework of EOMCC method. The chapter 6 is devoted to the implementation of a lower scaling approximation to single and double spin flip EOMCC

method. In chapter 7, we have discussed the shortcomings of EOMIP-CCSD(2) approximation for calculation of ionization potential. The chapter 8 presents a new method which overcomes the limitations of EOM-IP-CCSD(2) approximation.

References:

1. Löwdin, P. O. In *Advances in Chemical Physics*; John Wiley & Sons, Inc.: 2007, p 207-322.
2. Fetter, A. L.; Walecka, J. D. *Quantum theory of many-particle systems*; Courier Dover Publications, 2003.
3. Lowdin, P. O. *Int. J. Quantum Chem.* **1968**, *2*, 867-931.
4. Oksuz, I.; Sinanoglu, O. *Phys. Rev.* **1969**, *181*, 42.
5. Roos, B. O.; Siegbahn, P. E. M.; Schaefer III, H. F., Ed.; Plenum: New York, 1977; Vol. 3, p 277.
6. Shavitt, I. In *Methods of electronic structure theory*; Schaefer III, H. F., Ed.; Springer: 1977, p 189-275.
7. Shavitt, I.; Bartlett, R. J. *Many-body methods in chemistry and physics: MBPT and coupled-cluster theory*; Cambridge University Press, 2009.
8. Szabo, A.; Ostlund, N. S.; MacMillan Pub. Inc., New York: 1982.
9. Westhaus, P.; Sinanoglu, O. *Phys. Rev.* **1969**, *183*, 56.
10. Fock, V. *Zeitschrift fur Physik* **1930**, *61*, 126-148.
11. Hartree, D. R. *Math. Proc. Cambridge.* **1928**, *24*, 89-110.
12. Slater, J. C. *Phys. Rev.* **1930**, *35*, 210-211.
13. Roothaan, C. C. J. *Rev. Mod. Phys.* **1951**, *23*, 69.
14. Roothaan, C. C. J. *Rev. Mod. Phys.* **1960**, *32*, 179-185.
15. Goddard III, W. A. *Phys. Rev.* **1967**, *157*, 73.
16. Freed, K. F. *Ann. Rev. Phys. Chem.* **1971**, *22*, 313-346.
17. Paldus, J. In *New Horizons of Quantum Chemistry*; Springer: 1983, p 31-60.
18. Bartlett, R. J.; Dykstra, C. E.; Paldus, J. *Coupled-cluster methods for molecular calculations*; Springer, 1984.
19. Linderberg, J.; Ohrn, Y. *Second Quantization Based Methods in Quantum Chemistry* **1981**.

20. Kaldor, U. *Phys. Rev.* **1968**, *176*, 19.

21. Kaldor, U.; Schaefer, H. F.; Harris, F. E. *Int. J. Quantum Chem.* **1968**, *2*, 13-20.

22. Pople, J. A.; Binkley, J. S.; Seeger, R. *Int. J. Quantum Chem.* **1976**, *10*, 1-19.

23. Bartlett, R. J. *Ann. Rev. Phys. Chem.* **1981**, *32*, 359-401.

24. Mukherjee, D.; Pal, S. *Adv. Quant. Chem* **1989**, *20*, 291.

25. Chaudhary, R.; Mukherjee, D.; Prasad, M. D. *Lecture notes in chemistry* **1989**, *50*, 3.

26. Primas, H. *Modern Quantum Chemistry: Action of light and organic crystals*; Academic Press, 1965; Vol. 2.

27. Sinanoğlu, O. *J. Chem. Phys.* **1962**, *36*, 706-717.

28. Urban, M.; Noga, J.; Kello, V. *Theor. Chem. Acc.* **1983**, *62*, 549-562.

29. Raimes, S. *Many-electron theory*; North-Holland Amsterdam, 1972.

30. Manne, R. *Int. J. Quantum Chem.* **1977**, *12*, 175-192.

31. Lindgren, I.; Morrison, J. *Atomic many-body theory*; Springer, 1986.

32. Harris, F. E.; Monkhorst, H. J.; Freeman, D. L.; Oxford University Press, New York: 1992.

33. Kucharski, S. A.; Bartlett, R. J. *Adv. Quant. Chem* **1986**, *18*, 281-344.

34. Brueckner, K. A. *Phys. Rev.* **1955**, *97*, 1353-1366.

35. Goldstone, J. *Proc. R. Soc. A* **1957**, *239*, 267-279.

36. Kelly, H. P. *Phys. Rev.* **1963**, *131*, 684.

37. Sinanoğlu, O. In *Adv. Chem. Phys.*; John Wiley & Sons, Inc.: 1964, p 315-412.

38. Nesbet, R. K. In *Adv. Chem. Phys*; John Wiley & Sons, Inc.: 1965, p 321-363.

39. Freed, K. F. *Phys. Rev.* **1968**, *173*, 24-33.

40. Robb, M. A. In *Computational techniques in quantum chemistry and molecular physics*; Springer: 1975, p 435-503.

41. Kutzelnigg, W. In *Methods of Electronic Structure Theory*; Schaefer, H., III, Ed.; Springer US: 1977; Vol. 3, p 129-188.

42. Hurley, A. C. *Electron correlation in small molecules*; Academic Press New York, 1976.

43. Meyer, W. *Int. J. Quantum Chem.* **1971**, *5*, 341-348.

44. Ahlrichs, R.; Lischka, H.; Staemmler, V.; Kutzelnigg, W. *J. Chem. Phys.* **1975**, *62*, 1225-1234.

45. Ahlrichs, R. *Comput. Phys. Commun.* **1979**, *17*, 31-45.

46. Čížek, J. *J. Chem. Phys.* **1966**, *45*, 4256-4266.

47. Čížek, J. In *Advances in Chemical Physics*; John Wiley & Sons, Inc.: 1969, p 35-89.

48. Čižek, J.; Paldus, J. *Int. J. Quantum Chem.* **1971**, *5*, 359-379.

49. Bartlett, R. J.; Purvis, G. D. *Int. J. Quantum Chem.* **1978**, *14*, 561-581.

50. Pople, J. A.; Krishnan, R.; Schlegel, H. B.; Binkley, J. S. *Int. J. Quantum Chem.* **1978**, *14*, 545-560.

51. Raghavachari, K.; Trucks, G. W.; Pople, J. A.; Head-Gordon, M. *Chem. Phys. Lett.* **1989**, *157*, 479-483.

52. Noga, J.; Bartlett, R. J. *J. Chem. Phys.* **1987**, *86*, 7041-7050.

53. Kucharski, S. A.; Bartlett, R. J. *J. Chem. Phys.* **1992**, *97*, 4282-4288.

54. Pal, S.; Prasad, M.; Mukherjee, D. *Pramana* **1982**, *18*, 261-270.

55. Pal, S.; Durga Prasad, M.; Mukherjee, D. *Theor. Chem. Acc.* **1983**, *62*, 523.

56. Bartlett, R. J.; Noga, J. *Chem. Phys. Lett.* **1988**, *150*, 29-36.

57. Bartlett, R. J.; Kucharski, S. A.; Noga, J. *Chem. Phys. Lett.* **1989**, *155*, 133-140.

58. Arponen, J. S.; Bishop, R. F.; Pajanne, E. *Phys. Rev. A* **1987**, *36*, 2539-2549.

59. Arponen, J. S.; Bishop, R. F.; Pajanne, E. *Phys. Rev. A* **1987**, *36*, 2519-2538.

60. Vaval, N.; Pal, S. *Phys. Rev. A* **1996**, *54*, 250-258.

61. Stanton, J. F.; Gauss, J. In *Advances in Chemical Physics*; John Wiley & Sons, Inc.: 2003, p 101-146.

62. Andrews, J. S.; Jayatilaka, D.; Bone, R. G. A.; Handy, N. C.; Amos, R. D. *Chem. Phys. Lett.* **1991**, *183*, 423-431.

63. Davidson, E. R.; Borden, W. T. *J. Phys. Chem.* **1983**, *87*, 4783-4790.

64. Cizek, J.; Paldus, J. *J. Chem. Phys.* **1967**, *47*, 3976-3985.

65. Thouless, D. J. *The Quantum Mechanics Of Many-Body Systems*; Academic: New York, 1961.

66. Lund, A.; Shiotani, M.; Bally, T. In *Radical Ionic Systems*; Springer Netherlands: 1991; Vol. 6, p 3-54.

67. Bordon, W. T. *Encyclopedia of computational chemistry*; John Wiley & Sons, 1998.

68. Pople, J. A.; Nesbet, R. K. *J. Chem. Phys.* **1954**, *22*, 571-572.

69. McWeeny, R.; Diercksen, G. *J. Chem. Phys.* **1968**, *49*, 4852-4856.

70. Davidson, E. R. *Chem. Phys. Lett.* **1973**, *21*, 565-567.

71. Stanton, J. F. *J. Chem. Phys.* **1994**, *101*, 371.

72. Schlegel, H. B. *J. Phys. Chem.* **1988**, *92*, 3075-3078.

73. Bartlett, R. J. In *Geometrical Derivatives of Energy Surfaces and Molecular Properties*; Jorgensen, P., Simons, J., Eds.; Springer Netherlands: 1986; Vol. 166, p 35-61.

74. Crawford, T. D.; Stanton, J. F.; Allen, W. D.; Schaefer, H. F. *J. Chem. Phys.* **1997**, *107*, 10626-10632.

75. Weaver, A.; Arnold, D. W.; Bradforth, S. E.; Neumark, D. M. *J. Chem. Phys.* **1991**, *94*, 1740-1751.

76. Stanton, J. F.; Gauss, J.; Bartlett, R. J. *J. Chem. Phys.* **1991**, *94*, 4084-4087.

77. Pearson, R. G. *Symmetry Rules for Chemical Reactions*; Wiley: New York, 1976.

78. Stanton, J. F. *J. Chem. Phys.* **2001**, *115*, 10382-10393.

79. Crawford, T. D.; Kraka, E.; Stanton, J. F.; Cremer, D. *J. Chem. Phys.* **2001**, *114*, 10638-10650.

80. Saeh, J. C.; Stanton, J. F. *J. Chem. Phys.* **1999**, *111*, 8275-8285.

81. Crawford, T. D.; Stanton, J. F. *J. Chem. Phys.* **2000**, *112*, 7873-7879.

82. Roos, B. O. *Advances in Chemical Physics, AB INITIO Methods in Quantum Chemistry II*; John Wiley & Sons, 1987; Vol. 67.

83. Ruedenberg, K.; Schmidt, M. W.; Gilbert, M. M.; Elbert, S. T. *Chem. Phys.* **1982**, *71*, 41-49.

84. Roos, B. O.; Taylor, P. R.; Siegbahn, P. E. M. *Chem. Phys.* **1980**, *48*, 157-173.

85. Lischka, H.; Shepard, R.; Pitzer, R. M.; Shavitt, I.; Dallos, M.; Muller, T.; Szalay, P. G.; Seth, M.; Kedziora, G. S.; Yabushita, S. *Phys. Chem. Chem. Phys.* **2001**, *3*, 664-673.

86. Gdanitz, R. J.; Ahlrichs, R. *Chem. Phys. Lett.* **1988**, *143*, 413-420.

87. Szalay, P. t. G.; Bartlett, R. J. *J. Chem. Phys.* **1995**, *103*, 3600-3612.

88. Hirao, K. *Recent advances in multireference methods*; World Scientific, 1999; Vol. 4.

89. Andersson, K.; Malmqvist, P. A.; Roos, B. r. O.; Sadlej, A. J.; Wolinski, K. *J. Phys. Chem.* **1990**, *94*, 5483-5488.

90. Helgaker, T.; Jorgensen, P.; Olsen, J. *Molecular electronic-structure theory*; Wiley, 2000.

91. Pittner, J.; Nachtigall, P.; Carsky, P.; Masik, J.; Hubac, I. *J. Chem. Phys.* **1999**, *110*, 10275-10282.

92. Masik, J.; Hubac, I. *Advances in quantum chemistry* **1998**, *31*, 75-104.

93. Mahapatra, U. S.; Datta, B.; Mukherjee, D. *Mol. Phys.* **1998**, *94*, 157-171.

94. Evangelista, F. A.; Simmonett, A. C.; Allen, W. D.; Schaefer, H. F.; Iii; Gauss, J. *J. Chem. Phys.* **2008**, *128*, 124104-13.

95. Evangelista, F. A.; Allen, W. D.; Schaefer, H. F.; Iii *J. Chem. Phys.* **2007**, *127*, 024102-17.

96. Hanrath, M. *J. Chem. Phys.* **2008**, *128*, 154118-10.

97. Hanrath, M. *J. Chem. Phys.* **2005**, *123*, 084102-12.

98. Hanauer, M.; Kohn, A. *J. Chem. Phys.* **2012**, *134*, -.

99. Balkova, A.; Kucharski, S. A.; Meissner, L.; Bartlett, R. J. *J. Chem. Phys.* **1991**, *95*, 4311-4316.

100. Balkova, A.; Bartlett, R. J. *J. Chem. Phys.* **1994**, *101*, 8972-8987.

101. Pal, S. *Mol. Phys.* **2010**, *108*, 3033-3042.

102. Mukherjee, D.; Pal, S. In *Advances in Quantum Chemistry*; Per-Olov, L., Ed.; Academic Press: 1989; Vol. Volume 20, p 291-373.

103. Mukherjee, D. *Int. J. Quant. Chem.* **1986**, *30*, 409-435.

104. Pal, S.; Rittby, M.; Bartlett, R. J.; Sinha, D.; Mukherjee, D. *J. Chem. Phys.* **1988**, *88*, 4357-4366.

105. Meissner, L. *J. Chem. Phys.* **1998**, *108*, 9227-9235.

106. Malrieu, J. P.; Durand, P.; Daudey, J. P. *J. Phys. A* **1985**, *18*, 809.

107. Sinha, D.; Mukhopadhyay, S. K.; Chaudhuri, R.; Mukherjee, D. *Chem. Phys. Lett.* **1989**, *154*, 544-549.

108. Landau, A.; Eliav, E.; Kaldor, U. *Chem. Phys. Lett.* **1999**, *313*, 399-403.

109. Gupta, J.; Vaval, N.; Pal, S. *J. Chem. Phys.* **2013**, *139*, 074108.

110. Stanton, J. F.; Bartlett, R. J. *J. Chem. Phys.* **1993**, *98*, 7029-7039.

111. Nooijen, M.; Bartlett, R. J. *J. Chem. Phys.* **1995**, *102*, 3629-3647.

112. Stanton, J. F.; Gauss, J. *J. Chem. Phys.* **1994**, *101*, 8938-8944.

113. Stanton, J. F. *J. Chem. Phys.* **1993**, *99*, 8840-8847.

114. Kállay, M.; Gauss, J. *J. Chem. Phys.* **2004**, *121*, 9257-9269.

Chapter 2

NO_x Catalyzed Pathway of Stratospheric Ozone Depletion: A Coupled Cluster Investigation

"This earth is his, to him belong those vast and boundless Skies: Both seas within him rest, and yet that in small pool He lies "

ATHARVA VEDA

Block 4, Hymn 16

In this chapter, we report a theoretical investigation on the NO_x catalyzed pathways of stratospheric ozone depletion using highly accurate coupled cluster methods. These catalytic reactions present a great challenge to state-of-the-art ab initio methods, while their mechanisms remain unclear to both experimentalists and theoreticians. In this work, we have used the so-called "gold standard of quantum chemistry," the CCSD(T) method, to identify the saddle points on NOx-based reaction pathways of ozone hole formation. Energies of the saddle points are calculated using the multi-reference variants of coupled cluster methods. The calculated activation energies and rate constants show good agreement with available experimental results. Tropospheric precursors to stratospheric NO_x radicals have been identified, and their potential importance in stratospheric chemistry has been discussed. Our calculations resolve previous conflicts between ab initio and experimental results for a trans nitro peroxide intermediate, in the NOx catalyzed pathway of ozone depletion

2.1 Introduction:

The stratospheric ozone layer constitutes an important part of earth's atmosphere. It absorbs light of wavelengths below 240 nm and saves the planet earth and life on it from the lethal solar ultraviolet (UV) radiation. The past 50 years have seen a remarkable decrease in the concentration of the ozone layer. Thus, understanding the pathways of ozone depletion and its chemistry is of great importance for the prevention of it's decline (Figure 2.1).

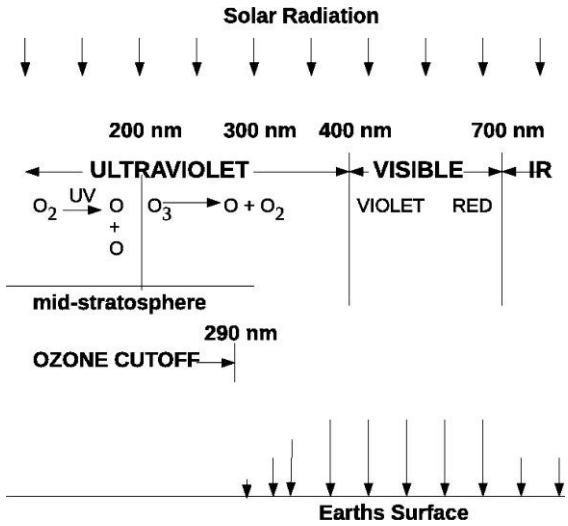

Figure2.1 : Atmospheric window for solar radiation

It is well established that the "ozone hole" forms over the Antarctic due to reactions of ClO with ozone in the Antarctic spring [1-4]. This occurs because the vortex is strong over the Antarctic (due to fewer land masses relative to the northern hemisphere) and thus long-lived, and also because all of the nitrogen compounds are frozen out on polar stratospheric clouds (PSC) in the winter, and these "fall" out of the stratosphere into the troposphere, thereby depleting the air in the vortex of nitrogen. This is important, because the main reservoir compound for Cl is $ClONO_2$. Hence, in the springtime, the existing Cl compounds in the Antarctic vortex (ClOOCl, ClOOH, HOCl, etc.) are photolyzed and begin to react catalytically to destroy ozone, which continues to occur until the vortex breaks up.

The possibility of stratospheric ozone depletion via the NO_x catalyzed pathway was first postulated by Johnston[5] and supported by several model calculations [6-9].

$$NO + O_3 \rightarrow NO_2 + O_2 \quad (2.1)$$

$$NO_2 + O \rightarrow NO + O_2 \quad (2.2)$$

Knowledge of the mechanism and kinetic parameters of reactions 2.1 and 2.2 is therefore of crucial importance in order to calculate ozone profiles in the stratosphere and to make reliable models of atmospheric ozone phenomena. Not surprisingly, the NO_x catalyzed reactions became much studied experimentally over the years so as to determine the associated rate constants and unravel the mechanistic details [10-14]. In spite of the relative abundance of experimental work, theoretical studies of NO_x based reactions of ozone depletion are rather scarce in the literature. The reported theoretical works are mostly done at the DFT and MP2 levels [15-16], which is inadequate to account for the correlation effects in a systematic manner. Some of the papers report single point calculations at the CCSD [17] level, which takes care of the dynamic correlation in a satisfactory way. However, T1 diagnosis [18] indicates large multi-reference character of the species involved. Thus, it becomes necessary to handle non-dynamic correlation in a proper way, which single reference coupled cluster fails to do. A multi-reference coupled cluster (MRCC) [24,25] method can account for both dynamic and non-dynamic correlation in a systematic way. However, so far, no multi-reference coupled cluster study has been done on NO_x catalyzed reactions. The objective of the present study is to carry out *ab-initio* calculations of a sufficiently high level and to get accurate results for the study of the reaction of NO_x molecules with ozone in the context of stratospheric ozone depletion. We have used Fock space multi reference (FSMRCC) theory for our study. FSMRCC is an effective Hamiltonian based theory and is known to give accurate direct difference energies [19-21]. It treats both N and $N \pm 1$ states on an equal footing. This method has

been used extensively for difference energies and response properties of open-shell molecules and molecular excited states [27].

This chapter is organized as follows. The next section presents computational details. Results and discussion are followed in section 2.3. The last section presents the conclusions and a brief discussion about the scope of future work.

2.2 Methodology and Computational Details

We have optimized all of the structures using the ROHF-CCSD(T) method. There exist several variants of ROHF-CCSD(T). Specifically, we have used the variant developed by Bartlett and co-workers [26]. The aug-cc-pVTZ basis set[33] has been used for geometry optimization. For all subsequent calculations presented in the chapter, the same basis set has been used. Following the geometry optimization, the frequency calculations have been done to determine the nature of the saddle point. Table 2.1.1 and 2.1.2 present results of IR spectra and equilibrium geometry using different methods. It is clear from both the table that only CCSD(T) results can give experimental accuracy. So, it is justified to use the CCSD(T) level of methods for the investigation of reactions involving NO_x and ozone, rather than MP2 and DFT.

Further, Table 2.2 presents the T1 diagnosis[18] values of reactants, products, and saddle points. It shows values higher than the permissible range of 0.02 (see Table 2.2), indicating the multi-reference nature of the wave function. To include the multi-reference effects, the FSMRCC method has been used to carry out the single point energy calculations on the optimized saddle points. FSMRCC is a valence-universal variant of multi-reference coupled cluster theory, and it is size-extensive for both ground and excited states.

Table 2.1.1 : Comparison of Theoretical Calculated Frequency in the aug-cc-pVTZ Basis Set with Experimental Values for Ozone

Method	r_e (Å)	θ (deg)	ω_1 (cm^{-1})	ω_2 (cm^{-1})	ω_3 (cm^{-1})
DFT (B3LYP)	1.255	118.2	745	1188	1248
MP2	1.283	116.6	741	1157	2244
CCSD(T)	1.269	117.1	720	1062	1160
EXP	1.272[a]	116.82[a]	716[b]	1089[b]	1135[b]

a :see ref 36a

b :see ref 36b

Table 2.1.2 : Comparison of Theoretical Calculated Frequency in the aug-cc-pVTZ Basis Set with Experimental Values for Nitric Oxide

Method	r_e (Å)	ω (cm^{-1})
DFT (B3LYP)	1.255	745
MP2	1.283	741
CCSD(T)	1.269	720
EXP	1.272[a]	716[b]

a :see ref 36a

b :see ref 36b

Photo dissociation energies are calculated using the Equation Of Motion Coupled Cluster (EOMCC)[28] method. EOMCC is similar to FSMRCC and was successfully used by Bartlett and co-workers for the simulation of UV/vis

absorption spectra for atmospheric modeling [29].

Table 2.2 : T1 diagnosis values in aug-cc-pVTZ Basis Set

species	T1 value
O_3	0.029
NO_2	0.026
NO	0.040
N_2O	0.028
N_2O_2 TS1	0.022
N_2O_2 min	0.021
N_2O_2 TS2	0.022
ONOOO	0.039
ONOO	0.035

All of the rate constants presented in this chapter have been estimated from theoretically calculated barrier heights, using the Arrhenius equation. Pre-exponential factors are obtained from experimental data [43].

All of the ROHF-CCSD(T) calculations on NO_x catalyzed reactions have been performed using CFOUR [30]. Gaussian09[31] has been used for some exploratory MP2, DFT-B3LYP, T1 diagnosis, and EOMCC calculations. FSMRCC single point calculations have been done using codes developed by Pal and co-workers [32].

2.3 Results and Discussion

First, it is necessary to find out among all of the NO_x radicals generated in the troposphere, which are probable candidates for stratospheric ozone depletion.

2.3.1 Tropospheric Precursors

To become a potential threat to the stratospheric ozone layer, NO_x radicals produced in the troposphere must satisfy certain conditions. First, it must be transparent to radiation of $\lambda > 290$ nm, so that it is not destroyed by visible solar radiation in the troposphere. Moreover, the radicals must be sufficiently inert to reach the stratosphere in intact condition.

Excitation of NO_x radicals to higher electronic states by visible (400–700 nm) and UV (10–400 nm) light actually causes photo dissociation. We have used the EOMCC method on previously reported potential energy surface s[39] to calculate the corresponding excitation energies. Calculated wavelengths for all three species correspond to the highest absorption cross-section in experimental UV–visible absorption spectra of the species [34]. So, light of this particular wavelength's can be taken as the major responsible radiation for the photo dissociation of the species. Table 2.3 represents photo dissociation wavelengths and oscillator strengths of the precursor species. From Table 2.3, it can be seen that NO_2 will be destroyed within the troposphere by visible solar radiation. Now, both NO and N_2O are transparent to visible light. But, nitric oxide, being an odd-electron molecule, is highly reactive toward hydroperoxide and organic radicals [40-41]. Thus, finally, a negligible amount of nitric oxide enters the stratosphere. Our calculated values of photo dissociation energy are in good agreement with the experimental values.

Now, N_2O does not have a significant sink in the troposphere. Therefore, nitrous oxide is the major source of odd nitrogen (NO_x) in the stratosphere and plays a fundamental role in regulating the ozone layer [9,42].

Table 2.3 : EOMCCSD Calculated Photo dissociation Energy of the NO_x Radicals

radical	excited state	photodiss. energy (nm)	oscillator strength	Expt. photodiss. energy (nm)[a]
NO_2	$^2B_2$	376	0.0099	372–402[b]
NO	$^2B_2$	198	0.0014	190–202[c]
N_2O	$^2A_1$	176	0.0000	176–187[b]

a : in units of $10^{20}\sigma$ (cm^2).

b : see ref 34.

c: see ref 35.

2.3.2 Generation of NO

Nitric oxide is the main active species in the NO_x catalytic cycle of stratospheric ozone depletion. Tropospheric N_2O, after reaching the stratosphere, reacts with the present odd oxygen atom (^1D) to form NO. This nitric oxide enters into the catalytic ozone depletion cycle.

$$N_2O + O \rightarrow NO + NO \qquad (2.3)$$

Figure 2.2 gives a schematic description of the reaction. The first step of the reaction is the formation of a saddle point of order 1 (TS1). It has C_S symmetry and has an imaginary frequency of 431 cm^{-1} at the ROHF-CCSD(T) level of theory. The imaginary frequency corresponds to the vibration of normal modes along the reaction coordinate. The evolution of the saddle point is thus toward an ONNO intermediate with C_2 symmetry. This point has been characterized as a minimum (MINIMA), and it is the intermediate compound in the reaction, responsible for the generation of nitric oxide in the stratosphere.

From the MINIMA, nitric oxides are finally reached through a second transition state (TS2). This saddle point shows an imaginary frequency of 157 cm^{-1}. It shows very small perturbations of the geometrical parameter, compared to those of MINIMA, as expected from their small energy difference. Figure 2.2 shows the evolution from MINIMA to TS2 and from TS2 to products accompanies gradual shortening of the terminal N–O bonds and the consequent stretching of the N–N bond.

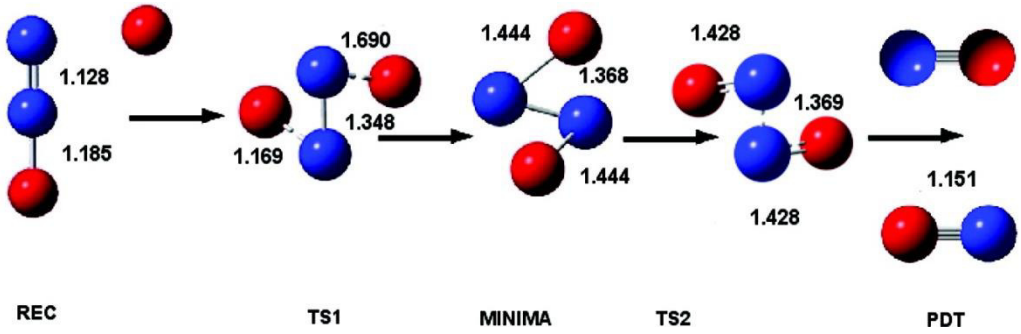

Figure 2.2 : Formation of NO from N_2O

We have plotted the energies of the reactants, products, and saddle points, calculated using the FSMRCC method, in an energy profile diagram (Figure 2.3). It shows a barrierless formation of the first transition state (TS1). It is 4.6 kcal/mol more stable than the reactants. There exists a minimum which is of 6.9 kcal/mol more stable than the TS1. The evolution from MINIMA to TS2 is the rate determining step in the reaction. The step shows a very low barrier height of 0.18 kcal/mol. This is expected from the very small perturbation of the geometrical parameter of TS2, compared to that of MINIMA. Table 2.4 shows that the calculated rate constant for the reaction is 4.9×10^{-11} cm^3 $molecule^{-1}$ S^{-1} at 298 K, which is very close to the experimental value of 6.7×10^{-11} cm^3 $molecule^{-1}$ S^{-1}) [43]. The value of the used prefactor is 6.7×10^{-11} cm^3 $molecule^{-1}$ S^{-1}.

Table 2.4 : Kinetic Parameter of the Reaction between N_2O and O

Parameter	Calculated	Experimental(43)
E_a(kcal/mol)	0.18	
k (cm^3 $molecule^{-1}$ S^{-1}) at 298 K	4.9×10^{-11}	6.7×10^{-11}

All of the saddle points considered above are of trans configuration. There may be a possibility of a cis pathway. But all cis conformers have been found to be of equal energy to the corresponding trans isomer.

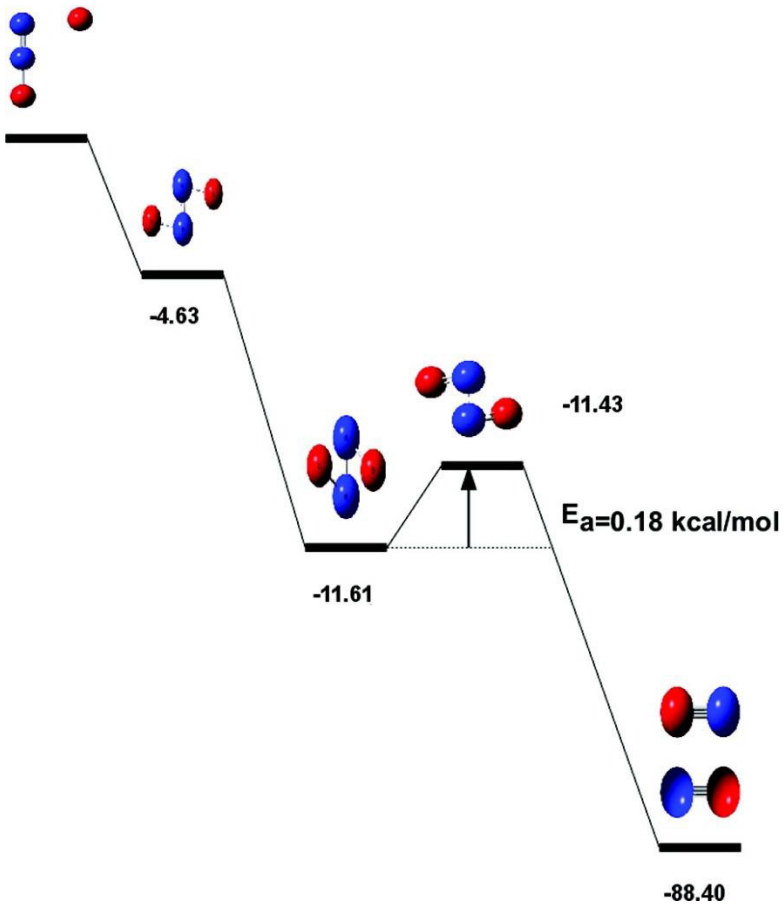

Figure 2.3 Energy profile diagram of the reaction between N_2O and O.

2.3.3 Beginning of the Catalytic Cycle

The nitric oxide generated from N_2O comes in contact with stratospheric ozone.

According to the previous theoretical work of Dupuis et. al.[44] for the H + O_3 reaction, the approach of the NO radical to the ozone molecule is determined by π orbitals of the terminal oxygen atom of ozone, as depicted in Figure 2.4.

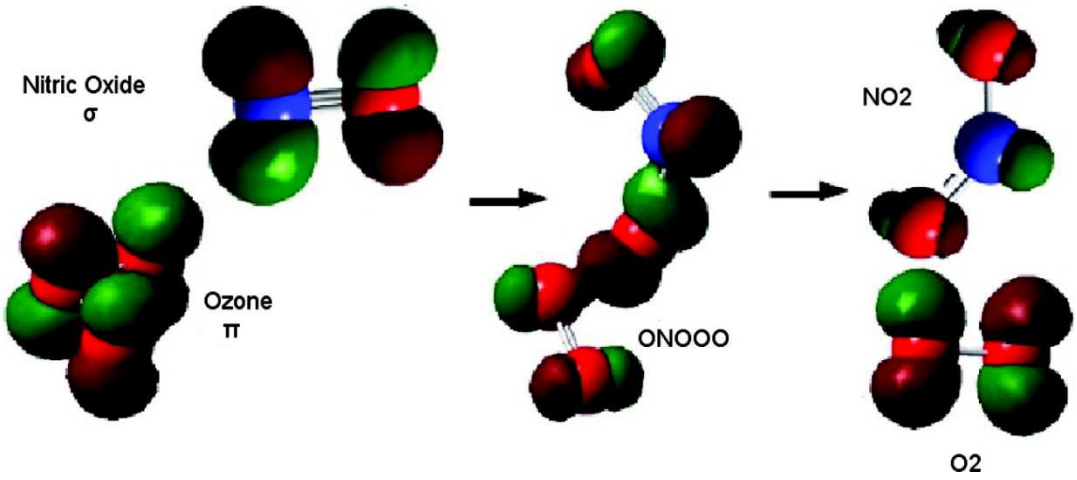

Figure 2.4 : MO diagram representation of the reaction between O_3 and NO

The first step of the reaction mechanism is the formation of a trans TS of C_1 symmetry. The imaginary frequency corresponding to the reaction coordinates is 292 cm^{-1}. Figure 2.5 shows that the formation of the TS involves stretching of one O–O bond of ozone, with subsequent formation of an O–N bond with nitric oxide. The TS then breaks down to nitric oxide and molecular oxygen. Table 2.5 reports the calculated value of activation energy and rate constants at the FSMRCC level of theory for the trans ONOOO transition state along with the experimental values. The activation energy for the reaction, calculated at the FSMRCC level, is 3.14 kcal/mol. With ZPE correction, the value comes down to 3.11 kcal/mol, which is well within the range of experimentally determined values between 1.44 and 3.18 kcal/mol (Figure 2.6) [45].

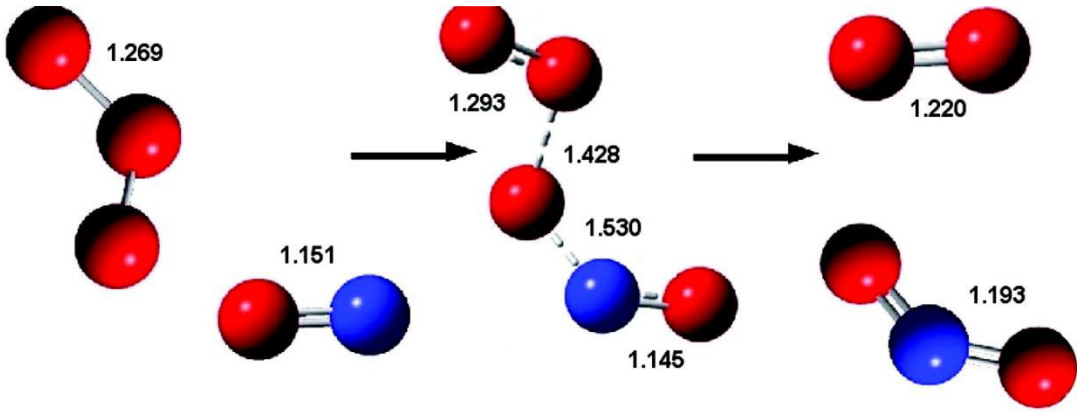

Figure 2.5: Trans pathway of the reaction between ozone and NO

Taking the standard prefactor (A) of 2×10^{-12}, the rate constant becomes 1.0×10^{-14} cm^3 $molecule^{-1}$ S^{-1}, at 298 K, which shows excellent agreement with the experimental value[43] of 1.8×10^{-14} cm^3 $molecule^{-1}$ S^{-1} (Table 2.5).

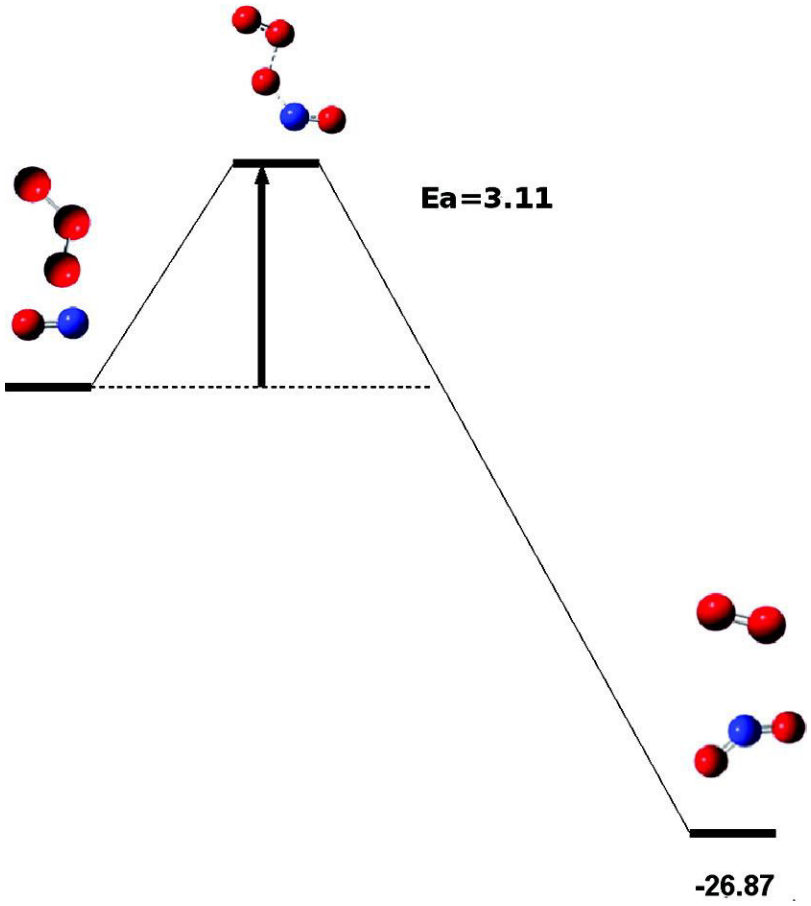

Figure 2.6 :Energy profile diagram of reaction between ozone and NO

It can be attributed to the high level of the method and the proper basis set being employed for the estimation of the barrier heights. However, there can always be a possibility of a fortuitous error cancellation leading to a better agreement.

Table 2.5 : Kinetic Parameter of the Reaction between NO and O_3 at 298 K

Parameter	**Calculated**	**Experimental**
E_a(kcal/mol)	3.11	1.4–3.18
k (cm^3 $molecule^{-1}$ S^{-1})	1.0×10^{-14}	1.8×10^{-14}

2.3.4 Regeneration of Nitric Oxide

The nitrogen dioxide molecule, thus formed, reacts with odd oxygen (O) to regenerate NO (Figure 2.7). The reaction involves the formation of a trans nitro-peroxide radical intermediate, which then undergoes photo dissociation to form two molecules of nitric oxide. Table 2.6 reports the EOMCC calculated photo dissociation energy and the corresponding experimental values. It can be seen that the wavelength of photo dissociation is 586 nm. This is well within the experimental range of 587 ± 4 nm [46]. The NO radical, thus regenerated, again reacts with another ozone molecule, and the catalytic depletion cycle continues.

Table 2.6 : EOMCCSD Calculated Photo dissociation Energy of the trans ONOO Radicals

Basis set	**Photo dissociation energy (nm)**	**Experimental (nm)[46]**
aug-cc-pVTZ	586	587 ± 4

However, there are controversies about the existence of the doublet trans peroxo nitrate intermediate in reality [47-48]. The only reliable experimental data come from an IR frequency study of a probable trans ONOO intermediate, by Hall and

Bhatia [14]. Their conclusion was based on the 50 cm^{-1} isotopic shift of an IR band at 1840 cm^{-1}. They have tried to further support their hypothesis using some limited *ab-initio* calculations [49] of structures and vibrational frequencies. However, their theoretically calculated results clearly deviate from experimental values.

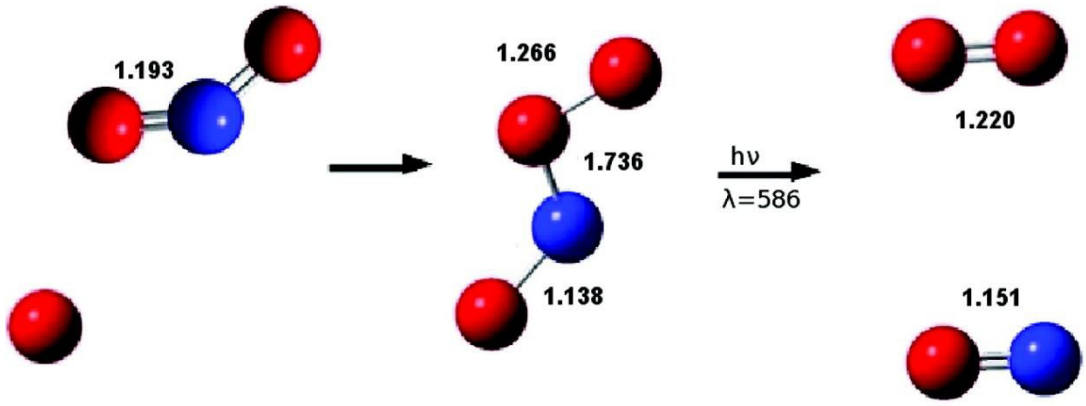

Figure 2.7 : Regeneration of nitric oxide from NO_2

When we revisited the problem with the highly correlated CCSD(T) method and the aug-cc-pVTZ basis set, we obtained a good agreement with experimental results. Table 2.7 reports the values of IR frequency, intensity, and isotropic shift calculated at the ROHF-CCSD(T) level of theory in the aug-cc-pVTZ basis set, along with the experimental results. Table 2.7 also presents the value of IR frequency and intensity calculated at the UHF level with a 6-31G* basis set. A close inspection of Table 2.7 shows that, with the UHF method, the IR peak nearest to the experimental value deviates by 181 wave number. Moreover, the mode is of very low intensity (6.5 $km \cdot mol^{-1}$). The only intense peak (100 $km \cdot mol^{-1}$) in the spectrum is at 975.5 cm^{-1}, which is nearly half of the experimental frequency. Therefore, these theoretical results are not at all consistent with experiments. The reason is the inadequacy of the theoretical method and small basis set. In the ROHF-CCSD(T) method with the aug-cc-pVTZ basis set, the

highest peak is at 1880 cm^{-1}, very close to the experimental value of 1840 cm^{-1}. Moreover this peak is of very high intensity (408 $km \cdot mol^{-1}$). This result is consistent with the experimental report of only one peak at 1840 cm^{-1}. Moreover, CCSD(T) calculation of the isotropic shift gives a value of −49 cm^{-1} for the highest peak, which is nearly identical to an experimental shift of −50 cm^{-1}. Thus, from the previous experimental data and our calculated results, it would be safe to conclude that a trans peroxo nitrate intermediate does get formed in the reaction between NO_2 and atomic oxygen.

Table 2.7 : Trans ONOO aug-cc-pVTZ IR Spectroscopy Results

Frequencies (ω), cm^{-1}	***I*^{IR}, $km \cdot mol^{-1}$**	**ω,[a] cm^{-1}**	**I^{IR},[a] $km \cdot mol^{-1}$**	**exptl freq cm^{-1}**	**Calc. iso shift, $km \cdot mol^{-1}$**	**Exp cm^{-1}**
123	1	207	1		–3	
198	1	469	1		–5	
271	3	671	13		–8	
719	3	976	100		–16	
1223	133	1287	14		–33	
1880	408	1659	7	1840	–49	–50

a : Values calculated by Hall et al. *J. Phys. Chem.* **1994**, *90*, 7414 at the UHF level with the 6-31G* basis set.

2.4 Conclusions:

In this chapter, the NO_x catalyzed pathway of stratospheric ozone depletion has been computationally investigated with the coupled cluster method. The

optimizations are performed at the ROHF-CCSD(T) level of theory in aug-cc-pVTZ basis set, while energetic of the reactions are investigated with the FSMRCC method in the same basis set

Our EOMCC calculations show that among several probable tropospheric precursor compounds, only nitrous oxide is photochemically inert enough to move through the troposphere to reach the stratosphere. In the stratosphere, it reacts with an odd oxygen atom (^1D) to form the active catalytic species nitric oxide. The reaction evolves through the formation of a four-membered reaction intermediate. Our calculations suggest that the breaking of the N–N bond of the intermediate is the rate-determining step of the reaction, which is consistent with the experimental value of the rate constant for the reaction.

The first step of the NO_x catalytic cycle is the reaction of NO with an ozone molecule to form NO_2 and O_2. The reaction proceeds through a five-membered transition state of trans configuration and shows a barrier height of 3.11 kcal/mol. This agrees perfectly with the experimental range of activation energy.

The regeneration of nitric oxide from NO_2 involves the formation of a trans peroxo nitrate intermediate. Our calculation resolves the previous conflict between theoretical calculations and experimental results. It has been shown that the compound gives an intense IR peak at 1880 cm^{-1}, which is consistent with the experimental results. Thus, theoretical calculations can not only predict but also supplement experimental findings.

Hence, high level theoretical studies can give a better understanding of the NO_x based pathways of stratospheric ozone depletion for both theoreticians and experimentalists. It would be interesting to extend by including the effect of non-dynamic correlation by doing a more extensive mapping of the PES in a MRCC

method. Furthermore, it would be interesting to study the other pathways of ozone depletion along with their inter-reactions. Such developments will be part of a planned systematic study of stratospheric ozone chemistry using a high level theoretical method.

References:

1. Molina, M. J.; Rowland, F. S. *Nature* **1974**, 249, 810– 814.
2. Crutzen, P. J. *Geophys. Res. Lett.* **1974**, 1, 205– 208.
3. Rowland, F. S. *Philos. Trans. R. Soc. London, Ser. B* **2006**, 361, 769– 790.
4. Solomon, S. *Rev. Geophys.* **1999**, 37, 275– 316.
5. Johnston, H. *Science* **1971**, 173, 517– 522
6. Chipperfield, M. P.; Feng, W. *Geophys. Res. Lett.* **2003**, 30, 1389– 1391.
7. Kinnison, D.; Johnston, H.; Wuebbles, D. *J. Geophys. Res.* **1988**, 93, 4165– 14176.
8. Randeniya, L. K.; Vohralik, P. F.; Plumb, I. C. *Geophys. Res. Lett.* **2002**, 29, 1051– 1054.
9. Ravishankara, A. R.; Daniel, J. S.; Portmann, R. W. **Science *2009***, 326, 123– 125.
10. Ghormley, J. A.; Ellsworth, R. L.; Hochanadel, C. J. *J. Phys. Chem.* **1973**, 77, 1341– 1345.
11. Davis, D. D.; Prusazcyk, J.; Dwyer, M.; Kim, P. *J. Phys. Chem.* **1974**, 75, 1775– 1779.
12. Graham, R. A.; Johnston, H. S. *J. Chem. Phys.* **1974**, 60, 4628– 4629.
13. Wu, C. H.; Morris, E. D., Jr.; Niki, H. *J. Phys. Chem*. **1973**, 77, 250– 2511.
14. Bhatia, S. C.; Hall, J. H., Jr. *J. Phys. Chem.* **1980**, 84, 3255– 3259.
15. Jaroszynska-Wolinska., J. *THEOCHEM* **2010**, 952, 74– 83.
16. Peiro-Garcia, J.; Nebot-Gil, I. *J. Comput. Chem*. **2003**, 47, 1657– 1663.
17. (a) Cizek, J. *J. Chem. Phys.* **1966**, 45, 4256– 4266.
    (b) Bartlett, R. J. *Annu. Rev. Phys. Chem.* **1981**, 32, 359– 402.
18. Lee, T. J.; Taylor, P. R. *Int. J. Quantum Chem*. **1989**, S23, 199– 207.
19. (a) Mukherjee, D. *Pramana* **1979**, 12, 203– 225.
    (b) Lindgren, I.; Mukherjee, D. *Phys. Rep.* **1987**, 151, 93– 127.
20. (a) Haque, A.; Kaldor, U. *Chem. Phys. Lett.* **1985**, 117, 347– 351.

(b) Haque, A.; Kaldor, U. *Chem. Phys. Lett.* **1985**, 120, 261– 265.

21. Stanton, J. F.; Bartlett, R. J.; Rittby, C. M. L *J. Chem. Phys*. **1992**, 97, 5560–5567.

22. (a) Scheiner, A. C.; Scuseria, G. E.; Rice, J. E.; Lee, T. J.; Schaefer, H. F. *J. Chem. Phys.* **1987**, 87, 5361– 5371.

(b) Fitzgerald, G.; Harrison, R. J.; Bartlett, R. J. *J. Chem. Phys.* **1986**, 85, 5143– 5150.

(c) Stanton., J. F.; Gauss., J. *J. Chem. Phys*. **1995**, 103, 1064– 1076.

23. (a) Salter, E.; Trucks, G.; Bartlett, R. J. *J. Chem. Phys.* **1989**, 90, 1752–1766.

(b) Helgaker, T.; Gauss, J.; Jørgensen, P.; Olsen, J. *J. Chem. Phys*. **1997**, 106, 6430– 6440.

24. (a) Banerjee, A.; Simons, J. *J. Chem. Phys.* **1982**, 76, 4548– 4559.

(b) Laidig, W. D.; Bartlett, R. *J. Chem. Phys. Lett.* **1984**, 104, 424– 430.

(c) Mukherjee, D.; Pal, S. *Adv. Quantum Chem*. **1989**, 20, 291– 373.

25. (a) Evangelista, F. A.; Allena, W. D.; Schaefer, H. F. *J. Chem. Phys.* **2007**, 127, 024102– 024117.

(b) Evangelista, F. A.; Simmonett, A. D.; Allen, W. D.; Schaefer, H. F.; Gauss, J. *J. Chem. Phys.* **2008**, 128, 124104– 124116.

26. (a) Gauss, J; Lauderdale, W. J.; Stanton, J. F.; Watts, J. D.; Bartlett, R. J. *Chem. Phys. Lett.* **1991**, 182, 207– 215.

(b) Watts, J. D.; Gauss, J.; Bartlett, R. J. *J. Chem. Phys.* **1993**, 98, 8718–8733.

27. (a) Pal, S.; Rittby, M.; Bartlett, R. J.; Sinha, D.; Mukherjee, D. *J. Chem. Phys.* **1988**, 88, 4357– 4366.

(b) Pal, S.; Rittby, M.; Bartlett, R. J.; Sinha, D.; Mukherjee, D. *Chem. Phys. Lett.* **1987**, 137, 273– 278.

(c) Rittby, M.; Pal, S.; Bartlett, R. J. *J. Chem. Phys.* **1989**, 90, 3214– 3220.

28. Stanton, J. F.; Bartlett, R. J. *J. Chem. Phys.* **1993**, 98, 7029– 7039.

29. Melnichuk, A.; Perera, A.; Bartlett, R. J. *Phys. Chem. Chem. Phys.* **2010**, 12,

9726– 9735.

30. CFOUR, coupled-cluster techniques for computational chemistry, a quantum-chemical program package by Stanton, J. F.; Gauss, J.; Harding, M. E.; Szalay, P. G., with contributions from Auer, A. A.; Bartlett, R. J.; Benedikt, U.; Berger, C.; Bernholdt, D. E.; Bomble, Y. J.; Cheng, L.; Christiansen, O.; Heckert, M.; Heun, O.; Huber, C.; Jagau, T.-C.; Jonsson, D.; Juselius, J.; Klein, K.; Lauderdale, W. J.; Matthews, D. A.; Metzroth, T.; ONeill, D. P.; Price, D. R.; Prochnow, E.; Ruud, K.; Schiffmann, F.; Schwalbach, W.; Stopkowicz, S.; Tajti, A.; Vazquez, J.; Wang, F.; Watts, J. D., and the integral packages MOLECULE (Almlof, J.; Taylor, P. R.), PROPS (Taylor, P. R.), ABACUS (Helgaker, T.; Jensen, H. J. Aa.; Jorgensen, P.; Olsen, J.), and ECP routines (Mitin, A. V.; van Wullen, C.) For the current version, see http://www.cfour.de.

31. Frisch, M. J.; Trucks, G. W.; Schlegel, H. B.; Scuseria, G. E.; Robb, M. A.; Cheeseman, J. R.; Scalmani, G.; Barone, V.; Mennucci, B.; Petersson, G. A.; Nakatsuji, H.; Caricato, M.; Li, X.; Hratchian, H. P.; Izmaylov, A. F.; Bloino, J.; Zheng, G.; Sonnenberg, J. L.; Hada, M.; Ehara, M.; Toyota, K.; Fukuda, R.; Hasegawa, J.; Ishida, M.; Nakajima, T.; Honda, Y.; Kitao, O.; Nakai, H.; Vreven, T.; Montgomery, J. A., Jr.; Peralta, J. E.; Ogliaro, F.; Bearpark, M.; Heyd, J. J.; Brothers, E.; Kudin, K. N.; Staroverov, V. N.; Kobayashi, R.; Normand, J.; Raghavachari, K.; Rendell, A.; Burant, J. C.; Iyengar, S. S.; Tomasi, J.; Cossi, M.; Rega, N.; Millam, N. J.; Klene, M.; Knox, J. E.; Cross, J. B.; Bakken, V.; Adamo, C.; Jaramillo, J.; Gomperts, R.; Stratmann, R. E.; Yazyev, O.; Austin, A. J.; Cammi, R.; Pomelli, C.; Ochterski, J. W.; Martin, R. L.; Morokuma, K.; Zakrzewski, V. G.; Voth, G. A.; Salvador, P.; Dannenberg, J. J.; Dapprich, S.; Daniels, A. D.; Farkas, A.; Foresman, J. B.; Ortiz, J. V.; Cioslowski, J.; Fox, D. J. Gaussian 09, revision A.1; Gaussian, Inc.: Wallingford, CT, 2009.

32. Vaval, N.; Ghose, K. B.; Pal, S.; Mukherjee, D. *Chem. Phys. Lett*. **1993**, 209, 292– 298.

33. Kendall, R. A.; Dunning, T. H.; Harrison, R. J. *J. Chem. Phys.* **1992**, 96,

6796– 6806.

34. Sander, S. P.; Abbatt, J.; Barker, J. R.; Burkholder, J. B.; Friedl, R. R.; Golden, D. M.; Huie, R. E.; Kolb, C. E.; Kurylo, M. J.; Moortgat, G. K.; Orkin, V. L.; Wine, P. H. *Chemical Kinetics and Photochemical Data for Use in Atmospheric Studies*, Evaluation No. 17, JPL Publication 10–6, Jet Propulsion Laboratory: Pasadena, CA, **2011**. http://jpldataeval.jpl.nasa.gov (accessed Mar. 2012) .

35. Thompson, B. A.; Harteck, P; Reeves, R. R. *J. Geophys. Res.* **1963**, 68, 6431– 6436.

36. (a) Barbe, A.; Secroun, C.; Jouve, P. *J. Mol. Spectrosc.* **1974**, 49, 171– 182.
(b) Tanaka, T.; Morino, Y. *J. Mol. Spectrosc.* **1970**, 33, 538– 551.

37. Huber, H. P.; Herzberg, G. *Molecular Structure and Molecular Spectra IV.Constants of Diatomic Molecules*; Van Nostrand Reinhold: Toronto, **1979**.

38. Ruden, T. A.; Helgaker, T.; Jørgensen, P.; Olsen., J. *J. Chem. Phys.* **200**4, 121, 5874– 5884.

39. (a) Wilkinson, I.; Whitaker, B. J. *J. Chem. Phys*. **2008**, 129, 154312 – 154326.
(b) Schinke, R; Suarez, J; Farantos, S. C. *J. Chem. Phys.* **2010**, 133, 091103– 091106.

40. Logan, J. A. *J. Geophys. Res.* **1983**, 88, 10785– 10807.

41. Crutzen, P. J. *Ann. Rev. Earth Planet. Sci.* **1979**, 7, 443– 472.

42. Logan, J. A.; Prather, M. J.; Wofsy, S. C.; McElroy, M. B. *EOS Trans. Am. Geophys. Union* **1978**, 59, 36– 42.

43. Demore, W. B.; Sander, S. P.; Golden, D. M.; Hampson, R. F.; Kurylo, M. J.; Howard, C. J.; Ravishankara, A. R.; Kolb, C. E.; Molina, M. J. *Chemical Kinetics and Photochemical Data for Use in Atmospheric Studies*, Evaluation No. 11, JPL Publication 94–26, Jet Propulsion Laboratory: Pasadena, CA, **1994**. http://jpldataeval.jpl.nasa.gov (accessed Mar 2012).

44. Dupuis, M.; Fitzgerald, G.; Hammond, B.; Lester, W. A.; Schaefer, H. F. J.

Chem. Phys. **1986**, 84, 2691– 2697.

45. (a) Clyne, M. A. A.; Thrush, B. A.; Wayne, R. P. *Trans. Faraday Soc.* **1964**, 60, 359– 370.

(b) Stedman, D. H.; Niki, H. *J. Phys. Chem.* **1973**, 77, 2604– 2609.

(c) Lippmann, H. H.; Jesser, B.; Schurath, U. *Int. J. Chem. Kinet.* **1980**, 12, 547– 554.

(d) Borders, R. A.; Birks, J. W. *J. Phys. Chem.* **1982**, 86, 3295– 3302.

46. Davis, H. F.; Kim, B. S.; Johnston, H. S.; Lee, Y. T. *J. Phys. Chem*. **1993**, 97, 2172– 2180.

47. Eisfield, W.; Morokuma, K. *J. Chem. Phys.* **2003**, 119, 4682– 4688.

48. Olson, L. P.; Kuwata, K. T.; Bartberger, M. D.; Houk, K. N. *J. Am. Chem. Soc.* **2002**, 124, 9469– 9475.

49. Morris, V. R.; Bhatia, S. C.; Hall, J. H. *J. Phys. Chem.* **1990**, 94, 7414– 7418.

Chapter 3

On potential stability of peroxo nitrate radical

"All beings are born to delusion . . . overcome by the dualities which arises from wish and hate . . . . But those men of virtuous deed in whom sin has come to an end, freed from the delusion of dualities, worship Me steadfast in their vows "

Bhagawat Gita

In this chapter, we report a comparative single-reference and multi-reference coupled cluster investigation on the structure, potential energy surface, and IR spectroscopic properties of the trans peroxo nitrate radical, one of the key intermediates in stratospheric NO_X chemistry. The previous single-reference *ab-initio* studies predicted an unbound structure for the trans peroxo nitrate radical. However, our Fock space multi reference coupled cluster calculation confirms a bound structure for the trans peroxo nitrate radical, in accordance with the experimental results reported earlier. Further, the analysis of the potential energy surface in FSMRCC method indicates a well-behaved minima, contrary to the shallow minima predicted by the single-reference coupled cluster method. The harmonic force field analysis, of various possible isomers of peroxo nitrate also reveals that only the trans structure leads to the experimentally observed IR peak at 1840 cm^{-1}. The present study highlights the critical importance of non-dynamic correlation in predicting the structure and properties of high-energy stratospheric NO_x radicals.

3.1 Introduction:

The NO_x radicals play a crucial role in stratospheric ozone chemistry and are involved in one of the major pathways of stratospheric ozone depletion [1-5]. Considerable efforts have been devoted to the study of these radicals, both theoretically[6-8] and experimentally [9-13].

$$NO + O_3 \rightarrow NO_2 + O_2 \quad (3.1)$$

$$NO_2 + O \rightarrow NO + O_2 \quad (3.2)$$

The above reactions represent the key steps in NO_x catalyzed pathway of stratospheric ozone depletion [2,14]. An analysis of the excitation energy spectra of NO_3 reveals that the radical undergoes a nonadiabatic transition and a rearrangement prior to dissociation [15], leading to the formation of ONOO intermediate. The ONOO intermediate further dissociates in the subsequent step to form NO and O_2.

$$NO_3 \rightarrow ONOO \rightarrow NO + O_2 \quad (3.3)$$

The existence of the ONOO intermediate was proposed by Ogg [16] for the first time, and since then, its presence has been debated considerably. Guillory and Johnston confirmed its presence, using infrared absorption spectroscopic analysis for a mixture of NO_x and oxygen, and proposed a trans planar structure for the molecule [17]. However, Morris and Johnston latter revised this interpretation due to the systematic errors in the experiments [18]. Finally, Hall and co-workers gave positive evidence [9,19] in favor of the stable trans ONOO radical from the isotopic labeling study of the reaction between NO and O_2, trapped in an argon matrix. Their conclusions were based on a 50 cm^{-1} isotopic shift of IR band at 1840 cm^{-1}, which was attributed to the presence of trans peroxo nitrate radical,

formed in the gas phase reaction between labeled O_2 and NO trapped in an argon matrix. The authors also used some limited *ab-initio* calculations [20] to support their results. However, the experimental and theoretical results were not consistent and showed considerable discrepancy. The first high-level *ab-initio* study (CCSD(T)) on this system was performed by Lee and Wright [21], who reported a weakly bound quartet complex of ONOO. The authors did not investigate the doublet spin coupled form of ONOO formed during the photodissociation of NO_3. Olson and co-workers [22] discarded the possibility of a bound structure for the doublet trans ONOO on energetic grounds. Their inference was partly based on the DFT and MP2 based results of Iwata and co-workers [23]. However, both DFT and MP2 methods are inadequate[24] for a proper description of the structure and properties of NO_x radicals. On the contrary, Eisfeld and Morokuma [25] located a bound structure for trans ONOO using CCSD(T)/aug-cc-pVTZ level of theory. The radical wave function was found to be dominated by more than one configuration and they concluded that the optimized geometry is an artifact of the single-reference nature of method, rather than a true minimum. Their conclusion is consistent with the fact that the single-reference description of wave function [26, 27] is inadequate in describing structure and properties of NO_3, which is a structural isomer of trans peroxo nitrate. In case of nitrogen trioxide, even the state of the art single-reference coupled cluster method predicts a C_{2v} geometry [28] contrary to the experimental geometry [29-32] of D_{3h}. However, the Fock space multi-reference coupled cluster calculations by Kaldor [33] and MRCI calculations by Morkuma and Eisfeld [34], both lead to a D_{3h} geometry of NO_3. Thus, a high-level multi-reference study on trans ONOO, is also necessary to draw firm conclusions about the structure and potential stability of this compound.

The objective of the present study is to investigate the structure, stability, and IR spectroscopic constants of doublet peroxo nitrate radical using multi-reference coupled cluster method, which incorporates dynamic and nondynamic correlation in a balanced way. The chapter is organized as follows: section 3.2 presents the

methodology; computational details, results, and discussion are presented in section 3.3; and section 3.4 contains the concluding remarks.

3.2 Methodology and Computational Details

The initial geometry optimization of the molecule has been done using single-reference coupled cluster method, with ROHF reference, in singles and doubles (CCSD) approximation [35]. The potential energy surfaces and IR spectroscopic constants are calculated for a proper characterization of the molecule. The effect of inclusion of partial triples [36,37] (CCSD(T)), which gives the so-called "chemical accuracy", is considered for the geometry, potential energy surface and spectroscopic properties. However, the trans peroxo nitrate radical shows high T1 diagnosis [38] value. T1 diagnosis is actually the Euclidian norm of the coupled cluster singles amplitudes. Lee and Taylor [38] have shown that a T1 diagnosis value above 0.02 indicates that the reference wave function (Hartree–Fock in this case) does not provide a correct zeroth-order description of the exact wave function. This is generally, but not necessarily, caused by the presence of quasi-degenerate configurations, each of which makes significant contribution to the reference wave function. The high T1 diagnosis value of trans ONOO radical shows that a proper description of its electronic structure requires a method capable of incorporating multi-configurational description of the wave function, where as accurate energetic requires calculation that include dynamic correlation.

A multi-reference coupled cluster (MRCC) method uses an exponential operator on the reference space, which is a linear combination of more than one configuration, in contrast with the single-reference based theory with one single determinant as the reference space. Thus, MRCC incorporates both dynamic and non-dynamic correlation in a systematic way. There are two basic variants of multi-reference coupled cluster theory in the literature: The first one describes a

specific root, known as state specific MRCC [39] and other is the multiroot description by effective Hamiltonian approach [40-42]. Various approaches are available for describing state specific MRCC wave function ansatz, such as the Brillouin–Wigner (BW) MRCC ansatz [43, 44], the state specific ansatz suggested by Mukherjee and co-workers (MK-MRCC) [45-48], exponential multi-reference wave function ansatz (MRexpT) [49, 50), and internally contracted multi-reference coupled cluster ansatz (ic-MRCC) [51, 52]. On the other hand, methods based on the effective Hamiltonian approach are divided into two subclasses: the Hilbert space (HS) [53-56] approach and Fock space (FS) [57-64] approach. In both approaches, energies are obtained by diagonalization of the effective Hamiltonian, defined within a pre-chosen model space and both approaches are fully size extensive. The HS-MRCC approach uses a state universal operator with different cluster operators for each determinant in the model space. The FS-MRCC approach, on the other hand, uses a valence universal wave operator, which correlates the model space with the reference space. However, both these approaches suffer from the convergence problem due to the presence of intruder states. The use of intermediate Hamiltonian [65, 66] (IH) or state specific (SS) MRCC approaches can circumvent this problem. Parallel to these approaches, the equation of motion coupled cluster (EOMCC) [67, 68] has been successfully used for the theoretical treatment of quasi-degenerate states [69, 70] and molecular-excited states [68, 71-74]. For the principal peaks in one-valence problems, the EOMCC method is equivalent[75] to the FSMRCC method. Although HS-MRCC is more frequently used for studying potential energy surfaces, Bernholdt and Bartlett [76], as well as Ghose and Pal [77], have used the FSMRCC method to study potential energy surfaces with great success.

We have used the FSMRCC method for our study. FSMRCC is known for accurate description of quasi-degenerate low lying states and has been successfully used for the calculation of energy [78-82] and properties [83-87] of ionized, electron-attached, and excited states.

The FSMRCC single-point calculations are performed using codes developed by Pal and co-workers [81-83]. The most time-consuming step in FS-MRCCSD calculation is the reference state closed-shell CCSD calculation, which scales as an iterative N^6 power of the basis set. The construction of $\bar{H}$ intermediates also scales as N^6. However, it has to be constructed only once in a single-point calculation. The FSMRCCSD calculation for (1,0) and (0,1) sectors of Fock space scales as an iterative N^5 power of the basis set. So, overall, the FSMRCCSD calculation scales as an iterative N^6 power of the basis set. However, it has a slightly higher prefactor and a slightly enhanced storage requirement than single-reference closed-shell CCSD calculations.

All the single-reference and multi-reference geometry optimization [88] and frequency calculations for the doublet radical were performed using CFOUR [89]. For optimizing the triplet state of oxygen, a numerical gradient based FSMRCC code has been used, with a model space of (4,3) [90]. The T1 diagnosis was performed using Gaussian09 [91]. The basis set convergence of the results was studied using a hierarchy of Dunning's [92] correlation-consistent aug-cc-pVXZ basis sets (X = D, T and Q) and all the electrons are used in correlation treatment. Total energies of the different isomers have been extrapolated to obtain the energy at the complete basis set (CBS) limit [93-95], using following formula [96] used by Kamiya and Hirata [97] in their benchmark study.

$$E(n) = E(\infty) + \eta_1 e^{-(n-1)} + \eta_2 e^{-(n-1)^2} \qquad (3.4)$$

where $E(\infty)$ is the energy at the CBS limit, and n = 2, 3, 4 corresponds to the aug-cc-pVDZ, aug- cc-pVTZ, and aug-cc-pVQZ basis sets, respectively. $E(n)$ are the corresponding energies, and η_1 and η_2 are parameters that are used to fit the energies.

3.3 Results and Discussion

The peroxo nitrate radical is made up of two open-shell fragments NO_2 and O_2 with the ground states of $^2\Pi$ and $^3\Sigma_g$, respectively, which could give rise to a single bond among them with one unpaired electron.

3.3.1 Single-Reference Coupled Cluster Calculations

The single-reference coupled cluster method, in CCSD approximation, is not suitable for a proper description of doublet radicals, with quasi-degenerate ground state. However, it can be a good starting point for a correlated *ab-initio* treatment of energy, structure, and properties of peroxo nitrate radical.

Table 3.1 presents the optimized geometries of trans peroxo nitrate. Optimization of the trans peroxo nitrate at the CCSD/aug-cc-pVDZ level of theory gives a bound complex with an ON–OO bond length of 1.664 Å, and it is similar to the earlier reported geometry by Eisfeld and Morokuma [25]. The optimized N–O and O–O bond lengths are 1.146 and 1.281 Å, respectively. Improving the basis set from aug-cc-pVDZ to aug-cc-pVTZ leads to shrinking of the ON–OO bond length to 1.558 Å. The N–O bond also shrinks to 1.130 Å in aug-cc-pVTZ basis set. On the other hand, the O–O bond gets stretched to 1.338 in CCSD/aug-cc-pVTZ level of theory. The O–O bond length (1.338 Å) in trans peroxo nitrate shows elongation from that of the free triplet oxygen (1.195 Å), whereas the N–O bond (1.130 Å) undergoes shrinking from the free nitric oxide bond length of 1.142 Å. This elongation of the O–O bond and shortening of the N–O bond indicate transfer of electron density from the antibonding orbital ($2\pi^*_g$) of nitric oxide to the antibonding orbital ($2\pi^*_g$) of oxygen. The harmonic frequencies computed for the optimized geometry are all real, confirming it to be a true minimum. The geometrical parameters in the aug-cc-pVQZ basis show very small deviation from that in the aug-cc-pVTZ basis set, and the results seem to approach the basis set convergence limit.

We have further refined the optimized geometry by including partial triples in the single-reference coupled cluster method (CCSD(T)), which takes care of the correlation in an improved manner. In the CCSD(T)/aug-cc-pVDZ level of theory,

Table 3.1 : Optimized Geometrical Parameters of Trans Peroxo Nitrate

method	**basis set**	R_{O-O} **(Å)**	$R_{(ON)-(OO)}$ **(Å)**	R_{N-O} **(Å)**	**α(ONO) (deg)**	**α(NOO) (deg)**
CCSD	aug-cc-pVDZ	1.281	1.664	1.146	108.0	108.4
	aug-cc-pVTZ	1.338	1.558	1.130	108.6	110.9
	aug-cc-pVQZ	1.333	1.556	1.129	108.6	111.2
CCSD(T)	aug-cc-pVDZ	does not converge				
	aug-cc-pVTZ	1.258	1.789	1.137	108.0	109.4
	aug-cc-pVQZ	1.255	1.789	1.136	107.9	109.7
FSMRCCSD	aug-cc-pVDZ	1.298	1.598	1.150	108.2	106.7
	aug-cc-pVTZ	1.287	1.556	1.135	108.3	107.4
	aug-cc-pVQZ	1.285	1.550	1.135	108.3	107.6

we have failed to obtain a bound structure for the trans peroxo nitrate. However, as

we go to the aug-cc-pVTZ basis set, the CCSD(T) method gives a bound structure for the trans peroxo nitrate. Inclusion of partial triples increases the ON–OO bond length from 1.558 to 1.789 Å (Table 3.1).

It also shrinks the O–O bond and subsequently stretches the N–O bond. Thus, it can be concluded that the inclusion of partial triples leads to less interaction between the constituting fragments and thereby weakening the ON–OO complex, which is also indicated by the very shallow minima present in the potential energy surface of trans ONOO, obtained using CCSD(T) method (Figure 3.1a). Interestingly, the bond angles in trans peroxo nitrate remain unaffected by inclusion of partial triples. Geometrical parameters show a very negligible change as we go from the aug-cc-pVTZ to the aug-cc-pVQZ basis, in both CCSD and CCSD(T) methods, and results seem to approach complete basis set limit.

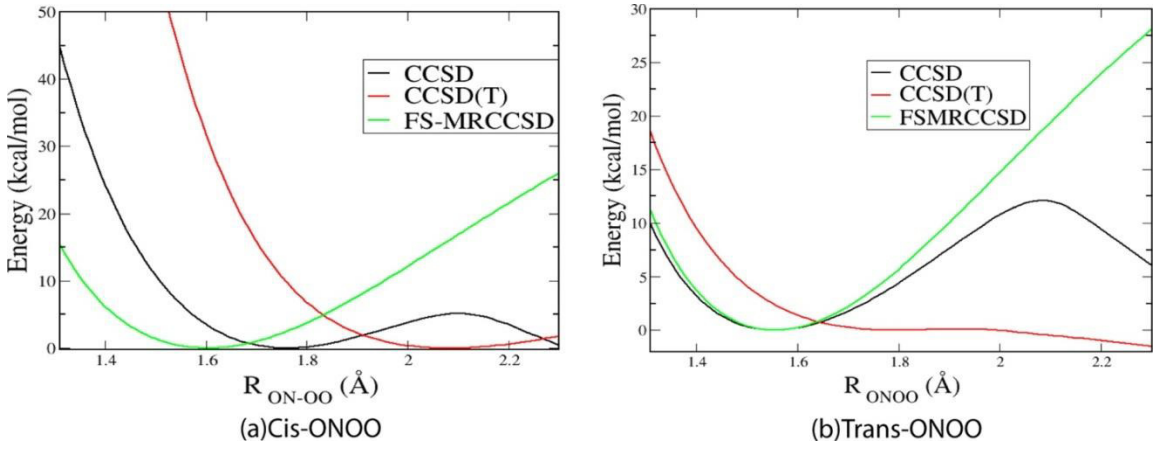

Figure 3.1 : Potential energy surface along the ON–OO bond.

A planar peroxo nitrate has an alternative possibility of existing as a cis isomer. Table 3.2 presents the optimized geometries of cis peroxo nitrate in single-reference and multi-reference coupled cluster methods.

The calculation at the CCSD/aug-cc-pVDZ level of theory reveals that the bond lengths of the cis isomer are considerably different from that of the corresponding

trans one. The ON–OO bond in case of the cis isomer is stretched to 1.846 Å, whereas O–O and N–O bonds shrink to 1.254 and 1.137 Å, respectively. The ONO and NOO bond angles are also slightly smaller than that in the trans isomer. On going from aug-cc-pVDZ to aug-cc-pVTZ, the ON–OO bond shrinks to 1.761 Å. The O–O and N–O bonds also shrink to 1.249 and 1.121 Å, respectively. On the other hand, ONO and NOO bond angles increase to 104.9° and 104.4°, respectively.

Table 3.2 : Optimized Geometrical Parameters of Cis Peroxo Nitrate

method	**basis set**	$R_{O–O}$ **(Å)**	$R_{(ON)–(OO)}$ **(Å)**	$R_{N–O}$ **(Å)**	**α(ONO) (deg)**	**α(NOO) (deg)**
CCSD	aug-cc-pVDZ	1.254	1.846	1.137	102.4	102.1
	aug-cc-pVTZ	1.249	1.761	1.121	104.9	104.4
	aug-cc-pVQZ	1.248	1.749	1.120	105.4	104.9
CCSD(T)	aug-cc-pVDZ	1.239	2.140	1.158	93.9	96.1
	aug-cc-pVTZ	1.228	2.084	1.134	95.1	96.1
	aug-cc-pVQZ	1.226	2.086	1.133	95.2	97.2
FSMRCCSD	aug-cc-pVDZ	1.306	1.660	1.137	113.2	111.6
	aug-cc-pVTZ	1.295	1.622	1.122	113.5	112.8
	aug-cc-pVQZ	1.292	1.620	1.121	113.5	112.8

However, the changes in both bond lengths and bond angles are small from the aug-cc-pVTZ to the aug-cc-pVQZ basis set, and the value approaches the

complete basis set limit.

The inclusion of partial triples in coupled cluster calculations shows considerable change in bond lengths, as well as in bond angles. The ON–OO bond stretches to 2.140 Å at the CCSD(T)/aug-cc-pVDZ level of theory. The O–O bond length shrinks to 1.239 Å, and the N–O bond stretches to 1.158 Å in the CCSD(T) method. However, the most striking change is observed in the case of bond angles. Unlike, in the case of the trans isomer, where the inclusion of triples keeps the bond angles almost unchanged, the ONO bond angle shrinks to 93.9° and the NOO bond angle shrinks to 96.1° in the cis isomer at the CCSD(T)/aug-cc-pVDZ level of theory. The bond angles close to 90° give cis peroxo nitrate a near rectangular structure. The ON–OO bond length shrinks to 2.084 Å, as we go from the aug-cc-pVDZ to the aug-cc-pVTZ basis. The O–O and N–O bonds also shrink to 1.228 and 1.134 Å, respectively, in the CCSD(T)/aug-cc-pVTZ level of theory. However, the bond angles are less affected by the improvement in the basis set. All the geometrical parameters show very small change from aug-cc-pVTZ to aug-cc-pVQZ basis set, and the values approach the complete basis set limit.

The huge change in the O–O and ON–OO bond lengths for the trans isomer and the ON–OO bond length and bond angles for cis with inclusion of partial triples at first glance may look puzzling. However, the potential energy surface scan (Figure 3.1a,b) along the ON–OO bond shows the two fragments constituting the molecule are very weakly bound. At the same time, the very high T1 diagnosis value (Figure 3.2 a,b) indicates that the ROHF reference orbitals do not provide a correct zeroth-order description of the exact wave function. Therefore, the inclusion of partial triples can induce a very large relaxation of the orbitals. Consequently, it can change the energy, as well as geometry and vibrational property, by a considerable amount. The change is more prominent at the intermonomer ON–OO bond and also the bond angles involving the ON–OO bond, rather than the strongly bound intramonomer O–O and O–N bonds.

The cis complex is energetically 24.03 kcal/mol more stable than the corresponding trans isomer at the CCSD/aug-cc-pVQZ level of theory (with ZPE correction of −0.72 kcal/mol). The relative stability of the cis isomer decreases to a value of 7.70 kcal/mol (with ZPE correction of −0.63 kcal/mol) at the CCSD(T) level. However, T1 diagnosis values indicate that the ROHF reference wave function is inadequate for a correct zeroth-order description of the exact wave function of both cis and trans peroxo nitrate. Plot a and b of Figure 3.2 show that the CCSD equilibrium geometry gives a T1 diagnosis value of 0.03, and it increases to 0.05 in the CCSD(T) equilibrium geometry, for both isomers.

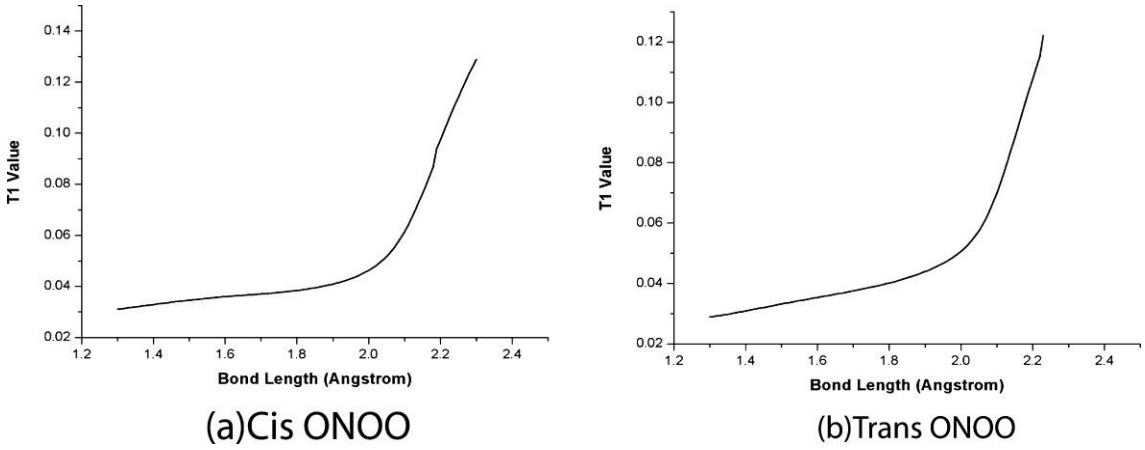

Figure 3.2 : ON–OO bond length vs T1 diagnosis value.

3.3.2 Multi-reference Coupled Cluster Calculations

The high T1 diagnosis value shown by the peroxo nitrate radical calls for a multi-reference description of the wave function. In FSMRCCSD/aug-cc-pVDZ level of theory trans peroxide shows an ON–OO bond length of 1.598 Å. The O–O and O–N bond lengths at the corresponding level of theory are 1.298 and 1.150 Å, respectively. All the bond lengths decrease from aug-cc-pVDZ to aug-cc-pVTZ basis. The comparison of O–O and N–O bond lengths in peroxo nitrate radical with their corresponding values in the free species can lead to some insight into the bonding of trans peroxo nitrate. In the FSMRCCSD/aug-cc-pVTZ level of

theory, the O–O bond stretches to 1.287 Å from the free oxygen bond length of 1.193 Å and the N–O bond shrinks to 1.135 Å compared to the free nitric oxide bond length of 1.150 Å. This change in the bond lengths indicates transfer of electron density from the antibonding ($2\pi^*_g$) of nitric oxide to the antibonding ($2\pi^*_g$) of oxygen, resulting in shrinking of the former and stretching of the latter. The Mulliken population analysis of species (Table 3.3) confirms the transfer of electron density from nitric oxide to oxygen. The O–O bond length shrinks and N–O bond length stretches, as compared to that in the CCSD method. In both cases, the trend in FSMRCCSD is comparable with that of the CCSD(T) method.

Table 3.3 : Mulliken Population Analysis of Trans ONOO at the FSMRCCSD/aug-cc-pVTZ Level of Theory

Atom center	Mulliken population
O	8.172
O	8.048
N	6.629
O	8.150

However, the ON–OO bond length (1.556 Å) in the FSMRCCSD method is much shorter than the CCSD(T) bond length and nearly identical to that with the CCSD method, which indicates higher bonding character in the complex as we go from single-reference to multi-reference coupled cluster, i.e., from CCSD to FSMRCCSD, method. To get a clearer picture about the stability of the trans peroxo nitrate, we have scanned the potential energy surface along the ON–OO coordinate from 1.30 to 2.30 Å with single-reference and multi-reference coupled cluster methods. The aug-cc-pVTZ basis set was used for the calculations, and the other geometrical parameters were kept fixed at their optimized equilibrium values

of the corresponding level of theory. The CCSD curve shows a minimum around 1.55 Å (Figure 3.1a). However, after 2.10 Å the curve rapidly starts falling off, which is consistent with the typical failures of the standard single-reference coupled cluster method in bond stretching [98] On the other hand, the CCSD(T) method shows a shallow minima around 1.79 Å and it does not fall off up to 2.30 Å, i.e., the entire width of the scan. However, the plot of bond length vs T1 diagnosis value (Figure 3.2a) indicates a progressive increase of the multi-reference character with the stretching of the bond. Therefore, the single-reference coupled cluster method can hardly be trusted for an accurate depiction of the potential energy curve at stretched bond lengths. The curve plotted with the FSMRCCSD method shows the trend similar to that of the CCSD curve, with the exception that the former does not fall off even at stretched bond lengths and behaves smoothly for the entire range of the scan. The above results, thus, lead us to the conclusion that the trans ONOO has a bound structure at the FSMRCCSD/aug-cc-pVTZ level of theory. The geometrical parameters show a very small change from the aug-cc-pVTZ to the aug-cc-pVQZ basis set, and results seem to converge with respect to the basis set. Figure 3.3a presents the optimized structure of trans peroxo nitrate at the FSMRCCSD/aug-cc-pVQZ level of theory.

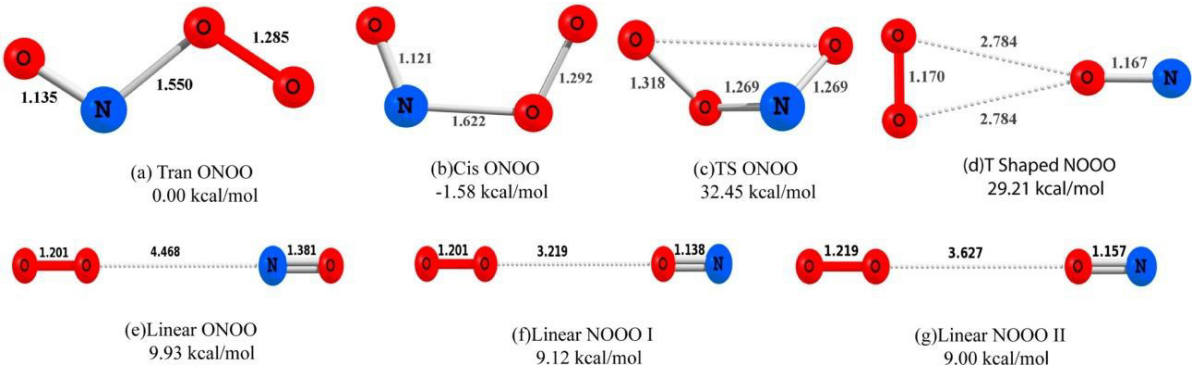

Figure 3.3 :. Different isomers of peroxo nitrate.

We have also optimized the cis structure of ONOO with the FSMRCCSD method.

At the FSMRCCSD/aug-cc-pVDZ level of theory, the cis isomer shows an ON–OO bond length of 1.660 Å, which is much smaller than the one predicted by CCSD and CCSD(T) methods. The O–O and O–N bond lengths at the FSMRCCSD/aug-cc-pVDZ level of theory are 1.306 and 1.137 Å, respectively. However, the bond angles in the FSMRCCSD method are much larger than those in the single-reference coupled cluster method. All the bond lengths in the FSMRCCSD method decrease with the larger aug-cc-pVTZ basis set. However, the bond angles are less affected by the basis set. The FSMRCCSD/aug-cc-pVTZ level of theory shows a slightly longer ON–OO bond length (1.622 Å) compared to that of the corresponding trans isomer (1.558 Å). The Mulliken population analysis of the species (Table 3.4) indicates transfer of electron density from antibonding orbital ($2\pi^*_g$) of nitric oxide to the antibonding orbital ($2\pi^*_g$) of oxygen, which results in shrinking of the N–O and stretching of the O–O bond lengths, as compared to their free molecular bond lengths.

Table 3.4 : Mulliken Population Analysis of Cis ONOO at the FSMRCCSD/aug-cc-pVTZ Level of Theory

Atom center	Mulliken population
O	8.050
O	8.199
N	6.671
O	8.079

A scan of the potential energy surface of the cis isomer along the ON–OO coordinate has also been performed using the same procedure as applied for the trans isomer (Figure 3.1b). The CCSD curve of the cis isomers shows a behavior similar to that of the trans isomer with a minima around 1.76 Å and starts to fall

off after 2.11 Å. The CCSD(T) curve shows a minima around 2.08 Å, which is slightly deeper than the corresponding trans isomer and, consequently, indicates a more bound structure. However, the plot of T1 value vs bond length (Figure 3.2b) shows heavy multi-reference character of the wave function, even at equilibrium distance, in the single-reference coupled cluster method. The FSMRCC calculation, on the other hand, gives a smooth curve. The geometrical parameters show very little change on moving from the aug-cc-pVTZ to the aug-cc-pVQZ basis, and the results seem to the approach basis set convergence limit. Figure 3.3b presents the optimized structure of cis peroxo nitrate at the FSMRCCSD/aug-cc-pVQZ level of theory.

The stability of the cis isomer relative to the trans isomer decreases with inclusion of non-dynamic correlation. Table 3.5 presents the effect of the basis set on the relative stability of the cis and trans isomer in the FSMRCCSSD method. In the aug-cc-pVDZ basis set, the cis isomer is only 2.12 kcal/mol (with inclusion of ZPE) lower in energy than the corresponding trans isomer. The relative stability of the cis isomer decreases to 1.47 kcal/mol (with inclusion of ZPE) at the FSMRCCSD/aug-cc-pVTZ level of theory; i.e., the cis isomer is now 1.47 kcal/mol lower in energy than the trans one. However, the change in the relative stability is small from aug-cc-pVTZ to aug-cc-pVQZ, and results seem to converged with respect to the basis set. In the complete basis set limit, the stability of the cis isomer decreases to 1.48 kcal/mol (without the ZPE correction). The inclusion of ZPE correction slightly changes the value, and the cis isomer is 1.58 kcal/mol lower in energy than the trans one, in the CBS limit with ZPE correction.

Lee and Wright [21] have described T-shaped and linear structures of quartet peroxo nitrate. We have also investigated these structures for the doublet peroxo nitrate in the FSMRCC method using a hierarchy of Dunning's [92] correlation-consistent aug-cc-pVXZ basis sets (X = D, T, and Q). All the isomers show similar

basis set behaviors. The bond lengths show a large change on going from the aug-cc-pVDZ to aug-cc-pVTZ basis. However, the change is negligible on moving from aug-cc-pVTZ to aug-cc-pVQZ, and the values seem to be converged with respect to the basis set. On the other hand, the bond angles are less affected by basis set and remain almost unchanged with a change in basis set.

Table 3.5 : Relative Stability of the Cis Perxo Nitrate Radical Compared to the Trans Isomer in the FSMRCCSD Method (kcal/mol)

basis set	trans isomer	cis isomer (without the ZPE correction)	cis isomer (with the ZPE correction)
aug-cc-pVDZ	0.00	1.92	2.12
aug-cc-pVTZ	0.00	1.37	1.47
aug-cc-pVQZ	0.00	1.43	1.53
CBS	0.00	1.48	1.58

The T-shaped structure (Figure 3.3d) of peroxo nitrate shows a long interfragment distance and is 29.21 kcal/mol higher in energy at the FSMRCCSD/CBS level of theory with inclusion of ZPE correction than the trans structure. In the T-shaped structure, the oxygen atom of the nitric oxide unit is pointed toward the middle of the O═O double bond. The Mulliken population analysis (Table 3.6) of atoms shows transfer of electron density from $2\pi^*_g$ of oxygen to $2\pi^*_g$ of NO, which is also reflected in the shrinking of the O═O bond to 1.173 Å and stretching of the NO bond to 1.167 Å in FSMRCCSD/aug-cc-pVQZ level of theory. Interestingly, this is opposite to the trend shown by cis and trans ONOO isomers, where the O═O bond stretches and NO bond shrinks, in their free species. The structure shows an imaginary frequency of 27 cm^{-1}, which indicates it to be a first-order

saddle point on the potential energy surface.

Among the various possible linear structures of peroxo nitrate, we have found only three bound structures. The first one is a linear ONOO structure with an elongated ON–OO bond length of 4.468 Å at the FSMRCCSD/aug-cc-pVQZ level of theory (Figure 3.3e). The O═O bond length is 1.201 Å, which is slightly longer than the corresponding free O═O bond length of 1.193 Å, where the N═O bond length is 1.138 Å, which is shorter than the corresponding free N═O bond of 1.150 Å. The linear ONOO structure is 9.93 kcal/mol higher in energy than the trans one at the FSMRCCSD/CBS level of theory (with ZPE correction). The structure shows an imaginary frequency of 7 cm^{-1} at the FSMRCCSD/aug-cc-pVQZ level of theory, indicating the structure to be a first-order saddle point.

Table 3.6 : Mulliken Population Analysis of T shaped ONOO at the FSMRCCSD/aug-cc-pVTZ Level of Theory

Atom center	Mulliken population
O	7.895
O	7.893
N	7.120
O	8.090

There also exist two alternative shapes of linear nitro peroxide (Figure 3.3f and g). At the aug-cc-pVQZ level of theory, both have similar O═O and N═O bond lengths, i.e., slightly elongated O═O bond and slightly shorter N═O bond than those in their free analogs. However, the isomers considerably differ among themselves in the ON–OO bond lengths. The first one (NOOO I in Figure 3.3f)

has an ON–OO bond length of 3.219 Å whereas the second one (NOOO II in Figure 3.3g) has an elongated ON–OO bond length of 3.645 Å. They have almost identical energies and are 9.12 and 9.00 kcal/mol higher in energy than the trans structure at the FSMRCCSD/CBS level of theory (with ZPE correction). An interesting observation for all the three linear isomer is that, though the intramonomer OO and ON distance, as well as their energies are virtually identical, the intermonomer distances are rather different, i.e., 4.468, 3.219, and 3.645 Å. All the three linear isomers of peroxo nitrate are made up of very weakly bound O═N and N═O monomer fragments. The potential energy surfaces along the intermonomer distance for all the three linear isomers are very flat, which indicate the linear isomers are very weakly bound. Consequently, all of them have nearly identical energies, in spite of having different intermonomer distances.

The NOOO II shows an imaginary frequency of 5 cm–1 at the FSMRCCSD/aug-cc-pVQZ level of theory, indicating the structure to be a first-order saddle point, whereas the NOOO I shows all real frequencies, indicating the structure to be a local minima.

3.3.3 Harmonic Frequency Calculation

The above-reported results demonstrate that the proposed ONOO complex can only have cis or trans geometry, on energetic grounds, which are stable and observable. The distinction between cis and trans structure can be made by comparing the computed IR frequencies with that of the experimentally determined values. The experimental evidence on the positive existence of trans peroxo nitrate is based on an IR band at 1840 cm^{-1}, observed due to a reaction product of NO and O_2 trapped in an argon matrix.

Table 3.7 reports the computed IR frequencies and intensities using single-

reference, FSMRCC, and UHF/6-311G* methods. We compare our results with the available experimental numbers. The lowest a″ torsion vibration is not of interest and was thus omitted. We also report results by Hall and co-workers[20] calculated using UHF/6-311G* for comparison.

Table 3.7 : Comparison of Frequencies of Trans ONOO Computed in Single-Reference and Multireference Coupled Cluster Method aug-cc pVTZ Basis Set with Experimental Values and Previous Theoretical Results

	CCSD		**CCSD(T)**		**FSMRCCSD[a]**		**UHF/6-31G*[b]**		**exp[c]**
Modes of vibration	**IR frequency (cm^{-1})**	**IR intensity (km mol^{-1})**	**IR frequency (cm^{-1})**	**IR intensity (km mol^{-1})**	**IR frequency (cm^{-1})**	**IR intensity (km mol^{-1})**	**IR frequency (cm^{-1})**	**IR intensity (km mol^{-1})**	
O–O–N deform	273	112	110	1	368 (182)	5	469	1	
O–N stretch	395	185	244	2	450 (367)	69	671	13	
O–N–O deform	733	171	680	1	870 (713)	89	976	100	
O–O stretch	989	24	1245	187	1251 (1365)	17	1287	14	
N–O stretch	1914	497	1880	420	1925 (1875)	273	1659	7	1840

a : The numbers in parentheses are frequencies with addition of partial triples to FSMRCCSD.

b : Values calculated by Hall and co-workers. See ref 20. c : See ref 19.

It can be seen that the most intense peak at the UHF/6-311G* level of theory is at 976 cm^{-1}, which is nearly half of the experimental peak at 1840 cm^{-1}. On the other hand, the peak at 1659 cm^{-1}, which is closest to the experimental value, is of very low intensity. Therefore, at the UHF/6-311G* level of theory, the computed spectrum of trans ONOO does not match with the experimental value.

The most intense peak using the CCSD/aug-cc-pVTZ spectrum is at 1914 cm^{-1}, which among the computed IR peaks, is closest to the experimental value. Inclusion of perturbative triples shifts the peak toward a lower value of 1880 cm^{-1}; i.e., it moves closer to the experimental value. The FSMRCCSD method also shows the same trend as that of the single-reference method. The most intense peak in the FSMRCCSD calculated spectrum is at 1925 cm^{-1}. The inclusion of partial triples [99, 100] lowers the frequency to 1875 cm^{-1} (reported in parentheses in Table 3.7), which is very close to the experimental value.

Table 3.8 presents the basis set convergence of IR frequencies of the trans peroxo nitrate radical computed with the single-reference and multi-reference coupled cluster methods. At the CCSD/aug-cc-pVDZ level of theory, the most intense peak is at 1915 cm^{-1}. It remains almost unchanged at 1914 cm^{-1} on moving to the aug-cc-pVTZ basis set. However, the intensity of the mode shows a large change from 418 to 497 km mol^{-1}, as we go from the aug-cc-pVDZ to the aug-cc-pVTZ basis set. Both the IR frequency and IR intensity show negligible change from aug-cc-pVTZ to aug-cc-pVQZ, and the results seem to approach the basis set convergence limit. In the case of the CCSD(T) method, we failed to obtain a bound structure for trans peroxo nitrate in the aug-cc-pVDZ basis. However, the intensity of the mode shows a large change from 418 to 497 km mol^{-1}, as we go from the aug-cc-pVDZ to the aug-cc-pVTZ basis set.

Table 3.8 : Basis Set Convergence of Frequencies of Trans ONOO at Various Levels of Theory

		CCSD		CCSD(T)		FSMRCCSD	
Basis	**Mode of vibration**	**IR frequency (cm^{-1})**	**IR intensity (km mol^{-1})**	**IR frequency (cm^{-1})**	**IR intensity (km mol^{-1})**	**IR frequency (cm^{-1})**	**IR intensity (km mol^{-1})**
aug-cc-pVDZ	O–O–N deform	301	15	Optimization does not converge		351	3
	O–N stretch	333	24			421	57
	O–N–O deform	779	33			848	74
	O–O stretch	1200	65			1207	29
	N–O stretch	1915	418			1902	315
aug-cc-pVTZ	O–O–N deform	273	112	110	1	368	5
	O–N stretch	395	185	244	2	450	69
	O–N–O deform	733	171	680	1	870	89
	O–O stretch	989	24	1245	187	1251	17
	N–O stretch	1914	497	1880	420	1925	273
aug-cc-pVQZ	O–O–N deform	276	116	98	1	373	6
	O–N stretch	397	185	247	2	457	70
	O–N–O deform	737	171	679	1	875	91
	O–O stretch	1001	26	1254	194	1262	16
	N–O stretch	1920	496	1894	422	1929	260

Both the IR frequency and IR intensity show negligible change from aug-cc-pVTZ to aug-cc-pVQZ, and the results seem to approach the basis set convergence limit. In the case of the CCSD(T) method, we failed to obtain a bound structure for trans peroxo nitrate in the aug-cc-pVDZ basis.

However, at the CCSD(T)/aug-cc-pVTZ level of theory, trans peroxo nitrate shows the most intense peak at 1880 cm^{-1} with an IR intensity of 420 km mol^{-1}. On moving to the aug-cc-pVQZ basis set, both the IR frequency and intensity seem to converge with respect to the basis set. The FSMRCCSD method with the aug-cc-pVDZ basis set shows the most intense peak at 1902 cm^{-1}, with an IR intensity of 315 km mol^{-1}. The peak shifts to 1925 cm^{-1} with an intensity of 273 km mol^{-1} in aug-cc-pVTZ. However, the change is very small from the aug-cc-pVTZ to the aug-cc-pVQZ basis set, and both the IR frequency and intensity in the FSMRCCSD method seem to converge with the basis set.

There is an even more sensitive test of the correlation between theory and experiment. The major argument in favor of a stable ONOO complex was based on the 50 cm^{-1} shift observed by Bhatia and Hall [9] when they performed the experiment with the $^{18}O_2$ isotopomer in place of a $^{16}O_2$ isotopomer. Their study reports an isotopic shift due to the $^{16}O^{14}N^{18}O^{18}O$ species, the only possible isotopomer that can form in an association reaction between $^{14}N^{16}O$ and $^{18}O_2$. Therefore, we have calculated the isotopic shift, at the FSMRCCSD/aug-cc-pVTZ level of theory, for all the possible isotopic combinations of $^{14}N^{16}O$ with $^{16}O_2$ or $^{18}O_2$, and the results are presented in Table 3.9.

The $^{16}O^{14}N^{18}O^{18}O$ isotopomer does not show any isotopic shift of peak at 1925 cm^{-1}, which at first glance contradicts the existence of a stable trans ONOO species. However, a careful look at Table 3.9 reveals that ONOO indeed shows an isotopic shift of nearly 50 cm^{-1}, only when the NO fragment contains an ^{18}O atom. Eisfeld and Morokuma [25] have indicated a possibility of formation of a $^{18}O^{14}N^{16}O^{18}O$ isotopomer, which may account for the 50 cm^{-1} isotopic shift. We have tried to find out a mechanism of formation of $^{18}O^{14}N^{16}O^{18}O$ isotopomer

from $^{16}O^{14}N^{18}O^{18}O$ isotopomer.

The isotope exchange reaction is found to proceed through a transition state (Figure 3.3c), which shows an imaginary frequency of 177 cm^{-1} at the FSMRCCSD/aug-cc-pVTTZ level of theory. The formation of the transition state is accompanied by stretching of the $^{18}O^{18}O$ and $^{14}N^{16}O$, and shrinking of the $^{18}O^{14}N$ bond (Figure 3.4). The transition state finally evolves to $^{18}O^{14}N^{16}O^{18}O$, and the reaction shows a barrier height of 32.45 kcal/mol at the FSMRCCSD/CBS level of theory (with inclusion of ZPE correction). Formation of $^{18}O^{14}N^{16}O^{18}O$ leads to an isotopic shift of 49 cm^{-1} of the peak at 1925 cm^{-1}, which is in excellent agreement with the experimental shift of 50 cm^{-1}.

Table 3.9 : Harmonic Frequencies (cm^{-1}) and Isotopic Shifts (cm^{-1}) of Trans ONOO Calculated at the FSMRCCSD/aug-cc-pVTZ Level of Theory

Isotopomer	O–O–N deform	O–N stretch	O–N–O deform	O–O stretch	N–O stretch
$^{16}O^{14}N^{16}O^{16}O$	368	450	870	1251	1925
$^{18}O^{14}N^{16}O^{16}O$	-3	–7	–10	0	–49
$^{16}O^{14}N^{16}O^{18}O$	-7	–2	–9	–30	0
$^{16}O^{14}N^{18}O^{16}O$	-5	–10	–11	–36	0
$^{16}O^{14}N^{18}O^{18}O$	–13	–13	–19	–68	0
$^{18}O^{14}N^{18}O^{16}O$	–8	–17	–20	–37	–50
$^{18}O^{14}N^{16}O^{18}O$	–10	–10	–18	–31	–49
$^{18}O^{14}N^{18}O^{18}O$	–16	–20	–29	–69	–50

In the previous section, we found the possibility of a cis isomer that is almost

degenerate with the trans isomer. However, the computed IR spectrum of cis ONOO shows very little resemblance with the experimental spectrum (Table 3.10). At the CCSD/aug-cc-pVDZ level of theory, the computed spectrum shows the most intense peak at 1973 cm^{-1}. On moving from aug-cc-pVDZ to aug-cc-pVTZ, the IR frequency corresponding to the most intense peak shifts to 1988 cm^{-1}, which is 148 cm^{-1} higher than that in the experimental spectrum. With inclusion of perturbative triples (CCSD(T)) the peak undergoes a red shift to 1927 cm^{-1}. However, the spectrum contains another peak at 1436 cm^{-1}, which is of comparable intensity to the peak at 1927 cm^{-1}. The experimental spectrum, on the other hand, contains only one intense peak. Therefore, the experimental peak in the spectrum of 1840 cm^{-1} cannot be due to cis ONOO. On going from the aug-cc-pVTZ to the aug-cc-pVQZ basis set, the IR frequency and intensity, in both CCSD and CCSD(T) methods, seem to converge with respect to the basis set. The FSMRCCSD computed spectrum shows the same behavior as that of the CCSD method and exhibits the most intense peak at 1970 cm^{-1}.

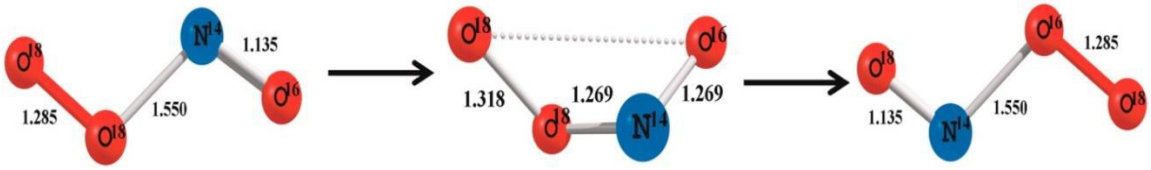

Figure 3.4 : Mechanism of the isotope exchange reaction of trans ONOO

The T-shaped structure apparently gives a single very low intensity peak at 1825 cm^{-1} in FSMRCCSD/aug-cc-pVDZ (Table 3.11). All the other peaks in the spectrum are of zero intensity. Both the IR frequency and IR intensity undergo a large change on going from aug-cc-pVDZ to aug-cc-pVTZ. However, the change is small from aug-cc-pVTZ to aug-cc-pVQZ, and the results seem to be approaching the complete basis set limit. At the FSMRCC/aug-cc-pVQZ level of theory, the most intense peak is at 1854 cm^{-1}, which is in very good agreement with the experimental peak at 1840 cm^{-1}.

Table 3.10 : Basis Set Convergence of Frequencies of Cis ONOO at Various Levels of Theory

		CCSD		CCSD(T)		FSMRCCSD	
Basis	**Mode of vibration**	**IR frequency (cm^{-1})**	**IR intensity (km mol^{-1})**	**IR frequency (cm^{-1})**	**IR intensity (km mol^{-1})**	**IR frequency (cm^{-1})**	**IR intensity (km mol^{-1})**
aug-cc-pVDZ	O–O–N deform	281	1	274	2	270	3
	O–N stretch	364	1	326	6	441	97
	O–N–O deform	708	0	551	0	681	39
	O–O stretch	1287	242	1420	186	1077	47
	N–O stretch	1973	410	1892	204	1938	602
aug-cc-pVTZ	O–O–N deform	303	2	253	8	342	2
	O–N stretch	394	17	280	4	474	55
	O–N–O deform	758	2	582	0	809	9
	O–O stretch	1304	157	1436	217	1263	74
	N–O stretch	1988	378	1927	224	1989	336
aug-cc-pVQZ	O–O–N deform	308	3	240	9	371.	0
	O–N stretch	394	20	287	4	398	22
	O–N–O deform	766	2	583	0	683	10
	O–O stretch	1310	148	1432	220	1234	128
	N–O stretch	1992	377	1920	224	1970	574

Table 3.11 : Frequencies T-Shaped Structure at the FSMRCCSD Method

	aug-cc-pVDZ		aug-cc-pVTZ		aug-cc-pVQZ	
Mode of vibration	**IR frequency (cm^{-1})**	**IR intensity (km mol^{-1})**	**IR frequency (cm^{-1})**	**IR intensity (km mol^{-1})**	**IR frequency (cm^{-1})**	**IR intensity (km mol^{-1})**
ip bending of O–O	260i	0	20	0	28i	0
N–O and O–O bond deform	126	0	41	1	52	1
ip bending of NO	225	0	110	63	104	62
oop bending of NO	244	0	118	0	119	0
O–O stretch	1764	0	1790	21	1801	13
N–O stretch	1825	1	1854	107	1854	99

However, a closer look across the spectrum reveals that there is another peak at 104 cm^{-1}, which is of comparable intensity. The experimental spectrum, on the other hand, shows a single intense peak. Therefore, the experimental peak at 1840 cm^{-1} cannot be due to the T-shaped structure of the peroxo nitrate radical.

The three linear isomers show similar behaviors for IR frequencies. The IR frequencies show a considerable change from aug-cc-pVDZ to aug-cc-pVTZ. However, the change is very small from aug-cc-pVTZ to aug-cc-pVQZ and the values seem to approach the basis set convergence limit.

Table 3.12 : Frequencies of Linear Isomers of Nitro Peroxide at the FSMRCCSD/aug-cc-pVQZ Level of Theory

	aug-cc-pVDZ		**aug-cc-pVTZ**		**aug-cc-pVQZ**	
Mode of vibration	**IR frequency (cm^{-1})**	**IR intensity (km mol^{-1})**	**IR frequency (cm^{-1})**	**IR intensity (km mol^{-1})**	**IR frequency (cm^{-1})**	**IR intensity (km mol^{-1})**
O–N bond stretching	7i	0	15	0	5i	0
Symm bending	16	0	31	0	24	0
Antisymm bending	16	0	32	0	26	0
O–O bond stretching	1626	0	1628	0	1627	0
N–O bond stretching	2034	46	2036	49	2035	45

Each of the three linear structures shows only one intense peak at 2034, 2036, and 2035 cm^{-1}, respectively (Table 3.12), at the FSMRCCSD/aug-cc-pVQZ level of theory. All the other peaks in the spectrum are of zero intensity. Visualizations of the vibrational peaks show that the single intense peak in the spectrum is due to an isolated stretching vibration of N═O, which is decoupled from the vibrations of other bonds. It shows that the N═O and O═O fragments in the linear isomers of

peroxo nitrate are very weakly attached and cannot lead to a bound structure of peroxo nitrate.

3.4 Conclusion

We have presented a benchmark investigation on the stability, structure, and properties of trans peroxo nitrate using the multireference coupled cluster method. Initial investigation on the structure and IR frequency using the CCSD method indicates a bound structure for the complex. Inclusion of perturbative triples in coupled cluster calculations (CCSD(T)) indicates weakening of the complex. However, high T1 diagnosis values indicate a quasi-degenerate nature of the ground state, which indicates the unreliability of the single-reference coupled cluster results. Our FSMRCC calculations indicate a bound structure for the complex, which is evident from the potential energy surface scan of the trans peroxo nitrate along the ON–OO bond. We have also investigated the cis, T-shaped, and linear structures of peroxo nitrate. However, except for the cis structure, all other structures are higher in energy than the trans structure. The cis structure is nearly degenerate with the trans structure at the FSMRCCSD/CBS level of theory (with ZPE correction). A scan of the potential energy surface of the cis isomer shows a shallow minimum in the FSMRCC method, which indicates weakly bound nature of the complex. To differentiate between the trans isomer and cis isomer, we have further investigated the correspondence of computed IR frequencies of both isomers with the experimentally determined frequency. It is found that the trans isomer gives only one intense peak at 1875 cm^{-1} at the FSMRCC/aug-cc-pVTZ level of theory, which is consistent with the experimental peak at 1840 cm^{-1}. The IR frequency of the cis isomer deviates considerably from the experimental value. We have studied the effect of basis set on the results obtained in both single-reference and multi-reference coupled cluster methods using a hierarchy of Dunning's [92] correlation-consistent aug-cc-pVXZ basis sets (X = D, T, and Q). The basis set has a significant effect on the computed results in

both single-reference and multi-reference coupled cluster. In all the methods, both bond lengths and IR frequencies show considerable change from the aug-cc-pVDZ to the aug-cc-pVTZ basis set. However, the change is very small from aug-cc-pVTZ to aug-cc-pVQZ and the values seem to be approaching the complete basis set limit. On the other hand, bond angles seem to be less affected by basis sets.

A more sensitive test of the correspondence between the computed and experimental IR frequency will be the reproduction of the 50 cm^{-1} isotopic shift reported by Hall and co-workers [9]. The most probable isotopomer obtained in the reaction between $^{14}N^{16}O$ and $^{18}O_2$ is $^{16}O^{14}N^{18}O^{18}O$, which does not show any isotopic shift. However, the species can undergo an isotope exchange reaction to form the $^{18}O^{14}N^{16}O^{18}O$ isotopomer and the reaction shows a barrier height of 32.45 kcal/mol at the FSMRCCSD/CBS level of theory, with inclusion of ZPE correction. The resulting $^{18}O^{14}N^{16}O^{18}O$ isotopomer shows an isotopic shift of 49 cm^{-1}, which is nearly identical to the experimental isotopic shift of 50 cm^{-1}. The FSMRCCSD computed peaks for T-shaped and linear isomers of peroxo nitrate differ considerably from the experimental spectrum. Thus, from the FSMRCC calculations, we can conclude that the trans peroxo nitrate has a stable bound structure and trans ONOO is the most probable structure of nitro peroxide, which can correspond to the experimental frequency of 1840 cm^{-1}. It resolves the previous contradiction between experiment and theory and can explain the observed NO_3 scavenging process described in the literature. The present study highlights the need for balanced description of dynamic and non-dynamic correlation in the ab initio study of stratospheric NO_x radicals.

In addition to the radical, the positively and negatively charged analogues of peroxo nitrate play an important role in ionospheric chemistry and the biological oxidation process. A comparative study of the stability, structure, and properties of the cationic, anionic, and radical system will be of considerable interest. Work is currently under way for the same

References:

1. Chipperfield, M. P.; Feng, W., *Geophys. Res. Lett*. **2003**, 30, 1389.
2. Johnston, H., *Science* **1971**, 173, 517-522.
3. Kinnison, D.; Johnston, H.; Wuebbles, D., *J. Geophys. Res.* **1988**, 93, 14165-14175.
4. Randeniya, L. K.; Vohralik, P. F.; Plumb, I. C., *Geophys. Res. Lett.* **2002**, 29, 1051.
5. Ravishankara, A. R.; Daniel, J. S.; Portmann, R. W., *Science*. **2009**, 326, 123-125.
6. Jaroszyńska-Wolińska, J.,. *J. Mol Struc-THEOCHEM*. **2009**, 952, 74-83.
7. Peiró-García, J.; Nebot-Gil, I., *J. Comput. Chem.* **2003**, 24, 1657-1663.
8. Savarino, J.; Bhattacharya, S. K.; Morin, S.; Baroni, M.; Doussin, J. F., *J. Chem. Phys.* **2008**, 128, 194303-12.
9. Bhatia, S. C.; Hall, J. H., *J. Phys. Chem.* **1980,** 84, 3255-3259.
10. Davis, D. D.; Prusazcyk, J.; Dwyer, M.; Kim, P.,. *J. Phys. Chem.* **1974**, 78, 1775-1779.
11. Ghormley, J. A.; Ellsworth, R. L.; Hochanadel, C. J., *J. Phys. Chem.* **1973**, 77, 1341-1345.
12. Wu, C. H.; Morris, E. D.; Niki, H., *J. Phys. Chem.* **1973**, 77, 2507-2511.
13. Graham, R. A.; Johnston, H. S., *J. Chem. Phys*. **1974**, 60, 4628-4629.
14. Crutzen, P. J., *Q. J. ROY. METEOR. SOC.* **1970**, 96, 320-325.
15. Eisfeld, W.; Morokuma, K., *J. Chem. Phys.* **2001**, 114, 9430-9440.
16. Ogg, J. R. A., *J. Chem. Phys.* **1953**, 21, 2079-2079.
17. Guillory, W. A.; Johnston, H. S., *J. Chem. Phys.* **1965**, 42, 2457-2461.
18. Morris, J. E. D.; Johnston, H. S., *J. Chem. Phys.* **1967**, 47, 4282-4282.
19. Morris, V. R.; Bhatia, S. C.; Hall, J. H., *J. Phys. Chem.* **1987**, 91, 3359-3361.
20. Morris, V. R.; Bhatia, S. C.; Hall, J. H., *J. Phys. Chem.* **1990**, 94, 7414-7418.
21. Lee, E. P. F.; Wright, T. G., *Chem. Phys. Lett.* **2001**, 347, 429-435.

22. Olson, L. P.; Kuwata, K. T.; Bartberger, M. D.; Houk, K. N., *J. Am. Chem. Soc*. **2002**, 124, 9469-9475.

23. Li, Y.; Iwata, S., *Chem. Phys.* **1997**, 219, 209-220.

24. Dutta, A. K.; Vaval, N.; Pal, S., *J. Chem. Theory Comput*. **2012**,. 8, 1895-1901.

25. Eisfeld, W.; Morokuma, K., *J. Chem. Phys.* **2003**, 119, 4682-4688.

26. Lauderdale, W. J.; Stanton, J. F.; Gauss, J.; Watts, J. D.; Bartlett, R. J., *Chem. Phys. Lett.* **1991**, 187, 21-28.

27. Lauderdale, W. J.; Stanton, J. F.; Gauss, J.; Watts, J. D.; Bartlett, R. J., *J. Chem. Phys.* **1992**, 97, 6606-6620.

28. Gauss, J.; Stanton, J. F.; Bartlett, R. J., *J. Chem. Phys.* **1991**, 95, 2639-2645.

29. Friedl, R. R.; Sander, S. P., *J. Phys. Chem*. **1987**, 91, 2721-2726.

30. Ishiwata, T.; Fujiwara, I.; Naruge, Y.; Obi, K.; Tanaka, I., *J. Phys. Chem.* **1983**, 87, 1349-1352.

31. Ishiwata, T.; Tanaka, I.; *J. Chem. Phys.* **1985**, 82, 2196-2205.

32. Weaver, A.; Arnold, D. W.; Bradforth, S. E.; Neumark, D. M.,. *J. Chem. Phys.* **1991**, 94, 1740-1751.

33. Kaldor, U., *Chem. Phys. Lett.* **1990**, 166, 599-601.

34. Eisfeld, W.; Morokuma, K., *J. Chem. Phys.* **2000**, 113, 5587-5597.

35. Rittby, M.; Bartlett, R. J., *J. Phys. Chem.* **1988**, 92, 3033-3036.

36. Scuseria, G. E., *Chem. Phys. Lett.* **1991**, 176, 27-35.

37. Watts, J. D.; Gauss, J.; Bartlett, R. J., *J. Chem. Phys.* **1993**, 98, 8718-8733.

38. Lee, T. J.; Taylor, P. R., *Int. J. Quant. Chem.* **1989**, 36, 199-207.

39. Paldus, J.; Li, X., A Critical Assessment of Coupled Cluster Method in Quantum Chemistry. *In Advances in Chemical Physics*, John Wiley & Sons, Inc.: **2007**; pp 1-175.

40. Durand, P., *Physical Review A* **1983**, 28, 3184-3192.

41. Durand, P.; Malrieu, J.-P., Effective Hamiltonians and Pseudo-Operators as Tools for Rigorous Modelling. In Advances in Chemical Physics, John Wiley & Sons, Inc.: 2007; pp 321-412.

42. Hurtubise, V.; Freed, K. F., The Algebra of Effective Hamiltonians and Operators: Exact Operators. In *Advances in Chemical Physics*, John Wiley & Sons, Inc.: **2007**; pp 465-541.

43. Mášik, J.; Hubač, I., Multireference Brillouin-Wigner Coupled cluster theory. Single-root approach. In *Advances in Quantum Chemistry*, John R. Sabin, M. C. Z., Erkki Brändas, S. Wilson ,J. Maruan,i Y. G. Smeyers, P. J. Grout; , R. M., Eds. Academic Press: **1998**; Vol. Volume 31, pp 75-104.

44. Pittner, J.; Nachtigall, P.; Carsky, P.; Masik, J.; Hubac, I., *J. Chem. Phys.* **1999**, 110, 10275-10282.

45. Chattopadhyay, S.; Mahapatra, U. S.; Mukherjee, D., *J. Chem. Phys.* **1999**, 111, 3820-3831.

46. Chattopadhyay, S.; Sinha Mahapatra, U.; Datta, B.; Mukherjee, D., + *Chem. Phys. Lett.***2002**, 357, 426-433.

47. Evangelista, F. A.; Allen, W. D.; Schaefer, H. F.; III, *J. Chem. Phys.* **2007**, 127, 024102-17.

48. Evangelista, F. A.; Simmonett, A. C.; Allen, W. D.; Schaefer, H. F.; III; Gauss, J.,. *J. Chem. Phys.* **2008**, 128, 124104-13.

49. Hanrath, M., *J. Chem. Phys.* **2005**, 123, 084102-12.

50. Hanrath, M., *J. Chem. Phys.* **2008**, 128, 154118-10.

51. Evangelista, F. A.; Gauss, J., *J. Chem. Phys*. **2011**, 134, 114102-15.

52. Hanauer, M.; Kohn, A., J. Chem. Phys. **2011**, 134, 204111-20.

53. Balkova, A.; Bartlett, R. J., *J. Chem. Phys.* **1994**, 101, 8972-8987.

54. Balkova, A.; Kucharski, S. A.; Meissner, L.; Bartlett, R. J., *J. Chem. Phys.* **1991**, 95, 4311-4316.

55. Jeziorski, B.; Monkhorst, H. J., *Phys. Rev. A* **1981**, 24, 1668-1681.

56. Piecuch, P.; Paldus, J., *Phys. Rev. A* **1994**, 49, 3479-3514.

57. Haque, A.; Kaldor, U., *Chem. Phys. Lett.***1985**, 120, 261-265.

58. Kaldor, U.; Haque, A., *Chem. Phys. Lett*.**1986**, 128, 45-48.

59. Kutzelnigg, W., *J. Chem. Phys.* **1982,** 77, 3081-3097.

60. Lindgren, I.; Mukherjee, D., *Phys. Rep.* **1987**, 151, 93-127.

61. Mukherjee, D., *Pramana* **1979**, 12, 203-225.

62. Mukherjee, D.; Pal, S., Use of Cluster Expansion Methods in the Open-Shell Correlation Problem. In *Advances in Quantum Chemistry*, Per-Olov, L. w., Academic Press: 1989; Volume 20, pp 291-373.

63. Pal, S.; Rittby, M.; Bartlett, R. J.; Sinha, D.; Mukherjee, D.,. *J. Chem. Phys*. **1988**, 88, 4357-4366.

64. Pal, S., *Mol. Phys.* **2010**, 108, 3033-3042.

65. Malrieu, J. P.; Durand, P.; Daudey, J. P.,. *J. Phys. A* **1985**, 18, 809.

66. Meissner, L., *J. Chem. Phys* **1998**, 108, 9227-9235.

67. Sekino, H.; Bartlett, R. J., *Int. J. Quant. Chem.* **1984**, 26, 255-265.

68. Stanton, J. F.; Bartlett, R. J., *J. Chem. Phys.* **1993**, 98, 7029-7039.

69. Nooijen, M.; Bartlett, R. J., *J. Chem. Phys.* **1995**, 102, 3629-3647.

70. Stanton, J. F.; Gauss, J., *J. Chem. Phys.* **1994**, 101, 8938-8944.

71. Kowalski, K.; Piecuch, P., *Chem. Phys. Lett*. **2001**, 347, 237-246.

72. Stanton, J. F., *J. Chem. Phys.* **1993**, 99, 8840-8847.

73. Stanton, J. F.; Gauss, J., *J. Chem. Phys.* **1994,** 100, 4695-4698.

74. Stanton, J. F.; Gauss, J., *Theor. Chem. Acc.***1995**, 91, 267-289.

75. Musial, M.; Bartlett, R. J., *J. Chem. Phys.* **2008**, 129, 134105-12.

76. Bernholdt, D. E.; Bartlett, R. J., A Critical Assessment of Multireference-Fock Space CCSD and Perturbative Third-Order Triples Approximations for Photoelectron Spectra and Quasidegenerate Potential Energy Surfaces. In *Advances in Quantum Chemistry*, Per-Olov, L., Ed. Academic Press: **1999**; Vol. Volume 34, pp 271-293.

77. Ghose, K. B.; Pal, S.,. *J. Chem. Phys.* **1992**, 97, 3863-3864.

78. Musial, M., *J. Chem. Phys.* **2012**, 136, 134111-14.

79. Musial, M.; Kucharski, S. A.; Zerzucha, P.; Kus, T; Bartlett, R. J., *J. Chem. Phys.* **2009**, 131, 194104-10.

80. Pal, S.; Rittby, M.; Bartlett, R. J.; Sinha, D.; Mukherjee, D., *Chem. Phys. Lett.* **1987**, 137, 273-278.

81. Vaval, N.; Ghose, K. B.; Pal, S.; Mukherjee, D., *Chem. Phys. Lett*. **1993**,

209, 292-298.

82. Vaval, N.; Pal, S.; Mukherjee, D., *Theor. Chem. Acc.* **1998**, 99, 100-105.

83. Bag, A.; Manohar, P. U.; Vaval, N.; Pal, S., *J. Chem. Phys.* **2009**, 131, 024102-8.

84. Barysz, M.; Rittby, M.; Bartlett, R. J., *Chem. Phys. Lett.* **1992**, 193, 373-379.

85. Bhattacharya, D.; Vaval, N.; Pal, S., *J. Chem. Phys.* **2012**, 138, 094108-9.

86. Manohar, P. U.; Pal, S., *Chem. Phys. Lett.* **2007**, 438, 321-325.

87. Ravichandran, L.; Vaval, N.; Pal, S., *J. Chem. Theory Comput.* **2011**, 7, 876-883.

88. The EOMCC method is equivalent to the FSMRCC methods for principle peaks in (1,0) and (0,1) sector(see ref 75). Therefore ,the EOMIP-CCSD method has been used for FSMRCCSD optimization and frequency calculations.

89. J.F. Stanton, J. Gauss., M.E. Harding, P.G. Szalay; w. c. f. A.A. Auer, R. J. B., U. Benedikt, C. Berger, D.E. Bernholdt, Y.J. Bomble, L. Cheng, O. Christiansen, M. Heckert, O. Heun, C. Huber, T.-C. Jagau, D. Jonsson, J. Jusélius, K. Klein, W.J. Lauderdale, D.A. Matthews, T. Metzroth, L.A. Mück, D.P. O'Neill, D.R. Price, E. Prochnow, C. Puzzarini, K. Ruud, F. Schiffmann, W. Schwalbach, S. Stopkowicz, A. Tajti, J. Vázquez, F. Wang, J.D. Watts and the integral packages MOLECULE (J. Almlöf and P.R. Taylor), PROPS (P.R. Taylor), ABACUS (T. Helgaker, H.J. Aa. Jensen, P. Jørgensen, and J. Olsen), and ECP routines by A. V. Mitin and C. van Wüllen. CFOUR. In a quantum chemical program package, 2009.

90. For ,one valence problem the model space is complete by definition .Therefore, for (1,0)and (0,1)sectors of FSMRCC , the results are independent of the choice of model space. However, that is not true for two valence problem, where the model space is quasi-complete. Therefore , in (1,1) sector of FSMRCC the result varies with choice of model space(see ref 63).

91. Frisch, M. J.; Trucks, G. W.; Schlegel, H. B.; Scuseria, G. E.; Robb, M. A.; Cheeseman, J. R.; Scalmani, G.; Barone, V.; Mennucci, B.; Petersson, G. A. et. al.

Gaussian 09, Revision B.01. In Gaussian 09, Revision B.01, Gaussian, Inc., Wallingford CT, Wallingford CT, 2009.

92. Kendall, R. A.; Dunning, J. T. H.; Harrison, R. J., *J. Chem. Phys.* **1992**, 96, 6796-6806.

93. Bak, K. L.; JØrgensen, P.; Olsen, J.; Helgaker, T.; Klopper, W., *J. Chem. Phys*. **2000**, 112, 9229-9242.

94 Halkier, A.; Helgaker, T.; JØrgensen, P.; Klopper, W.; Koch, H.; Olsen, J.; Wilson, A. K., *Phys. Lett.* **1998**, 286, 243-252.

95. Helgaker, T.; Klopper, W.; Koch, H.; Noga, J., *J. Chem. Phys.* **1997**, 106, 9639-9646.

96. Peterson, K. A.; Woon, D. E.; Dunning, T. H., *J. Chem. Phys.* **1994**, 100, 7410-7415.

97 Kamiya, M.; Hirata, S., *J. Chem. Phys.* **2006**, 125, 074111-14.

98. Laidig, W. D.; Saxe, P.; Bartlett, R. J., *J. Chem. Phys.* **1987**, 86, 887-907.

99. Stanton, J. F.; Gauss, J., *J. Chem. Phys.* **1999**, 111, 8785-8788.

100. Effect of partial triples to FSMRCC has been considered through continuum orbital approach in EOMCCSDT-3.See ref 99.

101. Dutta, A. K.; Dar, M; Vaval, N.; Pal, S., *J. Phys. Chem. A* **2014**, 118, 1350-1362.

Chapter 4

EOMIP-CCSD(2): an efficient N^5 scaling method for structure and properties of doublet radicals

"When we build, let us think that we build for ever"

John Ruskin

The Seven Lamps of Architecture

In this chapter, we present a benchmark study on the performance of the EOMIP-CCSD(2) method for computation of structure and properties of doublet radicals. The EOMIP-CCSD(2) method is a second-order approximation to the standard EOMIP-CCSD method. By retaining the black box nature of the standard EOMIP-CCSD method and adding favorable N^5 scaling, the EOMIP-CCSD(2) method can become the method of choice for predicting the structure and spectroscopic properties of large doublet radicals. The EOMIP-CCSD(2) method overcomes the typical problems associated with the standard single-reference *ab-initio* treatment of doublet radicals. We compare our results for geometries and harmonic vibrational frequencies with those obtained using the standard EOMIP-CCSD method, as well as unrestricted Hartree–Fock (UHF)- and restricted open-shell Hartree–Fock (ROHF)-based single-reference coupled cluster and second order many-body perturbation theory (MBPT(2)) methods. The effect of the basis set on the quality of the results has been studied using a hierarchy of Dunning's correlation-consistent aug-cc-pVXZ (X = D, T, Q) basis sets. Numerical results show that the EOMIP-CCSD(2) method, despite its N^5 scaling, gives better agreement with experimental results, compared to the UHF- and ROHF-based MBPT(2), as well as the single-reference coupled cluster methods.

4.1 Introduction:

In recent times, *ab-initio* quantum chemistry has become the trusted companion of researchers for the elucidation of structures and properties of complicated molecules. Among the plethora of methods available, the single-reference coupled cluster method [1, 2], because of its systematic treatment of electron correlation, has emerged as the method of choice for accurate prediction of structure [3-5], properties [6], and vibrational spectra [7-9] of closed-shell molecules. The extension of the single-reference coupled cluster method to open-shell systems, based on unrestricted Hartree–Fock (UHF) [10] or restricted open-shell Hartree–Fock (ROHF) [11, 12] references, has also been achieved. However, the single-reference coupled cluster method, even in the singles and doubles approximation, scales as N^6 power with the basis set, whereas the inclusion of partial triples [13-15] (CCSD(T)) increases the scaling to N^7. The development of parallel codes and a rapid increase in computational power, in recent times, may have made coupled cluster calculations for small- and medium-sized molecules possible (at least in small basis sets). However, the structure and property calculations of medium-sized molecules, in moderately sized or big basis sets, are still not routine. Moreover, N^6 scaling is computationally demanding to use in quantum molecular dynamics calculations, which involves multiple force constant calculations and is essential for predicting the time evolution and temperature effect on the molecules. Thus, a theoretical method with scaling lower than N^6, that is still able to predict the properties of the molecule accurately, is the need of the day.

The standard second order many-body perturbation theory (MBPT(2)) method offers the first correlation correction to the energy over the Hartree–Fock method and scales as N^5 power with the basis set. Over the years, the method has been extensively used as an accurate tool for the *ab-initio* investigation on a large variety of closed-shell molecules. But, standard UHF-based [16] or ROHF-based [17, 18] MBPT(2) methods perform poorly in the case of open-shell doublet radicals, because of multiple problems [19-21] associated with the open-shell

single reference wave function, such as spin contamination [22, 23], symmetry breaking [24], near-singularities of the HF solution [25, 26], pseudo-Jahn–Teller effects [27], and the presence of multi-reference character.

However, ab initio investigation of doublet radicals is extremely important, because of the key role of the radicals in biology and chemistry. The high energy and short lifetime of a doublet radical makes experimental characterization often tedious, and sometimes impossible. Theoretical calculations [28-34] can be helpful to understand the doublet radicals and their mechanism in chemistry and biology. However, this is more difficult for open-shell molecules, mainly because of two reasons:(1) The radical wave function has a more-complicated spin structure than that in the closed-shell molecules, in which all electrons are paired. (2) Two or more configurations make dominant contributions to the reference wave function in the radicals.

The multi-reference perturbation theory (MRPT) method [35-38], the multi reference configuration interaction (MRCI) method [39, 40], and the multi-reference coupled cluster (MRCC) method [41-51] can avoid the above-mentioned problems. However, the results are strongly dependent on the choice of active space, which requires experience and expertise. Subsequently, these calculations cannot be performed with a mere “push of a button”.

On the other hand, the equation of motion coupled cluster (EOM-CC) method [52-55] incorporates a balanced description of the dynamic and nondynamic correlation and presents a black box approach for the accurate calculation of energy [53-58], structure [59-61], and properties [62], of open-shell molecules and molecular excited states. The EOMIP-CCSD method has been successfully used[63-67] to investigate the structure and properties of problematic doublet radicals. However, despite having otherwise favorable characteristics, the EOMIP–CCSD method still has the problem of N^6 scaling. Stanton and Gauss [68]

proposed an N^5-scaled size-extensive modification of the standard EOMIP-CCSD method, by approximating the effective Hamiltonian based on perturbative orders. They have coined the term EOMIP-CCSD(2) for this black box method, and they have shown favorable numerical results for the formyl radical in the DZP basis set. One molecule is too inadequate to make a benchmark and the basis set used was too small to make a definitive conclusion. However, their results were very promising and if the trend generally holds, the EOMIP-CCSD(2) method can become the method of choice for the theoretical treatment of doublet radicals. The objective of this chapter is to perform a benchmark EOMIP-CCSD(2) study on the geometry and infrared (IR) spectroscopic properties for a variety of doublet radicals and compare the performance relative to experiment, with those obtained by standard EOM-IP-CCSD, single-reference MBPT(2), and CCSD methods.

The Chapter is organized as follows. Section 4.2 gives a brief discussion on the theory of the EOMIP-CCSD(2) method and computational details of the calculations. The trends in the numerical results for the geometry and IR frequency of a set doublet radicals are discussed in section 4.3. Section 4.4 contains the conclusions.

4.2 Theory and Computational Details

The non variational coupled cluster method generates the correlated wave function from a single Slater determinant reference state by the action of an exponential operator.

$$|\psi\rangle = e^{T} |\phi_0\rangle \tag{4.1}$$

$|\phi_0\rangle$ is generally, but not necessarily, the Hartree-Fock determinant and $T=T_1+T_2+T_3+\ldots\ldots T_n$, where

$$\hat{T}_1 = \sum_{ia} t_i^a \left\{ a_a^\dagger a_i \right\},$$

$$\hat{T}_2 = \frac{1}{4} \sum_{ijab} t_{ij}^{ab} \left\{ a_a^\dagger a_b^\dagger a_j a_i \right\} , \tag{4.2}$$

$$\hat{T}_3 = \frac{1}{6} \sum_{ijkabc} t_{ijk}^{abc} \left\{ a_a^\dagger a_b^\dagger a_c^\dagger a_k a_j a_i \right\}$$

These amplitudes are generally obtained by the iterative solution of a system of coupled nonlinear equations. Extending T up to the nth order, where n equals the total number of electrons in the system, leads to the full CI solution. However, for practical applications, T is truncated to finite order. The exponential structure of the correlation operator ensures the size extensivity, even at the truncated level of T. The truncation of T amplitudes at T_1 and T_2 leads to the popular coupled cluster singles and doubles (CCSD) approximation, which scales as N^6 with the basis set (where N is the number of basis functions). The inclusion of higher excitations leads to a systematic improvement in accuracy, but at the expense of a substantial increase in computational cost. The CCSDT method[69, 70] scales as N^8 and the inclusion of quadruples excitation (CCSDTQ)[71] advances the computational scaling to N^{10}.

The coupled cluster method shares an intimate relationship with the many-body perturbation theory (MBPT) [72]. Suitable lower-order iterations of coupled cluster equations recover the various orders of MBPT. For example, the lowest-order approximation to the coupled cluster T_2 amplitudes leads to the standard MBPT(2) method.

The single-reference coupled cluster method includes dynamic correlations in a systematic way. However, it fails to account for the non-dynamic correlation, which arises due to the quasi-degenerate states that prevail in radicals, bond stretching, and molecular excited states. Consequently, the single-reference coupled cluster methods, especially in the CCSD approximation, perform poorly in the above-mentioned cases. A multi-reference coupled cluster (MRCC)

method[41-51] addresses both dynamic and non-dynamic correlations in a systematic way. However, it has the active space dependency problem, as discussed previously.

Along with the MRCC methods, the EOM-CC method is known for its balanced treatment of both dynamic and non-dynamic correlations. In the EOM-CC method, the final states are obtained by diagonalizing the similarity transformed Hamiltonian

$$\bar{H} = e^{-T} H e^{T} = \left(H e^{T} \right)_c \tag{4.3}$$

The subscript c in the above equation represents the connectedness of T with the H. Since e^{T} is not unitary, $\bar{H}$ is not Hermitian. Therefore, the final states are represented by a biorthogonal set of bra and ket vectors, which are parameterized by left and right eigen vectors of $\bar{H}$, denoted by L and R respectively.

$$\left\langle \Psi \right| = \left\langle \phi_0 \right| L e^{-T} \tag{4.4}$$

$$\left| \Psi \right\rangle = e^{T} R \left| \phi_0 \right\rangle \tag{4.5}$$

For ionization problem, $\left\langle \Psi \right|$ and $\left| \Psi \right\rangle$ do not correspond to particle conserving operators, but rather involve net creation (L) and annihilation (R) of one electron. L and R can be expressed in second quantized notation as follows.

$$L \equiv \sum_i l^i i^{\dagger} + \frac{1}{2} \sum_{ija} l^{ij}_a i^{\dagger} a j^{\dagger} \tag{4.6}$$

$$R \equiv \sum_i r_i i + \frac{1}{2} \sum_{ija} r^a_{ij} a^{\dagger} i j \tag{4.7}$$

Diagonalization of $\bar{H}$ in the (N-1) electron space, gives the singly ionized states of a N electron state and the theory is called EOMIP-CC. It is equivalent to the

(0,1) sector of the Fock space multi reference coupled cluster (FSMRCC) method for the principal ionizations.[73] FSMRCC has been successfully implemented for spectra, [47,49,51,74-76] properties[77] and transition moments [78,79].

The energy in EOMIP-CC can be written in the illustrative functional form.

$$E = \langle \phi_0 | L\bar{H}R | \phi_0 \rangle = \langle \phi_0 | Le^{-T} He^{T} R | \phi_0 \rangle \tag{4.8}$$

The EOMIP-CC method is commonly used in singles and doubles approximation (EOMIP-CCSD). It has the same N^6 scaling as that of the single reference CCSD method and similar storage requirements, which prohibit its applications beyond the first row atoms, in a moderate basis set. Thus, it is highly desirable to develop methods, similar in spirit with the standard EOMIP-CCSD but with lower computational scaling and smaller storage requirements. Nooijen and Snijders[80] were the first to propose a simplification[81,82] to the standard EOM-IP-CCSD method, by approximating the full CCSD similarity transformed Hamiltonian as

$$\bar{H} \equiv \bar{H}_{NS} = e^{-T^{[1]}} He^{T^{[1]}} \tag{4.9}$$

$\bar{H}_{NS}$ is complete up to the first order in correlation and contains selective contributions from higher order terms. Diagonalization of $\bar{H}_{NS}$ in the (N-1) electron space leads to the loss of size- extensivity in energy. Nooijen and Snijders had eliminated the problem by diagonalizing matrix elements of a modified operator *A*, in place of the $\bar{H}_{NS}$, where

$$A_{\mu\nu} = \langle \phi_0 | \Omega_\mu \left[\bar{H}_{NS}, \Omega_\nu^\dagger \right] | \phi_0 \rangle \tag{4.10}$$

$\Omega^\dagger = \{ a_i ; a_i a_a^\dagger a_j \}$ and it represents the elements of the set of creation operator string that maps the $|\phi_0\rangle$ into the determinants spanning the diagonalization space. The commutator in the equation accounts for all the missing second order contributions to $\bar{H}_{NS}$, whereas, third or higher order terms in A do not contribute to the truncated diagonalization problem. This ensures the size-extensivity in energy.

However, the method does not provide a clear definition for the total energy, thus, becomes unsuitable for studying properties of the final state.

Stanton and Gauss provided an alternative approach[11] for approximating the conventional EOM-CCSD method. They have expanded the effective Hamiltonian in a perturbation series

$$\bar{H} = \left(He^{T} \right)_{c} = \bar{H}^{[1]} + \bar{H}^{[2]} + \bar{H}^{[3]} + ... + \bar{H}^{[n]} \tag{4.11}$$

The bracketed superscript in the above equation represents the order in perturbation and subscript c represents the connectedness of T with H. This leads to a set of hierarchical approximations to the full $\bar{H}$ and the diagonal representation of the modified effective Hamiltonian offers a set of hierarchical approximations to the corresponding EOM-CC final states, known as EOMCCSD(n). At a large value of n, the $\bar{H}^{[n]}$ converges to the full $\bar{H}$ and consequently EOMCCSD(n) converges to the standard EOM-CCSD. The approximate similarity transformed Hamiltonian, truncated at the n^{th} order, includes only the terms up to the order n in perturbation, which ensures the size-extensivety of the final energy for all values of n. Truncation at n=2, leads to EOMCCSD(2), with a MBPT(1) ground state reference wave function and MBPT(2) ground state energy. The EOMCCSD(2) method provides energy difference value identical to that of the Nooijen and Snijders's method and has the additional advantage of a clearly defined final energy.

The diagonalization of $H^{[2]}$ in a space spanned by a subset of $(N-1)$ determinants leads to the final ionized states of N-electron molecular problem, which can be performed by slight modification of any standard EOMIP-CCSD code. The explicit derivation of the expressions has been presented in ref [68]. The EOMIP-CCSD(2) method is naturally spin-adapted and equipped to deal with multi-reference situations, and, therefore, it is free from the problems that are associated with the standard single-reference treatment for doublet radicals.

The truncation of the effective Hamiltonian, based on perturbation order, leads to an obvious loss in accuracy. However, it gains significant computational simplifications, which lead to advantages in terms of both CPU timing and storage. The computational requirements of the standard EOMIP-CCSD method are dominated by the *N*-electron reference state CCSD calculation. Approximating the reference state using the MBPT(1) wave function reduces the computational scaling of the reference state calculation to N^5, as opposed to the iterative N^6 scaling of the CCSD reference-state calculation. Now, in IP calculation, the diagonalization (using Davidson's iterative method) of the $\bar{H}$ scales as N^5 and the superficially N^6 scaling intermediates can also be computed in an iterative N^5 scaling algorithm, by calculating them on the fly.[83] Thus, overall, the EOMIP–CCSD(2) method scales as N^5, which is vastly more economical[84, 85] than the standard EOMIP-CCSD method.

The terms containing the (*ab*|*cd*)-type integral present the most computationally demanding part of the coupled cluster iterations. The large file size of the four particle integrals often becomes the limiting factor for storage and memory. It also slows the overall speed of the calculation, by creating input/output (I/O) bottlenecks, even for small molecules. Now, (*ab*|*cd*) integrals only contribute to the reference-state CCSD calculation and, consequently, remain totally absent in the EOM part for the ionization problem. Thus, approximating the reference-state wave function at MBPT(1) leads to a significant savings in terms of disk space, since it does not require the (*ab*|*cd*) integrals. The favorable N^5 scaling and reduced storage requirements[86] make the EOMIP-CCSD(2) method applicable to the systems of considerably large dimension, where the use of the normal EOMIP-CCSD method is not possible.

T1 diagnosis values presented in the chapter are calculated using Gaussian 09.[87] All the other results presented in the chapter are calculated using CFOUR.[88] All of the electrons are used in the correlation calculations. Dunning's correlation-consistent aug-cc-pVXZ (X = D, T, Q) basis sets[89] are used in the calculations.

Equilibrium geometries (r_e) without any vibrational averaging and harmonic vibrational frequencies are used for comparison with the experiments.

4.3 Results and Discussion

To compare the timing of EOMIP-CCSD(2) with standard EOMIP-CCSD, we have calculated the ionization potential of water clusters($(H_2O)_n$, where n = 1–8) in cc-pVDZ basis set. The wall timings are presented in Table 4.1. The EOMIP-CCSD(2) method is found to be computationally significantly less expensive than the EOMIP-CCSD method.

Table 4.1 : Wall Timings for the EOMIP-CCSD(2) and EOMIP-CCSD Method[a,b] in the cc-pVDZ Basis Set

	Wall Timing (s)	
Number of H_2O units	**EOMIP-CCSD**	**EOMIP-CCSD(2)**
1	1.42	1.40
2	5.30	2.30
3	20.22	4.77
4	83.64	14.63
5	236.00	39.86
6	550.86	81.69
7	1385.21	223.21
8	3964.00	700.91

a : All the calculations were performed using an i7 desktop with 3.40 GHz CPU speed and 16 GB of RAM. Calculations were performed using single core.

b : Calculations were performed assuming C_1 symmetry.

To benchmark the reliability of the EOMIP-CCSD(2) method, we have calculated the geometry and vibrational frequencies of NO_2, NO_3, trans ONOO, NO, CN, F_2^+,

CO^+, O_2^+, and N_2^+ in aug-cc-pVDZ, aug-cc-pVTZ, and aug-cc-pVQZ basis. The above-mentioned radicals present a significant challenge for conventional ab initio methods. In all of the cases, the results are compared with those obtained by standard EOMIP-CCSD, UMP2, ROMP2, UCCSD, and ROCCSD methods, as well as with available experimental data.

4.3.1 Nitrogen Dioxide (NO_2)

Nitrogen dioxide (NO_2) is a very important molecule in atmospheric chemistry; consequently, it is subjected to many computational investigations [63, 90-92]. The triplet instabilities and second-order Jahn–Teller (SOJT) effect in NO_2, lead to the mixing of $^2A_1$ and $^2B_2$ states, which makes the description of vibrational modes—especially the asymmetric stretching problematic. The T1 diagnosis value of 0.026 (Table 4.2) indicates significant multi-reference character of the molecule. Table 4.3 presents the geometry and the vibrational frequencies for NO_2.

In the aug-cc-pVDZ basis set, the EOMIP-CCSD(2) method shows excellent agreement with the experiment for both bond lengths ($|\Delta r_e| = 0.006$ Å) and bond angles ($|\Delta_{angle}| = 0.3°$). The method also provides very good agreement with the experiment[93, 94] for the bending mode of vibration ($|\Delta\omega_e| = 6$ cm^{-1}). However, it overestimates both symmetric stretching modes (($|\Delta\omega_e| = 45$ cm^{-1}) and asymmetric stretching modes ($|\Delta\omega_e| = 120$ cm^{-1}), which are consistent with the previous theoretical reports.[61, 88] The performance of the EOMIP-CCSD method is similar to that of the EOMIP-CCSD(2) method, for both bond lengths ($|\Delta r_e| = 0.007$ Å) and bond angles ($|\Delta_{angle}| = 0.6°$). The asymmetric stretching ($|\Delta\omega_e| = 85$ cm^{-1}) mode is comparatively well described in the EOMIP-CCSD method. However, it shows more error than the EOMIP-CCSD(2) method for the bending mode ($|\Delta\omega_e| = 22$ cm^{-1}), as well as symmetric stretching mode ($|\Delta\omega_e| = 88$ cm^{-1}).

Table 4.2 : T1 Diagnosis Value of the Doublet Radicals

Molecule	T1 diagnosis
NO	0.023
CN	0.050
F_2^+	0.013
CO^+	0.046
O_2^+	0.014
N_2^+	0.022
NO_2	0.026
NO_3	0.035
ONOO	0.034

The UCCSD method performs very poorly for both geometry and vibrational frequencies; it especially underestimates the asymmetric stretching mode by a large value of 726 cm^{-1}. This is due to instabilities associated with the unrestricted reference wave function, which is indicated by a negative eigen value of the orbital rotation Hessian. The same reason leads to the disastrous performance of the UMP2 method. The performance of the ROCCSD method is similar to that of the EOMIP-CCSD method, with regard to geometry and harmonic vibrational frequencies. The ROMP2 method, on the other hand, shows more error than the EOM and ROCCSD methods for bond length ($|\Delta r_e|$ = 0.022 Å) and bond angle ($|\Delta_{angle}|$ = 1.3°), but performs significantly better than both the UCCSD and UMP2 methods. The ROMP2 method performs surprisingly well for bending and symmetric stretching modes of vibration. However, it significantly overestimates the asymmetric stretching mode ($|\Delta\omega_e|$ = 210 cm^{-1}).

Table 4.3 : Geometry and Harmonic Vibrational Frequency of Nitrogen Dioxide (NO_2)

method	bond length (Å)	bond angle (θ)	ω_1 (cm^{-1})	ω_2 (cm^{-1})	ω_3 (cm^{-1})
		aug-cc-pVDZ Basis Set			
EOMIP-CCSD(2)	1.200	134.2	756	1370	1754
EOMIP-CCSD	1.201	133.3	772	1413	1719
UCCSD	1.299	124.51	577	955	908*i*
ROCCSD	1.197	134.7	767	1412	1721
UMP2	1.284	125.0	671	1138	1629
ROMP2	1.216	132.6	753	1317	1844
		aug-cc-pVTZ Basis Set			
EOMIP-CCSD(2)	1.186	134.9	769	1384	1784
EOMIP-CCSD	1.186	133.7	795	1425	1745
UCCSD	1.283	124.9	139*i*	596	1190
ROCCSD	1.181	135.2	785	1438	1762
UMP2	1.270	125.4	609	1273	1071*i*
ROMP2	1.201	133.2	763	1329	1844
		aug-cc-pVQZ Basis Set			
EOMIP-CCSD(2)	1.185	135.7	773	1391	1782
EOMIP-CCSD	1.185	133.4	802	1450	1744
UCCSD	1.282	124.8	169*i*	603	1199
ROCCSD	1.180	135.0	790	1443	1762
UMP2	1.269	125.23	614	1279	1073*i*
ROMP2	1.200	133.0	767	1331	1840
		Experimental Results			
		1.194[a]	133.9[a]	750[b]	1325[b]

a : Values taken from ref 93. b:Values taken from ref 94.

Upon moving from the aug-cc-pVDZ basis set to the aug-cc-pVTZ basis set, the bond length shrinks and the bond angles are stretched for all of the theoretical methods. The EOMIP-CCSD(2) method continues to give a similar performance to that of the EOMIP-CCSD method, with regard to geometry, but gives better agreement with the experiment in the case of harmonic vibration frequencies. However, both methods overestimate the experimental asymmetric stretching frequency. The UCCSD method continues to give poor performance, with regard to geometry and harmonic vibrational frequencies. The imaginary value of the bending mode indicates that the optimized geometry in the UCCSD method is not actually the minimum on the potential energy surface, but rather is a first-order saddle point. The ROCCSD method avoids the disastrous failure of the UCCSD method, but gives inferior performance, compared to the EOM methods. The UMP2 method suffers from the spin contamination problem, similar to that of the UCCSD method; consequently, the results show a large deviation from the experimental bond length and bond angle. The asymmetric stretching mode in the UMP2 method shows an imaginary value, indicating that the geometry is a first-order saddle point. The ROMP2 method gives remarkable agreement with the experimental values with regard to geometry, as well as bending and stretching modes of vibration, but it overestimates the asymmetric stretching mode of vibration, and shows greater error ($|\Delta\omega_e|$ = 204 cm^{-1}) than the EOM-based methods.

The same trend persists in the aug-cc-pVQZ method, where the geometries and IR frequencies for all of the methods show very little deviation from their corresponding values in the aug-cc-pVTZ basis set.

3.3.2 Nitrogen Trioxide (NO_3)

The ground-state geometry of the nitrogen trioxide (NO_3) radical has been an issue of long-standing debate. Experimental studies [95-99] have provided evidence in

favor of D_{3h} geometry, whereas various theoretical studies have predicted different minimum energy structures for the molecule. Three structures have been found to be energetically most favorable: (a) a highly symmetric D_{3h} structure, (b) a C_{2v} structure with two long bonds and one short bond (2L1S), and (c) C_{2v} structure with one long bond and two short bonds (1L2S). Initial MCSCF studies [100] have predicted a Y-shaped structure for the NO_3 radical. In 1992, Bartlett and co-workers [101] have reported the C_{2v} structure to be 2.5 kcal/mol lower in energy than the more-symmetric D_{3h} structure in the B-CCD level of theory. Crawford and Stanton [102] latter revised this ordering, by placing the D_{3h} structure 0.5 kcal/mol below the C_{2v} structure in the B-CCD(T) method. The T1 diagnosis value of 0.035 (Table 4.2) indicates significant multi reference character for the species. Fock space multi reference coupled cluster (FSMRCC) calculations by Kaldor [103)], and MRCI calculations by Morkuma and Eisfield [104], both resulted in a D_{3h} ground-state geometry for the NO_3 radical.

The EOMIP-CCSD(2) and EOMIP-CCSD methods predict a D_{3h} ground-state geometry. In the aug-cc-pVDZ basis set, the EOMIP-CCSD(2) method shows better agreement with the experimental bond length than the EOMIP-CCSD method. Both methods slightly underestimate the bond length in the aug-cc-pVTZ and aug-cc-pVQZ basis sets. However, the EOMIP-CCSD(2) method continues to give better agreement with the experiment than the EOMIP-CCSD method. The UCCSD and ROCCSD methods predict a C_{2v} minimum energy structure (2L1S) for the ground state and both the methods predict identical geometries. In the aug-cc-pVDZ basis set, both methods overestimate the experimental bond length, in the case of the long bonds (2L) and underestimate the experimental bond length in the case of the short bond (1S). The two long bonds shrink in the aug-cc-pVTZ and aug-cc-pVQZ basis sets, bringing them closer to the experimental value. However, the use of a large basis set also shrinks the shorter bond, taking it further away from the experimental value. The UMP2 and ROMP2 methods follow the trend of their coupled cluster analogues, only with a larger error bar.

Table 4.4 : Geometry and Harmonic Vibrational Frequency of Nitrogen Trioxide (NO_3)

	Bond Length (Å)		Vibrational Frequency (cm^{-1})					
method	**L1**	**L2**	**ω_1 (asym bend)**	**ω_2 (asym bend)**	**ω_3 (umbr-ella)**	**ω_4 (sym strech)**	**ω_5 (asym stretch)**	**ω_6 (asym stretch)**
			aug-cc-pVDZ Basis Set					
EOMIP-CCSD(2)	1.240	1.240	163	163	783	1130	1198	1198
EOMIP-CCSD	1.235	1.235	310	310	813	1149	1183	1183
UCCSD	1.261	1.197	528	630	810	1129	1102	1667
ROCCSD	1.261	1.198	7792*i*	520	785	1116	1647	277833
UMP2	1.284	1.204	682	702	667	1058	791i	1650
ROMP2	1.267	1.220	521	655	833	1087	1642	2097
			aug-cc-pVTZ Basis Set					
EOMIP-CCSD(2)	1.228	1.228	66	66	800	1140	1176	1176
EOMIP-CCSD	1.221	1.221	305	305	836	1170	1191	1191
UCCSD	1.247	1.182	552*i*	857	826	1174	581	1700
ROCCSD	1.247	1.183	538	619	807	1139	998	1778
UMP2	1.270	1.191	701	908*i*	615	1081	716	1648
ROMP2	1.255	1.206	526	663	842	1097	1643	2123
			aug-cc-pVQZ Basis Set					
EOMIP-CCSD(2)	1.227	1.227	95	95	801	1142	1175	1175
EOMIP-CCSD	1.219	1.219	314	314	838	1174	1192	1192
UCCSD	1.246	1.182	547	7917	779	1152	1693	27249*i*
ROCCSD	1.246	1.182	442	623	809	1143	1005	1682
UMP2	1.269	1.190	703	910*i*	612	1085	718	1650
ROMP2	1.254	1.205	526	664	843	1099	1644	2126
			Experimental Results					
	1.240[a]	1.240[a]	250[b]	250[b]	762[c]	1060[c]	1480[c]	1480[c]

a : Values taken from ref 98. b : Values taken from ref 95. c : Values taken from ref 96.

The EOMIP-CCSD(2) method performs reasonably well for the IR frequencies of NO_3. It predicts the umbrella (ω_3) and the symmetric stretching (ω_4) mode of

vibrations with high accuracy. However, it underestimates the low-frequency asymmetric bending (ω_1 and ω_2) and high-frequency asymmetric stretching (ω_5 and ω_6) modes (see Table 4.4). The umbrella and symmetric stretching modes shift to higher values, when using larger basis sets; whereas, all of the other modes of vibration shrink to lower values. While the EOMIP-CCSD method shows significant improvement over the EOMIP-CCSD(2) method, for the asymmetric bending mode, it reduces the accuracy of the umbrella and symmetric stretching modes. Both EOMIP-CCSD(2) and EOMIP-CCSD methods, however, significantly underestimate the asymmetric stretching mode. Here, it should be noted that the experimental assignments of the asymmetric stretching at 1492 cm^{-1} is not unambiguous [64]. Detailed studies are required to make a concluding statement about these problematic modes, which are beyond the scope of the present study. The single-reference coupled cluster methods show large errors for the harmonic vibrational frequencies. The UCCSD method, in aug-cc-pVDZ basis, overestimates the two asymmetric bending modes and one of the asymmetric stretching modes, while it underestimates the other asymmetric stretching mode. These trends continue in the aug-cc-pVTZ basis, where the ω_1 shows an imaginary frequency, indicating that the geometry is a first-order saddle point. The UCCSD method in the aug-cc-pVQZ basis set shows a unphysical value for one of the asymmetric stretching modes (ω_2) and one of the asymmetric bending modes (ω_6) of vibration. The instability in the UHF reference wave function, indicated by the negative eigen value of the orbital rotation Hessian, leads to the catastrophic failure of the UCCSD method in the present case. The UMP2 method follows the same trend as that of its coupled cluster analogue and shows one imaginary frequency in all of the basis sets. The ROCCSD method shows an imaginary frequency for the asymmetric bending mode (ω_1) in the aug-cc-pVDZ basis set, indicating that the geometry is a first-order saddle point. It also gives an unphysical value for the asymmetric stretching mode (ω_6). Although these spurious results vanish at higher aug-cc-pVTZ and aug-cc-pVQZ basis sets, the calculated IR frequencies still show large deviations from the experimental results.

The ROMP2 method closely follows the trend of ROCCSD method, with the difference being that the former does not show any unphysical or imaginary frequencies in any of the basis sets used.

4.3.3 Trans Nitro Peroxide (ONOO)

The correlation of experiments and theory for the trans nitro peroxide has been a matter of long-standing debate [105, 106]. Bhatia and Hall [109)] have suggested a planar trans structure from IR spectroscopic investigation. However, later *ab-initio* studies [105, 108, 109], using different levels of theories, have shown contradictory results. The radical shows considerable multi-reference character (T1 diagnosis value = 0.034), making it a challenging case for standard ab initio methods. Geometry and IR frequencies of trans ONOO, computed at different levels of theory, are presented in Table 4.5. The EOMIP-CCSD(2) method shows an O–N bond length of 1.157 Å in the aug-cc-pVDZ basis set. The O–O bond length (1.285 Å) shows considerable elongation from the bare molecular oxygen bond length of 1.207 Å and, consequently, the N–O bond length (1.157 Å) decreases from the free nitric oxide bond length value of 1.160 Å. It indicates an electron transfer from the antibonding orbital of nitric oxide to the antibonding orbital of oxygen, leading to shrinkage of the former and stretching of the latter. In the EOMIP-CCSD(2) method, the IR frequency corresponding to the N–O bond stretching mode (ω_6) is underestimated by 40 cm^{-1}. The EOMIP-CCSD method predicts longer O–O and O–N bond lengths, compared to the EOMIP-CCSD(2) method. On the other hand, the N–O bond shrinks, from 1.157 Å to 1.149 Å, upon moving from the EOMIP-CCSD(2) method to the EOMIP-CCSD method, which leads to overestimation of experimental frequency (62 cm^{-1}) in the latter. The ROCCSD and ROMP2 methods follow the same trend as that of the EOMIP-CCSD method.

Table 4.5 : Geometry and Harmonic Vibrational Frequency of Trans Nitro Peroxide (ONOO)

	Bond Length (Å)			Bond Angle (deg)		Vibrational Frequency (cm^{-1})					
method	**O–O**	**N–O**	**O–N**	**N–O–O**	**O–N–O**	**ω_1**	**ω_2**	**ω_3**	**ω_4**	**ω_5**	**ω_6**
aug-cc-pVDZ Basis Set											
EOMIP-CCSD(2)	1.285	1.557	1.157	109.5	108.1	193	361	452	881	1287	1800
EOMIP-CCSD	1.298	1.598	1.149	106.6	108.2	150	351	421	848	1207	1902
UCCSD	1.216	3.316	1.159	88.3	166.1	61i	33	36	36	1581	1946
ROCCSD	1.352	1.605	1.143	110.1	108.3	192	260	368	701	929	1900
UMP2	1.259	3.146	1.141	73.4	171.0	8	58	65	170	1219	3658
ROMP2	1.328	1.762	1.137	110.9	108.7	170	226	310	675	913	1980
aug-cc-pVTZ Basis Set											
EOMIP-CCSD(2)	1.275	1.537	1.144	110.1	108.2	199	366	468	901	1307	1815
EOMIP-CCSD	1.287	1.556	1.136	107.4	108.3	158	368	450	870	1251	1925
UCCSD	1.196	3.224	1.142	79.3	169.2	102*i*	79	181	277	1646	1957
ROCCSD	1.281	1.582	1.136	107.8	108.2	181	280	338	723	1170	1867
UMP2	1.243	3.034	1.135	78.2	186.1	50	40	79	441	1329	3139
ROMP2	1.229	1.183	1.136	107.8	110.2	1916*i*	113	105	522	1055	1805
aug-cc-pVQZ Basis Set											
EOMIP-CCSD(2)	1.274	1.540	1.143	110.2	108.3	198	364	465	897	1307	1811
EOMIP-CCSD	1.287	1.557	1.135	107.5	108.3	157	368	451	870	1250	1919
UCCSD	1.196	3.332	1.141	79.6	169.6	17	34	43	53	1673	2000
ROCCSD	1.337	1.564	1.129	111.1	108.6	200	272	393	731	989	1912
UMP2	1.226	3.229	1.135	79.1	169.1	9*i*	41	50	63	1428	3169
ROMP2	1.227	1.849	1.136	108.2	110.2	117	197	202	700	1336	1924
Experimental Results											
											1840[a]

a : Value taken from ref 107. b : Diffused *g* functions were excluded from the basis

However, the UCCSD method predicts a weakly bound T-shaped geometry (Figure 4.1) with an elongated O–N bond length of 3.316 Å. The O–O and the N–O bond lengths are almost same as that of their free molecular form. The structure shows an imaginary frequency, which indicates that the geometry is a saddle point of order one. The IR frequency corresponding to the ω_6 mode shows a value of 1946 cm^{-1}, which is 106 cm^{-1} higher than the experimental value. The UMP2 method also shows a T-shaped structure, but with a larger O–O bond, and a shorter O–N bond, as well as a shorter N–O bond. The UMP2 method predicts an N–O bond stretching frequency of 3658 cm^{-1}, which is almost double the experimental frequency of 1840 cm^{-1}. The UHF instability, which is indicated by the negative value of the orbital rotation Hessian, is responsible for the unphysical behavior of the N–O stretching in the UMP2 method.

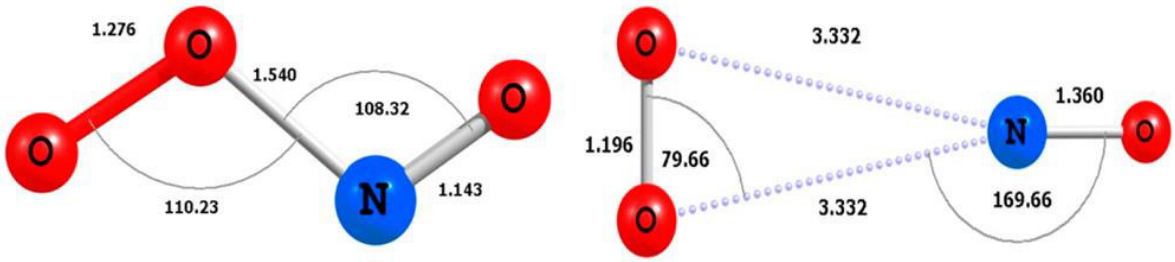

Figure 4.1 : EOMIP-CCSD(2) and UCCSD optimized structure of trans nitro peroxide (ONOO) in the aug-cc-pVQZ basis set.

The EOM methods, as well as the UCCSD method, lead to shrinkage of all of the bonds and an upward shifting of the IR frequencies in the aug-cc-pVTZ basis set. The ROCCSD and ROMP2 methods show similar trends for the bond length, but the IR frequency corresponding to the ω_6 mode undergoes a downward shift in both methods. The UMP2 method also shows a large downward shift of the ω_6 mode, but still overestimates the experimental frequency by more than a thousand wave numbers.

The results in the EOMIP-CCSD(2) and EOMCCSD methods in the aug-cc-pVQZ

basis set show very small deviations from those in the aug-cc-pVTZ basis set. The EOMIP-CCSD(2) method gives the best agreement ($|\Delta\omega_e|$ = 29 cm^{-1}) with the experimental frequency, among all the methods used. However, the UCCSD and UMP2 methods result in a longer O–N bond in the aug-cc-pVQZ basis set. It is interesting to note that both the N–O bond length and the N–O stretching frequency in the UCCSD and UMP2 methods are very similar to that in the free nitric oxide. It indicates that trans ONOO is a very weakly bound complex, contrary to the stable structure predicted by the EOM methods. In the aug-cc-pVQZ basis set, the ROCCSD method shows shrinkage of the N–O bond, which is reflected in the upward shift of the ω_6 mode. The ROMP2 method also results in an upward shift of the N–O stretching frequencies in the aug-cc-pVQZ basis set, but the N–O bond length remains unchanged from that in the aug-cc-pVTZ basis set.

4.3.4 The Diatomics

We have tested the performance of EOMIP-CCSD(2) method for diatomic molecules such as NO, CO^+, CN, F_2^+, O_2^+, and N_2^+. These diatomic molecules suffer from the notorious symmetry breaking problem and often represent a classic challenge for standard single-reference theories.

Nitric oxide acts as a catalyst for the ozone depletion reactions and plays a key role in stratospheric ozone chemistry. Table 4.6 contains the computed bond length and IR frequency of nitric oxide. In the aug-cc-pVDZ basis set, all the methods overestimate the N–O bond length, compared to the experimental value. The IR frequency in all of the methods shows reasonable agreement with the experiment, except in the UMP2 method, where the experimental frequency is overestimated by 1742 cm^{-1}. The bond length shrinks and, consequently, the IR frequency shifts to a higher value in both the aug-cc-pVTZ and aug-cc-pVQZ basis sets.

Table 4.6 : Geometry and Harmonic Vibrational Frequency of Nitric Oxide

method	bond length (Å)	frequency, ω (cm^{-1})
aug-cc-pVDZ Basis Set		
EOMIP-CCSD(2)	1.160	1981
EOMIP-CCSD	1.164	1957
UCCSD	1.160	1941
ROCCSD	1.159	1958
UMP2	1.142	3646
ROMP2	1.170	1897
aug-cc-pVTZ Basis Set		
EOMIP-CCSD(2)	1.146	2014
EOMIP-CCSD	1.150	1996
UCCSD	1.142	2000
ROCCSD	1.142	2000
UMP2	1.135	3179
ROMP2	1.154	1920
aug-cc-pVQZ Basis Set		
EOMIP-CCSD(2)	1.145	2022
EOMIP-CCSD	1.150	2005
UCCSD	1.141	2012
ROCCSD	1.141	2005
UMP2	1.341	3166
ROMP2	1.154	1922
Experimental Results		
	1.150[a]	1904[a]

a : Values taken from Huber and Herzberg.[110]

The EOMIP-CCSD(2) method underestimates the experimental bond length, but gives better agreement compared to the ROCCSD and UCCSD methods. For IR frequencies also, it gives a value ($|\Delta\omega_e|$ = 118 cm^{-1}) comparable to the EOMIP-CCSD ($|\Delta\omega_e|$ = 101 cm^{-1}), UCCSD ($|\Delta\omega_e|$ = 112 cm^{-1}), and ROCCSD ($|\Delta\omega_e|$ = 101 cm^{-1}) values, in the aug-cc-pVQZ basis set. The UMP2 method performs very poorly, with regard to bond length ($|\Delta r_e|$ = 0.019 Å) and IR frequency ($|\Delta\omega_e|$ = 1262 cm^{-1}). The ROMP2 method, on the other hand, shows surprisingly close agreement with the experiment,[110] with regard to bond length and IR frequency.

N_2^+ shows a T1 diagnostic value of 0.022 (Table 4.2); therefore, single-reference methods can treat it with reasonable accuracy. Table 4.7 shows that, in the aug-cc-pVDZ basis set, the EOMIP-CCSD method shows the best agreement with the experiment, with regard to bond length, but overestimates the experimental IR frequency by more than a hundred wave numbers. The EOMIP-CCSD(2) method, on the other hand, overestimates the bond length but reproduces the experimental[110] IR frequency ($|\Delta\omega_e|$ = 5 cm^{-1}) with high accuracy. The UHF- and ROHF-based single-reference coupled cluster methods give similar accuracy as that of the EOMIP-CCSD(2) method for bond length, but lead to greater error in IR frequency. Calculations in the aug-cc-pVTZ basis set result in shrinkage of the bond length and an upward shift of vibrational frequency. The results in the aug-cc-pVQZ basis set show negligible deviation from that in the aug-cc-pVTZ basis. The EOMIP-CCSD(2) method shows the best agreement with experiment for both bond length ($|\Delta r_e|$ = 0.004 Å) and IR frequency ($|\Delta\omega_e|$ = 42 cm^{-1}). The UCCSD and ROCCSD methods underestimate the bond length and consequently overestimate the IR frequency, by 94 and 101 cm^{-1}, respectively. The MBPT(2) methods overestimate the bond length and significantly underestimate the IR frequency. N_2^+ shows two significant exceptions to the trend shown by the previously discussed molecules. First, the UMP2 method performs better than the ROMP2 method; second, the EOMIP-CCSD method performs poorly for both bond length ($|\Delta r_e|$ = 0.010 Å) and IR frequency ($|\Delta\omega_e|$ = 152 cm^{-1}).

Table 4.7 : Geometry and Harmonic Vibrational Frequency of N_2^+

method	bond length (Å)	frequency, ω (cm^{-1})
	aug-cc-pVDZ Basis Set	
EOMIP-CCSD(2)	1.132	2212
EOMIP-CCSD	1.125	2316
UCCSD	1.130	2245
ROCCSD	1.129	2253
UMP2	1.148	2078
ROMP2	1.155	2008
	aug-cc-pVTZ Basis Set	
EOMIP-CCSD(2)	1.113	2250
EOMIP-CCSD	1.106	2359
UCCSD	1.110	2299
ROCCSD	1.109	2306
UMP2	1.127	2124
ROMP2	1.135	2055
	aug-cc-pVQZ Basis Set	
EOMIP-CCSD(2)	1.112	2249
EOMIP-CCSD	1.104	2359
UCCSD	1.108	2301
ROCCSD	1.107	2308
UMP2	1.126	2123
ROMP2	1.134	2054
	Experimental Results	
	1.116[a]	2207[a]

a : Values taken from Huber and Herzberg.[110]

O_2^+ shows a very small T1 diagnosis value of 0.014, which indicates that a single determinant reference will be sufficient for the accurate description of the wave function. Table 4.8 shows that, in the aug-cc-pVDZ basis set, the EOMIP-CCSD(2) method exhibits greater error for the bond length ($|\Delta r_e|$ = 0.011 Å), compared to the EOMIP-CCSD and single-reference coupled cluster methods, but performs significantly better than both the UMP2 method ($|\Delta r_e|$ = 0.049 Å) and the ROMP2 method ($|\Delta r_e|$ = 0.062 Å). However, the EOMIP-CCSD(2) method gives excellent agreement with the experimental value for IR frequency. The aug-cc-pVDZ basis set, however, is inadequate to rely upon. Calculations in the aug-cc-pVTZ and aug-cc-pVQZ basis sets lead to the contraction of the bond length and increment of the IR frequency, in all of the methods used. In the aug-cc-pVQZ basis set, the EOMIP-CCSD(2) method shows the best agreement with the experiment[110] for both bond length ($|\Delta r_e|$ = 0.004 Å) and harmonic vibrational frequency ($|\Delta \omega_e|$ = 37 cm^{-1}). The EOMIP-CCSD method gives comparable performance for bond length ($|\Delta r_e|$ = 0.009 Å), but performs poorly for IR frequency ($|\Delta \omega_e|$ = 117 cm^{-1}). The single-reference coupled cluster methods also show inferior results for both bond length ($|\Delta r_e|$ = 0.013 and 0.012 Å for the UCCSD and ROCCSD methods, respectively) and harmonic vibrational frequency ($|\Delta \omega_e|$ = 157 and 162 cm^{-1} for the UCCSD and ROCCSD methods, respectively). The UMP2 method performs very poorly with regard to bond length ($|\Delta r_e|$ = 0.030 Å) and IR frequency ($|\Delta \omega_e|$ = 362 cm^{-1}). However, the predicted values are better than those in the ROMP2 method ($|\Delta r_e|$ = 0.041 Å and $|\Delta \omega_e|$ = 476 cm^{-1}). O_2^+ follows the unique trend shown by MBPT(2) and the EOMIP-CCSD method in N_2^+, as discussed in the previous paragraph

The T1 diagnosis value (0.050) indicates significant multi reference character of the CN radical. Table 4.9 lists the computed bond lengths and IR frequencies of the CN radical. In the aug-cc-pVDZ basis set, however, both EOM methods give disastrous performance for bond length and IR frequency. The EOMIP-CCSD(2) method overestimates the bond length by 0.076 Å and underestimates the frequency by 264 cm^{-1}

Table 4.8 : Geometry and Harmonic Vibrational Frequency of O_2^+

method	bond length (Å)	frequency, ω (cm^{-1})
aug-cc-pVDZ Basis Set		
EOMIP-CCSD(2)	1.127	1908
EOMIP-CCSD	1.123	1981
UCCSD	1.120	2016
ROCCSD	1.119	2022
UMP2	1.166	1457
ROMP2	1.179	1326
aug-cc-pVTZ Basis Set		
EOMIP-CCSD(2)	1.114	1931
EOMIP-CCSD	1.109	2009
UCCSD	1.105	2049
ROCCSD	1.105	2054
UMP2	1.149	1526
ROMP2	1.160	1410
aug-cc-pVQZ Basis Set		
EOMIP-CCSD(2)	1.112	1942
EOMIP-CC	1.107	2022
UCCSD	1.103	2062
ROCCSD	1.102	2067
UMP2	1.146	1543
ROMP2	1.157	1429
Experimental Results		
	1.116[a]	1905[a]

a : Values taken from Huber and Herzberg.[110]

Table 4.9 : Geometry and Harmonic Vibrational Frequency of CN

method	bond length (Å)	frequency, ω (cm^{-1})
aug-cc-pVDZ Basis Set		
EOMIP-CCSD(2)	1.248	1805
EOMIP-CCSD	1.241	1877
UCCSD	1.183	2117
ROCCSD	1.185	2104
UMP2	1.138	2843
ROMP2	1.211	1753
aug-cc-pVTZ Basis Set		
EOMIP-CCSD(2)	1.165	2137
EOMIP-CCSD	1.163	2178
UCCSD	1.162	2187
ROCCSD	1.163	2167
UMP2	1.123	2916
ROMP2	1.186	1849
aug-cc-pVQZ Basis Set		
EOM-IP-CCSD(2)	1.164	2133
EOMIP-CCSD	1.161	2174
UCCSD	1.160	2188
ROCCSD	1.161	2164
UMP2	1.121	2923
ROMP2	1.185	1847
Experimental Results		
	1.171[a]	2069[a]

a : Values taken from Huber and Herzberg.[110]

The EOMIP-CCSD method improves the results, but still shows large error ($|\Delta r_e|$ = 0.069 Å and ($|\Delta\omega_e|$ = 192 cm^{-1}), compared to the experiment. This trend gets reversed in larger basis sets: the EOMIP-CCSD(2) method gives the best agreement with the experiment for both bond length ($|\Delta r_e|$ = 0.007 Å) and vibrational frequency ($|\Delta\omega_e|$ = 64 cm^{-1}) in the aug-cc-pVQZ basis set. The EOMIP-CCSD method slightly underestimates the bond length ($|\Delta r_e|$ = 0.010 Å) and overestimates the frequency ($|\Delta\omega_e|$ = 105 cm^{-1}). The performance of the single-reference coupled cluster methods is similar to that of the EOMIP-CCSD method, with regard to both bond length and IR frequency. The spin contamination of the UMP2 wave function introduces very large errors in bond length ($|\Delta r_e|$ = 0.050 Å) and IR frequency ($|\Delta\omega_e|$ = 854 cm^{-1}) . The ROMP2 method shows significant improvement over the UMP2 method, but the bond length ($|\Delta r_e|$ = 0.014 Å) and IR frequency ($|\Delta\omega_e|$ = 222 cm^{-1}) still deviate significantly from the experiment.[110]

The F_2^+ shows a T1 diagnosis value of 0.013, which makes it a suitable candidate for single-reference treatment. Table 4.10 shows that, in the aug-cc-pVDZ basis set, the EOMIP-CCSD(2) method reproduces the experimental[110] bond length and frequency with absolute accuracy. The EOMIP-CCSD method also gives comparable performance for bond length and IR frequency. However, the single-reference coupled cluster methods underestimate the bond length and overestimate the IR frequency. The UMP2 and ROMP2 methods also overestimate the bond length by a large value (0.073 and 0.115 Å, respectively), but give IR frequencies with accuracy comparable to that of their coupled cluster analogues. The UMP2 method overestimates the experimental frequency by 51 cm^{-1}, whereas the ROMP2 method underestimates the frequency by 68 cm^{-1}. In the aug-cc-pVTZ and aug-cc-pVQZ basis sets, both the EOM and single-reference coupled cluster methods underestimate the bond length and overestimate the frequency. The UCCSD and ROCCSD methods, in the aug-cc-pVQZ basis set, give significant error in bond length ($|\Delta r_e|$ = 0.041 and 0.040 Å, respectively), as well as in frequency ($|\Delta\omega_e|$ = 166 and 170 cm^{-1}, respectively).

Table 4.10 : Geometry and Harmonic Vibrational Frequency of F_2^+

method	bond length (Å)	frequency, ω (cm^{-1})
aug-cc-pVDZ Basis Set		
EOMIP-CCSD(2)	1.322	1081
EOMIP-CCSD	1.326	1065
UCCSD	1.312	1128
ROCCSD	1.310	1133
UMP2	1.395	1124
ROMP2	1.437	1005
aug-cc-pVTZ Basis Set		
EOMIP-CCSD(2)	1.299	1174
EOMIP-CCSD	1.299	1168
UCCSD	1.286	1230
ROCCSD	1.285	1234
UMP2	1.347	890
ROMP2	1.374	781
aug-cc-pVQZ Basis Set		
EOMIP-CCSD(2)	1.295	1178
EOMIP-CCSD	1.295	1176
UCCSD	1.281	1239
ROCCSD	1.280	1243
UMP2	1.343	897
ROMP2	1.369	788
Experimental Results		
	1.322[a]	1073[a]

a : Values taken from Huber and Herzberg.[110]

The EOMIP-CCSD(2) method gives better performance than the single-reference coupled cluster method, although it continues to underestimate the bond length ($|\Delta r_e|$ = 0.027 Å), and overestimates the harmonic vibrational frequency ($|\Delta \omega_e|$ = 105 cm^{-1}). The EOM-CCSD method gives a performance similar to that of the EOMIP-CCSD(2) method, in both the aug-cc-pVTZ and aug-cc-pVQZ basis sets. The UHF- and ROHF-based MBPT(2) methods overestimate the bond length and underestimate the IR frequency. The UMP2 shows a surprisingly accurate bond length of 1.341 Å and leads to an IR frequency that has accuracy comparable to that of the single-reference coupled cluster method. However, the ROMP2 method performs very poorly for both bond length ($|\Delta r_e|$ = 0.047 Å) and IR frequency ($|\Delta \omega_e|$ = 285 cm^{-1}) .

CO^+ is isoelectronic with N_2^+, but shows significant multi reference character (T1 value = 0.046). Table 4.11 shows that, in the aug-cc-pVDZ basis set, the EOM and the single-reference coupled cluster methods overestimate the bond length. For IR frequency, the EOMIP-CCSD(2) method gives the best agreement with the experiment[110] ($|\Delta \omega_e|$ = 7 cm^{-1}), whereas the EOMIP-CCSD and single-reference coupled cluster methods result in overestimation of the frequency. The UMP2 method underestimates the bond length ($|\Delta r_e|$ = 0.016 Å) and overestimates the frequency ($|\Delta \omega_e|$ = 636 cm^{-1}) by a considerable margin. The ROMP2 method shows greater error than the UMP2 method, with regard to bond length ($|\Delta r_e|$ = 0.023 Å), but gives a better result for harmonic vibrational frequency ($|\Delta \omega_e|$ = 149 cm^{-1}). In the aug-cc-pVTZ basis set, the bond length decreases and the IR frequency increases for all of the methods. The EOMIP-CCSD(2) method gives the best agreement with experiment for bond length ($|\Delta r_e|$ = 0.006 Å), as well as IR frequency ($|\Delta \omega_e|$ = 66 cm^{-1}). The EOMIP-CCSD method, as well as the single-reference coupled cluster method, show inferior performance than the EOMIP-CCSD(2) method in the aug-cc-pVTZ basis set. The UMP2 method severely underestimates the bond length ($|\Delta r_e|$ = 0.027 Å) and overestimates the frequency ($|\Delta \omega_e|$ = 666 cm^{-1}).

Table 4.11 : Geometry and Harmonic Vibrational Frequency of CO^+

method	bond length (Å)	frequency, ω (cm^{-1})
aug-cc-pVDZ Basis Set		
EOMIP-CCSD(2)	1.123	2221
EOMIP-CCSD	1.122	2257
UCCSD	1.124	2248
ROCCSD	1.123	2259
UMP2	1.100	2850
ROMP2	1.139	2065
aug-cc-pVTZ Basis Set		
EOMIP-CCSD(2)	1.109	2282
EOMIP-CCSD	1.106	2324
UCCSD	1.108	2322
ROCCSD	1.108	2327
UMP2	1.089	2881
ROMP2	1.124	2129
aug-cc-pVQZ Basis Set		
EOMIP-CCSD(2)	1.108	2288
EOMIP-CCSD	1.104	2331
UCCSD	1.106	2330
ROCCSD	1.106	2333
UMP2	1.088	2888
ROMP2	1.122	2132
Experimental Results		
	1.115[a]	2214[a]

a : Values taken from Huber and Herzberg.[110]

However, the ROMP2 method gives surprisingly good performance for the bond length ($|\Delta r_e|$ = 0.009 Å) as well as the vibrational frequency ($|\Delta \omega_e|$ = 79 cm^{-1}). The same trend holds in the aug-cc-pVQZ basis set, and the bond length and IR frequency show very small deviations from that determined in the aug-cc-pVTZ basis set.

4.3.5 Error Analysis

Tables 4.12 and 4.13 present the minimum, maximum, and average absolute deviations (AAD) of the computed (in the aug-cc-pVQZ basis set) bond lengths and harmonic vibrational frequencies from the experiment, for all of the molecules investigated in this chapter.

Table 4.12 : Comparison of the Maximum, Minimum, and Average Absolute Deviation Values of the Computed (aug-cc-pVQZ Basis Set) Equilibrium Bond Lengths from the Experiment

Method	**Deviation in Bond Length, $\|\Delta r_e\|$ (Å)**		
	Min	**Max**	**AAD**
IP-EOM-CCSD(2)	0.004	0.027	0.010
EOM-IP-CCSD	0.000	0.027	0.013
UCCSD	0.006	0.088	0.030
ROCCSD	0.006	0.058	0.016
UMP2	0.012	0.075	0.038
ROMP2	0.004	0.047	0.019

.

Among all the methods used in this work, the EOMIP-CCSD(2) method shows the lowest average absolute deviation for bond length ($|\Delta r_e|$ = 0.010 Å) as well as harmonic vibrational frequency ($|\Delta\omega_e|$ = 111 cm^{-1}); whereas the UCCSD and UMP2 methods show the highest maximum absolute deviations for bond length and harmonic vibrational frequency, respectively.

Table 4.13 : Comparison of the Maximum, Minimum, and Average Absolute Deviation Values of the Computed (aug-cc-pVQZ Basis Set) Harmonic Vibrational Frequencies from the Experiment

Method	**Deviation in Harmonic Vibrational Frequencies, $\|\Delta\omega_e\|$ (cm^{-1})**		
	Min	**Max**	**AAD**
IP-EOM-CCSD(2)	23	317	111
EOM-IP-CCSD	52	300	124
UCCSD	17	722	233
ROCCSD	40	487	155
UMP2	25	1337	482
ROMP2	6	634	197

Figure 4.2 and 4.3 reveal that the EOMIP-CCSD(2) method gives the best performance for both bond length and IR frequency; these values are very close to (and even better than, in some cases) the EOMIP-CCSD method, despite the latter being computationally more demanding. It is followed, in order of decreasing accuracy, by the ROCCSD method, the ROMP2 method, the UCCSD method, and, lastly, the UMP2 method.

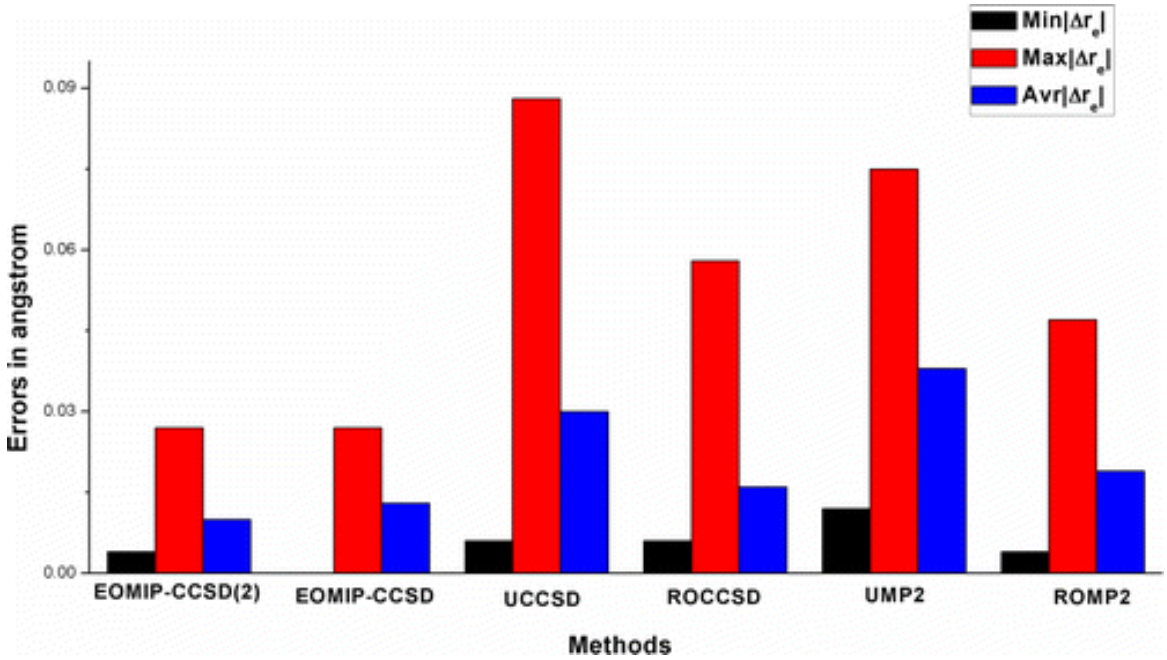

Figure 4.2 : Comparison of the maximum, minimum, and average absolute deviations of the computed (aug-cc-pVQZ basis set) bond length from the experiment.

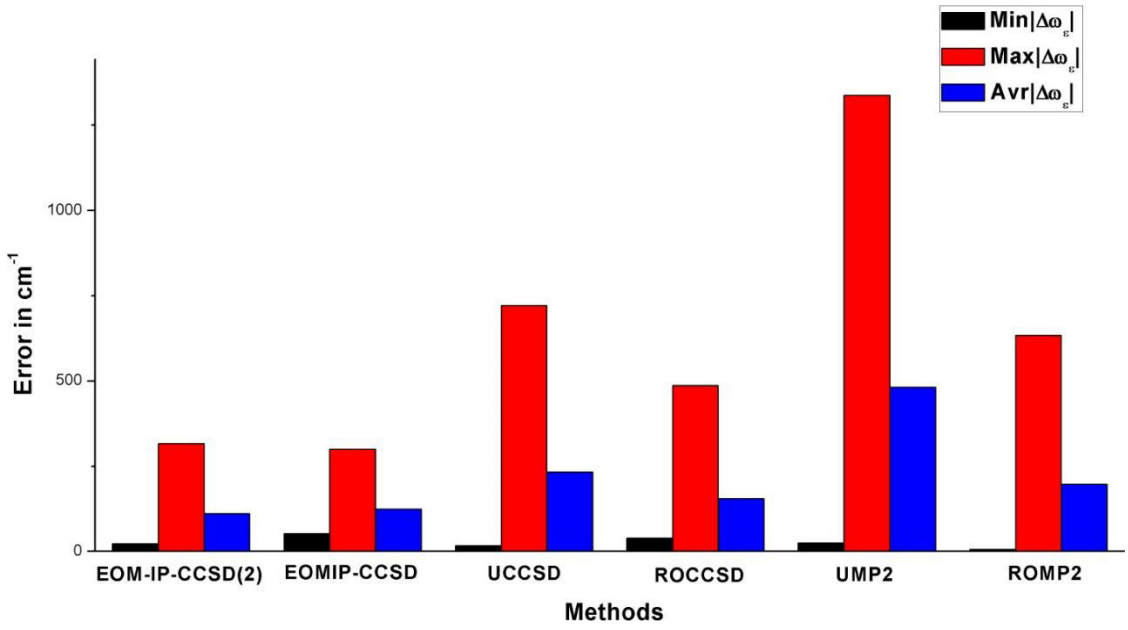

Figure 4.3 : Comparison of the maximum, minimum, and average absolute deviation of the computed (aug-cc-pVQZ basis set) harmonic vibrational frequency from the experiment.

4.4 Conclusion

We have presented a benchmark study on the performance of the EOMIP-CCSD(2) method for geometry and vibrational frequencies of doublet radicals. The method, being naturally spin-adapted and equipped to address multi reference situations, can avoid the problems associated with the standard single-reference *ab-initio* treatment of open-shell radicals. In addition to that, the method is computationally less expensive than the standard EOMIP-CCSD and single-reference coupled cluster methods, in terms of both computational scaling as well as storage requirements. The performance of the method is benchmarked, in a hierarchy of Dunning's correlation-consistent aug-cc-pVXZ (X = D, T, Q) basis sets, on a variety of doublet radicals, which are previously reported to be challenging cases for standard *ab-initio* methods. We have compared our results with the EOMIP-CCSD method, the UHF- and ROHF-based coupled cluster methods, and MBPT(2) method. The computed results demonstrate that the EOMIP-CCSD(2) method provides reasonable agreement with the experimental geometry and IR frequency. The calculated bond lengths and frequencies are strongly dependent on the basis sets used. The bond lengths decrease and IR frequencies shift to higher values upon changing the basis set from the aug-cc-pVDZ basis set to the aug-cc-pVTZ basis set. The change in the results is negligible upon moving from the aug-cc-pVTZ basis set to the aug-cc-pVQZ basis set; hence, the results in the aug-cc-pVQZ basis set can be taken as the complete basis set limit results. We have calculated the minimum, maximum, and average absolute deviations from the experiment for all of the methods, in the aug-cc-pVQZ basis set. The EOMIP-CCSD(2) method shows the smallest average absolute deviation in bond length ($|\Delta r_e| = 0.010$ Å), as well as in IR frequency ($|\Delta\omega_e| = 111$ cm^{-1}). The method performs similar to that of the standard EOMIP-CCSD method, even better in some particular cases, despite the latter being more computationally expensive. The UHF reference-based MBPT(2) and CCSD

methods fail to reproduce even the qualitative trends for most of the cases, which is indicated by the high value of the maximum and average absolute deviations in bond length and IR frequency. However, the ROHF-based CCSD and MBPT(2) method shows comparatively better results than the UHF-based CCSD and MBPT(2) method, but performs poorly compared to the EOMIP-CCSD(2) method. Inclusion of partial triples will obviously improve the results for the single-reference coupled cluster methods. However, it will also increase the scaling to N^7, which will make the method computationally unfeasible, even for the moderately sized molecules.

The EOMIP-CCSD(2) method offers an efficient black box approach for the theoretical treatment of doublet radicals and gives accuracy comparable to the robust EOMIP-CCSD method, at significantly lower computational cost. Therefore, the present approach should be extended to the other variants of EOM-CC and FSMRCC to obtain efficient lower scaling methods for calculation of direct difference of energy.

References:

1. Cizek, J., *J. Chem. Phys.* **1966,** 45, 4256-4266.
2. Bartlett, R. J., *Annu. Rev. Phys. Chem.* **1981,** 32, 359-401.
3. Adamowicz, L.; Laidig, W. D.; Bartlett, R. J., *Int. J. Quant. Chem.* **1984,** 26, 245-254.
4. Salter, E. A.; Trucks, G. W.; Bartlett, R. J., *J. Chem. Phys.* **1989,** 90, 1752-1766.
5. Scheiner, A. C.; Scuseria, G. E.; Rice, J. E.; Lee, T. J.; Schaefer III, H. F., *J. Chem. Phys.* **1987,** 87, 5361-5373.
6. Monkhorst, H. J., Calculation of properties with the coupled cluster method. *Int. J. Quant. Chem.* **1977,** 12, 421-432.
7. Besler, B. H.; Scuseria, G. E.; Scheiner, A. C.; Schaefer III, H. F., *J. Chem. Phys.* **1988,** 89, 360-366.
8. Koch, H.; Jensen, H. J. A.; Jorgensen, P.; Helgaker, T.; Scuseria, G. E.; Schaefer III, H. F., *J. Chem. Phys.* **1990,** 92, 4924-4940.
9. Salter, E. A.; Bartlett, R. J., *J. Chem. Phys.* **1989,** 90, 1767-1773.
10. Knowles, P. J.; Hampel, C.; Werner, H. J., *J. Chem. Phys.* **1993,** 99, 5219-5227.
11. Rittby, M.; Bartlett, R. J., *J. Phys. Chem.* **1988,** 92, 3033-3036.
12. Scuseria, G. E.,. *Chem. Phys. Lett.* **1991,** 176, 27-35.
13. Raghavachari, K.; Trucks, G. W.; Pople, J. A.; Head-Gordon, M., A *Chem. Phys. Lett.* **1989,** 157, 479-483.
14. Stanton, J. F., *Chem. Phys. Lett.* **1997,** 281, 130-134.
15. Bartlett, R. J.; Watts, J. D.; Kucharski, S. A.; Noga, J., *Chem. Phys. Lett.* **1990,** 165, 513-522.
16. Möller, C.; Plesset, M. S., *Phys. Rev.* **1934,** 46, 618-622.
17. Lauderdale, W. J.; Stanton, J. F.; Gauss, J.; Watts, J. D.; Bartlett, R. J., *Chem. Phys. Lett.* **1991,** 187, 21-28.
18. Lauderdale, W. J.; Stanton, J. F.; Gauss, J.; Watts, J. D.; Bartlett, R. J., *J. Chem. Phys.* **1992,** 97, 6606-6620.

19. Detailed discussion on the origin of the problems associated with theoretical treatment of doublet radicals is outside the scope of the present work. Ref 20 and 21 should be consulted for a elaborate review on the above mentioned subject.

20. Stanton, J. F.; Gauss, J., A Discussion of Some Problems Associated with the Quantum Mechanical Treatment of Open-Shell Molecules. In *Advances in Chemical Physics*, John Wiley & Sons, Inc.: **2003**; pp 101-146.

21. Szalay, P. G.; Vazquez, J.; Simmons, C.; Stanton, J. F., *J. Chem. Phys.* **2004,** 121, 7624-7631.

22. Andrews, J. S.; Jayatilaka, D.; Bone, R. G. A.; Handy, N. C.; Amos, R. D., *Chem. Phys. Lett.* **1991,** 183, 423-431.

23. W. J. Hehre, L. R., P. v. R. Schleyer, and J. A. Pople, *Ab Initio Molecular Orbital Theory* John Wiley & Sons, Inc.: New York, 1986.

24. Davidson, E. R.; Borden, W. T., *J. Phys. Chem.* **1983,** *87*, 4783-4790.

25. Cizek, J.; Paldus, J., *J. Chem. Phys.* **1967,** *47*, 3976-3985.

26. Thouless, D. J., *The Quantum Mechanics Of Many-Body Systems*. Academic: New York, 1961; pp 126.

27. Pearson, R. G., *Symmetry Rules for Chemical Reactions*. Wiley: New York, 1976.

28. Eisfeld, W., *Phys. Chem. Chem. Phys.* **2005,** *7*, 3924-3932.

29. Goddard, J. D.; Handy, N. C.; Schaefer III, H. F., *J. Chem. Phys.* **1979,** *71*, 1525-1530.

30. Golubeva, A. A.; Pieniazek, P. A.; Krylov, A. I., *J. Chem. Phys.* **2009,** *130*, 124113-10.

31. Gonzalez, M.; Valero, R.; Sayos, R., *J. Chem. Phys.* **2001,** 115, 2540-2549.

32. Hammond, J. R.; Mazziotti, D. A., *Phys. Rev. A* **2006,** 73, 012509.

33. McLean, A. D.; Lengsfield III, B. H.; Pacansky, J.; Ellinger, Y., *J. Chem. Phys.* **1985,** 83, 3567-3576.

34. Stanton, J. F.; Gauss, J., *Theor. Chim. Acta.* **1996,** 93, 303-313.

35. Andersson, K.; Malmqvist, P. A.; Roos, B. O., *J. Chem. Phys.* **1992,** 96,

1218-1226.

36. Hirao, K., *Chem. Phys. Lett.* **1992,** 190, 374-380.

37. Hirao, K., *Chem. Phys. Lett.* **1993,** 201, 59-66.

38. Malmqvist, P. A.; Rendell, A.; Roos, B. O.,. *J. Phys. Chem.* **1990,** 94, 5477-5482.

39. Lischka, H.; Shepard, R.; Brown, F. B.; Shavitt, I., *Int. J. Quant. Chem.* **1981,** 20, 91-100.

40. Meyer, W., *Methods of Electronic Structure Theory*. Plenum Press: New York, 1977; Vol. 4, pp 413.

41. Balkova, A.; Kucharski, S. A.; Meissner, L.; Bartlett, R. J., *J. Chem. Phys.* **1991,** 95, 4311-4316.

42. Chattopadhyay, S.; Sinha Mahapatra, U.; Datta, B.; Mukherjee, D., *Chemical Physics Letters* **2002,** 357, 426-433.

43. Evangelista, F. A.; Allen, W. D.; Schaefer, H. F.; III, *J. Chem. Phys.* **2007,** 127, 024102-17.

44. Evangelista, F. A.; Simmonett, A. C.; Allen, W. D.; Schaefer, H. F.; III; Gauss, J., *J. Chem. Phys.* **2008,** 128, 124104-13.

45. Hanrath, M., *J. Chem. Phys.* **2005,** 123, 084102-12.

46. Jeziorski, B.; Monkhorst, H. J., *Physical Review A* **1981,** 24, 1668-1681.

47. Kaldor, U.; Haque, A., **1986,** 128, 45-48.

48. Mukherjee, D.; Pal, S., Use of Cluster Expansion Methods in the Open-Shell Correlation Problem. In *Advances in Quantum Chemistry*, Per-Olov, L. w., Academic Press: **1989**; Volume 20, pp 291-373.

49. Pal, S.; Rittby, M.; Bartlett, R. J.; Sinha, D.; Mukherjee, D., *J. Chem. Phys.* **1988,** 88, 4357-4366.

50. Pittner, J.; Nachtigall, P.; Carsky, P.; Masik, J.; Hubac, I., *J. Chem. Phys.* **1999,** 110, 10275-10282.

51. Vaval, N.; Pal, S.; Mukherjee, D., *Theoretical Chemistry Accounts* **1998,** *99*, 100-105.

52. Sekino, H.; Bartlett, R. J., *Int. J. Quant. Chem.* **1984,** 26, 255-265.

53. Nooijen, M.; Bartlett, R. J.,. *J. Chem. Phys.* **1995,** 102, 3629-3647.

54. Stanton, J. F.; Bartlett, R. J., *J. Chem. Phys.* **1993,** 98, 7029-7039.

55. Krylov, A. I., *Annu. Rev. Phys. Chem.* **2008,** 59, 433-462.

56. Kowalski, K.; Piecuch, P., Full EOMCCSDt. *J. Chem. Phys.* **2001,** 115, 643-651.

57. Kucharski, S. A.; Wloch, M.; Musial, M.; Bartlett, R. J., *J. Chem. Phys.* **2001,** 115, 8263-8266.

58. Manohar, U. M.; Stanton, J. F.; Krylov, A. I., *J. Chem. Phys.* **2009,** *131*, 114112.

59. Stanton, J. F.; Gauss, J., *J. Chem. Phys.* **1994,** 101, 8938-8944.

60. Levchenko, S. V.; Wang, T.; Krylov, A. I., *J. Chem. Phys.* **2005,** 122, 224106-11.

61. Stanton, J. F., *J. Chem. Phys.* **1993,** *99*, 8840-8847.

62. Kállay, M.; Gauss, J., *J. Chem. Phys.* **2004,** 121, 9257-9269.

63. Saeh, J. C.; Stanton, J. F., *J. Chem. Phys.* **1999,** 111, 8275-8285.

64. Stanton, J. F., *J. Chem. Phys.* **2007,** 126, 134309-20.

65. Stanton, J. F., *Mol. Phys.* **2009,** 107, 1059-1075.

66. Bravaya, K. B.; Epifanovsky, E.; Krylov, A. I., *J. Phys. Chem. Lett.,* **2012,** 3, 2726-2732.

67. Epifanovsky, E.; Wormit, M.; Kuś, T.; Landau, A.; Zuev, D.; Khistyaev, K.; Manohar, P.; Kaliman, I.; Dreuw, A.; Krylov, A. I., *J. Comput. Chem.*, **2013,** 34, 2293-2309.

68. Stanton, J. F.; Gauss, *J. Chem. Phys.* **1995,** 103, 1064-1076.

69. Watts, J. D.; Bartlett, R. J., *J. Chem. Phys.* **1990,** 93, 6104-6105.

70. Noga, J.; Bartlett, R. J., *J. Chem. Phys.* **1987,** 86, 7041-7050.

71. Oliphant, N.; Adamowicz, L., *J. Chem. Phys.* **1991,** 95, 6645-6651.

72. Kucharski, S. A.; Bartlett, R. J., In *Advances in Quantum Chemistry*, Academic Press: **1986**; Vol. Volume 18, pp 281-344.

73. Musial, M.; Bartlett, R. J., *J. Chem. Phys.* **2008,** 129, 134105-12.

74. Vaval, N.; Ghose, K. B.; Pal, S.; Mukherjee, D., *Chemical Physics Letters* **1993,** 209, 292-298.

75. Musial, M., *J. Chem. Phys.* 136, 134111-14.

76. Musial, M.; Kucharski, S. A.; Zerzucha, P.; Kus, T; Bartlett, R. J., *J. Chem. Phys.* **2009,** 131, 194104-10.

77. Bag, A.; Manohar, P. U.; Vaval, N.; Pal, S., *J. Chem. Phys.* **2009,** 131, 024102-8.

78. Barysz, M.; Rittby, M.; Bartlett, R. J., *Chem. Phys. Lett.* **1992,** 193, 373-379.

79. Bhattacharya, D.; Vaval, N.; Pal, S., *J. Chem. Phys.* 138, 094108-9.

80. Nooijen, M.; Snijders, J. G., *J. Chem. Phys.* **1995,** 102, 1681-1688.

81. The CIS(D) method of Head-Gordon and coworkers is in similar spirit to a second order approximation to the EOMEE-CCSD. See ref 82

82. Head-Gordon, M.; Rico, R. J.; Oumi, M.; Lee, T. J., *Chem. Phys. Lett.* **1994,** 219, 21-29.

83. By using the same strategy generally used to evaluate non-iterative N7 scaling three body terms in H in an iterative N^5 way

84. N^5 simplifications to EOMCCSD were presented by other groups also. Bartlett and coworkers have presented the P-EOM-MBPT(2) (ref85) method. Krylov and coworkers have persuade the IP-CISD method (ref 30).But rigorous benchmarking of geometry and IR frequency, with other theoretical methods and experiment were not performed in both of the cases.

85. Gwaltney, S. R.; Nooijen, M.; Bartlett, R. J., *Chem. Phys. Lett.* **1996,** 248, 189-198.

86. The advantage will not be present in case of EOMEA-MBPT(2) method. The EA calculation will require the (ab|cd) integrals, consequently will have the same storage requirement as that of EOMEA-CCSD .However, the EOMEA-CCSD(2) method will still have the reduced scaling of N^5.

87. Frisch, M. J.; Trucks, G. W.; Schlegel, H. B.; Scuseria, G. E.; Robb, M. A.; Cheeseman, J. R.; Scalmani, G.; Barone, V.; Mennucci, B.; Petersson, G. A.;

Nakatsuji, H.; Caricato, M.; Li, X.; Hratchian, H. P.; Izmaylov, A. F.; Bloino, J.; Zheng, G.; Sonnenberg, J. L.; Hada, M.; Ehara, M.; Toyota, K.; Fukuda, R.; Hasegawa, J.; Ishida, M.; Nakajima, T.; Honda, Y.; Kitao, O.; Nakai, H.; Vreven, T.; Montgomery, J. A.; Peralta, J. E.; Ogliaro, F.; Bearpark, M.; Heyd, J. J.; Brothers, E.; Kudin, K. N.; Staroverov, V. N.; Kobayashi, R.; Normand, J.; Raghavachari, K.; Rendell, A.; Burant, J. C.; Iyengar, S. S.; Tomasi, J.; Cossi, M.; Rega, N.; Millam, J. M.; Klene, M.; Knox, J. E.; Cross, J. B.; Bakken, V.; Adamo, C.; Jaramillo, J.; Gomperts, R.; Stratmann, R. E.; Yazyev, O.; Austin, A. J.; Cammi, R.; Pomelli, C.; Ochterski, J. W.; Martin, R. L.; Morokuma, K.; Zakrzewski, V. G.; Voth, G. A.; Salvador, P.; Dannenberg, J. J.; Dapprich, S.; Daniels, A. D.; Farkas; Foresman, J. B.; Ortiz, J. V.; Cioslowski, J.; Fox, D. J., Gaussian 09, Revision B.01. In *Gaussian 09, Revision B.01, Gaussian, Inc., Wallingford CT*, Wallingford CT, 2009.

88. CFOUR. Coupled cluster techniques for Computational Chemistry. a quantum-chemical program package by J.F. Stanton, J. G., M.E. Harding, P.G. Szalay; with contributions from A.A. Auer, R. J. B., U. Benedikt, C. Berger, D.E. Bernholdt, Y.J. Bomble, L. Cheng, O. Christiansen, M. Heckert, O. Heun, C. Huber, T.-C. Jagau, D. Jonsson, J. Jusélius, K. Klein, W.J. Lauderdale, D.A. Matthews, T. Metzroth, L.A. Mück, D.P. O'Neill, D.R. Price, E. Prochnow, C. Puzzarini, K. Ruud, F. Schiffmann, W. Schwalbach, S. Stopkowicz, A. Tajti, J. Vázquez, F. Wang, J.D. Watts and the integral packages MOLECULE (J. Almlöf and P.R. Taylor), PROPS (P.R. Taylor), ABACUS (T. Helgaker, H.J. Aa. Jensen, P. Jørgensen, and J. Olsen), and ECP routines by A. V. Mitin and C. van Wüllen. For the current version, see http://www.cfour.de.

89. Kendall, R. A.; Dunning, J. T. H.; Harrison, R. J., *The Journal of Chemical Physics* **1992,** 96, 6796-6806.

90. Burton, N. A.; Yamaguchi, Y.; Alberts, I. L.; Schaefer III, H. F., *J. Chem. Phys.* **1991,** 95, 7466-7478.

91. Jackels, C. F.; Davidson, E. R., *J. Chem. Phys.* **1976,** 64, 2908-2917.

92. Kaldor, U., *Chem. Phys. Lett.* **1991,** 185, 131-135.

93. Lafferty, W. J.; Sams, R. L., *J. Mol. Spectrosc.* **1977,** 66, 478-492.

94. Morino, Y.; Tanimoto, M.; Saito, S.; Hirota, E.; Awata, R.; Tanaka, T., *J. Mol. Spectrosc.* **1983,** 98, 331-348.

95. Weaver, A.; Arnold, D. W.; Bradforth, S. E.; Neumark, D. M., *J. Chem. Phys.* **1991,** 94, 1740-1751.

96. Friedl, R. R.; Sander, S. P., *J. Phys. Chem.* **1987,** 91, 2721-2726.

97. Ishiwata, T.; Fujiwara, I.; Naruge, Y.; Obi, K.; Tanaka, I., *J. Phys. Chem.* **1983,** 87, 1349-1352.

98. Ishiwata, T.; Tanaka, I.; Kawaguchi, K.; Hirota, E., *J. Chem. Phys.* **1985,** *82*, 2196-2205.

99. Kawaguchi, K.; Hirota, E.; Ishiwata, T.; Tanaka, I., *J. Chem. Phys.* **1990,** *93*, 951-956.

100. Davy, R. D.; Schaefer Iii, H. F., *J. Chem. Phys.* **1989,** 91, 4410-4411.

101. Stanton, J. F.; Gauss, J.; Bartlett, R. J., *J. Chem. Phys.* **1992,** 97, 5554-5559.

102. Crawford, T. D.; Stanton, J. F., *J. Chem. Phys.* **2000,** 112, 7873-7879.

103. Kaldor, U., *Chem. Phys. Lett.* **1990,** 166, 599-601.

104. Eisfeld, W.; Morokuma, K., *J. Chem. Phys.* **2000,** 113, 5587-5597.

105. Eisfeld, W.; Morokuma, K., *J. Chem. Phys.* **2003,** 119, 4682-4688.

106. Olson, L. P.; Kuwata, K. T.; Bartberger, M. D.; Houk, K. N., *J. Am. Chem. Soc.* **2002,** 124, 9469-9475.

107. Bhatia, S. C.; Hall, J. H., *J. Phys. Chem.* **1980,** 84, 3255-3259.

108. Dutta, A. K.; Vaval, N.; Pal, S., *J. Chem. Theory Comput.* 8, 1895-1901.

109. Morris, V. R.; Bhatia, S. C.; Hall, J. H., *J. Phys. Chem.* **1990,** 94, 7414-7418.

110. Huber, K. P.; Herzberg, G., *Molecular Spectra and Molecular Structure. IV. Constants of Diatomic Molecules* Van Nostrand Reinhold: Van Nostrand Reinhold, **1979**.

Chapter 5

Partitioned EOMEA-CCSD(2): an efficient N^5 scaling method for calculation of electron affinity

"It is likely that out of ten possible heads
I have seen only one true tail, or vice versa.
In fact it's possible, and there are no excuses,
for these lips can only describe what these eyes actually see"

Ernesto 'CHE' Guevara

The Motorcycle Diaries

In this chapter, we present an N^5 scaling modification to the standard EOMEA-CCSD method, based on the matrix partitioning technique and perturbative approximations. The method has lower computational scaling and smaller storage requirements than the standard EOMEA-CCSD method and, therefore, can be used to calculate electron affinities of large molecules and clusters. The performance and capabilities of the new method have been benchmarked with the standard EOMEA-CCSD method, for a test set of 20 small molecules, and the average absolute deviation is only 0.03 eV. The method is further used to investigate electron affinities of DNA and RNA nucleobases, and the results are in excellent agreement with the experimental values.

5.1 Introduction:

Electron affinities are one of the intrinsic properties of atoms and molecules and are of interest to both theoreticians and experimentalists. In spite of its immense importance in chemistry and biology, experimental determination of electron affinities is rather complicated. The main reason behind the experimental uncertainty is the ambiguous nature of the anion formed after electron attachment. There are two alternative possibilities: valence bound (VB), which involves attachment of an additional electron to the antibonding molecular orbital, leading to significant structural change of the molecule. On the other hand, there exists an alternative possibility in polar molecules (dipole moment equal to or higher than 2.5 D), where the additional electron remains weakly bound to the molecule by charge-dipole interaction (DB)[1, 2], and the structure remains almost unchanged from that of the neutral precursor. Now, energetically VB and DB can be near degenerate, and depending on the experimental condition, either of them can be formed, which makes experimental determination of electron affinity complicated. Theoretical calculations can be helpful for the reliable determination of electron affinities. The *ab-initio* computation of electron affinity is also challenging, however, due to different reasons. The Hartree–Fock approximation often does not bind the excess electron or bind it very weakly [3, 4]. Therefore, calculations of electron affinities require systematic inclusion of both dynamic and non-dynamic correlation [5).] At the same time, a highly diffused basis set, with maximum possible radical and angular flexibility [6], is required to model the weakly bound electron, and it often makes the correlated calculations very time-consuming, sometimes impossible.

Among the various approaches available, the equation of motion coupled cluster (EOM-CC) [7, 8] approach has been proved to be an accurate and systematic method for the calculation of electron affinities [9-12], as a direct difference of energies. The EOM-CC approach for electron affinity (EOMEA-CC) is size-

consistent, naturally spin adapted, and equivalent [13] to the (1, 0) sector of the Fock space multi-reference coupled cluster (FSMRCC) [14-17] method for the principal peaks. The EOMEA-CC method is generally used in singles and doubles approximations (EOMEA-CCSD). It scales as iterative N^6, and has similar storage requirements as that of the single-reference coupled cluster, which restrict its application beyond small molecules in moderate basis sets.

The single-reference coupled cluster theory has an intriguing relationship with many-body perturbation theory (MBPT) [18]. Therefore, a natural way of approximating the coupled cluster effective Hamiltonian would be based on perturbation orders. Nooijen and Snijders [19] were the first to propose an approximation of the CCSD effective Hamiltonian by replacing the CCSD amplitudes with MBPT(2) amplitudes. Stanton and Gauss [20] generalized the approach by proposing a hierarchy of perturbative approximations to full EOM-CCSD, termed EOM-CCSD(*n*), where the effective Hamiltonian contains terms up to order *n* in perturbation. At a large value of *n*, EOM-CCSD(*n*) leads to full EOM-CCSD. The lowest order approximation to the EOM-CCSD(*n*) leads to EOM-CCSD(2) with MBPT(2) as ground state energy. The extension of this method to the ionization problem (EOMIP-CCSD(2)) leads to an N^5 scaling method with significantly less storage requirements than that of the standard EOMIP-CCSD method. Pal and co-workers [21] have recently shown that the EOMIP-CCSD(2) method can be used to study the geometry and vibrational frequencies of large doublet radicals with accuracy comparable to that of the standard EOM-CCSD method. Ghosh and co-workers [22] have extended a similar idea in spin flip EOMCC and shown that the approximate effective Hamiltonian based EOMCC can be used for accurate description of potential energy surfaces.

The original implementation of EOM-CCSD(2) by Stanton and Gauss [20] was for the ionization problem (EOMIP-CCSD(2)) and excitation energy (EOMEE-

CCSD(2)). The obvious extension of the EOM-CCSD(2) approach will be to the electron affinity problem. Recently, Jordan and co-workers [23, 24] have used the EOMEA-CCSD(2) method to study electron attachment to water clusters and C60. The EOMEA-CCSD(2) method scales as N^5. However, unlike in the case of EOMIP-CCSD(2), the EOMEA-CCSD(2) has the same storage requirement as that of EOMEA-CCSD, which prohibits its usages beyond moderate size molecules. Bartlett and co-workers [25] have used a partitioned EOM matrix along with a MBPT(2) ground state, to reduce the scaling and storage requirement of the EOM-CCSD method for excitation energy. Taking inspiration from their work [25-27], we have implemented a partitioning technique to the EOM based approach to the electron affinity problem, which leads to significant reduction in the storage requirements.

The aim of this chapter is to benchmark the comparative accuracy (relative to standard EOMEA-CCSD) of this new method (P-EOMEA-CCSD(2)) against the former EOMEA-CCSD(2) method and investigate its suitability to calculate electron affinities of large molecule and clusters. The Chapter is organized as follows. The next section contains the theory and implementation details of P-EOMEA-CCSD(2). Numerical results are discussed in section 5.3. Section 5.4 gives the concluding remarks.

5.2 Theory and Computational Details

5.2.1 EOMEA-CC

The equation of motion coupled cluster (EOM-CC) method [7] is a single-reference approach, where the excited state wave functions are generated by the action of a linear CI like operator on the correlated reference state wave function.

The Schrödinger equation for the reference state and the exited state (can be electron attached or ionized state also) can be described by

$$\hat{H}\Psi_0 = E_0\Psi_0 \tag{5.1}$$

$$\hat{H}\Psi_k = E_k\Psi_k \tag{5.2}$$

The excited state wave function Ψ_k is related to the reference state wave function by

$$\Psi_k = \hat{\Omega}_k\Psi_0 \tag{5.3}$$

Left multiplying equation 5.1 with $\hat{\Omega}_k$ and subtracting from equation 5.2, we get

$$\left[\hat{H},\hat{\Omega}\right]\Psi_0 = \omega_k\Omega_k\Psi_0 \tag{5.4}$$

Where $\omega_k = E_k - E_0$

The form of Ω_k defines the particular EOM method corresponding to the target state. For the electron affinity problem [9]

$$\Omega_k^{EA} = \sum_a R^a(k)\hat{a}^\dagger + \sum_{a>b,j} R_j^{ab}(k)\hat{a}^\dagger\hat{j}\hat{b}^\dagger + \text{.....} \tag{5.5}$$

Coupled cluster theory is introduced by generating the correlated wave function by action of an exponential operator on a Slater determinant, which is generally, but not necessarily, a Hartree–Fock determinant.

$$\Psi_0 = e^{\hat{T}}\left|\Phi_0\right\rangle \tag{5.6}$$

Where, $\hat{T} = \hat{T}_1 + \hat{T}_2 + \text{.....}$ and $\hat{T}_1 = \sum_{ia} t_i^a\left\{a_a^\dagger a_i\right\}$, $\hat{T}_2 = \frac{1}{4}\sum_{ijab} t_{ij}^{ab}\left\{a_a^\dagger a_b^\dagger a_j a_i\right\}$ .....

Since, $\hat{\Omega}$ and $\hat{T}$ commutes among themselves, we can write equation 4 as

$$\left[\bar{H},\hat{\Omega}\right]\Phi_0 = \left(\bar{H}\Omega\right)_c = \omega_k\hat{\Omega}_k\Phi_0 \tag{5.7}$$

Where, $\bar{H} = e^{-\hat{T}} H e^{\hat{T}}$, and c denotes the connectedness of $\bar{H}$ and Ω .

Since $\bar{H}$ is non Hermitian, there exist different right(R) and left(L) eigenvectors which are biorthogonal and can be normalized to satisfy

$$L_k R_l = \delta_{kl} \tag{5.8}$$

The method is equivalent to (1,0) sector of Fock space multi-reference coupled cluster(FSMRCC) method for the principal peaks [13].

In a typical EOMEA-CCSD calculation, the electron affinities are obtained by diagonalization of the non-symmetric effective Hamiltonian matrix in the (N+1) electron space

$$\left(\bar{H}\right) = \begin{bmatrix} \bar{H}_{SS} & \bar{H}_{SD} \\ \bar{H}_{DS} & \bar{H}_{DD} \end{bmatrix} \tag{5.9}$$

Where $\bar{H}_{SS}$ stands for the singles-singles block of the matrix and so on. The diagonalization is generally performed by Davidson iterative technique.

The major step in the Davidson method is the multiplication of the matrix by trial vector *R*. In the case of EA, the equations for the multiplications are as follows (as described in ref 9)

$$\left[H_{SS} R\right]^a = \sum_c F_{ac} R^c \tag{5.10}$$

$$\left[H_{SD} R\right]^a = \sum_{id} F_{id} \left(2R_i^{ad} - R_i^{da}\right) + \sum_{cdi} R_i^{cd} (2W_{aicd} - W_{aidc}) \tag{5.11}$$

$$\left[H_{DS} R\right]_j^{ab} = \sum_c W_{abcj} R^c \tag{5.12}$$

$$
\begin{aligned}
\left[H_{DD}\right]_j^{ab} &= \sum_c F_{ac} R_j^{cb} + \sum_d F_{bd} R_j^{ad} - \sum_i F_{ij} R_j^{ab} \\
&+ \sum_{id} \left(2W_{ibdj} - W_{bidj}\right) R_i^{ad} - \sum_{ci} W_{aicj} R_i^{cb} \\
&- \sum_{ci} W_{bicj} R_i^{ca} + \sum_{cd} W_{abcd} R_j^{cd} - \sum_k \left(\sum_{icd} \left[2V_{kicd} - V_{kidc}\right] R_i^{cd} \right) t_{kj}^{ab}
\end{aligned}
\tag{5.13}
$$

In the above equation, V denotes the normal mo integrals and expression for F and W intermediates are given in Appendix I.

5.2.2 EOMEA-CCSD(2)

Approximating the coupled cluster amplitudes in eq 5.7 by MBPT(2) amplitudes leads to the EOMEA-CCSD(2) method. It is an obvious extension of EOMIP-CCSD(2) and EOMEE-CCSD(2), by Stanton and Gauss,[20] to the electron affinity problem. The method can be trivially implemented by modifying the F and W intermediates in any standard EOMEA-CCSD code. The expressions for the modified F and W intermediates are given in Appendix I.

The EOMEA-CCSD(2) scales as N^5 power of the basis set, but it has the same storage requirement as the normal EOMEA-CCSD. Especially, the computation of the W_{abcd} intermediate is the most time-consuming step in an EOMEA-CCSD(2) calculation and also the bottleneck of the method, which prohibits its applicability to large molecules.

Following Bartlett and co-worker's suggestion,[25] we propose a further approximation to the EOMEA-CCSD(2) method based on the partitioning of the EOM matrix.

5.2.3 P-EOMEA-CCSD(2)

Following Löwdin's partitioning technique[28], equation 5.7 can be partitioned into P and Q space, where P represents the principal configuration space, and Q represents its orthogonal complement.

$$\begin{bmatrix} \bar{H}_{pp} & \bar{H}_{pq} \\ \bar{H}_{qp} & \bar{H}_{qq} \end{bmatrix} \begin{bmatrix} R_p \\ R_q \end{bmatrix} = \omega \begin{bmatrix} R_p \\ R_q \end{bmatrix} \tag{5.14}$$

and

$$\begin{bmatrix} L_p & L_q \end{bmatrix} \begin{bmatrix} \bar{H}_{pp} & \bar{H}_{pq} \\ \bar{H}_{qp} & \bar{H}_{qq} \end{bmatrix} = \begin{bmatrix} L_p & L_q \end{bmatrix} \omega \tag{5.15}$$

Where, R_p (L_p) and R_q(L_q) represent the projection of the right (left) eigenvector on P and Q spaces.

Expanding equation 5.14 we get

$$\bar{H}_{pp} R_p + \bar{H}_{pq} R_q = \omega R_p \tag{5.16}$$

$$\bar{H}_{qp} R_p + \bar{H}_{qq} R_q = \omega R_q \tag{5.17}$$

Rearranging equation 5.17

$$R_q = \left[\omega - \bar{H}_{qq} \right]^{-1} \bar{H}_{qp} R_p \tag{5.18}$$

Inserting R_q back into equation 5.16 we get

$$\bar{H}_{eff} R_p \equiv \left(\bar{H}_{pp} + \bar{H}_{pq} \left[\omega - \bar{H}_{qq} \right]^{-1} \bar{H}_{qp} \right) R_p = \omega R_p \tag{5.19}$$

Projecting equation 5.19 with L_p

$$\left\langle L_p \middle| \bar{H}_{eff} \middle| R_p \right\rangle \equiv \left\langle L_p \middle| \left[\bar{H}_{pp} + \bar{H}_{pq} \left[\omega - \bar{H}_{qq} \right]^{-1} \bar{H}_{qp} \right] \middle| R_p \right\rangle = \omega \left\langle L_p \middle| R_p \right\rangle \tag{5.20}$$

The eigenvalues of H_{eff} are solely defined in the P space, for first several eigenvalues.

Now if the exact eigenvalue ω is written as the sum of zeroth order energy ω_0, as of yet undetermined, and an energy correction $\Delta\omega$, we can write the operator inverse in equation 5.20 as

$$\left[\omega - \bar{H}_{qq}\right]^{-1} = \left[\omega_0 + \Delta\omega - \bar{H}_{qq}^{[0]} - \bar{H}_{qq}^{[1]} - \bar{H}_{qq}^{[2]} .....\right]^{-1}$$
$$= \left[\left(\omega_0 - \bar{H}_{qq}^{[0]}\right)\left(1 - \left[\omega_0 - \bar{H}_{qq}^{[0]}\right]^{-1}\left[\bar{H}_{qq}^{[1]} + \bar{H}_{qq}^{[2]} ..... - \Delta\omega\right]\right)\right]^{-1} \quad (5.21)$$
$$\equiv \left[\left(\omega_0 - \bar{H}_{qq}^{[0]}\right)\left(1 - \left[\omega_0 - \bar{H}_{qq}^{[0]}\right]^{-1}\left[V_{qq} - \Delta\omega\right]\right)\right]^{-1}$$

Where $V_{qq} = \bar{H}_{qq}^{[1]} + \bar{H}_{qq}^{[2]} + ...$

Now equation 5.21 can be expanded in an inverse series

$$\left[\omega - \bar{H}_{qq}\right]^{-1} = \left[\omega_0 - \bar{H}_{qq}^{[0]}\right]^{-1}$$
$$+\left[\omega_0 - \bar{H}_{qq}^{[0]}\right]^{-1}\left(V_{qq} - \Delta\omega\right)\left[\omega_0 - \bar{H}_{qq}^{[0]}\right]^{-1} \quad (5.22)$$
$$+\left[\omega_0 - \bar{H}_{qq}^{[0]}\right]^{-1}\left(V_{qq} - \Delta\omega\right)\left[\omega_0 - \bar{H}_{qq}^{[0]}\right]^{-1}\left(V_{qq} - \Delta\omega\right)\left[\omega_0 - \bar{H}_{qq}^{[0]}\right]^{-1}$$
$$+.....$$

The lowest order approximation to equation 5.22 will be

$$\left[\omega - \bar{H}_{qq}\right]^{-1} \equiv \left[\omega_0 - \bar{H}_{qq}^{[0]}\right]^{-1} \quad (5.23)$$

Where $\bar{H}_{qq}^{[0]}$ is the usual MØller-Plesset unperturbed Hamiltonian in Q space.

In other words, the unfolded matrix in equation 5.9 is approximated as

$$\left(\bar{H}\right) \equiv \begin{bmatrix} \bar{H}_{SS} & \bar{H}_{SD} \\ \bar{H}_{DS} & \bar{H}_{DD}^{[0]} \end{bmatrix} \quad (5.24)$$

and equation 5.13 becomes

$$\left[H_{DD}^{[0]}\right]_j^{ab} = \sum_c f_{ac} R_j^{cb} + \sum_d f_{bd} R_j^{ad} - \sum_i f_{ij} R_j^{ab} \quad (5.25)$$

Here, f is the Fock operator. In the case of RHF or UHF reference $H_{DD}^{[0]}$ becomes diagonal with the difference of orbital energy in the diagonal.

An examination of equation 5.10-5.12 and equation 5.25 reveals that there is no four particle intermediate in partition–EOMEA-CC(P-EOMEA) method. The four particle $\langle ab|cd\rangle$ integrals can indeed contract with T_1 amplitudes to contribute into the W_{abci} intermediate. However, an MBPT(2) ground state reference for RHF or UHF case will lead to zero T_1 amplitudes. So P-EOMEA-CCSD(2) does not contain any four particle terms, which leads to significant decrease in the storage requirements compared to the standard EOMEA-CCSD and EOMEA-CCSD(2). The P-EOMEA-CCSD(2) method is effectively N^5 scaling. A few N^6 scaling terms remain in $\bar{H}$, but these terms needed to be calculated only once. Alternatively, these terms can be calculated in iterative N^5 scaling algorithm, following the approach presented in ref 5.7 and 5.20. However, the results presented in this chapter were calculated using the former approach.

Here, it should be noted that the H_{DD} block in EOMEA matrix accounts for the electron attached states dominated by double-excitation character, i.e. states, which are formed by addition of an extra electron to the virtual orbitals of the reference state accompanied by excitation of electron from occupied to virtual orbital. In the EOMEA-CCSD method, these doubly excited states are treated only in an approximate manner. As it is well known that the doubly excited determinant gives the major contribution in any correlation method. However, the R_2 operator in EOMEA method can account for the only one electron excitations. On the other hand, the two electron excited determinants are accurately taken care in the reference state by the T_2 amplitudes in the CCSD method. This leads to an imbalance in the description of the reference and the target state in EOMEA-CCSD method and requires inclusion of triples, in both reference and target state calculation, for an accurate description of the electron attached state dominated by double excitations. In Partitioned EOMEA method, this H_{DD} block is further approximated to include only the diagonal terms. Therefore, the P-EOM based method is expected to give inferior performance for the states dominated by

double excitations compared to the standard EOM method with untruncated H_{DD} doubles-doubles block.

5.2.4 Size Consistency of P-EOMEA-CCSD(2)

Size consistency is defined in the literature[29, 30] as the additive separability of energy in the limit of non-interacting fragments.

$$E_{AB} = E_A + E_B \tag{5.26}$$

Where E_{AB} is the energy of the system AB consists of two non-interacting fragments. E_A and E_B are individual energies of fragment A and B, respectively.

Now the P-EOMEA-CCSD(2) to be size-consistent, the sum of the reference energy and the transition energy (electron attachment in this case) has to be size-consistent. Stanton and Gauss have shown that truncation of effective Hamiltonian based on the perturbation orders will ensure size-consistency of the ground state energy for each order of perturbation. The detailed derivation is presented in ref [20].

Now for investigating the separability of the electron attachment energies, one needs to put attention to the CI like linear operator Ω.

Let us consider that the electron attachment is taking place on fragment A.

The Hamiltonian of the system AB is the sum of the fragment A and B in the non-interacting limit

$$\hat{H}_{AB} = \hat{H}_A + \hat{H}_B \tag{5.27}$$

To ensure the additive separability of the energy, the Hamiltonian should be expressible in the block diagonal form.

$$\hat{H}_{AB} = \begin{pmatrix} H_{0,0} & H_{0,A} & H_{0,B} & H_{0,AB} \\ H_{A,0} & H_{A,A} & H_{A,B} & H_{A,AB} \\ H_{B,0} & H_{B,A} & H_{B,B} & H_{B,AB} \\ H_{AB,0} & H_{AB,A} & H_{AB,B} & H_{AB,AB} \end{pmatrix} \tag{5.28}$$

where, $H_{AB,AB} = \langle \Psi_A \Psi_B | H_A + H_B | \Psi_A \Psi_B \rangle$, $H_{AB,0} = \langle \Psi_A \Psi_B | H_A + H_B | \Psi_0 \Psi_0 \rangle$ and so on. 0_A, 0_B, Ψ_A and Ψ_B represent reference and electron attached states on A and B respectively. Following reference 28 and 29, most of the terms in Hamiltonian $\hat{H}_{AB}$ can be shown to be zero. The reference state and the target state cannot be connected through the Hamiltonian, as they differ in spin multiplicity (singlet and doublet respectively). Therefore, the terms $H_{X,0}$ and $H_{0,X}$ are zero, where X=A, B, AB. It should be noted that these terms are not necessarily be zero for the excitation energy case.

Thus, $\hat{H}_{AB}$ simplifies to

$$\hat{H}_{AB} = \begin{pmatrix} H_{0,0} & 0 & 0 & 0 \\ 0 & H_{A,A} & H_{A,B} & H_{A,AB} \\ 0 & H_{B,A} & H_{B,B} & H_{B,AB} \\ 0 & H_{AB,A} & H_{AB,B} & H_{AB,AB} \end{pmatrix} \tag{5.29}$$

In the non-interacting limit, the $\hat{H}_A$ acts only on states of A and $\hat{H}_B$ acts only on states of B. Consequently the terms H_{AB} and H_{BA} are zero.

$$\begin{aligned} H_{A,B} &= \langle \Psi_A 0_B | \hat{H}_A + \hat{H}_B | 0_A \Psi_B \rangle \\ &= \langle \Psi_A 0_B | \hat{H}_A | 0_A \Psi_B \rangle + \langle \Psi_A 0_B | \hat{H}_B | 0_A \Psi_B \rangle \\ &= \langle 0_B | \Psi_B \rangle \langle \Psi_A | \hat{H}_A | 0_A \rangle + \langle \Psi_A | 0_B \rangle \langle 0_B | \hat{H}_B | \Psi_B \rangle \\ &= 0.\langle \Psi_A | \hat{H}_A | 0_A \rangle + 0.\langle 0_B | \hat{H}_B | \Psi_B \rangle = 0 \end{aligned} \tag{5.30}$$

Now little attention has to be paid towards the term $H_{A,AB}$

$$\begin{aligned} H_{A,AB} &= \langle \Psi_A 0_B | \hat{H}_A + \hat{H}_B | \Psi_A \Psi_B \rangle \\ &= \langle 0_B | \Psi_B \rangle \langle \Psi_A | \hat{H}_A | \Psi_A \rangle + \langle \Psi_A | \Psi_A \rangle \langle 0_B | \hat{H}_B | \Psi_B \rangle \\ &= 0 + \langle \Psi_A | \Psi_A \rangle \langle 0_B | \hat{H}_B | \Psi_B \rangle \end{aligned} \tag{5.31}$$

The first term of equation 5.31 is trivially zero. Let us take the electron attachment takes place on fragment A. As the determinant Ψ_A includes at least one electron attachment, the excitation level in the determinant Ψ_B will be restricted to a maximum of single substitution. Thus, $\langle 0_B | \hat{H}_B | \Psi_B \rangle$ becomes zero due to the Brillouin's theorem. Following the similar analogy, $H_{B,AB}$, $H_{AB,A}$ and $H_{AB,B}$ can also be shown to be zero. The proof is same if the electron attachment takes place in fragment B.

All the above condition holds true, even for a partitioned form of the Hamiltonian

The target states are obtained by the diagonalization of $\hat{H}_{AB}$ and are, thus, defined by the following secular equation.

$$\begin{pmatrix} H_{0,0} - \omega I & 0 & 0 & 0 \\ 0 & H_{A,A} - \omega I & 0 & 0 \\ 0 & 0 & H_{B,B} - \omega I & 0 \\ 0 & 0 & 0 & H_{AB,AB} - \omega I \end{pmatrix} = 0 \tag{5.32}$$

Where I stands for the unity matrix and ω is the corresponding eigen value.

The equation 5.32 is satisfied when

$$\left| H_{0,0} - \omega I \right| \times \left| H_{A,A} - \omega I \right| \times \left| H_{B,B} - \omega I \right| \times \left| H_{AB,AB} - \omega I \right| = 0 \tag{5.33}$$

which means the eigen values of the individual fragment are also the eigen value of the combined system.

Therefore, the transition energies in P-EOMEA-CCSD(2) method are size-intensive.

Hence, the total energy, which is sum of the reference state energy and transition energies, is also size-consistent.

5.2.5 Computational Details

Vertical electron affinities are calculated for small molecules like N_2, H_2O, NO^+, O_3, and H_2CO using the P-EOMEA-CCSD(2) method, in a hierarchy of Dunning's correlation consistent aug-cc-pVXZ (X = D, T, Q) basis sets [31]. Experimental geometries are used in all of the cases. The results are compared with the standard EOMEA-CCSD, P-EOMEA-CCSD, and EOMEA-CCSD(2) methods.

After estimating the accuracy of the P-EOMEA-CCSD(2) method, we have used it to calculate the electron affinities of DNA and RNA nucleobases (NAB). We have calculated the electron affinities of adenine, guanine, thymine, cytosine, and uracil in the aug-cc-pVDZ and aug-cc-pVTZ basis sets, and the results are compared with the available experimental and theoretical values. Diffused f functions are removed from the aug-cc-pVTZ basis set, in the calculations for DNA nucleic acid bases, to keep it computationally viable. All the calculations are performed using our in-house coupled cluster and EOMCC codes. Converged Hartree–Fock coefficients, eigenvectors, and one and two electron atomic integrals are taken from the GAMESS-US package [32]. All the calculations are performed assuming C_1 symmetry, and all the electron are used in correlation treatment.

5.3 Results and Discussion

5.3.1 Benchmarking

The performance of the newly implemented P-EOMEA-CCSD(2) method is benchmarked for small molecules like N_2, H_2O, NO^+, O_3, and H_2CO in a hierarchy

of Dunning's correlation consistent aug-cc-pVXZ (X = D, T, Q) basis set (Tables 5.1–5.5). For the sake of comparison, we also quote the corresponding P-EOMEA-CCSD and EOMEA-CCSD(2) results.

Table 5.1 presents the electron affinity values for first five states of N_2. It is well know that N_2^- is a temporary bound anion, which is evident from its negative electron affinity. It can be seen that all four methods give electron affinity values which are in good agreement with each other in all three basis sets, except for the $^2\Pi_g$ state, where both the P-EOM-CCSD and P-EOM-CCSD(2) underestimate the electron affinity value as compared to the EOM-CCSD and EOM-CCSD(2) methods, which are in good agreement with each other. Here it should be noted that the $^2\Pi_g$ state has significant double-excitation character, which is not properly taken care of by the partitioned EOM methods, due to a truncated doubles–doubles block of the EOM matrix. This leads to inferior performance of both the P-EOM-CCSD and P-EOM-CCSD(2) methods for the $^2\Pi_g$ state. The $^2\Sigma_u^-$, $^2\Sigma_g^+$, and $^2\Pi_u$ states, which are dominated by single excitation, are accurately reproduced by the partitioned methods. The increment of basis set from aug-cc-pVDZ to aug-cc-pVTZ leads to an increase in electron affinity for all the states. It also accompanies change in relative ordering of states. The $^2\Sigma_g^+$ state, which has been the fourth highest electron attached state, changes to the second highest electron attached state, on changing the basis from aug-cc-pVDZ to aug-cc-pVTZ. The discrepancy between the P-EOM vs EOM results, for the $^2\Pi_g$ states, slightly decreases in the aug-cc-pVTZ basis set. The electron affinity values of N_2 further increase from aug-cc-pVTZ to the aug-cc-pVQZ basis; however, the state ordering remains unchanged from that in the aug-cc-pVTZ basis set.

In Table 5.2, we report the electron affinity values for the first five states of water. Water also gives rise to a temporarily bound anion on electron attachment. The Hartree–Fock wave function provides a very good zeroth order description of the wave function of the ground state of water, as indicated by the small T1 diagnosis

value.

Table 5.1 : Electron Affinities of N_2 (in eV)

state	EOMEA-CCSD	P-EOMEA-CCSD	EOMEA-CCSD(2)	P-EOMEA-CCSD(2)
		aug-cc-pVDZ Basis Set		
$^2\Sigma_u^-$	–2.64	–2.66	–2.64	–2.65
$^2\Pi_g$	–2.69	–2.86	–2.68	–2.85
$^2\Sigma_g^+$	–3.15	–3.18	–3.15	–3.18
$^2\Pi_u$	–3.78	–3.80	–3.79	–3.80
		aug-cc-pVTZ Basis Set		
$^2\Sigma_u^-$	–2.08	–2.07	–2.06	–2.07
$^2\Sigma_g^+$	–2.26	–2.28	–2.26	–2.27
$^2\Pi_g$	–2.46	–2.58	–2.43	–2.54
$^2\Pi_u$	–2.94	–2.95	–2.94	–2.95
		aug-cc-pVQZ Basis Set		
$^2\Sigma_u^-$	–1.70	–1.70	–1.69	–1.70
$^2\Sigma_g^+$	–1.70	–1.71	–1.70	–1.71
$^2\Pi_g$	–2.33	–2.41	–2.29	–2.37
$^2\Pi_u$	–2.41	–2.41	–2.41	–2.41

At the same time, the first five electron attached states are predominantly single-reference in nature. This leads to very good agreement of electron affinity values in all four methods, with each other, in all three basis sets. Incrementing in the basis set leads to an increase in electron affinity values for all five states in water.

Table 5.2 : Electron Affinities of H_2O (in eV)

state	EOMEA-CCSD	P-EOMEA-CCSD	EOMEA-CCSD(2)	P-EOMEA-CCSD(2)
		aug-cc-pVDZ Basis Set		
$1\ ^2A_1$	-0.78	-0.80	-0.77	-0.80
$^2B_2$	-1.50	-1.51	-1.50	-1.52
$2\ ^2A_1$	-4.36	-4.40	-4.38	-4.43
$3\ ^2A_1$	-5.17	-5.20	-5.20	-5.24
$^2B_1$	-5.54	-5.61	-5.57	-5.64
		aug-cc-pVTZ Basis Set		
$1\ ^2A_1$	-0.62	-0.64	-0.63	-0.64
$^2B_2$	-1.23	-1.24	-1.24	-1.24
$2\ ^2A_1$	-3.26	-3.28	-3.27	-3.30
$3\ ^2A_1$	-4.04	-4.06	-4.06	-4.08
$^2B_1$	-4.20	-4.24	-4.22	-4.26
		aug-cc-pVQZ Basis Set		
$1\ ^2A_1$	-0.54	-0.56	-0.55	-0.56
$^2B2$	-1.10	-1.11	-1.11	-1.11
$2\ ^2A_1$	-2.70	-2.71	-2.71	-2.72
$3\ ^2A_1$	-3.29	-3.30	-3.30	-3.32
$^2B_1$	-3.45	-3.48	-3.45	-3.49

Table 5.3 reports the electron affinity value for the five states of NO^+. The electron attachment to NO^+ is energetically favorable and, therefore, leads to positive values of electron affinities. We observe that the electron affinity values for the two $^2\Pi$ states is slightly underestimated in both P-EOM-CCSD and P-EOM-CCSD(2) methods. The slightly higher double excitation character for the $^2\Pi$ state is responsible for the discrepancy. The other three states, which are dominated by single excitation, are well described by the partitioned EOM methods. The electron affinity values for all five states increase with larger basis sets. The discrepancy between the P-EOM and EOM method for the $^2\Pi$ state also decreases in the aug-cc-pVTZ basis set. The electron affinity values for all five states further increase from aug-cc-pVTZ to the aug-cc-pVQZ basis, and in the aug-cc-pVQZ basis set, all the methods are in good agreement with each other.

The first five electron attached states of ozone are reported in Table 5.4. We observe that the electron affinity of the 1 $^2B_1$ state is positive, while the rest of the four states have negative electron affinity, which indicates that only the first state is stable upon electron attachment. The electron affinity values in all four methods increase with a better basis set. It can be seen that both the EOMEA-CCSD(2) as well as P-EOMEA-CCSD(2) methods significantly underestimate the electron affinity value for the 1 $^2B_1$ state, compared to the EOMEA-CCSD method. On the other hand, the electron affinity value for the 1 $^2B_1$ state in the P-EOMEA-CCSD method is in good agreement with the EOMEA-CCSD value for all three basis sets. Here, it should be noted that the presence of multi-reference character makes the restricted Hartree–Fock method wave function a poor choice for the correct zeroth order description for the ground state of ozone, which is indicated by the large T1 diagnosis values (see Table 5.6). In the case of both EOMEA-CCSD and P-EOMEA-CCSD methods, the T_1 amplitudes take care of the orbital relaxation. This is missing in both EOMEA-CCSD(2) and P-EOMEA-CCSD(2) methods and

leads to the failure of both the methods for the 1 $^2B_1$ state. The picture in higher electron attached states is dominated by the large structural relaxation caused by the addition of an extra electron, which is properly taken care of by the EOM method.

Table 5.3 : Electron Affinities of NO^+ (in eV)

state	EOMEA-CCSD	P-EOMEA-CCSD	EOMEA-CCSD(2)	P-EOMEA-CCSD(2)
		aug-cc-pVDZ Basis Set		
X $^2\Pi$	9.38	9.25	9.39	9.25
X $^2\Pi$	9.38	9.25	9.39	9.25
A $^2\Sigma^+$	3.33	3.31	3.31	3.29
D $^2\Sigma^+$	2.10	2.10	2.14	2.12
C $^2\Pi$	1.91	1.91	1.92	1.92
		aug-cc-pVTZ Basis Set		
X $^2\Pi$	9.65	9.59	9.66	9.60
X $^2\Pi$	9.65	9.59	9.66	9.60
A $^2\Sigma^+$	3.52	3.51	3.51	3.50
D $^2\Sigma^+$	2.39	2.39	2.41	2.40
C $^2\Pi$	2.24	2.25	2.25	2.26
		aug-cc-pVQZ Basis Set		
X $^2\Pi$	9.74	9.72	9.77	9.74
X $^2\Pi$	9.74	9.72	9.77	9.74
A $^2\Sigma^+$	3.65	3.65	3.65	3.65
D $^2\Sigma^+$	2.54	2.54	2.55	2.55
C $^2\Pi$	2.43	2.44	2.43	2.44

Therefore, both EOMEA-CCSD(2) and P-EOMEA-CCSD(2) give satisfactory performance for all of the higher electron attached states.

Table 5.4 : Electron Affinities of O_3 (in eV)

state	EOMEA-CCSD	P-EOMEA-CCSD	EOMEA-CCSD(2)	P-EOMEA-CCSD(2)
		aug-cc-pVDZ Basis Set		
$1\,^2B_1$	1.62	1.58	1.18	1.16
$^2B_2$	-3.05	-3.03	-3.09	-3.08
$1\,^2A_1$	-3.07	-3.03	-3.10	-3.09
$2\,^2A_1$	-3.43	-3.41	-3.46	-3.46
$2\,^2B_1$	-4.47	-4.48	-4.53	-4.54
		aug-cc-pVTZ Basis Set		
$1\,^2B_1$	1.84	1.88	1.42	1.49
$^2B_2$	-2.47	-2.45	-2.50	-2.49
$1\,^2A_1$	-2.55	-2.53	-2.55	-2.54
$2\,^2A_1$	-2.59	-2.55	-2.63	-2.60
$1\,^2B_1$	1.84	1.88	1.42	1.49
		aug-cc-pVQZ Basis Set		
$1\,^2B_1$	1.94	2.03	1.53	1.65
$^2B_2$	-1.91	-1.89	-1.92	-1.90
$1\,^2A_1$	-2.01	-1.99	-2.03	-2.01
$2\,^2A_1$	-2.14	-2.12	-2.14	-2.13
$2\,^2B_1$	-2.85	-2.85	-2.88	-2.87

The detailed analysis on the origin and the trends of the errors are presented in the next section.

Table 5.5 : Electron Affinities of H_2CO (in eV)

state	EOMEA-CCSD	P-EOMEA-CCSD	EOMEA-CCSD(2)	P-EOMEA-CCSD(2)
		aug-cc-pVDZ Basis Set		
$1\ ^2A_1$	-0.75	-0.77	-0.73	-0.75
$^2B_2$	-1.25	-1.32	-1.24	-1.31
$1\ ^2B_1$	-1.31	-1.36	-1.29	-1.35
$2\ ^2A_1$	-2.19	-2.22	-2.21	-2.24
$2\ ^2B_1$	-3.10	-3.19	-3.08	-3.17
		aug-cc-pVTZ Basis Set		
$1\ ^2A_1$	-0.59	-0.60	-0.56	-0.58
$^2B_2$	-1.07	-1.08	-1.05	-1.06
$1\ ^2B_1$	-1.08	-1.14	-1.05	-1.12
$2\ ^2A_1$	-1.85	-1.87	-1.86	-1.88
$2\ ^2B_1$	-2.48	-2.53	-2.44	-2.50
		aug-cc-pVQZ Basis Set		
$1\ ^2A_1$	$1\ ^2A_1$	-0.50	-0.50	-0.48
$^2B_2$	$^2B_2$	-0.96	-0.97	-0.95
$1\ ^2B_1$	$1\ ^2B_1$	-0.99	-1.03	-0.96
$2\ ^2A_1$	$2\ ^2A_1$	-1.58	-1.59	-1.59
$2\ ^2B_1$	$2\ ^2B_1$	-2.11	-2.14	-2.07

Electron affinity values for the five states of formaldehyde are presented in Table 5.5. The electron affinity values for all five states are negative, which indicates that the electron attachment to formaldehyde leads to temporary bound anions. The electron affinity values for all five states increase with incrementation in the basis set. All four methods show very good agreement with each other in all three basis sets.

As a passing remark, it should be mentioned that the calculated electron affinity values in all four methods have not converged with respect to basis set even in the aug-cc-pVQZ basis set. Therefore, it may be necessary to go for explicit correlation technique based [33] EOM methods to get the basis set convergence in the electron affinity values.

Table 5.6 : T1 Diagnosis Values in aug-cc-pVTZ Basis Set

molecule	T1 value
N_2	0.013
H_2O	0.010
NO^+	0.022
ozone	0.028
H_2CO	0.016

5.3.2 Error Analysis

To understand the trends and source of the errors in different approximations to the EOMEA-CCSD method, we have calculated the vertical electron affinities of 20 small molecules like N_2, H_2O, CH^+, F_2, C_2, CO, NH, NO^+, O_2, BH, O_3, C_2H_2, C_2H_4, CO_2, LIF, NaH, Cl_2, BeO, H_2S, and H_2CO, in a hierarchy of Dunning's correlation consistent aug-cc-pVXZ (X = D, T, Q) basis sets.[31] The statistical

analysis shows that the P-EOMEA-CCSD(2) method has an average absolute deviation (AAD) and root-mean-square deviation (RMSD) of 0.03 and 0.07 eV from the standard EOMEA-CCSD values (Table 5.7). The error bars are smaller than that in both P-EOMEA-CCSD and EOMEA-CCSD(2) methods. From Figure 5.1, it can be seen that the P-EOMEA-CCSD(2) method shows the least error in the electron affinity values among the three approximations to the standard EOMEA-CCSD method.

Table 5.7 : Maximum Absolute, Average Absolute, and Root Mean Square Deviation of Calculated Electron Affinity (in eV) from EOMEA-CCSD Values in the aug-cc-PVQZ Basis Set

method	P-EOMEA-CCSD	EOMEA-CCSD(2)	P-EOMEA-CCSD(2)
max abs dev	0.63	0.50	0.49
avr abs dev	0.04	0.05	0.03
RMS dev	0.10	0.11	0.07

Ghosh and co-workers [22] have shown that the use of EOM-CCSD(2) approximation leads to systematic underestimation of excitation energy in the spin-flip EOM method and proposed a linear relationship between the errors in reference and target state. However, in the case of the electron affinity problem, the correlation between error in the reference state and that in the target state will be less straightforward, as the reference and target states differ in the total number of electrons, unlike in the case of the excitation energy problem.

In general, the P-EOMEA-CCSD method overestimates and the EOMEA-CCSD(2) method underestimates the electron affinity values as compared to the standard EOMEA-CCSD method. However, the trends are less systematic. The

truncated $\bar{H}_{DD}$ block of the partition EOMEA matrix leads to a rise in energy of the target state which in turn increases the energy difference between the reference and target states (if the target state is higher in energy than the reference state, see Figure 5.2), i.e., electron affinity value. This leads to systematic overestimation of electron affinity by the P-EOMEA-CCSD method.

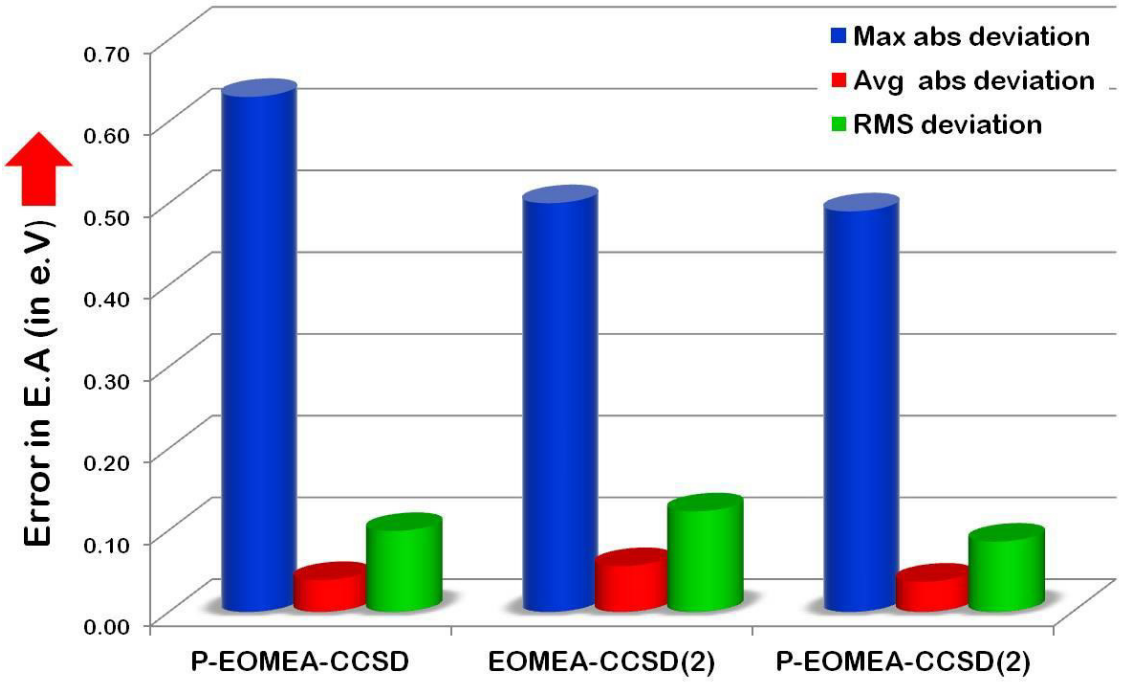

Figure 5.1: Maximum abs deviation, average abs deviation, and RMS deviation of different approximate EOMEA-CC methods from the full EOMEA-CCSD method (in eV).

In the case of the EOMEA-CCSD(2) method, the difference between E_{target}(EOMEA-CCSD) and E_{target}(EOMEA-CCSD(2)) is smaller than that in E_{ref}(CCSD) and E_{ref}(CCSD(2)), since the EOM operators R1 and R2 partly correct the error introduced due to the truncated T amplitudes. Thus, the electron affinity value ($E_{target} - E_{ref}$) calculated by the EOMEA-CCSD(2) method is lower than that calculated in the standard EOMEA-CCSD method. This leads to persistent

underestimation of electron affinity values in the EOMEA-CCSD(2) method. In the P-EOMEA-CCSD(2) method, the truncated $\bar{H}_{DD}$ block reduces the power of the R_1 and R_2 operators to correct for the error in the target state, due to the truncated T amplitudes.

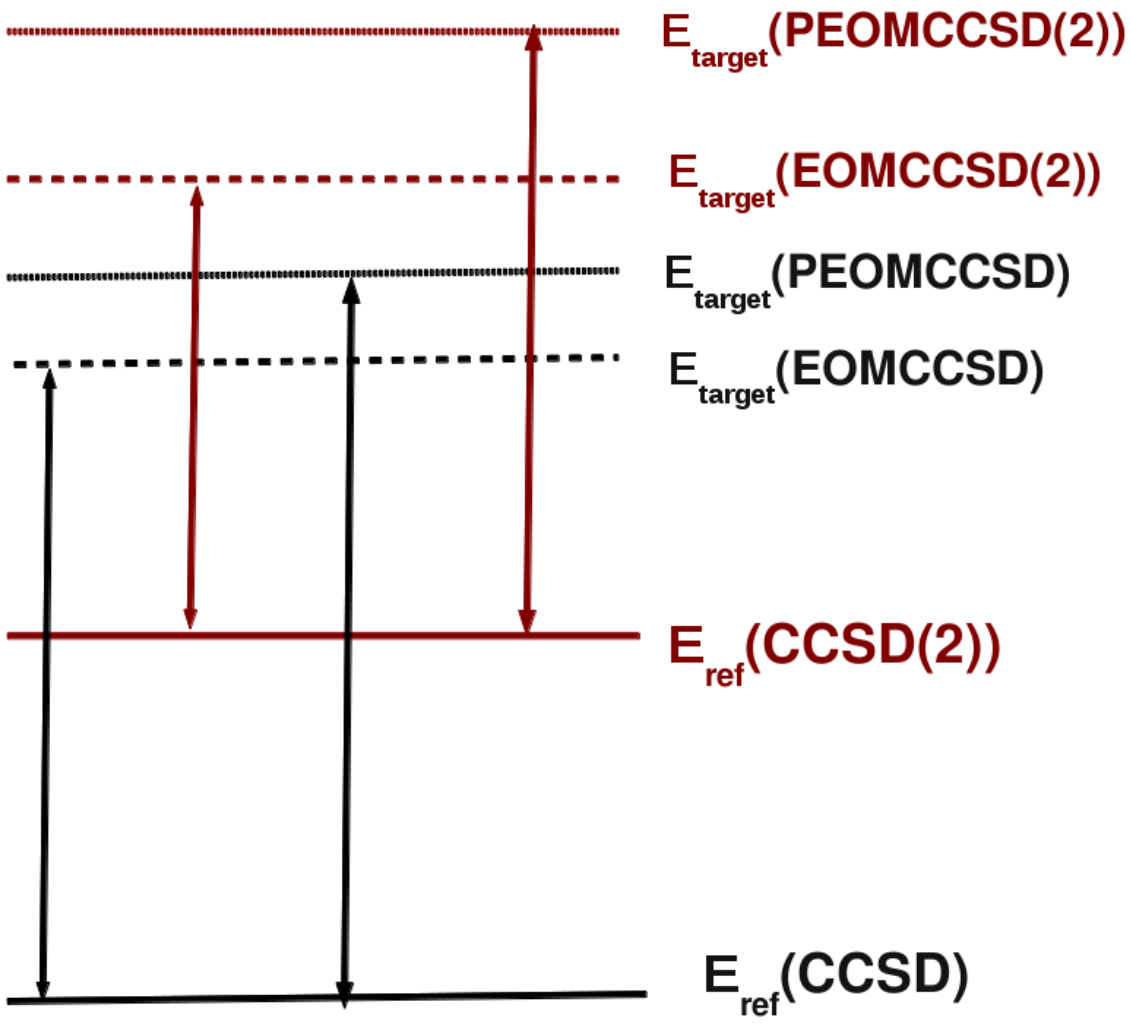

Figure 5.2 .The error cancellation in the difference of energies between reference and target states.

This leads to a better balance in the errors in the E_{ref} and E_{target} states of the P-EOMEA-CCSD(2) method, resulting in systematic error cancelation to give a more accurate value of electron affinity ($E_{target} - E_{ref}$) values than that in the P-

EOMEA-CCSD and EOMEA-CCSD(2) methods. However, the EOM vs P-EOM and the CCSD vs CCSD(2) errors are not exactly additive. The slightly higher error introduced by the P-EOM method in the target state compared to that caused by the CCSD(2) method in the reference state leads to underestimation of the electron affinity values in the P-EOMEA-CCSD(2) method. However, the magnitude of the errors in both the reference state and target state is small in most of the cases.

After gaining some confidence about the sufficient accuracy of the P-EOMEA-CCSD(2) method, we proceed to investigate the vertical electron affinities of DNA and RNA nucleic acid bases (NAB). The electron affinities of NAB are difficult to treat accurately with conventional *ab-initio* methods, and NABs are too big to be investigated in the standard EOMEA-CCSD method, especially with modest computational resources.

5.3.3 Vertical Electron Affinities of DNA and RNA Nucleic Acid Bases

Accurate determination of electron affinities (EA) of DNA and RNA bases (Figure 3) plays a crucial role in understanding the electron donor and acceptor properties of NAB, such as charge transfer and charge transport along the DNA strand [34], radiation damage and repair of the genetic material [35] DNA protein interaction [36], DNA phototherapy [37] and DNA based molecular technologies [38]. A large number of experimental studies [39-46] has been performed for accurate determination of electron affinities. At the same time, numerous theoretical studies [47] with a wide range of theoretical methods, starting from DFT [48-51] to highly correlated CCSD(T) [52, 53] and CASPT2 methods, [52] have also been used for the elucidation of vertical and adiabatic electron affinities of NAB. Theoretical determination of EA of NAB is rather difficult, due to multiple reasons. The density functional theory (DFT) calculations show high dependence [47] on the exchange correlation functional. On the other hand, the state-of-the-art *ab-initio* quantum mechanical calculations, although being more accurate, are difficult to

perform due to the use of a highly diffused basis set, having the maximum radial and angular flexibility [54] required to model the weakly bound electrons. The standard EOMEA-CCSD method, because of its systematic inclusion of dynamic and nondynamic correlation, is the ideal method for accurate theoretical estimations of EA of NAB. However, the prohibitively large computational cost has restricted the application of the EOMEA-CCSD method to NAB. To the best of our knowledge, no EOMCC study has been performed on electron affinities of NAB. The P-EOMEA-CCSD(2) method, because of its N^5 scaling and lesser storage requirements, can easily be applied to calculate the EA of NAB. Table 8 compiles the earlier reported theoretical results and present P-EOMEA-CCSD(2) values for the vertical EA of NAB, together with the available experimental data.

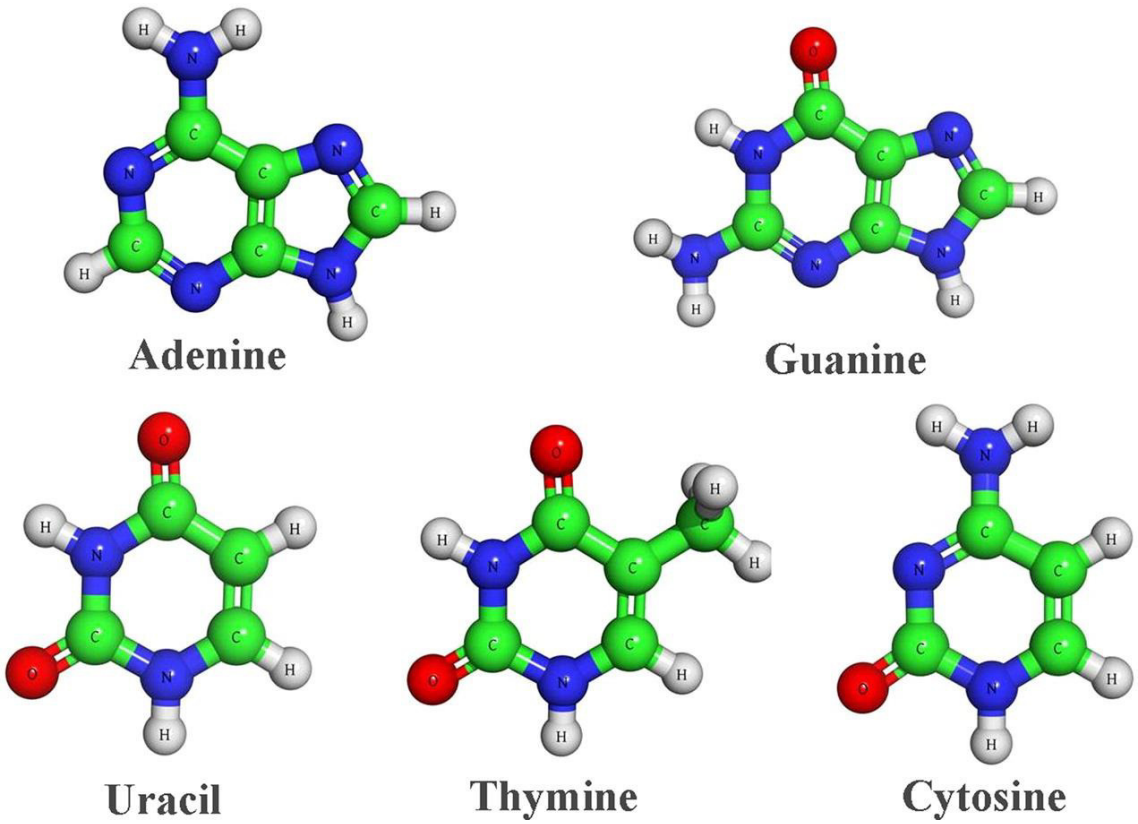

Figure 5.3 : DNA and RNA Nucleic Acid Bases.

Table 5.8 : Low-Lying Vertical Electron Affinities (eV) of DNA and RNA Nucleobases Obtained by Different Experimental, P-EOMEA-CCSD(2), and Other Theoretical Methods

Method	Uracil	Thymine	Cytosin	Adenine	Guanine
Experimental range[a]	−0.30 to −0.22	−0.53 to −0.29	−0.55 to −0.32	−0.56 to −0.45	…
Expt. (ETS)[b]	−0.22	−0.29	−0.32	−0.54	…
Scaled Koopman/D95V[c]	−0.11	−0.32	−0.40	−0.74	−1.23
B3LYP range[d]	−1.09 to −0.11	−1.05 to −0.28	−1.42 to −0.31	−1.57 to −0.34	−2.07 to −0.08
MP2/6-31G(*d*)[e]	−1.77	−1.85	−1.97	−2.54	−2.82
PMP2//MP2/6-31G(*d*)[e]	−1.63	−1.69	−1.76	−2.07	−2.48
MP2/aug-cc-pVDZ	−0.69	−0.73	−0.91	−1.42	−1.57
PMP2//MP2/aug-cc-pVDZ[e]	−0.56	−0.58	−0.73	−0.99	−1.30
CCSD//CCSD/aug-cc-pVDZ[e]	−0.63	−0.65	−0.77	…	…
CCSD(T)//CCSD/aug-cc-pVD[e]	−0.64	−0.65	−0.79	…	…
CASPT2//CASSCF/cc-pVDZ[e]	−1.42	−1.44	−1.49	−1.65	−2.14
CASPT2//CASSCF/ANO-L 431/21[e]	−0.68	−0.69	−0.76	−1.06	−1.30
CASPT2/ANO-L 4321/321//CASSCF/ANO-L 431/21[e]	−0.49	−0.45	−0.59	−0.74	−0.94
P-EOMEA-CCSD(2)/aug-cc-pVDZ/B3LYP/aug-cc-pVTZ[f]	-0.17	-0.28	-0.46	-0.46	-0.34
P-EOMEA-CCSD(2)/aug-cc-pVTZ/B3LYP/aug-cc-pVTZ[f,g]	-0.14	-0.24	-0.41	-0.41	-0.30

a : Values taken from refs 41−43. b: Values taken from ref 41. c : Values taken from ref 55.

d : Values taken from ref 47. e : Values taken from ref 52. f : Present work.

g :aug-cc-pVDZ basis used for hydrogen.

It can be seen that the experimental and theoretical methods provide negative vertical EA values for all the levels, which indicates that the NAB anions are temporary bound states or resonance states, existing in a short period of time and prone to autodetachment.

An analysis of the theoretical methodologies employed for the calculation of vertical EA of NAB reveals that the DFT method gives the most scattered values, ranging from highly negative to nearly equal to zero, strongly dependent upon the functional and the quality of the basis set used. The simplest approach, i.e., via Koopman's approach [55] with some scale factor, gives values more or less similar to experimental values. The MP2 methods[52] lead to very high negative values in the 6-31G(d) basis set. However, the values become less negative with the use of diffused aug-cc-pVDZ. Spin contamination also has a significant effect on electron affinities calculated in the MP2 method. The use of the projected MP2 method makes the predicted electron affinity value less negative, i.e., closer to the experimental values. The CCSD(T)[52] and CASPT(2)[52] give similar values, and both underestimate (i.e., gives more negative value) compared to the experimental results.

The P-EOMEA-CCSD(2) method gives the best agreement with the experimental values. There exists a striking difference in the trends of electron affinity values calculated in the P-EOMEA-CCSD(2) method with the earlier reported values. The electron affinities calculated using the P-EOMEA-CCSD(2) method are much less negative compared to that obtained in the MP2 and CCSD(T) method by Serrano-Andres and co-workers.[52] Especially the vertical EA for uracil is very small in the P-EOMEA-CCSD(2)/aug-cc-pVTZ level of theory, unlike that reported in the earlier theoretical investigation. It should be noted that the above CCSD(T) calculations by Serrano-Andres and co-workers[52] were performed in the small aug-cc-pVDZ basis set. The OVOS-CCSD(T) calculation in aug-cc-

pVTZ by Urban and co-workers[53] has resulted in a vertical EA value of −0.15 eV for urcail, which is nearly identical with our P-EOMEA-CCSD(2) value of −0.14 eV. It is also interesting to note that the purine NAB, adenine and guanine, show significantly less negative values in P-EOMEA-CCSD(2) method than that in the CCSD(T) method.

The loosely bound electron in NAB anions may lead to multiple near-degenerate configurations requiring systematic inclusion of non-dynamic correlation, which CCSD(T) fails to include in a balanced way. The electron affinity values calculated in the CASPT(2) method shows that with inclusion of non-dynamic correlation, electron affinities become less negative. However, the CASPT(2) values strongly depend on the choice of active space. The EOM based methods, on the other hand, provide a balanced description of both dynamic and non-dynamic correlation and is "black box" to use. Therefore, detailed studies of electron attachment and the electron attachment induced structural changes of NAB using EOMCC methods are required to get a better analysis of the experimental values. However, it is outside the scope of the present study and will be followed in a subsequent study.

5.4 Conclusion

Electron attachment variant of EOM-CC offers a versatile approach to model electron attachment to atoms and molecules. In this work, we present an N^5 scaling, size-consistent modification to the standard EOMEA-CCSD method based on perturbation order analysis and the matrix partitioning technique. The proposed approximation (P-EOMEA-CCSD(2)) has significantly less storage than the earlier proposed EOMEA-CCSD(2) method. We have benchmarked the new method with standard EOMEA-CCSD methods. Statistical analysis of the results

shows that P-EOMEA-CCSD(2) provides an inexpensive way for accurate determination of the electron affinities, when the ground state of the system is well described by the MBPT(1) wave function. For systems where the MBPT(1) wave function fails to properly describe the ground-state reference, no EOM-CCSD(2) method can give quantitatively accurate values and can only be used to get a mere qualitative picture. The P-EOMEA-CCSD(2) approximation gives similar accuracy to that of the previous EOMEA-CCSD(2) method, even better in most of the cases, in spite of the former having significantly lesser storage requirements. We have used the P-EOMEA-CCSD(2) method to calculate the electron affinities of DNA and RNA nucleic acid bases. The results have shown excellent agreement with experimental values.

The newly developed P-EOMEA-CCSD(2) method has immense potential to be used in the study of electron attachment to biological molecules and large clusters. The implementation of analytic derivatives is required for the purpose. Work is currently under way toward that direction.

References:

1. Crawford, O. H.; Garrett, W. R., *J. Chem. Phys.* **1977,** *66*, 4968-4970.
2. Desfrancois, C.; Abdoul-Carime, H.; Khelifa, N.; Schermann, J. P., *Phys. Rev. Lett.* **1994,** *73*, 2436-2439.
3. Sommerfeld, T.; DeFusco, A.; Jordan, K. D., *J. Phys. Chem. A* **2008,** *112*, 11021-11035.
4. Herbert, J. M.; Head-Gordon, M., *Phys. Chem. Chem. Phys.* **2006,** *8*, 68-78.
5. Hughes, S. R.; Kaldor, U., *J. Chem. Phy.s* **1993,** *99*, 6773-6776.
6. Raghavachari, K.,. *J. Chem. Phys.* **1985,** *82*, 4142-4146.
7. Stanton, J. F.; Bartlett, R. J., *J. Chem. Phys.* **1993,** *98*, 7029-7039.
8. Krylov, A. I., *Annu. Rev. Phys. Chem.* **2008,** *59*, 433-462.
9. Nooijen, M.; Bartlett, R. J., *J. Chem. Phys.* **1995,** *102*, 3629-3647.
10. Nooijen, M.; Bartlett, R. J., *J. Chem. Phys.* **1995,** *102*, 6735-6756.
11. Musial, M.; Bartlett, R. J., *J. Chem. Phys.* **2003,** *119*, 1901-1908.
12. Gour, J. R.; Piecuch, P., *J. Chem. Phys.* **2006,** *125*, 234107-17.
13. Musial, M.; Bartlett, R. J., *J. Chem. Phys.* **2008,** *129*, 134105-12.
14. Pal, S.; Rittby, M.; Bartlett, R. J.; Sinha, D.; Mukherjee, D., *J. Chem. Phys.* **1988,** *88*, 4357-4366.
15. Pal, S., *Mol. Phys* **2010**. *108*, 3033-3042.
16. Musial, M.; Bartlett, R. J.,. *J. Chem. Phys* **2008,** *129*, 044101-10.
17. Kaldor, U.; Haque, A., *Chem. Phys. Lett.* **1986,** *128*, 45-48.
18. Bartlett, R. J., *Annu. Rev. Phys. Chem.* **1981,** *32*, 359-401.
19. Nooijen, M.; Snijders, J. G., *J. Chem. Phys.* **1995,** *102*, 1681-1688.
20. Stanton, J. F.; Gauss, J., *J. Chem. Phys.* **1995,** *103*, 1064-1076.
21. Dutta, A. K.; Vaval, N.; Pal, S., *J. Chem. Theory Comput.* **2013,** *9*, 4313–4331.
22. Dutta, A. K.; Pal, S.; Ghosh, D., *J. Chem. Phys.* **2013,** *139*, 124116-11

23. Voora, V. K.; Cederbaum, L. S.; Jordan, K. D., *J. Phys. Chem. Lett.* **2013,** *4*, 849-853.

24. Vysotskiy, V. P.; Cederbaum, L. S.; Sommerfeld, T.; Voora, V. K.; Jordan, K. D., *J. Chem. Theory Comput.* **2012,** *8*, 893-900.

25. Gwaltney, S. R.; Nooijen, M.; Bartlett, R. J., *Chem. Phys. Lett.* **1996,** *248*, 189-198.

26. Gwaltney, S. R.; Bartlett, R. J., *J. Chem. Phys.* **1999,** *110*, 62-71.

27. Nooijen, M.; Ajith Perera, S.; Bartlett, R. J.,. *Chem. Phys. Lett.* **1997,** *266*, 456-464.

28. Löwdin, P.O., *J. Mol. Spectros*. **1963,** *10*, 12-33.

29. Krylov, A. I., *Chem. Phys. Lett.* **2001,** *350*, 522-530.

30. Stanton, J. F., *J. Chem. Phys.* **1994,** *101*, 8928-8937.

31. Kendall, R. A.; Dunning, J. T. H.; Harrison, R. J., *J. Chem. Phys.* **1992,** *96*, 6796-6806.

32. Schmidt, M. W.; Baldridge, K. K.; Boatz, J. A.; Elbert, S. T.; Gordon, M. S.; Jensen, J. H.; Koseki, S.; Matsunaga, N.; Nguyen, K. A.; Su, S.; Windus, T. L.; Dupuis, M.; Montgomery, J. A., *J. Comput. Chem.* **1993,** *14*, 1347-1363.

33. Bokhan, D.; Ten-no, S., *J. Chem. Phys.* **2010,** *132*, 021101-4.

34. Steenken, S., *Chem. Rev.* **1989,** *89*, 503-520.

35. Colson, A.. O.; Sevilla, M. D., *J. Phys. Chem.* **1995,** *99*, 3867-3874.

36. Wintjens, R.; Lièvin, J.; Rooman, M.; Buisine, E., *J. Mol. Biol.* **2000,** *302*, 393-408.

37. Bonnett, R., *Chemical aspects of photodynamic therapy*. CRC Press: 2000.

38. Prasad, P. N., *Introduction to biophotonics*. John Wiley & Sons: 2004.

39. Wiley, J. R.; Robinson, J. M.; Ehdaie, S.; Chen, E. C. M.; Chen, E. S. D.; Wentworth, W. E., *Biophys. Res. Commun.* **1991,** *180*, 841-845.

40. Chen, E. C. M.; Wiley, J. R.; Batten, C. F.; Wentworth, W. E., *J. Phys. Chem.* **1994,** *98*, 88-94.

41. Aflatooni, K.; Gallup, G. A.; Burrow, P. D., *J. Phys. Chem. A* **1998,** *102*, 6205-6207.

42. Periquet, V.; Moreau, A.; Carles, S.; Schermann, J. P.; Desfrancois, C., *J. Electron. Spectrosc. Relat. Phenom.* **2000,** *106*, 141-151.

43. Harinipriya, S.; Sangaranarayanan, M. V., *J. Mol. Struct.* **2003,** *644*, 133-138.

44. Chen, E. C. M.; Chen, E. S., *J. Phys. Chem. B* **2000,** *104*, 7835-7844.

45. Desfrancois, C.; Periquet, V.; Bouteiller, Y.; Schermann, J. P., *J. Phys. Chem. A* **1998,** *102*, 1274-1278.

46. Compton, R. N.; Carman, J. H. S.; Desfrancois, C.; Abdoul-Carime, H.; Schermann, J. P.; Hendricks, J. H.; Lyapustina, S. A.; Bowen, K. H., *J. Chem. Phys.* **1996,** *105*, 3472-3478.

47. Gu, J.; Leszczynski, J.; Schaefer, H. F., *Chem. Rev.* **2012,***112*, 5603-5640.

48. Wetmore, S. D.; Boyd, R. J.; Eriksson, L. A., *J. Phys. Chem. B* **1998,** *102*, 10602-10614.

49. Richardson, N. A.; Wesolowski, S. S.; Schaefer, H. F., *J. Phys. Chem. B* **2002,** *107*, 848-853.

50. Gu, J.; Xie, Y.; Schaefer, H. F., *J. Phys. Chem. B* **2006,** *110*, 19696-19703.

51. Richardson, N. A.; Wesolowski, S. S.; Schaefer, H. F., *J. Am. Chem. Soc.* **2002,** *124*, 10163-10170.

52. Roca-Sanjuan, D.; Merchan, M.; Serrano-Andres, L.; Rubio, M., *J. Chem. Phys.* **2008,** *129*, 095104-11.

53. Dedíková, P.; Demovíc, L.; Pitoňák, M.; Neogrády, P.; Urban, M., *Chem. Phys. Lett.* **2009,** *481*, 107-111.

54. Rienstra-Kiracofe, J. C.; Tschumper, G. S.; Schaefer, H. F.; Nandi, S.; Ellison, G. B., *Chem. Rev.* **2002,** *102*, 231-282.

55. Sevilla, M. D.; Besler, B.; Colson, A.. O., *J. Phys. Chem.* **1995,** *99*, 1060-1063.

Chapter 6

Perturbative approximations to single and double spin flip equation of motion coupled cluster methods

"If the red slayer think he slays,
Or if the slain think he is slain,
They know not well the subtle ways
I keep, and pass, and turn again"

Ralph Waldo Emerson
Brahma

Spin flip equation of motion coupled cluster (EOM-SF-CC) can correctly treat situations involving electronic degeneracies or near-degeneracies, e.g., bond breaking, di- and tri-radicals, etc. However, for large systems EOM-SF-CC (even in single and double excitations) is computationally prohibitively expensive. Therefore, earlier approximations to EOM-SF-CC methods such as spin flip configuration interaction singles with perturbative doubles (SF-CIS(D)) have been proposed. In this chapter, we present a new perturbative approximation to EOM-SF-CC, which has been found to be more accurate than SF-CIS(D). The capabilities, advantages, and timings of the new approach have been demonstrated considering the singlet-triplet gaps in di- and tri-radicals as well as bond breaking examples. The method is extended to double spin flip EOM-CC, and its capabilities have been tested. We have shown that the second order approximation to single and double spin flip EOM-CC can generate very accurate potential energy surface and their geometrical derivatives.

6.1 Introduction:

Prediction and explanation of gas phase molecular spectra have been one of the major focus of theoretical chemistry in the last few decades. The single reference coupled cluster (SRCC) approach[1–8] has proved incredibly successful for closed shell molecules. SRCC considers dynamic correlation in a very systematic way, but leaves out the non-dynamic component of the correlation and therefore, fails for open shell molecules and bond breaking.

In order to treat both dynamic and non-dynamic correlations, coupled cluster (CC) ansatz starting from a multi-determinantal reference (multi-reference coupled cluster (MRCC)) has been developed over the years [9–21]. Within the SRCC formalism, renormalized coupled cluster methods (renormalized coupled cluster singles doubles (RCCSD)) [22–24], have been developed, which are more successful in tolerating situations with limited non-dynamic correlation. However, there are difficulties associated with all the MRCC methods, such as active space selection, need of state averaging, etc., that prohibit its routine application [25]. To circumvent these problems, alternative approaches such as equation-of-motion (EOM) [26–28] and linear response (LR) coupled cluster [29–33] have been developed. Equation-of-motion-coupled-cluster (EOM-CC) [26,28,34–39] has emerged as one of the most reliable methods for the calculation of ionization energy [38,40–42], excitation energy, and electron affinity [27,39,43].

However, traditional EOM-CC has been limited in its application by the initial "single determinantal" coupled cluster reference. Therefore, it is difficult to treat truly multi-reference problems such as di- or tri-radicals and bond breaking where the consideration of non-dynamic correlation is crucial [41,44–48]. Krylov and co-workers have used single or double spin flip (SF or DSF) [49–56] operators to introduce multi-configurational character to the traditional EOM-CC calculations. The main advantage of the SF or DSF approach lies in its simplicity and the ease

of implementation. Additionally, by construction SF or DSF does not have the problems associated with genuine MRCC.

Despite the success of EOM-SF-CC method and the CC methods in general, it remains limited to small systems due to the rather steep computational scaling (N^6) for coupled cluster singles doubles (CCSD) and (N^7) for the non-iterative triples corrected CCSD(T). There have been various attempts at reducing the computational cost of EOM-CC, such as the use of frozen natural orbitals (FNO) [57,58] and restricted active spaces in the EOM part [59]. However, these methods can only reduce the pre-factor and not the intrinsic computational scaling [60]. An alternative approach taken by Nooijen et al. [61,62] and Stanton and Gauss [63], and later generalized by Hirata et al. [64], has been to approximate the coupled cluster effective Hamiltonian based on many body perturbed Hamiltonians. The benefit of this approach, especially when considering the second order perturbed Hamiltonian is the reduction in scaling in the form of EOM-CCSD(2) or EOM-MBPT(2) (iterative (N^6) for CCSD vs iterative (N^5) for CCSD(2) or MBPT(2)). EOM-CCSD(2) has been implemented and tested for excitation energies and ionization energies [63]. Recently, Pal and co-workers have shown that EOMIP-CCSD(2) can be used to predict bond length and IR frequencies of large doublet radicals, with accuracy comparable to that of conventional EOMIP-CCSD method [65]. On the other hand, there have been approximations to SF and ionization potential (IP) versions of the EOM-CCSD method, where the effective Hamiltonian has been defined as the Hartree Fock (HF) Hamiltonian. This is the so-called equation-of-motion-configuration interaction singles with perturbative doubles (EOM-CISD) or the EOM-CIS(D) depending on the different levels of approximation in the EOM excitation operator. Here, it should be mentioned that SF-CISD has the same computational scaling as EOM-SF-CCSD while the scaling of IP-CISD is lower than EOM-IP-CCSD. Taking our motivation from the previous works [63,65] we have implemented EOM-SF-CCSD(2) and EOM-DSF-CCSD(2)[2,3] variants where the effective Hamiltonian (similar to EOM-IP-

CCSD(2)) is the second order perturbed (MP2) Hamiltonian and EOM-SF or EOM-DSF is carried out on top of that. In this work, we will show that this approximation is capable of breaking single and double bonds. It can reproduce singlet triplet gaps within an accuracy of 0.1 eV for small molecules, with respect to full EOM-SF-CCSD. We compare the performance of this new method with the existing EOM-SF-CCSD and EOM-DSF-CCSD[2,3], SF-CIS(D), double spin flip configuration interaction doubles triples as well as complete active space methods such as complete active space second order perturbation theory (CASPT2).

The organization of the chapter is as follows. The theory of the new approximation and computational details of the calculations are provides in the next section. The section 6.3 consists of the results and discussions of the various test cases. We summarize our conclusions in section 6.4 .

6.2 Theory and Computational Details

6.2.1 EOM-SF-CCSD(2) and EOM-DSF-CCSD(2)[2,3]

The central premise of the CC theory starts with the uncorrelated Hartree-Fock (HF) wave-function $|\phi_0\rangle$ and the exponential ansatz that assumes the correlated wave-function can be calculated from

$$|\psi_{CC}\rangle = \exp\left(\hat{T}\right)|\phi_0\rangle \tag{6.1}$$

where $|\psi_{CC}\rangle$ is the coupled cluster correlated wave-function. The operator $\hat{T}$ can be written as

$$\begin{aligned} T &= T_1 + T_2 + ... \\ &= \sum_{i,a} t_i^a a^\dagger i + \frac{1}{4}\sum_{i,j,a,b} t_{ij}^{ab} a^\dagger b^\dagger ij + ... \end{aligned} \tag{6.2}$$

in the traditional CCSD form. The *i, j* indices refer to the occupied orbitals and *a, b* refer to the virtual orbitals in the HF reference orbitals. The EOM-CC method is a conceptually single reference approach for the description of excited states starting from this CC reference. The kth excited state eigen functions are written as linear excitations from the ground state CC reference,

$$\left|\psi_{CC,k}\right\rangle = \hat{R}_k \left|\psi_{CC,0}\right\rangle \tag{6.3}$$

where 0 and k refers to the ground state and kth excited states, respectively. The operator $\hat{R}_k$ for the different flavors of EOM-CC can be expanded as

$$\begin{aligned}
\hat{R}_k^{IP} &= \sum_i R_i(k) i + \sum_{i>j,a} R_{ij}^a(k) \hat{a}^\dagger \hat{j}\hat{i} + \ldots\ldots\ldots \\
\hat{R}_k^{EA} &= \sum_a R^a(k) \hat{a}^\dagger + \sum_{a>b,j} R_j^{ba}(k) \hat{b}^\dagger \hat{j}\hat{a}^\dagger + \ldots\ldots\ldots \\
\hat{R}_k^{EE} &= R_0(k) + \sum_{i,a} R_i^a(k) \hat{a}^\dagger i + \sum_{a>b,i>j} R_{ij}^{ab}(k) \hat{a}^\dagger \hat{b}^\dagger ij + \ldots\ldots\ldots \\
\hat{R}_k^{SF} &= R_0(k) + \sum_{i,a} R_{i\uparrow}^{a\downarrow}(k) \hat{a}_\downarrow^\dagger i_\uparrow + \sum_{a>b,i>j} R_{i\uparrow j\uparrow}^{a\downarrow b\uparrow}(k) \hat{a}_\downarrow^\dagger \hat{b}_\uparrow^\dagger i_\uparrow j_\uparrow + \ldots\ldots\ldots
\end{aligned} \tag{6.4}$$

where EE, IE, EA, and SF refer to excitation energy, ionization energy, electron affinity, and spin flip, respectively. In case of the SF operator, α and β spins are denoted by ↑ and ↓ respectively, the equation shows the case where one starts with an excess α electrons (this can be easily generalized to the reference with excess β electrons). The operator $\hat{R}$ is an excitation operator truncated at a certain order of excitation. Reference [66] gives a detailed description of the method. For a system with significant non-dynamic correlation, one needs to consider multiple possible configurations. This can be achieved through the SF operator which changes the spin of the system ($\Delta M_s = \pm 1$) but not the number of particles ($\Delta N = 0$), thus generating the configurations shown in Figure 6.1. One starts with a high spin triplet state (with excess α/β electrons) which is predominantly single reference in nature. From that reference, the $\hat{R}^{[SF]}$ operator moves one electron with α/β spin to β/α spin, which changes the state from high spin ($M_s = 1$) to low spin (singlet and M s = 0 triplet), and in the process considers various configurations. Analogously

extending to DSF-CCSD one can consider double bond breaking, i.e., the operator $\hat{R}^{[DSF]}$ causes $\Delta M_s = \pm 2$. The operator $\hat{R}_2^{[DSF]}$ can be written as

$$\hat{R}_k^{DSF} = R_0(k) + \sum_{a>b,i>j} R_{i\uparrow j\uparrow}^{a\downarrow b\downarrow}(k)\hat{a}_\downarrow^\dagger \hat{b}_\downarrow^\dagger i_\uparrow j_\uparrow + ... \tag{6.5}$$

assuming one starts with a quintet reference with an excess α or ↑ electrons.

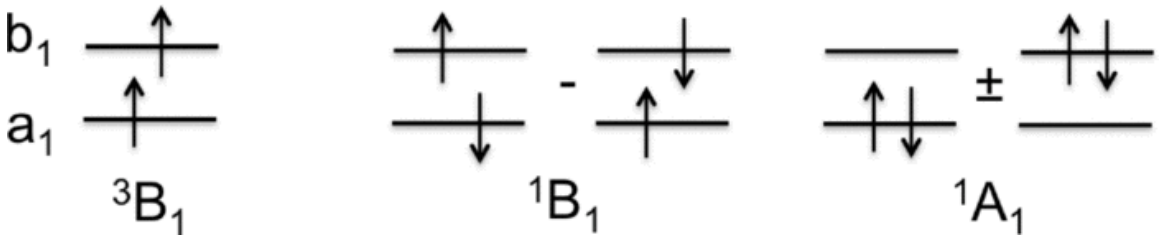

Figure 6.1 : Starting with $^3B_1$ reference state, spin flip operator creates target open shell $^1B_1$ state and closed shell singlet states 1 $^1A_1$ and 2 $^1A_1$.

The CC theory and many body perturbation theory (MBPT) are closely related techniques for the calculation of many body effects. [2,67] Therefore, a natural way of analyzing and reducing the computational cost of CC based methods is to look at the possible perturbative approximations. One can express the effective Hamiltonian $\bar{H}$ as the connected terms in $\left[H\exp\left(\hat{T}\right)\right]$. This effective Hamiltonian can also be expanded as a Baker-Campbell-Hausdorff (BCH) expansion,

$$\bar{H} = H + [H,T] + \frac{1}{2}[[H,T],T] + \frac{1}{6}[[[H,T],T],T] + ... \tag{6.6}$$

and alternatively as a perturbative expansion,

$$\bar{H} = \bar{H}^{[0]} + \bar{H}^{[1]} + \bar{H}^{[2]} + \bar{H}^{[3]} + ... \tag{6.7}$$

Two slightly different perturbative approaches have been reported in the literature [61,63]. Nooijen and Snijders[61] first proposed a truncation of the CCSD effective Hamiltonian based on the above perturbative scheme and Stanton and Gauss [63] generalized it within the EOM approach. Truncations at the nth level of

the effective Hamiltonian give rise to n^{th} order of MBPT ground state, e.g., CCSD(2) for MBPT[(2), CCSD(3) for MBPT(3), etc. The detailed working expressions for the approximations are given in Ref. [63] . According to the n^{th} truncation in the perturbative series, approximate EOM-CCSD(n) can be formulated. The lowest order expansion is the EOM-CCSD(2), where the $\bar{H}$ is truncated at the second order perturbative level (MBPT(2)).

In case of truncated effective Hamiltonians (at the level of $H^{[2]}$), the CC amplitudes can be expressed as the MBPT(2) amplitudes [62],

$$\begin{aligned} \bar{H} &= \left(H \, \mathrm{e}^{T} \right)_c \\ &\approx \left(H \, \mathrm{e}^{T'} \right)_c \end{aligned} \tag{6.8}$$

where the perturbative approximation to the T amplitudes can be written as

$$\begin{aligned} T_1' &= \frac{f_{ia}}{\varepsilon_i - \varepsilon_a} \\ T_2' &= \frac{\langle ab || ij \rangle}{\varepsilon_i + \varepsilon_j - \varepsilon_a - \varepsilon_b} \end{aligned} \tag{6.9}$$

T_1 is zero for restricted closed shell and unrestricted MBPT(2) reference. Using these T' amplitudes one can calculate a modified effective $\bar{H}'$, which can be used as the reference for subsequent EOM calculation. Thus, this is necessarily an EOM calculation on a MBPT(2)reference state. In our implementation of EOM-SF-CCSD(2), we use the later approach of perturbatively approximating the amplitudes T′, which is slightly different from the original Nooijen and Snijders' approach. Reference 63 gives a good discussion on the differences of these two methods as well as the fact that both the methods give exactly the same ionization energies within the EOM-IP framework.

Of course, in our approach the CC ground state energy reduces to the MBPT(2) ground state energy, with the reduction of computational scaling from iterative N^6 to non-iterative N^5. There are still some elements of $\bar{H}$ that need to be calculated

that scale as N^6, but the scaling of the ground state is dominated by the iterative part. Therefore, our approach gives significant saving in terms of reference state calculation. However, the total scaling of the method is still determined by the EOM part and the total computational scaling of EOM-SF-CCSD and EOM-SF-CCSD(2) are O(N^6), but the total timings of the EOM-SF-CCSD(2) is much lower than the EOM-SF-CCSD. Table 6.1 compares the approaches in the existing SF methods with the new EOM-SF-CCSD(2) method. The corresponding method for DSF has been named EOM-DSF-CCSD(2)[2,3], where [2,3] denotes that we use amplitudes up to 2nd order to calculate the effective Hamiltonian and in the EOM part we use up to 3 hole, 3 particle (3h,3p) operators. In the original DSF formalism it has been noticed that significantly better results are obtained when 3h,3p operators are used than 2h,2p in the EOM part [55].

Table 6.1 : Hierarchy of spin flip methods. For explicit forms see Eqs. (6.10)–(6.12) .

Reference	**Method**	**Wave-function**
SCF	SF-CIS	$R_1\phi_0$
SCF(MP2)	SF-CIS(D)	$R_1\phi_0 + R_2\phi_0$ *by PT*
SCF	SF-CISD	$(R_1 + R_2)\phi_0$
CCSD(2)	SF-CCSD(2)	$(R_1 + R_2)\exp(T_1' + T_2')\phi_0$
CCSD	SF-CCSD	$(R_1 + R_2)\exp(T_1 + T_2)\phi_0$

6.2.2 Comparison of EOM-SF-CCSD(2) with other SF methods

SF-CIS, SF-CIS(D), and SF-CISD form the class of methods that start from a HF reference as the effective Hamiltonian. EOM-SF-CCSD on the other hand contains the full CCSD effective Hamiltonian and therefore, a CCSD reference state. EOM-SF-CCSD(2) lies in between these two approximations, where we start from a MBPT(2) reference state, i.e., truncated CCSD effective Hamiltonian.

It is especially important to compare SF-CIS(D) and EOM-SF-CCSD(2) because both of these have a perturbative correction. However, their difference can be explained by "excite then perturb" (CIS(D)) vs "perturb then excite" technique (CCSD(2)). SF-CIS and SF-CIS(D) have single excitation ($\hat{R}_1$) while SF-CISD and EOM-SF-CCSD(2) also include double excitations ($\hat{R}_1 + \hat{R}_2$).

The energy expressions for the various related methods can be written as

$$E^{EOM-CCSD} = \langle 0 | Le^{-T} He^{T} R | 0 \rangle = \langle 0 | L\bar{H}R | 0 \rangle \tag{6.10}$$

$$E^{EOM-CCSD(2)} = \langle 0 | Le^{-T'} He^{T'} R | 0 \rangle = \langle 0 | L\bar{H}'R | 0 \rangle \tag{6.11}$$

$$E^{CIS(D)} = \langle 0 | L^{[1]} H R^{[2]} | 0 \rangle + \langle 0 | L^{[1]} H T_{[2]} R^{[1]} | 0 \rangle \tag{6.12}$$

where T_2 creates the first order MBPT wave-function when it acts on $|0\rangle$. For the CIS(D) energy, the first term takes care of the direct electron correlation and the second term takes care of correlation between pairs of electrons that are not connected by singles. We should also mention a related method, CIS-MP2, which fares worse than the CIS(D) due to the presence of disconnected terms [68]. From the energy expressions and the wave-functions listed in the hierarchy of methods (Table 6.1), we expect the accuracy as well as computational timings of the newly developed EOM-SF-CCSD(2) to be in between that of EOM-SF-CCSD and SF-CIS(D).

6.2.3 Size Consistency

We start by defining size-consistency as the capacity to partition the energy of two non-interacting fragments correctly. As explained in the literature [52,69], this means that the reference energy (ground state) needs to be size-consistent as well as the transition/excitation energy. Stanton and Gauss [63] have proved that approximating the effective Hamiltonians based on perturbative orders lead to size

extensivity of the ground state for every order of perturbation, which fulfils the first condition. Reference 63 shows the detailed derivation.

The second condition requires consideration of the linear excitation operators $R\hat{}n$ (similar to CI). One starts with the Hamiltonian which is the sum of the Hamiltonians of the fragments in the non-interacting limit,

$$\hat{H} = \hat{H}_A + \hat{H}_B \tag{6.13}$$

In order to show that the energies are separable, one needs to show that this Hamiltonian of both the fragments can be represented in a block diagonal form

$$\hat{H} = \begin{pmatrix} H_{0,0} & H_{0,A} & H_{0,B} & H_{0,AB} \\ H_{A,0} & H_{A,A} & H_{A,B} & H_{A,AB} \\ H_{B,0} & H_{B,A} & H_{B,B} & H_{B,AB} \\ H_{AB,0} & H_{AB,A} & H_{AB,B} & H_{AB,AB} \end{pmatrix} \tag{6.14}$$

where, $H_{AB,AB} = \langle \Psi_A \Psi_B | H_A + H_B | \Psi_A \Psi_B \rangle$, $H_{AB,0} = \langle \Psi_A \Psi_B | H_A + H_B | \Psi_0 \Psi_0 \rangle$ and so on. 0_A, 0_B, Ψ_A and Ψ_B refer to the ground and excited states on A and B, respectively.

References 52 and 70 show that most of the terms of this Hamiltonian can be easily shown to be zero. The terms $H_{0,P}$ and $H_{P,0}$, where P = A, B, AB, are zero since the initial and final states differ in their spin (triplet to singlet) and therefore, cannot be connected through the Hamiltonian. Note that these terms are not necessarily zero for non-SF CI expansions. Thus, $\hat{H}$ can be expressed as

$$\hat{H} = \begin{pmatrix} H_{0,0} & 0 & 0 & 0 \\ 0 & H_{A,A} & H_{A,B} & H_{A,AB} \\ 0 & H_{B,A} & H_{B,B} & H_{B,AB} \\ 0 & H_{AB,A} & H_{AB,B} & H_{AB,AB} \end{pmatrix} \tag{6.15}$$

The terms $H_{A,B}$ and $H_{B,A}$ are zero since $\hat{H}_A$ acts only on states in A and $\hat{H}_B$ on states in B, in the non-interacting limit. These terms would be zero even for non-

SF CI. The only intriguing term arises as $H_{A,AB}$, assuming one starts with a triplet state on A. Now, expanding the term $H_{A,AB}$,

$$\begin{aligned} H_{A,AB} &= \langle \Psi_A 0_B | \hat{H}_A + \hat{H}_B | \Psi'_A \Psi_B \rangle \\ &= \langle 0_B | \Psi_B \rangle \langle \Psi_A | \hat{H}_A | \Psi'_A \rangle + \langle \Psi_A | \Psi'_A \rangle \langle 0_B | \hat{H}_B | \Psi_B \rangle \\ &= 0 + \langle \Psi_A | \Psi'_A \rangle \langle 0_B | \hat{H}_B | \Psi_B \rangle \end{aligned} \tag{6.16}$$

Where, the first part of the equation is trivially zero since $\langle 0_B | \psi_B \rangle$ is zero. The second part of the equation is non-zero for general CISD expansion. One can show that for SF case this reduces to zero due to Brillouin condition. It can be generally proved that such terms will be zero for nSF if excitations up to (n + 1) are considered in the CI expansion. Following this condition, both EOM-SF-CCSD(2) and EOM-DSF-CCSD(2)[2,3], the later containing up to triple excitation in the EOM part, are size consistent.

6.2.4 Computational Details

We have implemented the methods (EOM-SF-CCSD(2) and EOM-DSF-CCSD(2)[2,3] energies) in a developers version of the quantum chemistry package Q-CHEM [71]. The truncation of the effective Hamiltonian in perturbative order will only need modification of $\bar{H}$ intermediates, which can easily be achieved by modifying an existing EOM-CC code. The Appendix II gives the expressions for the modified $\bar{H}$. The effect of basis set on the EOM-CCSD(2) singlet triplet gap is studied for small diradicals for the basis sets cc-pVDZ, cc-pVTZ, and cc-pVQZ. The method is benchmarked with EOM-CCSD method for singlet triplet (ST) energy gaps of diradicals. Complete active space self-consistent field (CASSCF) and CASPT2 calculations (with no frozen core, without state averaging) for benchmarking are carried out with GAUSSIAN 09 [72] and full configuration interaction (FCI) calculations are carried out with PSI4 [73]. The potential energy surfaces (PES) are calculated with cc-pVDZ basis set, unless otherwise mentioned. In order to study the oxirane ring opening with EOM-SF-CCSD(2), we have

optimized the geometries along the reaction coordinate, in this case ∠COC. The geometries at each angle has been constrained optimized with B3LYP/cc-pVDZ.

6.3 Results and Discussion

The wall timings for the spin flip computations of singlet triplet gap in carbenes with long aliphatic chains (R C̈ H) are shown in Table 6.2 . EOM-SF-CCSD(2) is found to be considerably cheaper computationally than EOM-SF-CCSD. The timings reported are with CCMAN module with cc memory set to 25 000. Our method has also been implemented in the newer module, which is parallel and therefore, the EOM-SF-CCSD(2) method can trivially utilize this parallelization. In this work, we have not dealt with the parallelization in details.

Table 6.2 : Wall timings (in s) for SF-CIS(D), EOM-SF-CCSD, and EOM-SF-CCSD(2) calculations of long chain carbenes. The computations were performed with single core on an i7 workstation (3.50 GHz) with 32 GB RAM.

Number of C	SF-CIS(D)	EOM-SF-CCSD	EOM-SF-CCSD(2)
1	0.21	1.74	1.18
2	1.22	6.37	3.57
3	5.27	30.95	14.94
4	23.31	148.06	70.58
5	61.61	514.87	229.0
6	158.77	1507.95	538.51
7	355.60	7476.40	1353.97

6.3.1 CH_2, NH_2^+, O_3

The calculation of singlet-triplet gaps in hypovalent compounds such as methylene (or other substituted carbenes) and nitrenium ion is complicated due to the presence of both dynamic and non-dynamic correlations. The singlet states are multi-configurational in nature, while the triplet states are single reference and the inclusion of dynamic correlation is important. Thus, for estimating the energy difference one needs to have a balanced description of both. These compounds have been used as test cases for many multi-reference theories. Moreover, understanding the nature of ground states (singlet or triplet) of the substituted carbenes and nitrenium ions are important due to their implications in reactivity [74].

The triplet state of both the isoelectronic compounds, methylene and nitrenium ion, is given by the single determinant – $(1a_1)^2\ (2a_1)^2\ (1b_2)^2\ (3a_1)^1\ (1b_1)^1$. The symmetry of this state is $^3B_1$. The 3 low-lying singlet states are $1\ ^1A_1$, $1\ ^1B1$, and $2\ ^1A_1$. Due to spin flip operations, we can describe these states as shown in Figure 6.1 .

Table 6.3 shows the ST gaps for the diradicals calculated by various methods. The numbers inside and outside the bracket denote the vertical and adiabatic excitation energies, respectively. Excellent agreement is noticed between EOM-SF-CCSD and EOM-SF-CCSD(2) (errors not exceeding 0.08 eV in adiabatic excitation energies and 0.05 eV in vertical excitation energies). The absence of singles amplitude T_1 in the reference state is corrected to a large extent by the presence of R_1 amplitude in the EOM part. Therefore, the excitation energies are systematically underestimated. The detailed error analysis is shown in section 6.3.4 .

The reference triplet state for ozone is $^3B_2$, i.e., $(1a_1)^2\ (1b_2)^2\ (2a^1)^2\ (3a_1)^2\ (2b_2)^2\ (4a_1)^2\ (1b_1)^2\ (3b_2)^2\ (5a_1)^2\ (4b_2)^2\ (6a_1)^2\ (1a_2)^1\ (2b_1)^1$, and the ground state is closed shell singlet $^1A_1$.

Table 6.3 : ST energy gaps (in eV) in CH_2 and NH_2^+ calculated by various methods. The reference energy for the triplet state is in a.u. The values in bracket refer to the vertical excitation energies and outside bracket are the adiabatic excitation energies. The geometries are taken from EOM-SF-CCSD/cc-pVDZ optimization.

Methylene (CH_2)				
State	$^3B_1$	1^1A_1	1^1B_1	2^1A_1
EOM-SF-CCSD(2)	−39.075287	0.466 (0.931)	1.487 (1.523)	2.603 (3.270)
EOM-SF-CCSD	−39.087983	0.486 (0.950)	1.497 (1.523)	2.678 (3.283)
SF-CIS(D)	−39.051184	0.227	1.229	2.553
SF-TDDFT(50-50) [a]	−39.10937	−0.249	0.858	1.711
CASSCF SOCI [b]	−39.064939	0.482	1.558	2.697
FCI [c]	−39.066738	0.483	1.542	2.674
Expt. [d]	-	0.390	1.425	-
Nitrenium ion (NH_2^+)				
State	$^3B1$	1^1A1	1^1B1	2^1A1
EOM-SF-CCSD(2)	−55.385950	1.273 (1.785)	1.891 (1.909)	3.313 (3.504)
EOM-SF-CCSD	−55.398751	1.307 (1.823)	1.932 (1.943)	3.399 (3.568)
SF-CIS(D)	−55.371817	1.337	1.947	3.620
SF-TDDFT(50-50) [a]	−55.405373	0.255	1.016	2.045
CASSCF SOCI [e]	−55.388368	1.281	1.935	3.380
Expt. [f]	-	1.306	-	-

a : Reference 75. b : Reference 76 , TZ2P basis set. c : Reference 77, TZ2P basis set.

d : Reference 78 e : Reference 79 f : Reference 80

The 1 $^1A_1$ state of ozone has stronger diradical character than methylene and nitrenium ion. EOM-SF-CCSD(2) vertical excitation energies are shown in Table 6.4 . EOM-SF-CCSD(2) is in excellent agreement with EOM-SF-CCSD, and reasonable agreement with Fock space multi-reference coupled cluster (FS-MRCC) and large active space CASPT2 methods.

Table 6.4 : Vertical excitation energies (in eV) with respect to the ground state of ozone. The energy of ground state is given in a.u.

State	^{1}A1	^{3}B2	^{1}A2	^{1}B1
EOM-SF-CCSD(2)	−225.124407	1.457	2.001	1.952
EOM-SF-CCSD	−225.145111	1.579	2.036	1.990
SF-CIS(D)	−225.113399	1.206	2.139	2.123
CASPT2(4,3) [a]	-	1.61	4.33	4.51
CASPT2(6,3) [a]	-	1.66	2.27	2.51
CASPT2(9,3) [a]	-	1.72	2.26	2.37
FS-MRCC [b]	-	1.82	2.54	2.45
Expt. [c]	-	1.43	1.92	2.10

a : Reference 81 b : Reference 82, aug-cc-pVTZ. c : Reference 83

.

Basis set has a prominent effect on the excitation energy calculated in EOM-SF-CC methods energy. Table 6.5 shows the effect of basis set on the excitation energies of methylene, nitrenium ion, and ozone. We notice that the excitation energies for all the states decrease with increasing basis set. The change is small from cc-pVTZ to cc-pVQZ and the results seems to approach complete basis set limit.

Table 6.5 : Effect of basis set on the excitation energies calculated with EOM-SF-CCSD(2).

Methylene (CH_2)				
State	$^3B_1$	1^1A_1	1^1B_1	2^1A_1
cc-pVDZ	−39.027275	0.498	1.719	2.839
cc-pVTZ	−39.075287	0.466	1.487	2.603
cc-pVQZ	−39.098732	0.440	1.442	2.542
Expt. [a]	-	0.390	1.425	-
Nitrenium ion (NH_2^+)				
State	$^3B_1$	1^1A_1	1^1B_1	2^1A_1
cc-pVDZ	−55.329713	1.305	2.029	3.433
cc-pVTZ	−55.385950	1.272	1.891	3.314
cc-pVQZ	−55.414647	1.250	1.848	3.276
Expt. [b]	-	1.306	-	-
Ozone				
State	$^1A_1$	$^3B_2$	$^1A_2$	$^1B_1$
cc-pVDZ	−224.880223	1.481	2.034	1.960
cc-pVTZ	−225.124407	1.457	2.001	1.952
cc-pVQZ	−225.244718	1.443	1.991	1.949
Expt. [c]	-	1.43	1.92	2.10

a : Reference 78. b: Reference 80. c : Reference 83

6.3.2 Potential energy curves

6.3.2.1 Bond breaking with EOM-SF-CCSD(2)

6.3.2.1.1 F_2

Potential energy curve for the bond breaking in F_2 molecule is a complicated and interesting test case. From the molecular orbital (MO) picture of F_2, it is clear that

as we elongate the F–F bond, the configurations that need to be considered deal with the σ and σ* orbitals. Therefore, we start the SF calculations from a $^3\Sigma$ reference state. Figure 6.2 shows the potential energy curves calculated with EOM-SF-CCSD(2) compared to EOM-SF-CCSD, SF-CIS(D), and CASPT2. Single reference calculations with UCCSD(T) and UMP2 are known to fail at large bond lengths due to absence of non-dynamic correlation.[51] EOM-SF-CCSD(2) shows excellent agreement with EOM-SF-CCSD.

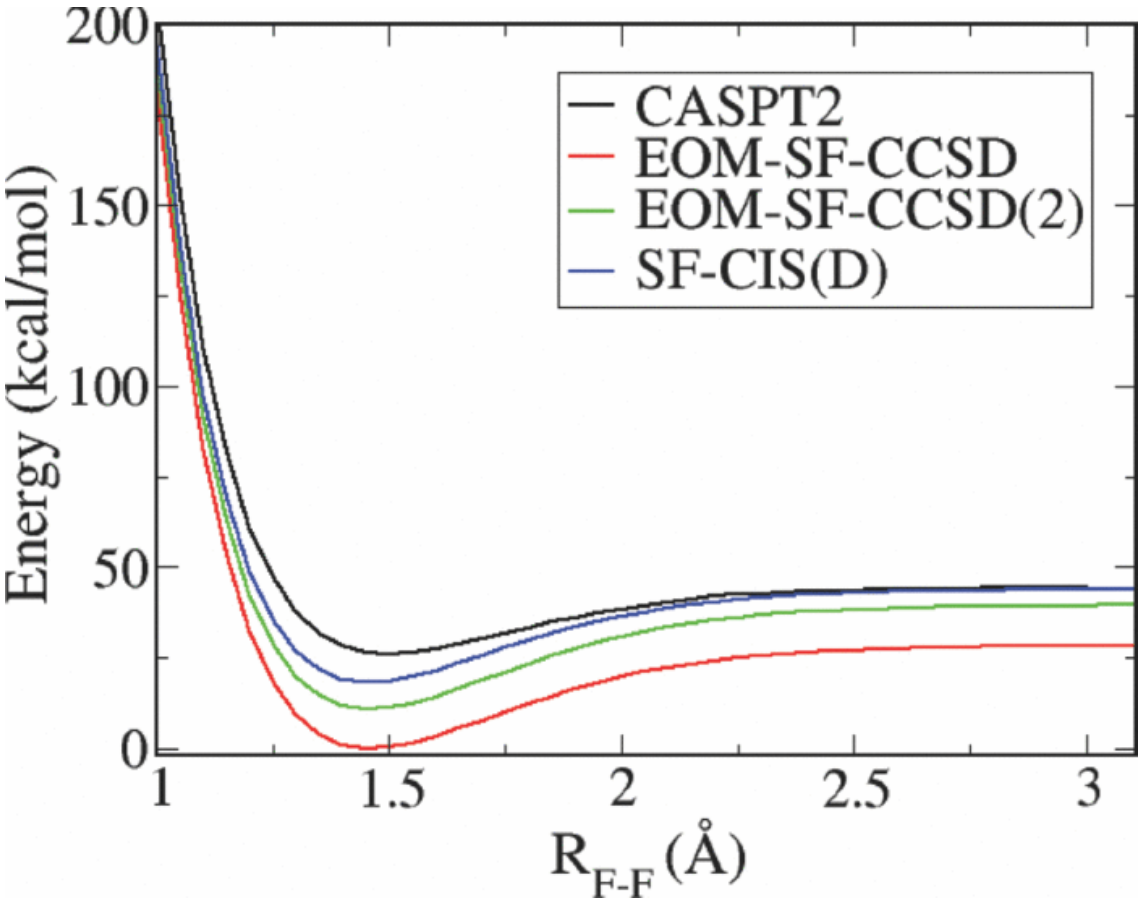

Figure 6.2: Dissociation curves for F_2 molecule calculated using CASPT2, EOM-SF-CCSD, SF-CIS(D), and EOM-SF-CCSD(2). The energies are given in kcal/mol.

The dissociation energies calculated by EOM-SF-CCSD(2) is 1.25 eV as compared to 1.24 eV with EOM-SF-CCSD and 1.12 eV with SF-CIS(D). The position of the minima in the dissociation curve is accurately reproduced by EOM-

SF-CCSD(2) when compared to EOM-SF-CCSD. However, none of the dissociation energies are comparable to the experimental dissociation energies (1.5–1.6 eV) due to inadequate size of basis set.

6.3.2.1.2 Cyclobutadiene rectangular to square geometry.

The anti-aromatic cyclobutadiene ring is formed by two double bonds and two single bonds in a strained rectangular geometry (D_{2h}). It can automerize between the two different rectangular geometries (geometry 1 with C1-C2 and C3-C4 as double bonds vs geometry 2 with C1-C3 and C2-C4 as double bonds), through a square transition state (D_{4h}). The ground state in the D_{2h} geometry is a closed shell singlet A_g state which becomes B_{1g} in the square geometry. This transition state is open shell in nature and therefore, multi-reference calculations are required for the correct estimation of the barrier for the transition (automerization). The multi-reference character can be understood from the two equivalent double bonds on opposite ends of the square butadiene. Thus, theoretical description of this automerization is challenging. Single reference methods have been known to severely overestimate the barrier heights.

In order to calculate the transition energy for the automerization as well as various low-lying excited states, we start with the optimized geometries in the square and rectangular geometries calculated using CCSD(T)/cc-pVTZ level of theory. The geometrical parameters are listed in Table 6.6. To create intermediate structural parameters, we interpolate between the rectangular and square geometrical parameters with a scaling parameter λ, such that,

$$R(i) = (1-\lambda) R_0(i) + \lambda R_i(i) \tag{6.17}$$

where $R(i)$ is the value of the ith parameter interpolated from $R_0(i)$ in the rectangular geometry to $R_1(i)$ in the square geometry, i goes over all the parameters (bond lengths, angles, etc.).

Table 6.6 : Geometrical parameters of cyclobutadiene in its rectangular and square geometries. The bond lengths are given in Å, and bond angles in degrees. The value in the bracket for the ∠HCC is the complementary angle.

Bonds	C–C	C=C	C–H	∠HCC
Rectangular	1.566	1.343	1.074	134.91 (135.09)
Square	1.439	1.439	1.073	135.0

Figure 6.3 shows the PESs of $1\ ^1A_g$, $2\ ^1A_g$, $^1B_{1g}$, and $^3B_{1g}$ states calculated with EOM-SF-CCSD, EOM-SF-CCSD(2), and SF-CIS(D) using cc-pVDZ basis set. It should be noted that as one goes from rectangular to square geometry (i.e., D_{2h} to D_{4h} symmetry), the term symbols for the states change. The term symbols of the states change as $1\ ^1A_g \rightarrow\ ^1B_{1g}$, $2\ ^1A_g \rightarrow 1\ ^1A_{1g}$, $^1B_{1g} \rightarrow\ ^1B_{2g}$, and $^3B_{1g} \rightarrow\ ^3A_{2g}$, when the cyclobutadiene changes from D_{2h} rectangular geometry to D_{4h} square geometry. We notice good agreement between all the methods especially in the two lowest states.

Table 6.7 : Energy barriers (in kcal/mol) for automerization reaction of cyclobutadiene obtained with different methods. We have denoted EOM-SF-CCSD by SF-CCSD and EOM-SF-CCSD(2) by SF-CCSD(2) for brevity.

CCSD	MR-CISD+Q	MR-AQCC	MR-CCSD	MR-BW-CCSD	SF-CCSD	SF-CCSD(2)
19.8–20.4 [a]	7.6 [b]	7.7 [b]	6.5 [c]	6.4 [d]	6.33 [a]	7.36

a : References 84 and 85. b : Reference 86. c : Reference 84.

d : Reference .85

Table 6.7 compares energy barriers for the automerization reaction of cyclobutadiene computed with EOM-SF-CCSD(2) and selected methods. We notice that the EOM-SF-CCSD(2) method reproduces the activation energy barrier comparable to multi-reference configuration interaction (MRCI) and multi-reference averaged quadratic coupled cluster (MRAQCC) methods and slightly over-estimates it with respect to the MRCC as well as EOM-SF-CCSD methods.

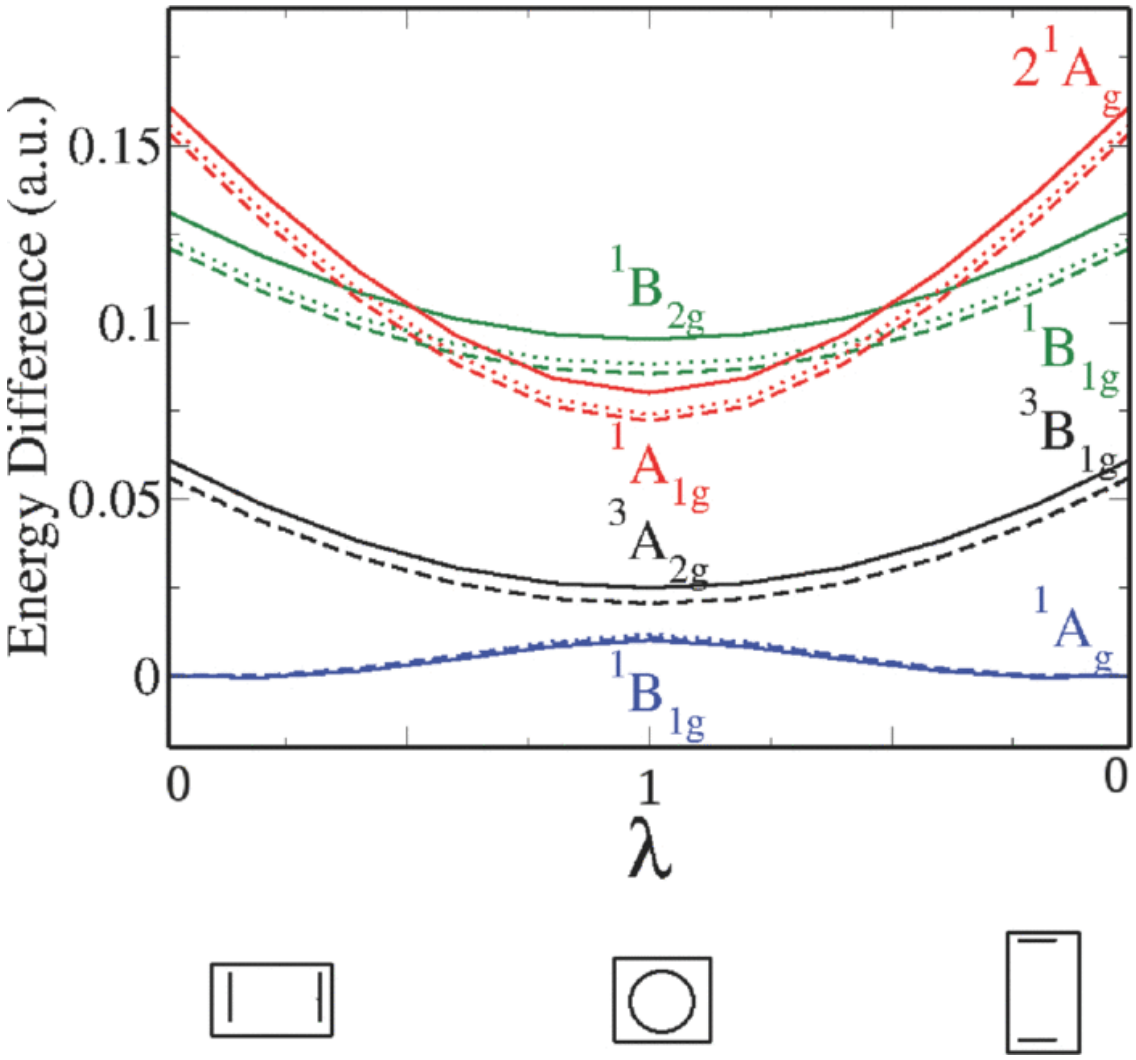

Figure 6.3 : The low-lying excited states (singlet and triplet) of cyclobutadiene along the reaction coordinate for automerization reaction. The figure shows the excitation energies calculated with EOM-SF-CCSD (bold lines), EOM-SF-CCSD(2) (dotted lines), and SF-CIS(dashed lines).

Table 6.8 compares the vertical excitation energies of the excited states at the rectangular and square geometries calculated with EOM-SF-CCSD and EOM-SF-CCSD(2). We notice reasonable agreement between the two methods with error <0.3 eV. The difficulty in comparing these results with experimental barrier heights is the extreme sensitivity of the barrier heights to the geometry of the molecule as well as size of basis set.

Table 6.8 : Vertical excitation energies (in eV) of $^3B_{1g}$, 2 ^1A_g , and $^1B_{1g}$ states of cyclobutadiene in the rectangular D2h geometry and $^3A_{2g}$, $^1B_{2g}$, and ^1A_g states in the square D_{4h} geometry.

	Rectangular D_{2h}			**Square D_{4h}**		
Method	**$^3B_{1g}$**	**$^1B_{1g}$**	**2 ^1A_g**	**$^3A_{2g}$**	**$^1B_{2g}$**	**^1A_g**
EOM-SF-CCSD(2)/cc-pVDZ	1.533	3.381	4.281	0.240	2.080	1.690
EOM-SF-CCSD/cc-pVDZ	1.678	3.586	4.416	0.404	2.317	1.904
EOM-SF-CCSD/cc-pVTZ	1.659	3.420	4.369	0.369	2.143	1.824
EOM-CCSD/cc-pVTZ	1.351	3.319	…	−0.590	1.534	…
EOM-SF-CCSD(fT)/cc-pVTZ	1.515	3.256	4.200	−0.590	1.534	…
EOM-SF-CCSD(dT)/cc-pVTZ	1.468	3.205	4.170	−0.590	1.534	…
SCF-CI/[5s5p/5s]	1.622	5.984	4.767	0.590	4.914	2.754

6.3.2.1.3 Oxirane ring opening

Stereo-specific ring opening of oxirane is another complicated test case due to the change in nature of the low lying excited states, when the ∠COC changes around 120°. Cordova et al. give a good description of the various singlet and triplet states that can explain the spectra of this molecule as well as the challenges they offer to

the various theoretical approaches [88]. They use CASSCF and diffusion Monte Carlo (DMC) to adequately account for both dynamic and non-dynamic correlation. Parkhill *et. al.* show the failure of UCCSD(T) to describe the ground state of oxirane as its ring opening occurs [89].

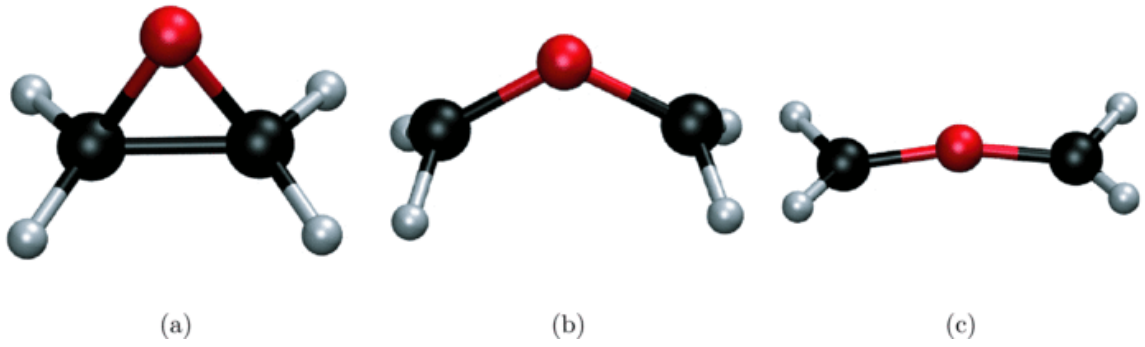

Figure 6.4 : Optimized geometries of oxirane along ring opening, at angles 60°, 120°, and 165° of the COC angle. (a) 60° (RCO = 1.447 Å). (b) 120° (RCO = 1.382 Å). (c) 165° (RCO = 1.290 Å).

The optimized structures along the ring opening coordinate is given in Fig. 6.4 (see Sec. 6.2.4 for details). Figure 6.5 compares the ground and low lying excited states of EOM-SF-CCSD and EOM-SF-CCSD(2) with change in ∠COC, as well as EOM-CCSD(T) method for the 2 $^1A_1$ and ^{3}A1 states. We have plotted only the singlet and triplet A_1 and B_2 states (1 $^1A_1$, 2 $^1A_1$, 1 $^1B_2$, $^3B_2$, and $^3A_1$) for clarity. EOM-SF-CCSD(2) gives excellent results when compared with EOM-SF-CCSD for all the states.

One notices that the EOM-SF-CCSD(2) excitation energies are systematically underestimated (≈0.2 eV) with respect to EOM-SF-CCSD and the reason for this is analyzed in Sec. 6.3.4 . One distinguishing feature of the curves is the ^{3} B 2 and ^{1} A 1 state crossing at 120°. This feature is seen in both EOM-SF-CCSD and EOM-SF-CCSD(2) methods.

The corresponding states for oxirane calculated with CASSCF and DMC are

presented in Ref [88]. The 2 $^1A_1$ state is an open shell singlet ((a_1)^1(a_1)^1 or (b_2)^1(b_2)^1) and, therefore, needs a balanced description of both dynamic and non-dynamic correlation. The nature of 2 $^1A_1$ state changes as we go along the ring opening co-ordinate (single Rydberg excitation below 100° and dominated by two electron excitations between 100° and 150°). Therefore, the most problematic part is getting the correct 2 $^1A_1$ state energies between 105 and 150, which in turn shows up as the singlet triplet gap between this singlet and the $^3A_1$ state.

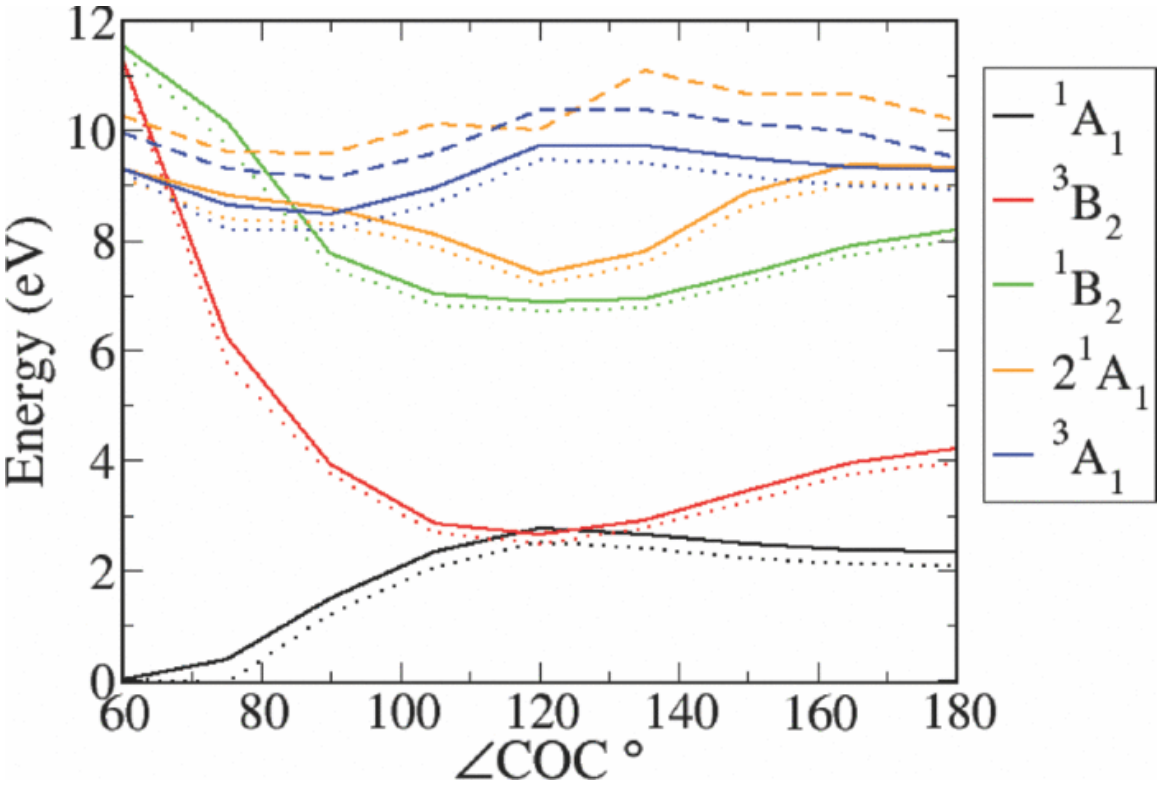

Figure 6.5 : The low-lying excited states (singlet and triplet) of oxirane along the COC angle (ring opening). The figure shows the excitation energies calculated with EOM-SF-CCSD (solid line) and EOM-SF-CCSD(2) (dotted line) and EOM-CCSD(T) (dashed line).

Since traditional EOM-CCSD(T) starts with a single reference singlet state, the target state obtained through subsequent EOM operators does not sufficiently capture the non-dynamic correlation. Thus, EOM-CCSD(T) fails qualitatively to

capture the shape of the 2 $^1A_1$ state between 105° and 150°. On the other hand, methods such as CASSCF which include the non-dynamic correlation but not the dynamic correlation, capture the shape of the curve qualitatively but fail to achieve quantitative accuracy and therefore, the singlet triplet gap (≈ 1 eV). [88] However, EOM-SF-CCSD, EOM-SF-CCSD(2), as well as DMC, which consider both dynamic and non-dynamic correlation in a balanced way, calculate the singlet triplet gap as 2.34 eV, 2.28 eV, and 1.92 eV, respectively [88].

6.3.2.2 Double bond breaking with EOM-DSF-CCSD(2)[2,3]

6.3.2.2.1 H_2O

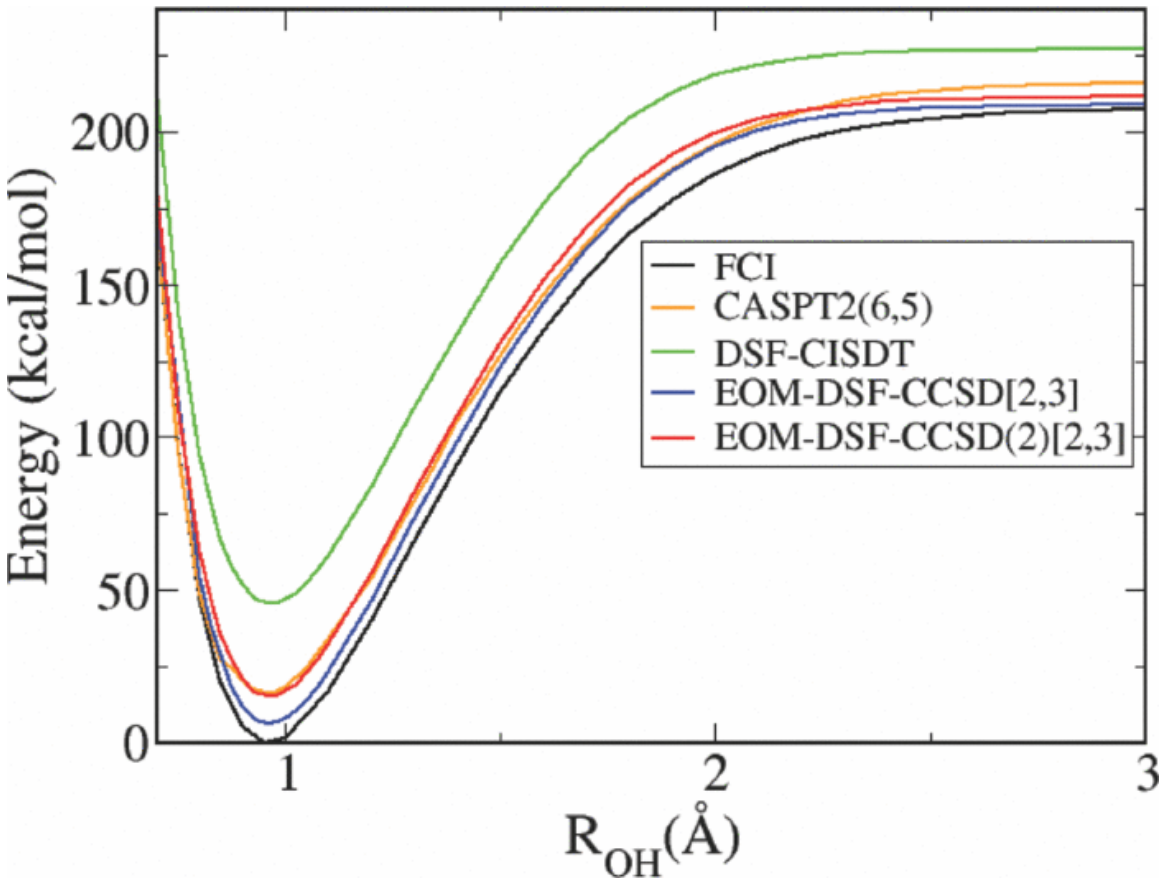

Figure 6.6 : Simultaneous OH bond stretching curves for H_2O molecule calculated using FCI, CASPT2, EOM-DSF-CCSD[2,3], DSF-CISDT, and EOM-DSF-CCSD(2)[2,3]. The energies are given in kcal/mol.

Simultaneous OH bond stretching potential energy curves for water dissociation have been used as a benchmark for DSF methods. We test our EOM-DSF-CCSD(2)[2,3] against existing EOM-DSF-CCSD[2,3] as well as DSF-CISDT, CASPT2, and FCI methods. We start from a quintet reference and use double spin flip operators to target the open shell singlet states along the bond breaking coordinate. The quintet reference is formed by singly populating the σ, σ*, and 2 lone pair on O atom.

Figure 6.6 shows the dissociation curves for the various methods and we clearly see the excellent agreement of EOM-DSF-CCSD(2)[2,3] with EOM-DSF-CCSD[2,3], CASPT2, and FCI methods. The DSF-CISDT is shifted vertically, i.e., in the absolute energy values. The nature of agreement can be better understood from the non-parallelity errors (NPE) in the attractive part of the curve which is 0.0137 a.u. for EOM-DSF-CCSD[2,3] and 0.0204 a.u. for EOM-DSF-CCSD(2)[2,3] with respect to FCI.

6.3.3 Geometrical Derivatives

Table 6.9 presents the geometry and IR frequencies of Ozone in aug-cc-pVTZ basis set. The ground state of ozone contains significant multi-reference character, and acts as a challenging test case for the EOM-CCSD(2) method. The SF-CCSD(2) method gives a bond length of 1.258 Å and bond angle of 116.4º in aug-cc-pVTZ basis set. Both of them are in reasonable agreement with experimental value and the agreement is better than the single-reference CCSD method. The improved agreement is also seen for the IR frequencies also. It also gratifying to note that SF-CCSD(2) method gives almost identical performance to that of the SF-CCSD(2) method for both geometry and IR frequency.

So, it can be seen that the SF-CCSD(2) method not only works well for the

potential energy surfaces, it also successful in simulating its geometrical derivatives. Detailed benchmarking is necessary to reach into any firm conclusions. However, it is outside the scope of this chapter.

Table 6.9 : ***Geometry and Harmonic Vibrational Frequency of Ozone (O_3) in aug-cc-pVTZ basis set***

Method	Bond length(Å)	Bond Angle(θ)	ω_1	ω_2	ω_3
SF-CCSD(2)	1.258	116.4	744	1188	1208
SF-CCSD	1.261	116.7	741	1185	1240
CCSD	1.244	117.8	767	1270	1285
Experiment [90,91]	1.278	116.8	705	1042	1142

6.3.4 Error analysis

We notice that the EOM-SF-CCSD(2) method systematically underestimates the energy difference between reference and target states, with respect to EOM-SF-CCSD, as reflected by the excitation energies in Tables 6.3 and 6.4. In the dissociation curves (for F_2 and H_2O), we further notice that the EOM-SF-CCSD(2) curve is almost parallel and shifted higher in energy than the EOM-SF-CCSD curve. In order to explain these observations as well as understand the limitations of our method, we have plotted the errors in the reference energy (CCSD(2)-CCSD) versus the orbital energy spacing (see Fig. 6.7(a)). As expected, when the frontier orbitals are degenerate or quasi-degenerate the errors in the reference energies (triplet state) are higher, since the $(\varepsilon_i - \varepsilon_a)$ in the denominators of the perturbed amplitudes are small.

We further notice there is a linear relationship between the error in the reference state (E_{ref}) and the error in the target state (E_{target}). Figures 6.7(b) and 6.7(c) show

that there is significant error cancellation between the target and reference states. The difference between $E_{target(EOM\text{-}SF\text{-}CCSD)}$ and $E_{target(EOM\text{-}SF\text{-}CCSD(2))}$ is smaller than that in $E_{ref(CCSD)}$ and $E_{ref(CCSD(2))}$, since the EOM operators (R_1 and R_2) corrects for the errors in T_1 and T_2 amplitudes in the EOM-SF-CCSD(2) method. Thus, the magnitude of the excitation energies ($E_{target} - E_{ref}$) calculated by EOM-SF-CCSD(2) is lower than that calculated by EOM-SF-CCSD (if target state is higher in energy than reference state; see Fig. 6.7(c)). This unbalanced error cancellation is responsible for the persistent trend of the underestimated excitation energy values calculated by EOM-SF-CCSD(2) method.

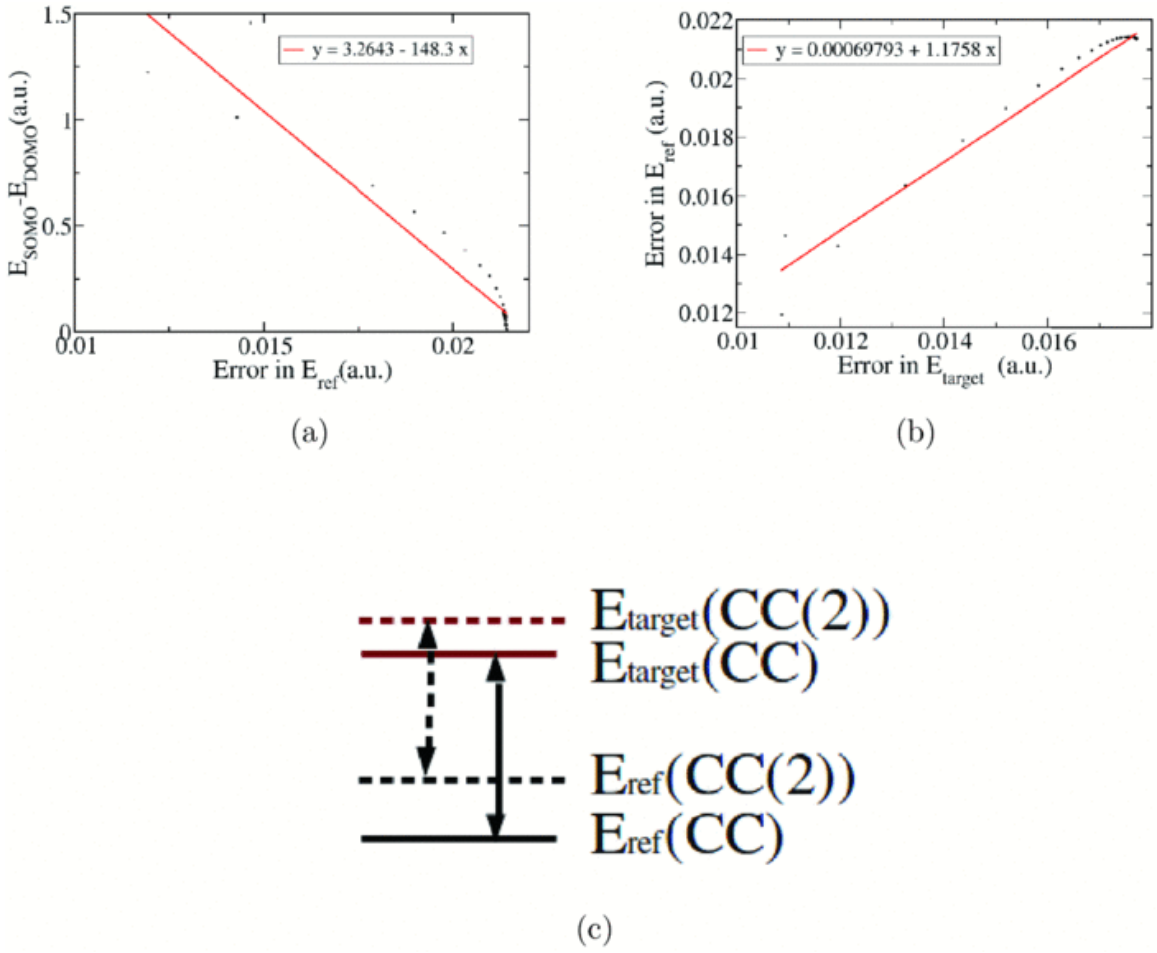

Figure 6.7:(a) The correlation between the energy differences (singly occupied MO – highest doubly occupied MO) and the error in the reference state. The errors refer to difference between EOM-SF-CCSD(2) and EOM-SF-CCSD energies for the F_2 dissociation curve. (b) The correlation between the errors in target state energies and reference state energies is shown for the F_2 dissociation curve. (c) The error cancellation in the difference of energies between reference and target states is shown.

6.4 CONCLUSION

Spin flip variant of EOM-CC has been found to be a versatile tool for modeling open shell singlet states in diradicals as well as bond breaking problems. This work presents a cheaper EOM-SF-CCSD(2) approach, which uses perturbative approximations to truncate the effective Hamiltonian. We have shown the improved timing data for our method with respect to the full EOM-SF-CCSD, as well as good agreement in the ST gaps in small molecules. Several complicated bond breaking examples were also studied to prove the accuracy of EOM-SF-CCSD(2). The method is successful even for calculating first and second geometrical derivatives of the potential energy surface.

The reference state as well as each of the target state energies calculated with EOM-SF-CCSD(2) method, are individually overestimated with respect to EOM-SF-CCSD energies. This is because perturbation captures less correlation than CC method (overestimation of reference state) and the subsequent EOM-SF operators does not completely correct for this effect (target state). This partial correction of target state energy by the EOM-SF operator leads to partial error cancellation in the excitation energy. This unbalanced error cancellation systematically underestimates the excitation energies (energy differences). However, as detailed error analysis shows, this underestimation occurs as long as the reference state is below the target state.

This approach can be used for large molecules with significant non-dynamic correlations and work is underway towards that direction.

References:

1. Cizek, J. *J. Chem. Phys.*, **1966**, *45*, 4256–4266.

2. Bartlett, R. J. *Ann. Rev. Phys. Chem.*, **1981**, *32*, 359.

3. Pople, J.; Krishnan, R.; Schlegel, H.; Binkley, J. *Int. J. Quant. Chem.*, **1978**, *14*, 545–560.

4. Scuseria, G.; Lee, T.; Schaefer, H. *Chem. Phys. Lett.*, **1986**, *130*, 236–239.

5. Harris, F. *Int. J. Quant. Chem. Symp.*, **1977**, *11*, 403–411.

6. Bartlett, R.; Musial, M. *Rev. Mod. Phys.*, **2007**, *79*, 291–352.

7. Bartlett, R. in *Theory and Applications of computational chemistry*, Dykstra, C.; Frenking,G.; Scuseria, G., Eds. Elsevier, **2005**.

8. Bartlett, R. *Mol. Phys.*, **2010**, *108*, 2905–2920.

9. Pal, S.; Rittby, M.; Bartlett, R.; Sinha, D.; Mukherjee, D. *J. Chem. Phys.*, **1988**, *88*(7),4357–4366.

10. Rittby, M.; Pal, S.; Bartlett, R. *Chem. Phys. Lett.*, **1989**, *164*, 57–62.

11. Kaldor, U. *Theor. Chim. Acta*, **1991**, *80*, 427–439.

12. Kaldor, U. in *Applied Many-Body Methods in Spectroscopy and Electronic Structure*, Mukherjee, D., Ed., pp 213–231. Plenum Press, **1992**.

13. Mukherjee, D. *Proc. Ind. Acad. Sci.*, **1986**, *96*, 145.

14. Ivanov, V.; Adamowicz, L. *J. Chem. Phys.*, **2000**, *112*(21), 9258–9268.

15. Haque, M.; Mukherjee, D. *J. Chem. Phys.*, **1984**, *80*(10), 5058–5069.

16. Balkova, A.; Kucharski, S. A.; Meissner, L.; Bartlett, R. J. *J. Chem. Phys.*, **1991**, *95*, 4311.

17. Chattopadhyay, S.; Mahapatra, U. S.; Datta, B.; Mukherjee, D. *Chem. Phys. Lett.*, **2002**,*5*, 357.

18. Evangelista, F. A.; Simmonett, A. C.; Allen, W. D.; Schaefer, H. F.; Gauss, J. *J. Chem.Phys.*, **2008**, *128*, 124104.

19. Hanrath, M. *J. Chem. Phys.*, **2005**, *123*, 084102.

20. Jeziorski, B.; Monkhorst, H. J. *J. Chem. Phys.*, **1981**, *24*, 1668.

21. Pittner, J.; Nachtigall, P.; C'arsky, P.; Masik, J.; Huba..c, I. *J. Chem. Phys.*, **1999**, *110*,10275.

22. Piecuch, P.; Hirata, S.; Kowalski, K.; Fan, P.; Windus, T. *Int. J. Quant. Chem.*, **2006**,*106*, 79–97.

23. Piecuch, P.; WAloch, M.; Gour, J.; Kinal, A. *Chem. Phys. Lett.*, **2006**, *418*, 467–474.

24. Piecuch, P.; WAloch, M. *J. Chem. Phys.*, **2005**, *123*, 224105–224115.

25. Bartlett, R. J. *Int. J. Mol. Sci.*, **2002**, *3*, 579.

26. Stanton, J.; Bartlett, R. *J. Chem. Phys.*, **1993**, *98*, 7029–7039.

27. Nooijen, M.; Bartlett, R. *J. Chem. Phys.*, **1995**, *102*, 3629–3647.

28. Bartlett, R. *Wiley Interdisciplinary Reviews: Computational Molecular Science*, **2011**.

29. Mukherjee, D.; Mukherjee, P. *Chem. Phys.*, **1979**, *39*, 325–335.

30. Koch, H.; Kobayashi, R.; de Mer'as, A. S.; Jorgensen, P. *J. Chem. Phys.*, **1994**, *100*,4393–4400.

31. Rico, R.; Head-Gordon, M. *Chem. Phys. Lett.*, **1993**, *213*, 224–232.

32. Sattelmeyer, K.; Stanton, J.; Olsen, J.; Gauss, J. *Chem. Phys. Lett.*, **2001**, *347*, 499–504.

33. Sekino, H.; Bartlett, R. J. *Int. J. Quant. Chem.*, **1984**, *26*, 255.

34. Chen, T.; Simons, J.; Jordan, K. *Chem. Phys.*, **1976**, *14*, 145.

35. Chaudhuri, R.; Mukhopadhyay, D.; Mukherjee, D. *Chem. Phys. Lett.*, **1989**,

162, 393.

36. Stanton, J.; Gauss, J. *Theor. Chim. Acta*, **1996**, *93*, 303.

37. Stanton, J.; Gauss, J. *Adv. Chem. Phys.*, **2003**, *125*, 101–146.

38. MusiaAl, M.; Kucharski, S.; Bartlett, R. *J. Chem. Phys.*, **2003**, *118*, 1128.

39. MusiaAl, M.; Bartlett, R. *J. Chem. Phys.*, **2003**, *119*, 1901.

40. Bartlett, R.; Bene, J.; Perera, S.; Mattie, R.-P. *J.Mol.Struct.:THEOCHEM*, **1997**, *400*,157–168.

41. Sattelmeyer, K.; Schaefer, H.; Stanton, J. *Chem. Phys. Lett.*, **2003**, *378*, 42–46.

42. Stanton, J. F.; Gauss, J. *J. Chem. Phys.*, **1994**, *101*, 8938.

43. Simons, J.; Smith, W. D. *J. Chem. Phys.*, **1973**, *58*, 4899–4907.

44. Piecuch and co-workers in Ref 47 and Musial *et al* in Ref 48 have shown that EOM-DIP-CCSD can be used to calculate the bond breaking curve and other truly multi-reference problems.

45. Demel, O.; Shamasundar, K.; Kong, L.; Nooijen, M. *J. Phys. Chem. A*, **2008**, *112*,11895–11902.

46. Kong, L.; Nooijen, M. *Int. J. Quant. Chem.*, **2008**, *108*, 2097–2107.

47. Shen, J.; Piecuch, P. *J. Chem. Phys.*, **2013**, *138*, 194102.

48. Musial, M.; Kowalska-Szojda, K.; Lyakh, D. I.; Bartlett, R. J. *J. Chem. Phys.*, **2013**, *138*,194103.

49. Levchenko, S.; Krylov, A. *J. Chem. Phys.*, **2004**, *120*(1), 175–185.

50. Krylov, A. *Chem. Phys. Lett.*, **2001**, *338*, 375–384.

51. Krylov, A.; Sherrill, C. *J. Chem. Phys.*, **2002**, *116*, 3194–3203.

52. Krylov, A. *Chem. Phys. Lett.*, **2001**, *350*, 522–530.

53. Slipchenko, L.; Krylov, A. *J. Chem. Phys.*, **2002**, *117*, 4694–4708.

54. Golubeva, A.; Nemukhin, A.; Harding, L.; Klippenstein, S.; Krylov, A. *J. Phys. Chem. A*, **2007**, *111*, 13264–13271.

55. Casanova, D.; Slipchenko, L.; Krylov, A.; Head-Gordon, M. *J. Chem. Phys.*, **200**9, *130*,044103.

56. Manohar, P.; Krylov, A. *J. Chem. Phys.*, **2008**, *129*, 194105.

57. Taube, A. G.; Bartlett, R. J. *J. Chem. Phys.*, **2008**, *128*, 164101.

58. Landau, A.; Khistyaev, K.; Dolgikh, S.; Krylov, A. *J. Chem. Phys.*, **2010**, *132*, 014109.

59. Krylov, A.; Sherrill, C.; Byrd, E.; Head-Gordon, M. *J. Chem. Phys.*, **1998**, *109*(24),10669–10678.

60. Nooijen, M.; Snijders, J. G. *J. Chem. Phys.*, **1995**, *102*, 1681.

61. Nooijen, M. *J. Chem. Phys.*, **1999**, *111*, 10815.

62. Stanton, J. F.; Gauss, J. *J. Chem. Phys.*, **1995**, *103*, 1064.

63. Hirata, S.; Nooijen, M.; Grabowski, I.; Bartlett, R. J. *J. Chem. Phys.*, **2001**, *114*, 3919.

64. Dutta, A. K.; Vaval, N.; Pal, S., *J. Chem. Theory Comput.* **2013,** *9*, 4313–4331

65. Krylov, A. *Acc. Chem. Res.*, **2006**, *39*, 83–91.

66. Kucharski, S. A.; Bartlett, R. J.; Per-Olov, L. *J. Chem. Phys.*, **1986**, *1986*, 281.

67. Head-Gordon, M.; Rico, R.; Oumi, M.; Lee, T. *Chem. Phys. Lett.*, **1994**, *219*, 21–29.

68. Koch, H.; Jensen, H. J. A.; Jorgensen, P.; Helgaker, T. *J. Chem. Phys.*, **1990**, *93*, 3345.

69. Sears, J.; Sherrill, C.; Krylov, A. *J. Chem. Phys.*, **2003**, *118*, 9084–9094.

70. Y. Shao, L. Fusti-Molnar, Y. Jung, J. Kussmann, C. Ochsenfeld, S. Brown,

A.T.B. Gilbert,L.V. Slipchenko, S.V. Levchenko, D.P. O'Neill, R.A. Distasio Jr, R.C. Lochan, T. Wang,G.J.O. Beran, N.A. Besley, J.M. Herbert, C.Y. Lin, T. Van Voorhis, S.H. Chien, A. Sodt,R.P. Steele, V.A. Rassolov, P. Maslen, P.P. Korambath, R.D. Adamson, B. Austin, JBaker, E.F.C. Bird, H. Daschel, R.J. Doerksen, A. Dreuw, B.D. Dunietz, A.D. Dutoi, T.R.Furlani, S.R. Gwaltney, A. Heyden, S. Hirata, C.-P. Hsu, G.S. Kedziora, R.Z. Khalliulin, P. Klunziger, A.M. Lee, W.Z. Liang, I. Lotan, N. Nair, B. Peters, E.I. Proynov, P.A. Pieniazek, Y.M. Rhee, J. Ritchie, E. Rosta, C.D. Sherrill, A.C. Simmonett, J.E. Subotnik, H.L. Woodcock III, W. Zhang, A.T. Bell, A.K. Chakraborty, D.M. Chipman, F.J. Keil, A. Warshel, W.J. Hehre, H.F. Schaefer III, J. Kong, A.I. Krylov, P.M.W. Gill, M. Head-Gordon. *Phys. Chem. Chem. Phys.*, **2006**, *8*, 3172–3191.

71. Frisch, M. J.; Trucks, G. W.; Schlegel, H. B.; Scuseria, G. E.; Robb, M. A.; Cheeseman, J. R.; Scalmani, G.; Barone, V.; Mennucci, B.; Petersson, G. A.; Nakatsuji, H.; Caricato,M.; Li, X.; Hratchian, H. P.; Izmaylov, A. F.; Bloino, J.; Zheng, G.; Sonnenberg, J. L.; Hada, M.; Ehara, M.; Toyota, K.; Fukuda, R.; Hasegawa, J.; Ishida, M.; Nakajima, T.; Honda, Y.; Kitao, O.; Nakai, H.; Vreven, T.; Montgomery, J. A. Jr.; Peralta, J. E.; Ogliaro, F.; Bearpark, M.; Heyd, J. J.; Brothers, E.; Kudin, K. N.; Staroverov, V. N.; Kobayashi, R.; Normand, J.; Raghavachari, K.; Rendell, A.; Burant, J. C.; Iyengar, S. S.; Tomasi, J.; Cossi, M.; Rega, N.; Millam, J. M.; Klene, M.; Knox, J. E.; Cross, J. B.; Bakken, V.; Adamo, C.; Jaramillo, J.; Gomperts, R.; Stratmann, R. E.; Yazyev, O.; Austin, A. J.; Cammi, R.; Pomelli, C.; Ochterski, J. W.; Martin, R. L.; Morokuma, K.; Zakrzewski, V. G.; Voth, G. A.; Salvador, P.; Dannenberg, J. J.; Dapprich, S.; Daniels, A. D.; Farkas,.; Foresman, J. B.; Ortiz, J. V.; Cioslowski, J.; Fox, D. J. Gaussian 09 Revision A.1. Gaussian Inc. Wallingford CT **2009**.

72. Frisch, M. J. ; Trucks, G. W. ; Schlegel, H. B. et al., Gaussian 09, Revision A.1, Gaussian, Inc., Wallingford, CT, **2009**.

73. Turney, J. M.; Simmonett, A. C.; Parrish, R. M.; Hohenstein, E. G.; Evangelista, F.;Fermann, J. T.; Mintz, B. J.; Burns, L. A.; Wilke, J. J.; Abrams, M.

L.; Russ, N. J.;Leininger, M. L.; Janssen, C. L.; Seidl, E. T.; Allen, W. D.; Schaefer, H. F.; King, R. A.;Valeev, E. F.; Sherrill, C. D.; Crawford, T. D. *WIREs Comput. Mol. Sci.*, **201**2, *2*, 556.

74. Hirai, K.; Itoh, T.; Tomioka, H. *Chem. Rev.*, **2009**, *109*, 3275.

75. Yamaguchi, Y.; Sherrill, C.; H.F. Schaefer III. *J. Phys. Chem.*, **1996**, *100*, 7911–7918.

76. Bernard, Y. A. ; Shao, Y. ; Krylov, A. I. *J. Chem. Phys., **2012**, 136*, 204103

77. Sherrill, C.; Leininger, M.; Van Huis, T.; Schaefer III, H. *J. Chem. Phys.*, **1998**, *108*(3),1040–1049.

78. Jensen, P.; Bunker, P. *J. Chem. Phys.*, **1988**, *89*, 1327–1332.

79. Stefens, J.; Yamaguchi, Y.; Sherrill, C.; H.F. Schaefer III. *J. Phys. Chem.*, **1998**, *102*,3999–4006.

80. Gibson, S.; Greene, J.; Berkowitz, J. *J. Chem. Phys.*, **1985**, *83*, 4319.

81. Borowski, P.; F..ulscher, M.; Malmqvist, P.-A.; Roos, B. O. *Chem. Phys.Lett.*,**1995**, *237*,195.

82. Musial, M.; Kucharski, S. A.; Zerzucha, P.; Ku's, T.; Bartlett, R. J. *J. Chem. Phys.*, **2009**,*131*, 194104.

83. Anserson, S. M.; Morton, J.; Mauesberger, K. *J. Chem. Phys.*, **1990**, *93*, 3826.

84. Baklov'a, A.; Bartlett, R. J. *J. Chem. Phys.*, **1994**, *101*, 8972.

85. Sancho-Garcia, J. C.; Pittner, J.; C'arsky, P.; Huba..c, I. *J. Chem. Phys.*, **2000**, *112*, 8785.

86. Eckert-Maksi'c, M.; Vazdar, M.; Barbatti, M.; Lischka, H.; Maksi'c, Z. B. *J. Chem. Phys.*,**2006**, *125*, 064310.

87. Buenker, R.; Peyerimhoff, S. *J. Chem. Phys.*, **1968**, *48*, 354–373.

88. Cordova, F.; Doriol, L. J.; Ipatov, A.; Casida, M. E.; Filippi, C. *J. Chem. Phys.*, **2007**,*127*, 164111.

89. Parkhill, J. A.; Azar, J.; Head-Gordon, M. *J. Chem. Phys.*, **2011**, *134*, 154112.

90. Barbe, A.; Secroun, C.; Jouve, P. *J. Mol. Spectrosc.* **1974**, 49, 171– 182.

91. Tanaka, T.; Morino, Y. *J. Mol. Spectrosc.* **1970**, 33, 538– 551.

Chapter 7

How good is the EOMIP-CCSD(2) approximation for calculation of ionization potential?

"Between the conception and the creation
Between the emotion and the response
Falls the Shadow"

T. S. Eliot
The Hollow Men

In this chapter, we present a benchmark investigation on the performance of EOMIP-CCSD(2) method for calculation of ionization potential. The calculated ionization potential (IP) values are found to be significantly overestimated compared to that obtained in the standard EOMIP-CCSD method. However, the EOMIP-CCSD(2) method correctly reproduces the basis set convergence behavior of standard EOMIP-CCSD method, and a small basis set EOMIP-CCSD calculation, extrapolated with large basis set EOMIP-CCSD(2) results can correct the errors of the original EOMIP-CCSD(2) approximation to a large extend. However, the method gives inferior performance for the cases where relaxation effect plays an important role.

7.1 Introduction:

Ionization energies are one the intrinsic properties of atoms and molecules, which has continued to fascinate generations of experimentalists and theoreticians. The accurate determinations of ionization energies are of extreme importance in biology and chemistry[1]. In spite of the tremendous advancement of spectroscopic techniques in recent times, experimental determination of ionization energies are often troublesome. Therefore, theoretical calculations are generally utilized as the supportive, some time the sole, mean of understanding of electron detachment induced phenomenon.

The various available theoretical methods for calculations of ionization potential (IP) are broadly classified into two categories. The first one is the so-called Δ techniques, where two separate calculations are required for the ion and the neutral species and the IP is obtained as the difference of energies obtained in two separate calculations[2]. The second strategy consists of the so-called 'direct difference of energy' scheme, which describes ionization as a transition process between the neutral molecule and the ion. The coupled cluster linear response theory[3, 4], quasi-degenerate perturbation theories[5, 6], and Green function based method[7, 8] fall into this second category and can be unified under the general framework of equation of motion (EOM) approach. The direct difference of energy has significant advantage over the Δ technique. Firstly, the direct difference of energy approach generates the IP in a single calculation, not as the difference of two big numbers as in Δ technique. Secondly, it gives information about the transition process and transition probability, which allows the simulation of experimental spectroscopic signatures.

Among the various EOM approaches available, equation of motion coupled cluster (EOM-CC) method[4, 9, 10] provides the most systematic way of balanced inclusion of dynamic and non-dynamic correlations. The EOM-CC approach for the ionization

problem (EOMIP-CC) is generally used in singles and doubles approximation (EOMIP-CCSD)[9] and provides a easy way to (0,1) sector of Fock space[11] without going into the conceptual difficulties of the corresponding multi-reference coupled cluster theory (FSMRCC). The EOMIP-CCSD method scales as N^6 power of the basis set and has similar storage requirement as that of the single-reference coupled cluster method, which prohibit its use beyond systems containing ten atoms in a reasonable basis set.

The coupled cluster theory has an intrigue relationship with many body perturbation theory[12]. So, the most obvious way of approximating the coupled cluster theory would be based on perturbation orders. Nooijen and Sniders[13] were the first, to propose an MBPT(2) amplitudes in place of coupled cluster ansatz in the context of IP calculations. Stanton and Gauss[14] latter generalized this idea to define a hierarchy of approximation to standard EOM-CCSD method called EOM-CCSD(n), where the reference state energy is complete up to n^{th} order in perturbation. The method is size-extensive for each values of n and the lowest order of approximation to it leads to EOM-CCSD(2) method with MBPT(2) ground state. Similar ideas were persuaded by Bartlett and co-workers in the context of excitation energy[15], and Dutta *et. al.* for electron affinity[16] and spin-flip variants[17] of EOM-CC.

For ionization problem, the EOM-CCSD(2) approximation offers significant cost cutting in computational requirements. The EOMIP-CCSD(2) method is N^5 scaling and does not involve (ab|cd) integral, leading to drastic decrease in storage requirements. Therefore, it can be applied to very large molecules. Pal and coworkers[18] have recently shown that the EOMIP-CCSD(2) method can be used to predict geometry and IR frequency of doublet radicals with accuracy comparable to that of standard EOMIP-CCSD method. However, no such benchmark studies are available for IP itself. An initial study[19] has shown that the EOMIP-CCSD(2) tends to overestimates the IP values a little bit, as compared to the EOMIP-CCSD method. However, the low computational cost of the method makes it too attractive to be discarded on the above ground, especially if the errors happen to be

systematic and within a reasonable limit. Therefore, a systematic study to investigate the source and estimate the magnitude of the error is absolutely necessary for proceeding with the further application of this method. The aim of this chapter is perform a benchmark study IP in EOMIP-CCSD(2) method against the standard EOMIP-CCSD method and other approximate variants of it, and to rationalize the source of error in the former.

The chapter is organized as follows. Section 7.2 gives a brief discussion on the theory of the EOMIP-CCSD(2) method and computational details of the calculations. The trends in the numerical results and sources of errors are discussed in section 7.3. Section 7.4 gives the concluding remarks.

7.2 Theory and Computational Details

7.2.1 EOM-IP-CCSD(2)

In the EOM frame work the kth excited state is generated from a reference state by action of a linear operator $\hat{R}_k$

$$|\psi_k\rangle = \hat{R}_k |\psi_0\rangle \tag{7.1}$$

The explicit form of $\hat{R}_k$ depends upon the nature of the excited state. For ionized state,

$$\hat{R}_k^{IP} = \sum_i R_i(k) i + \sum_{i>j,a} R_{ij}^a(k) \hat{a}^\dagger \hat{j}\hat{i} + ... \tag{7.2}$$

This is general EOM framework. The coupled cluster enters into the picture with the fact that in EOM-CC the correlated wave function is generated from a single Slater determinant reference state by the action of an exponential operator as following

$$|\psi_0\rangle = e^T |\phi_0\rangle \tag{7.3}$$

$|\phi_0\rangle$ is generally, but not necessarily, the Hartree-Fock determinant and $T=T_1+T_2+T_3+\ldots\ldots T_n$, where

$$\hat{T}_1 = \sum_{ia} t_i^a \left\{ a_a^\dagger a_i \right\},$$

$$\hat{T}_2 = \frac{1}{4} \sum_{ijab} t_{ij}^{ab} \left\{ a_a^\dagger a_b^\dagger a_j a_i \right\}, \tag{7.4}$$

$$\hat{T}_3 = \frac{1}{6} \sum_{ijkabc} t_{ijk}^{abc} \left\{ a_a^\dagger a_b^\dagger a_c^\dagger a_k a_j a_i \right\}$$

These amplitudes are generally obtained by the iterative solution of a system of coupled nonlinear equations.

In the EOMCC framework, the final states are obtained by diagonalizing the similarity transformed Hamiltonian within (N-1) electron space.

$$\bar{H} = e^{-T} H e^{T} = \left(H e^{T} \right)_c \tag{7.5}$$

The resulting method is equivalent to the (0,1) sector of the Fock space multi reference coupled cluster (FSMRCC) method for the principal ionization.

The energy in EOMIP-CC can be written in the illustrative functional form.

$$E = \langle \phi_0 | L \bar{H} R | \phi_0 \rangle = \langle \phi_0 | L e^{-T} H e^{T} R | \phi_0 \rangle \tag{7.6}$$

The EOMIP-CC method is generally used in singles and doubles approximation (EOMIP-CCSD). It has the N^6 scaling and similar storage requirements as that of the single reference CCSD method, which makes it unsuitable for large applications. Now, the coupled cluster method has an intrigue relationship with many body perturbation theory (MBPT). Various orders of MBPT can be recovered from the suitable lower order iteration of coupled cluster equations[12]. For example, the lowest order approximation to CCSD leads to the MBPT(2) method. Therefore, the natural choice of truncating the

CCSD similarity transformed Hamiltonian should be based on perturbational orders. Two slightly different perturbative approaches have been reported in the literature[13, 14]. Nooijen and Snijders[13] first proposed a truncation of the CCSD effective Hamiltonian based on the perturbative scheme. Stanton and Gauss [14] latter generalized it within the EOM framework. They have expanded the effective Hamiltonian in a perturbation series

$$\bar{H} = \left(He^{T}\right)_{c} = \bar{H}^{[1]} + \bar{H}^{[2]} + \bar{H}^{[3]} + ... + \bar{H}^{[n]} \tag{7.7}$$

The bracketed superscript in the above equation represents the order in perturbation and subscript c represents the connectedness of T with H. Equation (7.7) leads to a set of hierarchical approximation to the full $\bar{H}$ and the diagonal representation of the modified effective Hamiltonian offers a set of hierarchical approximation to the corresponding EOM-CC final states, known as EOMCCSD(n). The similarity transformed Hamiltonian truncated at n^{th} order, contains terms only up to n^{th} order in perturbation, which ensures the size extensivity of the method for all values of n. At large value of n, the $\bar{H}^{[n]}$ converges to the full $\bar{H}$ and consequently EOM-CCSD(n) converges to the standard EOM-CCSD method. Truncation at n=2, leads to EOM-CCSD(2), with a MBPT(1) ground state reference wave function and MBPT(2) ground state energy.

In case of second order truncated effective Hamiltonian ($H^{[2]}$), the CC amplitudes can be approximated by the MBPT(2) amplitudes

$$\begin{aligned} \bar{H} &= \left(H\,\mathrm{e}^{T}\right)_{c} \\ &\approx \left(H\,\mathrm{e}^{T'}\right)_{c} \end{aligned} \tag{7.8}$$

Where the second order perturbative approximation to the T amplitudes can be written as

$$\begin{aligned} T_1' &= \frac{f_{ia}}{\varepsilon_i - \varepsilon_a} \\ T_2' &= \frac{\langle ab||ij\rangle}{\varepsilon_i + \varepsilon_j - \varepsilon_a - \varepsilon_b} \end{aligned} \tag{7.9}$$

T_1 is zero for restricted closed shell and unrestricted MBPT(2) reference. Using these T' amplitudes one can generate a modified similarity transformed Hamiltonian $\bar{H}'$, which can be used as the reference for subsequent EOMIP calculations. Thus, this is necessarily an EOM calculation on a MBPT(2)reference state. This approach is slightly different from that originally proposed by Nooijen and Snijders [13]. Reference [14] should be consulted for an elaborate discussion on the differences of these two approaches.

In this approach the reference state energy reduces to the MBPT(2) ground state energy, with the accompanied reduction in the computational scaling from iterative N^6 to non-iterative N^5 for the reference state. There are still some terms of $\bar{H}$ that scale as N^6, however, scaling of those steps can be reduced to iterative N^5 by calculating them on the fly. Moreover, the truncation at MBPT(2) ensures the absence of 4 particle intermediates, which anyways remain absent from the EOM part in IP calculations. Therefore, the EOMIP-CCSD(2) gives significant saving in terms of scaling, as well as storage requirement.

The IP-CISD approach of Krylov and co-workers[20] provides another N^5 scaling approximation to standard EOMIP-CCSD method, where uncorrelated HF wave-function is used as a reference.

Table 7.1 : Hierarchy of EOMIP-CCSD methods.

Reference	**Method**	**Wave-function**
SCF	EOMIP-CISD	$(R_1 + R_2)\phi_0$
CCSD(2)	EOMIP-CCSD(2)	$(R_1 + R_2)\exp(T_2')\phi_0$
CCSD(2)	P-EOMIP-CCSD(2)	$(R_1' + R_2')\exp(T_2')\phi_0$
CCSD	EOMIP-CCSD	$(R_1 + R_2)\exp(T_1 + T_2)\phi_0$

Another related development is the generalization of Partition EOM-MBPT(2) approach[15, 16] to the ionization problem. It essentially means that the doubles-doubles block of EOM matrix is approximated as its diagonal terms. The exact programmable expressions are provided in Appendix III. It is observed that partitioned version of EOM-CCSD(2) method provides improvement in results compared to the standard EOM-CCSD(2) for both EA[16] and EE[15]. Therefore, it would be interesting to extend the idea to IP problem. Here, it should be noted that partitioning approach does not provide any significant decrease in storage requirement in EOMIP-CCSD(2) method, unlike in the case of electron affinity problem, where it reduces the storage requirements drastically[16].

Table 7.1 compares the various approximations to EOMIP-CCSD method.

7.2.2 Computational Details

The reliability of the EOMIP-CCSD(2) method has been benchmarked by calculating the vertical ionization potential of few small molecules in a hierarchy of Dunning's correlation consistent cc-pVXZ (X= D, T, Q) basis sets [21]. The values are compared with the standard EOMIP-CCSD method. To improve the EOMIP-CCSD(2) ionization potential values, the following extrapolation scheme has been defined [22].

$$IP_{\text{Extrapolated EOMIP-CCSD(2)}} = IP_{\text{small basis}} + (IP_{\text{big basis EOMIP-CCSD(2)}} - IP_{\text{small basis EOMIP-CCSD(2)}})$$

Where $IP_{\text{small basis}} = IP_{\text{small basis EOMIP-CCSD}}$, when $IP_{\text{small basis EOMIP-CCSD}} < IP_{\text{small basis EOMIP-CCSD(2)}}$

Otherwise, $IP_{\text{small basis}} = IP_{\text{small basis EOMIP-CCSD(2)}}$

All the EOMIP-CCSD and EOMIP-CCSD(2) calculations are performed using CFOUR [23]. EOMIP-CISD and P-EOMIP-CCSD(2) calculations are performed by our in-house coupled cluster codes. All the T1 diagnosis calculations are performed using Gaussian09 [24].

7.3 Results and Discussion

7.3.1 Valence Ionization Spectra

The performance of the EOMIP-CCSD(2) method for valence ionization energies is benchmarked for small molecules like N_2, H_2O, H_2CO, C_2H_4, and CO in a hierarchy of Dunning's correlation consistent cc-pVXZ (X = D, T, Q) basis set [21] (Tables 7.2–7.6). For the sake of comparison, we also quote the corresponding P-EOMIP-CCSD and EOMIP-CISD results.

The Table 7.2 presents the valence ionization energies of first five states of N_2. The EOMIP-CISD method fails to reproduce the corresponding EOMIP-CCSD results, even qualitatively. The lack of correlation effect in the reference state can be held responsible for these drastic failures. The EOMIP-CCSD(2) method gives qualitatively correct values, but the IP values are slightly overestimated compared to the corresponding EOMIP-CCSD method. The P-EOMIP-CCSD(2) also overestimates the IP values except the $2\sigma_g$ state, where the IP is underestimated in P-EOMIP-CCSD(2) method and the resulting errors for all the states are more than that in EOMIP-CCSD(2) method. It should be noted that the ionization from the $2\sigma_g$ state involves significant double excitation character, which cannot be properly taken care by the truncated doubles-doubles block of the P-EOMIP-CCSD(2) method. On increasing the basis set from cc-pVDZ to cc-pVTZ, the IP values in all the methods increase, except the double excitation dominated $2\sigma_g$ state in P-EOMIP-CCSD(2) method, where the value is slightly decreased. Although, the EOMIP-CCSD(2) method continue to overestimate compared to the EOMIP-CCSD method, the extrapolated EOMIP-CCSD(2) method gives very good agreement. The IP values further increase from cc-pVTZ to cc-pVQZ, although, the deviation is much smaller compared to that from cc-pVDZ to cc-pVTZ, and the trend remains the same.

Table 7.2 : Ionization Energies of N_2 (in eV)

state	EOMIP-CCSD	EOMIP-CISD	EOMIP-CCSD(2)	P-EOMIP-CCSD(2)	Extrapolated EOMIP-CCSD(2)
			cc-pVDZ Basis Set		
$3\sigma_g$	15.19	13.27	15.39	15.48	-
$1\pi_u$	16.96	14.61	17.14	17.18	-
$1\pi_u$	16.96	14.61	17.14	17.18	-
$2\sigma_u$	18.45	16.38	18.56	18.84	-
$2\sigma_g$	38.61	28.68	38.78	35.93	-
			cc-pVTZ Basis Set		
$3\sigma_g$	15.59	13.26	15.85	15.85	15.65
$1\pi_u$	17.22	14.49	17.48	17.46	17.30
$1\pi_u$	17.22	14.49	17.48	17.46	17.30
$2\sigma_u$	18.81	16.35	18.98	19.15	18.87
$2\sigma_g$	38.65	28.60	38.90	35.86	38.73
			cc-pVQZ Basis Set		
$3\sigma_g$	15.72	13.25	16.02	15.99	15.82
$1\pi_u$	17.34	14.47	17.64	17.59	17.46
$1\pi_u$	17.34	14.47	17.64	17.59	17.46
$2\sigma_u$	18.93	16.34	19.15	19.27	19.04
$2\sigma_g$	38.74	28.57	39.04	35.93	38.87

Table 7.3 presents the vertical ionization energies corresponding to the valence orbitals of water.

Table 7.3 : Ionization Energies of H_2O (in eV)

state	EOMIP-CCSD	EOMIP-CISD	EOMIP-CCSD(2)	P-EOMIP-CCSD(2)	Extrapolated EOMIP-CCSD(2)
			cc-pVDZ Basis Set		
$1b_2$	11.80	9.76	11.74	11.60	-
$3a_1$	14.11	12.06	14.04	13.91	-
$1b_1$	18.47	16.43	18.37	18.27	-
$2a_1$	32.17	31.68	32.07	33.31	-
			cc-pVTZ Basis Set		
$1b_2$	12.40	9.88	12.43	12.17	12.43
$3a_1$	14.63	12.12	14.63	14.39	14.63
$1b_1$	18.83	16.40	18.81	18.62	18.81
$2a_1$	32.61	29.78	32.57	33.28	32.57
			cc-pVQZ Basis Set		
$1b_2$	12.62	9.92	12.69	12.36	12.69
$3a_1$	14.82	12.16	14.87	14.57	14.87
$1b_1$	19.00	16.42	19.01	18.77	19.01
$2a_1$	32.81	29.83	32.81	33.31	32.81

It can be seen that in cc-pVDZ basis set, the EOMIP-CCSD(2) method gives very good agreement with the standard EOMIP-CCSD method. On the other hand, the EOMIP-CISD method leads to results, which are not even qualitatively correct. The P-EOMIP-CCSD(2) method significantly underestimates the IP values compared to standard

EOMIP-CCSD method, except the $2a_1$ state, where it is significantly overestimated. The trend in P-EOMIP-CCSD(2) results are just opposite to that in N_2, where it is significantly overestimated compared to the EOMIP-CCSD method. On increasing the basis set, from cc-pVDZ to cc-pVTZ the ionization potential in all the coupled cluster methods increases, except the $2a_1$ state in P-EOMIP-CCSD(2) method, where the value remains almost unchanged. The $2a_1$ state contains significant double excitation character, which explains the discrepancies. The change in EOMIP-CISD values are very small and lacks even qualitative trend. The formula (7.10) used for performing basis set extrapolation leads to the fact that the extrapolated EOMIP-CCSD(2) method gives identical results as that of original EOMIP-CCSD(2) method, in case of water and they are in excellent agreement with the standard EOMIP-CCSD method. The Ionization energies show a small increase from cc-pVTZ to cc-pVQZ method and the relative trend in different methods remain unchanged from that in the cc-pVTZ basis set.

The first five ionized states of formaldehyde are reported in Table 7.4. The EOMIP-CISD method gives significantly underestimated values compared to the standard EOMIP-CCSD method. The EOMIP-CCSD(2) method also leads to underestimated IP values. However, the extent of underestimation is very small and the values are in excellent agreement with the EOMIP-CCSD method. The trends in P-EOMIP-CCSD(2) method is not very systematic. The IP values for first three states are underestimated and the last two states are overestimated. In cc-pVTZ basis, the IP values in all the coupled cluster methods increases, whereas the IP in EOMIP-CISD method mostly remains unchanged. The EOMIP-CCSD(2) values are overestimated compared to the standard EOMIP-CCSD method and the trend is opposite to that in cc-pVDZ basis set. The P-EOMIP-CCSD(2) method, however, follows the same trend as that in the cc-pVDZ basis set, i.e. the first three states in P-EOMIP-CCSD(2) method are underestimated and the rest two states are overestimated compared to EOMIP-CCSD method.

Table 7.4 : Ionization Energies of H_2CO (in eV)

state	EOMIP-CCSD	EOMIP-CISD	EOMIP-CCSD(2)	P-EOMIP-CCSD(2)	Extrapolated EOMIP-CCSD(2)
			cc-pVDZ Basis Set		
$2b_2$	10.34	8.03	10.25	10.09	-
$1b_1$	14.29	11.57	14.18	14.12	-
$5a_1$	15.71	13.19	15.63	15.44	-
$1b_2$	17.08	15.21	17.03	17.15	-
$4a_1$	21.35	19.61	21.33	21.74	-
			cc-pVTZ Basis Set		
$2b_2$	10.75	8.04	10.77	10.51	10.77
$1b_1$	14.57	11.50	14.58	14.43	14.58
$5a_1$	16.05	13.11	16.07	15.78	16.07
$1b_2$	17.37	15.19	17.39	17.43	17.39
$4a_1$	21.62	19.57	21.66	21.99	21.66
			cc-pVQZ Basis Set		
$2b_2$	10.90	8.05	10.97	10.68	10.97
$1b_1$	14.69	11.49	14.77	14.57	14.77
$5a_1$	16.19	13.11	16.28	15.95	16.28
$1b_2$	17.48	15.20	17.54	17.55	17.54
$4a_1$	21.72	19.57	21.80	22.10	21.80

The extrapolated EOMIP-CCSD(2) values are identical with that of the original EOMIP-CCSD(2) method. The IP values in all the coupled cluster methods show relatively small

change from cc-pVTZ to cc-pVQZ basis and follow the same trend as that in cc-pVTZ basis set. The IP-CISD values remain almost unchanged from that in cc-pVTZ basis set.

Table 7.5 : Ionization Energies of C_2H_4 (in eV)

state	EOMIP-CCSD	EOMIP-CISD	EOMIP-CCSD(2)	P-EOMIP-CCSD(2)	Extrapolated EOMIP-CCSD(2)
			cc-pVDZ Basis Set		
B_{1u}	10.42	8.24	10.30	10.32	-
B_{1g}	12.92	11.18	12.79	12.90	-
A_g	14.61	12.69	14.59	14.65	-
B_{2u}	16.06	14.13	15.94	16.12	-
B_{3u}	19.37	17.45	19.24	19.68	-
			cc-pVTZ Basis Set		
B_{1u}	10.63	8.21	10.63	10.61	10.63
B_{1g}	13.11	11.14	13.07	13.15	13.07
A_g	14.84	12.60	14.91	14.93	14.91
B_{2u}	16.26	14.07	16.22	16.36	16.22
B_{3u}	19.54	17.36	19.50	19.86	19.50
			cc-pVQZ Basis Set		
B_{1u}	10.71	8.21	10.77	10.74	10.77
B_{1g}	13.18	11.13	13.18	13.24	13.18
A_g	14.93	12.59	15.06	15.05	15.06
B_{2u}	16.34	14.06	16.34	16.45	16.34
B_{3u}	19.61	17.35	19.62	19.95	19.62

The first five vertical ionization potentials of ethylene are presented in table 7.5. The EOMIP-CISD method significantly underestimates the values compared to the standard EOMIP-CCSD method. The EOMIP-CCSD(2) method also underestimates the IP values, but the results are generally in good agreement with the EOMIP-CCSD values. The P-EOMIP-CCSD(2) method shows a mixed trend, it underestimates for the B_{1u} and B_{1g} states and overestimates for the rest three states. In cc-pVTZ basis, the IP values in all the three coupled cluster methods increase. However, the EOMIP-CISD method shows slight decrease in the IP values. The IP values in EOMIP-CCSD(2) method give very good agreement with its EOMIP-CCSD counterpart. The extrapolated EOMIP-CCSD(2) method give rise to IP values, which are identical to that of the original EOMIP-CCSD(2) method. The P-EOMIP-CCSD(2) method also give very good agreement with the EOMIP-CCSD method, except the B_{3u} state, where it is significantly overestimated. The IP values in all the coupled cluster methods slightly increase from cc-pVTZ to cc-pVQZ method, but the trend in the results remain same as that in cc-pVTZ basis set. The IP-CISD values, on the other hand, remain practically unchanged with increase in the basis set.

Table 7.6 presents the ionization potential corresponding to first five states of ozone. The ozone ground state is known to have significant multi-reference character and hence possess considerable challenge for all the approximate EOMCC methods based on a MBPT(2) reference. In cc-pVDZ basis set, the EOMIP-CISD method significantly underestimates the IP values, as compared to the standard EOMIP-CCSD method. The EOMIP-CCSD(2) method, on the other hand, significantly overestimates the IP values for all the states. The P-EOMIP-CCSD(2) gives relatively better agreement with the EOMIP-CCSD results, except for the b_2 state, which has significant double excitation character. As we go from cc-pVDZ to cc-pVTZ basis set, the IP values in all the EOM method increase, except the CISD one, where the IP values decrease with the increment in basis set. The EOMIP-CCSD(2) method significantly overestimates the IP values compared to EOMIP-CCSD method with error as high as 0.77 eV (for $1b_2$ state).

Table 7.6 : Ionization Energies of O_3 (in eV)

state	EOMIP-CCSD	EOMIP-CISD	EOMIP-CCSD(2)	P-EOMIP-CCSD(2)	Extrapolated EOMIP-CCSD(2)
			cc-pVDZ Basis Set		
$1a_2$	12.35	9.48	12.76	12.28	-
$6a_1$	12.45	9.58	12.84	12.33	-
$3b_1$	13.11	9.66	13.52	13.36	-
$1b_2$	18.20	16.11	18.91	18.96	-
$2b_1$	19.21	19.06	19.76	19.20	-
			cc-pVTZ Basis Set		
$1a_2$	12.77	9.39	13.24	12.66	12.83
$6a_1$	12.85	9.45	13.30	12.68	12.91
$3b_1$	13.41	9.52	13.93	13.68	13.52
$1b_2$	18.68	15.97	19.45	19.23	18.74
$2b_1$	19.56	18.92	20.18	19.49	19.63
			cc-pVQZ Basis Set		
$1a_2$	12.97	9.39	13.49	12.85	13.08
$6a_1$	13.05	9.45	13.54	12.86	13.15
$3b_1$	13.58	9.51	14.15	13.84	13.74
$1b_2$	18.90	15.97	19.71	19.38	19.00
$2b_1$	19.75	18.91	20.41	19.66	19.86

The P-EOMIP-CCSD(2) method gives relatively better agreement but the trends are not quite systematic. The values are overestimated for $3b_1$ and $1b_2$ state, whereas, they are

underestimated for rest of the three states. The extrapolated EOMIP-CCSD(2) method shows significant improvement over the standard EOMIP-CCSD(2) method, specially the high error of 0.77 eV in $1b_2$ state is reduced to 0.06 eV in extrapolated EOMIP-CCSD(2) method. With further increase in the basis set from cc-pVTZ to cc-pVQZ, the IP values in all the CC method increase, however, the trends remain same. The IP values in EOMIP-CISD method, on the other hand, remain unchanged from cc-pVTZ to cc-pVQZ basis.

7.3.2 Core Ionization Spectra

The large relaxation effect, associated with the core orbitals, makes the computation of the core-ionization spectra, in standard *ab-initio* methods, a challenging task. The EOMIP-CC method, even in the CCSD approximation, often does not lead to satisfactory results[25]. Therefore, it will be interesting to test the performance of EOMIP-CCSD(2) method, where a significant amount of the relaxation effect is missing due to lack of T_1 amplitude in the reference state.

We have calculated the core-ionization energies of H_2O, CH_4, CO(C(1s)), HF and NH_3 in a hierarchy of Dunning's core-valence correlation consistent cc-pCVXZ basis sets (X=D,T and Q)[26]. The EOMIP-CISD method significant underestimates the IP values compared to the EOMIP-CCSD method for core-ionization energy. On the other hand, EOMIP-CCSD(2) method in cc-pCVDZ basis overestimates the core-ionization energy, except in the case of HF, where it gives very good agreement with standard EOMIP-CCSD method. The P-EOMIP-CCSD(2) method gives inferior performance for the core-ionization energies and overestimates the IP values compared to the standard EOMIP-CCSD method, except in the case of HF, where it underestimates. The error bars in P-EOM-CCSD(2) method are much higher than that in the EOMIP-CCSD(2) method, as the ionization from the core orbitals involves significant double excitation character, which the truncated doubles-doubles block of P-EOMIP-CCSD(2) method fails to take

care of.

Table 7.7 : Core-ionized energies in EOMCC methods. (in eV)

Molecule	EOMIP-CCSD	EOMIP-CISD	EOMIP-CCSD(2)	P-EOMIP-CCSD(2)	Extrapolated EOMIP-CCSD(2)	Experimental
			cc-pCVDZ Basis Set			
H_2O	542.69	538.96	542.81	542.78	-	539.75
CH_4	293.18	290.68	293.31	294.62	-	290.86
CO	298.87	297.06	299.50	300.75	-	296.20
HF	697.24	693.16	697.19	696.36	-	693.80
NH_3	408.17	405.02	408.36	409.11	-	405.52
			cc-pCVTZ Basis Set			
H_2O	541.13	537.20	541.65	542.20	541.53	539.75
CH_4	291.99	289.36	292.40	294.07	292.27	290.86
CO	297.63	295.52	298.39	300.17	297.76	296.20
HF	695.41	691.10	695.81	695.62	695.81	693.80
NH_3	406.84	403.53	407.36	408.56	407.17	405.52
			cc-pCVQZ Basis Set			
H_2O	541.35	537.27	541.92	542.41	541.80	539.75
CH_4	291.99	289.33	292.49	294.14	292.36	290.86
CO	297.64	295.30	298.51	300.16	297.86	296.20
HF	695.74	691.27	696.19	695.96	696.19	693.80
NH_3	406.99	403.59	407.59	408.72	407.40	405.52

a : Values taken from ref [27] . b:Values taken from ref [28] .

With increase in the basis set from cc-pCVDZ to cc-pCVTZ basis, the core IP values in

all the methods undergo red shift. The IP values in EOMIP-CCSD(2) method continue to be overestimated as compared to EOMIP-CCSD method, even in the case of HF. The extrapolated EOMIP-CCSD(2) method shows slight improvement over the normal EOMIP-CCSD(2) method, however, the values continue to be grossly overestimated. The EOMIP-CISD and P-EOMIP-CCSD(2) method both give inferior performance but in a different way. The P-EOMIP-CCSD(2) method overestimate and EOMIP-CISD method underestimate the core IP values compared to the standard EOMIP-CCSD method by a large extent.

Further increasing the basis set from cc-pCVTZ to cc-pCVQZ, the IP values in all the method increase slightly, however, the trends remain the same. The comparison with the experimental results is out of the question as the EOMIP-CCSD method itself overshoots the experimental numbers by values as high as 2.0 eV in some of the cases, not to speak of the approximate EOM methods.

7.3.3 Error analysis

One of the main aim of this study is to estimate the error introduced in the EOMIP-CCSD(2) approximation due to truncated T amplitudes and rationalize the reasons behind it, so that this knowledge can be used to rectify the problem. The five test molecules (N_2, H_2O, H_2CO, C_2H_4, and CO), which we have studied in the previous subsection for valence IP, fetch out some clear trends.

The EOMIP-CISD method grossly underestimates the IP values and results are not even qualitatively correct. The EOMIP-CCSD(2) method overestimates the values compared to the standard EOMIP-CCSD method and this trend is more clear in large basis sets. The previous studies on the electron affinity and excitation energies have shown that the EOM-CCSD(2) approximation gives inferior performance only for molecules, where the Hartree-Fock orbitals do not provide a correct zeroth order description of the reference state. It was suggested by *Dutta et. al*[16] that the T1 diagnosis values can be used as an

marker of the suitability of the EOM-CCSD(2) approximation i.e. a T1 diagnosis value more than 0.02 indicates that the transition properties of the system will not be well reproduced by the EOM-CCSD(2) approximation. However, the situation is quite different for the IP case. The EOMIP-CCSD(2) method grossly over estimates the IP value for N_2, which has T1 diagnosis value of 0.13 (see Table 7.8), which is well within the acceptable range. On the other hand, C_2H_4 that has almost similar T1 diagnosis value (0.14), shows very good agreement with the corresponding EOMIP-CCSD results. So T1 diagnosis values in this case cannot be used as a marker for the reliability of the results. The P-EOMIP-CCSD(2) method gives an inconsistent performance depending upon the double excitation character associated with the concerned ionized state and in general gives inferior performance compared to the original EOMIP-CCSD(2) method. The P-EOMIP-CCSD(2) approximation fails drastically for states dominated by double excitation, which is to be expected from its truncated doubles-doubles block.

Table 7.8 : T1 Diagnosis Values in cc-pVTZ Basis Set

molecule	T1 value
N_2	0.013
H_2O	0.007
H_2CO	0.015
C_2H_4	0.014
ozone	0.028

The error in the different approximations to EOMIP-CCSD method can be rationalized in terms of the error introduced in the reference and the target state. The total energy in both reference and target state has three main components, namely: Hartree-Fock energy, correlation energy coming from the interaction of various excited determinants, and the

relaxation effects coming from the orbital rotations. In all the approximate schemes to the standard EOMIP-CCSD method, any truncation of the T and R operators leads to inferior description of the correlation and relaxation effect in both reference and target state, as compared to its full description and thereby increasing its energy w.r.t. the standard EOMIP-CCSD method. The delicate balance between the errors in the reference and the target state determines the over-all accuracy of the method.

Figure 7.1 provides a qualitative picture of the relative ordering of the reference and the target state in different variants of EOM approach to IP problem. In EOMIP-CISD approximation, the reference state is only bare Hartree-Fock wave function from which both relaxation and correlation effect are missing. On the other hand, the R_1 and R_2 operators introduce a significant amount of correlation and relaxation in the target state, which causes more rise in the reference state energy compared to the target state energy, resulting in underestimation of IP values. The situation is more complicated in case of EOMIP-CCSD(2) approximation. It is well known that generally the T_2 amplitudes introduce the correlation effect and T_1 amplitudes bring the relaxation effect. Now, the MBPT(2) amplitudes account for the dominant part of the correlation effect in CCSD method and relaxation effect is generally negligible for a closed shell reference state, unless dominated by more than one configuration. Therefore, the truncated T amplitudes in EOMIP-CCSD(2) method recover most part of the correlation energy in full CCSD model. However, the relaxation effect is significant in case of the ionized target state and large error is introduced in the target state due to the missing relaxation effect caused by the absence of T_1 amplitudes. Consequently, this leads to greater rise in the target state energy as compared to the reference state energy and IP values get overestimated in EOMIP-CCSD(2) method. The missing relaxation effect also leads to the fact that the truncated doubles-doubles block in P-EOM-CCSD(2) method, which has yielded great dividends in case of EA[16] and EE problem[15], only results in worsening of results in case of IP. This is due to the fact that already partly missing relaxation effect is further diminished by the truncated R operators in P-EOMIP-CCSD(2) methods. However, it

should be kept in mind that all the above-mentioned arguments are qualitative in nature and it may not be very straightforward to draw any quantitative relationship.

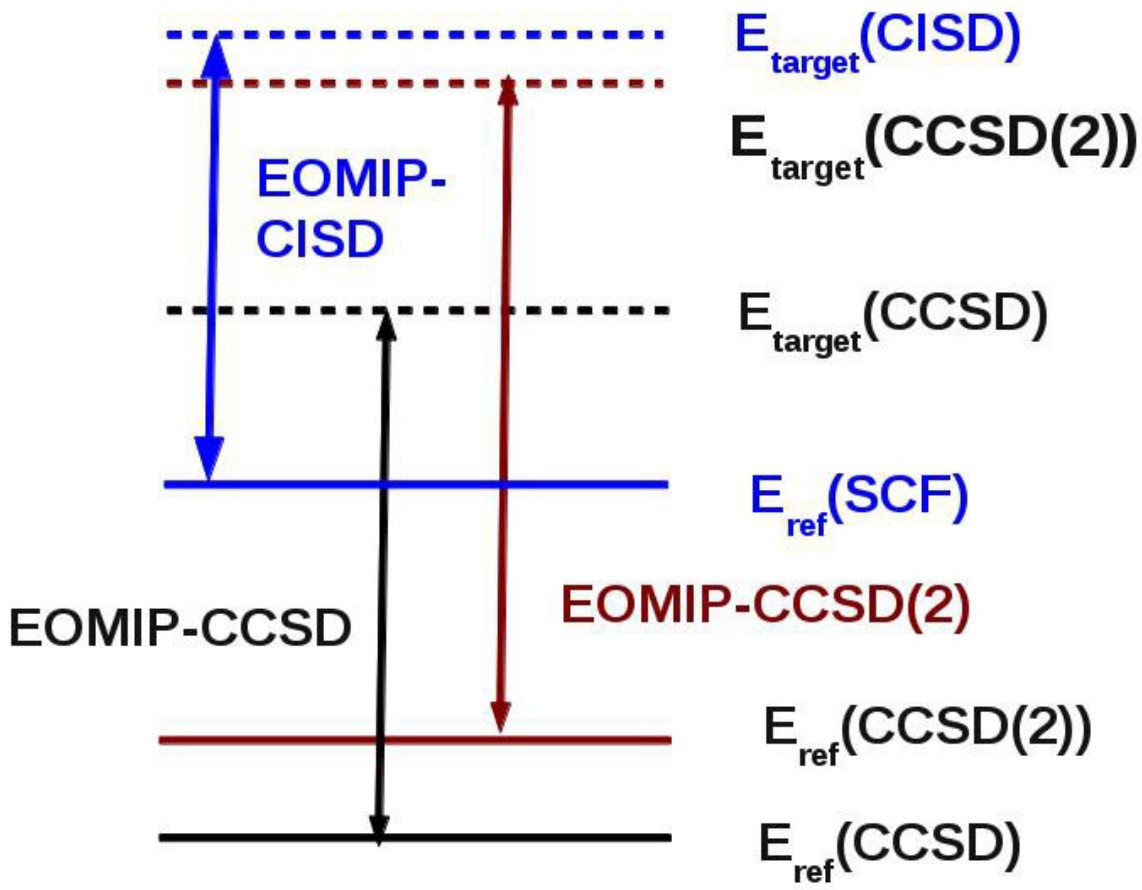

Figure 7.1: The relative ordering of reference and target state in different variants of EOM approach to IP problem

Another interesting point to be noted in the results presented in Table 7.2-7.6 is that the EOMIP-CCSD(2) method reproduces the basis set dependence of the EOMIP-CCSD method quite well and the extrapolated EOMIP-CCSD(2) method, as given by equation 7.10, corrects for the errors observed in the original EOMIP-CCSD(2) method to a large extent. However, five molecules are too small to construct a benchmark data set. Therefore, we have calculated the IP values corresponding to first five states of a test set of twenty molecules consisting of N_2, H_2O, ClF, H_2CO, CO, NO^-, C_2H_2, C_2H_4, O_3, NH_3,

F_2, CO_2, SO_2, CN^- , N_2O, BN, HF, S_2, P_2 and O_2 in EOMIP-CCSD(2)/cc-pVQZ level of theory and compared the values with the standard EOMIP-CCSD results. Table 7.9 contains the statistical analysis of the errors.

Table 7.9 : Maximum absolute, average absolute and root mean square deviation of calculated valence ionization potentials(e.V) from EOMIP-CCSD values in aug-cc-PVQZ basis set

Method	EOMIP-CCSD(2)	Extrapolated EOMIP-CCSD(2)
Max abs dev	0.81	0.28
Avr Abs dev	0.17	0.09
RMS dev	0.24	0.11

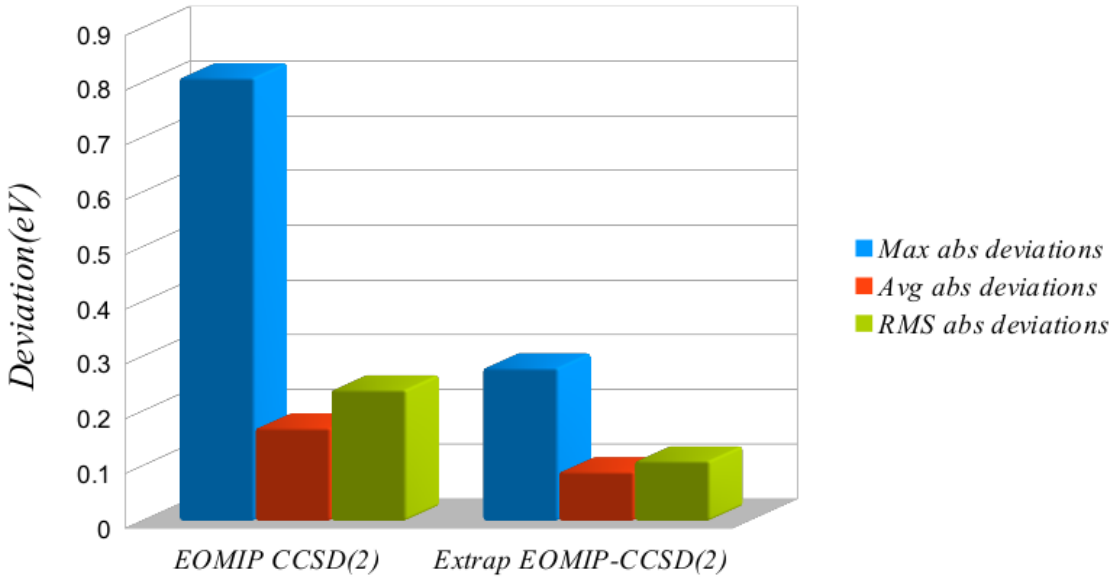

Figure 7.2 : Maximum abs deviation, average abs deviation, and RMS deviation of EOMIP-CCSD(2) method and its extrapolated version from the full EOMIP-CCSD method (in eV).

The average absolute deviation in extrapolated EOMIP-CCSD(2) method is less than 0.1 eV and maximum error is 0.28 eV, which is significantly less than the high value of

0.81eV seen in the original EOMIP-CCSD(2) method. The RMSD value in extrapolated EOMIP-CCSD(2) method is 0.11 eV, which is nearly half of the original EOMIP-CCSD(2) approximation. Figure 7.2 shows that the extrapolated EOMIP-CCSD(2) method gives significant improvement for valence IP, over its original implementation and at least it saves in the cases where the original EOMIP-CCSD(2) method drastically fails.

In the case of core ionization spectra the EOMIP-CCSD(2) fails terribly and the extrapolated version hardly provides any respite. This also emphasizes the importance of missing relaxation effect as the determining factor in the errors obtained in the EOMIP-CCSD(2) calculated IP values.

7.4 CONCLUSION

In this chapter, we have analyzed the performance of the EOMIP-CCSD(2) method for valence and core-ionization energies. It is found that among various proposed approximations to standard EOMIP-CCSD method, the EOMIP-CCSD(2) method gives the best performance. The EOMIP-CISD method heavily underestimates the IP values and the results are not even qualitatively correct. The partitioned version of EOMIP-CCSD(2) gives inconsistent performance and in general shows more error than the standard EOMIP-CCSD(2) method. Therefore, approximating the doubles-doubles block of the EOM matrix by its diagonal terms, which has been extremely successful in reducing the errors in EA and EE EOM-CC method, does not work in the case of IP. The EOMIP-CCSD(2) method, although, overestimates the IP values but it correctly reproduces the basis set dependence of standard EOMIP-CCSD method. The extrapolated EOMIP-CCSD(2) method gives reasonable agreement with the standard EOMIP-CCSD method and shows an average absolute deviation of only 0.09 eV for the valence IP.

However, the EOMIP-CCSD(2) approximation fails drastically for ionization of core electrons and even the extrapolated version does not provide any reasonable improvement.

Therefore, the EOMIP-CCSD(2) approximation, which has been extremely successful for geometries and properties of doublet radicals, does not provide good results for the ionization potential itself. Although, the extrapolation techniques give some respite for valence IP, it hardly saves in the case of core-ionization. The analysis of the results has shown that the missing relaxation effect due to the truncated T amplitudes in EOM-CCSD(2) is responsible for the overestimation of the IP values. Therefore, new theoretical developments introducing more relaxation effect within the framework of EOMIP-CCSD(2) approximation is necessary to rectify the problem.

References:

1. Marcus, R. A.; Sutin, N., *Bio. Biophys. Acta.* **1985,** *811*, 265-322.
2. Born, G.; Kurtz, H. A.; ohrn, Y., *J. Chem. Phys.* **1978,** *68*, 74-85.
3. Sekino, H.; Bartlett, R. J., *Int. J. Quant. Chem.* **1984,** *26*, 255-265.
4. Stanton, J. F.; Bartlett, R. J., *J. Chem. Phys.* **1993,** *98*, 7029-7039.
5. Hubac, I.; Kvasnicka, V.; Holubec, A., *Chem. Phys. Lett.* **1973,** *23*, 381-385.
6. Hirao, K., *Chem. Phys. Lett.* **1993,** *201*, 59-66.
7. Cederbaum, L. S.; Domcke, W., *Adv. Chem. Phys.*, John Wiley & Sons, Inc.: 2007; pp 205-344.
8. Herman, M. F.; Freed, K. F.; Yeager, D. L., , *Adv. Chem. Phys.* John Wiley & Sons, Inc.: 2007; pp 1-69.
9. Stanton, J. F.; Gauss, J., *J. Chem. Phys.* **1994,** *101*, 8938-8944.
10. Nooijen, M.; Bartlett, R. J.,. *J. Chem. Phys.* **1995,** *102*, 3629-3647.
11. Musial, M.; Bartlett, R. J., *J. Chem. Phys.* **2008,** *129*, 134105-12.
12. Bartlett, R. J., *Annu. Rev. Phys. Chem.* **1981,** *32*, 359-401.
13. Nooijen, M.; Snijders, J. G., *J. Chem. Phys.* **1995,** *102*, 1681-1688.
14. Stanton, J. F.; Gauss, J., *J. Chem. Phys.* **1995,** *103*, 1064-1076.
15. Gwaltney, S. R.; Nooijen, M.; Bartlett, R. J., *Chem. Phys. Lett.* **1996,** *248*, 189-198.
16. Dutta, A. K.; Gupta, J.; Pathak, H.; Vaval, N.; Pal, S., *J. Chem. Theor. Comp.* **2014,** *10*, 1923-1933.
17. Dutta, A. K.; Pal, S.; Ghosh, D., *J. Chem. Phys.* **2013,** *139*, 124116-11
18. Dutta, A. K.; Vaval, N.; Pal, S., *J. Chem. Theor. Comp.* **2013,** *9*, 4313-4331.
19. Ghosh, D., *J. Chem. Phys.* **2014,** *140*, 094101.
20. Anna, A. G.; Piotr, A. P.; Anna, I. K., *J. Chem. Phys.* **2009,** *130*, 124113.
21. Dunning, T. H., *J. Chem. Phys.* **1989,** *90*, 1007-1023.
22. The formula used is slightly different from that used in ref 19.

23. Stanton, J. F.; Gauss, J.; Harding, M. E.; Szalay, P. G.; Auer, A. A.; Bartlett, R. J.; Benedikt, U.; Berger, C.; Bernholdt, D. E.; Bomble, Y. J., CFOUR, a quantum chemical program package. *For the current version, see http://www. cfour. de* **2009**.

24. Frisch, M. J.; Trucks, G. W.; Schlegel, H. B.; Scuseria, G. E.; Robb, M. A.; Cheeseman, J. R.; Scalmani, G.; Barone, V.; Mennucci, B.; Petersson, G. A., Gaussian 09, revision B. 01. *Gaussian, Inc., Wallingford, CT*.

25. Jana, D.; Bandyopadhyay, B.; Mukherjee, D., *Theor. Chem. Acc.* **1999,** *102*, 317-327.

26. Woon, D. E.; Dunning, T. H., *J. Chem. Phys.* **1995,** *103*, 4572-4585.

27. Ohtsuka, Y.; Nakatsuji, H., *J. Chem. Phys.* **2006,** *124*, -.

28. Ehara, M.; Nakatsuji, H., G *Collect. Czek. Chem. Comm.* **2008,** *73*, 771-785.

Chapter 8

EOMIP-CCSD(2)* : an efficient method for calculation of ionization potential

" Life had already given him sufficient reasons for knowing that no defeat was the final one "

Gabriel García Márquez

The General in His Labyrinth

In this chapter, we present a new approximation to the standard EOMIP-CCSD method. The new method (EOMIP-CCSD(2)*) scales as non-iterative N^6 and has significantly low storage requirement. The problem of over estimation of ionization potential in EOMIP-CCSD(2) approximation is corrected in this new method and the EOMIP-CCSD(2)* method gives excellent agreement with experimental the values. It also gives very good with experiments for bond-length and IR frequencies and produces value comparable to CCSD(T) method, in significantly less computational cost. The EOMIP-CCSD(2)* approximation works even for the core-ionization and satellite IP, where the previous EOMIP-CCSD(2) approximation drastically fails.

8.1 Introduction:

The equation of motion coupled cluster approach has emerged as one of the most robust method for the calculation of direct difference of energies like excitation energies (EE) [1], ionization potential (IP) [2], and electron affinities (EA) [3]. It includes a balanced description of dynamic and non-dynamic correlation and provides a "black box" way to different sectors of Fock space without going into the complicacies of so-called multi-reference coupled cluster methods [4].

The equation of motion coupled cluster (EOM-CC) is generally used in singles and doubles approximation (EOM-CCSD) [1]. It has iterative N^6 scaling and similar storage requirement as that of the standard single-reference CCSD method, which prohibits its use beyond ten second-row atoms in any reasonable basis set. This calls for the development of lower scaling and smaller storage requiring approximation to the standard EOM-CCSD, which can be applied to large systems. There exists an intrigue relationship between coupled cluster method and many body perturbation theory (MBPT) [5]. So, a natural way of approximating any coupled cluster method would be based on perturbational orders. Nooijen and Sniders [6] were the first to develop the idea of replacing coupled cluster T amplitudes with their MBPT(2) analogues in the context of ionization problem. This leads to a method, which is N^5 scaling and has lower storage requirement, as it is free from the four particle intermediates. Although, the method has been successful in calculating the ionization potential, it does not provide a straightforward definition of total energy and therefore not suitable for final state calculations. Stanton and Gauss [7] latter generalized this approach to provide a hierarchical approximation to the standard EOM-CCSD method. They have coined the term EOM-CCSD(n), where n denoted the order in perturbation and at large values of n, the EOM-CCSD(n) method converges to standard EOM-CCSD method. The new method can calculate difference of energy, at the same time has the added advantage of clearly

defined total energy, which makes them suitable for final state property calculations. The lowest order approximation to EOM-CCSD(n) is EOM-CCSD(2), where the reference state is truncated at MBPT(2). The EOM-CCSD(2) approximation was originally implemented by Stanton and Gauss [7] for ionization problem(EOMIP-CCSD(2)) and excitation energies(EOMEE-CCSD(2)). Similar developments were latter persuaded by Dutta *.et. al.* [8] in the context of electron affinity and spin flip variants of EOMCC. Recently, Pal and co-workers [9] have shown that the EOMIP-CCSD(2) method can be used for the calculation of geometry and IR frequency of large doublet radicals with accuracy comparable to that of the standard EOMIP-CCSD method. In the previous chapter, we have shown that although the EOMIP-CCSD(2) method is very good for the study of final state properties, it is not particularly suitable for calculation of IP itself. The missing relaxation effect due to the truncated T amplitudes leads to systematic overestimation of IP in EOMIP-CCSD(2) method. The aim of this chapter is to suggest a modification of the standard EOMIP-CCSD(2) method, which can account for the missing relaxation effect.

The chapter is organized as follows. The next section gives the theory and computational details of the new method. The numerical performance of the new method are discussed in the section 8.3. The section 8.4 gives the concluding remarks.

8.2 Theory and Computational Details

The main source of error in the EOMIP-CCSD(2) approximation, as pointed out in the previous chapter, is the missing relaxation effect due to truncated T amplitudes, which cannot be compensated by the R_1 and R_2 operators. A straightforward way to account for the missing relaxation effect is to include higher order terms in the EOM matrix. The full inclusion of R_3 *o*perator will shoot up the scaling to iterative N^7, which is not feasible to use except for very small molecules. However, it is possible to perform a selective inclusion of R_3 in a non-iterative way with a N^6 scaling. Among the various possible

schemes available for non-iterative inclusion of R_3 operator, we have followed the scheme described by Stanton and co-workers [10].

8.2.1 EOM-IP-CCSD*

In the EOMIP-CC frame work, the final states are obtained by diagonalizing the similarity transformed Hamiltonian in (N-1) electron space.

$$\bar{H} = e^{-T} H e^{T} = \left(H e^{T} \right)_c \tag{8.1}$$

In the eigen value equation form it can be written as

$$\left[\bar{H}, \hat{\Omega} \right] \Phi_0 = \left(\bar{H} \Omega \right)_c = \omega_k \hat{\Omega}_k \Phi_0 \tag{8.2}$$

where ω_k is the IP value corresponding to kth state and $\hat{\Omega}_k$ is the corresponding EOM operator and for the IP problem it has the following form.

$$\Omega_k^{IP} = \sum_i R_i(k) i + \sum_{i>j,a} R_{ij}^{a}(k) \hat{a}^{\dagger} \hat{j} \hat{i} + ... \tag{8.3}$$

Since $\bar{H}$ is non Hermitian, there exist different right(R) and left(L) eigenvectors which are biorthogonal and can be normalized to satisfy

$$L_k R_l = \delta_{kl} \tag{8.4}$$

The resulting method is equivalent to the (0,1) sector of the Fock space multi-reference coupled cluster (FSMRCC) method for the principal ionizations [11].

In deriving the R_3 correction to EOMIP-CCSD, Löwdin's matrix partitioning technique [12] is used.

Following Löwdin's partitioning technique [12], equation 8.2 can be partitioned into *P* and *Q* space, where *P* represents the principal configuration space, and *Q* represents its orthogonal complement.

$$\begin{bmatrix} \bar{H}_{pp} & \bar{H}_{pq} \\ \bar{H}_{qp} & \bar{H}_{qq} \end{bmatrix} \begin{bmatrix} R_p \\ R_q \end{bmatrix} = \omega \begin{bmatrix} R_p \\ R_q \end{bmatrix} \tag{8.5}$$

and

$$\begin{bmatrix} L_p & L_q \end{bmatrix} \begin{bmatrix} \bar{H}_{pp} & \bar{H}_{pq} \\ \bar{H}_{qp} & \bar{H}_{qq} \end{bmatrix} = \begin{bmatrix} L_p & L_q \end{bmatrix} \omega \tag{8.6}$$

Where, R_p (L_p) and R_q(L_q) represent the projection of the right (left) eigenvector on *P* and *Q* spaces.

Expanding equation 8.5 we get

$$\bar{H}_{pp} R_p + \bar{H}_{pq} R_q = \omega R_p \tag{8.7}$$

$$\bar{H}_{qp} R_p + \bar{H}_{qq} R_q = \omega R_q \tag{8.8}$$

Rearranging equation 8.8

$$R_q = \left[\omega - \bar{H}_{qq} \right]^{-1} \bar{H}_{qp} R_p \tag{8.9}$$

Inserting R_q back into equation 8.7 we get

$$\bar{H}_{eff} R_p \equiv \left(\bar{H}_{pp} + \bar{H}_{pq} \left[\omega - \bar{H}_{qq} \right]^{-1} \bar{H}_{qp} \right) R_p = \omega R_p \tag{8.10}$$

Projecting equation 8.10 with L_p

$$\left\langle L_p \middle| \bar{H}_{eff} \middle| R_p \right\rangle \equiv \left\langle L_p \middle| \left[\bar{H}_{pp} + \bar{H}_{pq} \left[\omega - \bar{H}_{qq} \right]^{-1} \bar{H}_{qp} \right] \middle| R_p \right\rangle = \omega \left\langle L_p \middle| R_p \right\rangle \tag{8.11}$$

The eigen values of H_{eff} are solely defined in the *P* space, for first several eigen values. Now the exact eigen value ω can be expressed as the sum of zeroth order energy ω_0, as of yet undetermined, and an energy correction $\Delta\omega$.

The operator inverse in equation (8.11) can be expressed as

$$\left[\omega - \bar{H}_{qq}\right]^{-1} = \left[\omega_0 + \Delta\omega - \bar{H}_{qq}^{[0]} - \bar{H}_{qq}^{[1]} - \bar{H}_{qq}^{[2]}.....\right]^{-1}$$
$$= \left[\left(\omega_0 - \bar{H}_{qq}^{[0]}\right)\left(1 - \left[\omega_0 - \bar{H}_{qq}^{[0]}\right]^{-1}\left[\bar{H}_{qq}^{[1]} + \bar{H}_{qq}^{[2]}..... - \Delta\omega\right]\right)\right]^{-1} \quad (8.12)$$
$$\equiv \left[\left(\omega_0 - \bar{H}_{qq}^{[0]}\right)\left(1 - \left[\omega_0 - \bar{H}_{qq}^{[0]}\right]^{-1}\left[V_{qq} - \Delta\omega\right]\right)\right]^{-1}$$

Where $V_{qq} = \bar{H}_{qq}^{[1]} + \bar{H}_{qq}^{[2]} + ...$

Now equation 8.12 can be expanded in an inverse series

$$\left[\omega - \bar{H}_{qq}\right]^{-1} = \left[\omega_0 - \bar{H}_{qq}^{[0]}\right]^{-1}$$
$$+\left[\omega_0 - \bar{H}_{qq}^{[0]}\right]^{-1}\left(V_{qq} - \Delta\omega\right)\left[\omega_0 - \bar{H}_{qq}^{[0]}\right]^{-1} \quad (8.13)$$
$$+\left[\omega_0 - \bar{H}_{qq}^{[0]}\right]^{-1}\left(V_{qq} - \Delta\omega\right)\left[\omega_0 - \bar{H}_{qq}^{[0]}\right]^{-1}\left(V_{qq} - \Delta\omega\right)\left[\omega_0 - \bar{H}_{qq}^{[0]}\right]^{-1}$$
$$+.....$$

Now, the energy correction to EOMIP-CCSD can be derived by defining p as $p \equiv h \cup 2hp$, $\bar{H}_{pp}$ is taken as zeroth order and ω_0 can be taken as the EOMIP-CCSD energy. Equation (8.11) can be written as

$$\left\langle L_p \middle| \bar{H}_{eff} \middle| R_p \right\rangle = E_{EOMIP} + \Delta\omega = E_{EOMIP} + \left\langle \delta L \middle| D \middle| \delta R \right\rangle \quad (8.14)$$

and

$$\left\langle \delta L \right| = \left\langle L \middle| \bar{H}_{pq}\left[\omega_0 - H_{qq}^{[0]}\right]^{-1} \right. \quad (8.15)$$

$$\left| \delta R \right\rangle = \left[\omega_0 - H_{qq}^{[0]}\right]^{-1} H_{qp} \left| R \right\rangle \quad (8.16)$$

Now, the similarity transformed Hamiltonian can be expressed in perturbational orders

$$\bar{H} = \left(He^T\right)_c = \bar{H}^{[1]} + \bar{H}^{[2]} + \bar{H}^{[3]} + \bar{H}^{[4]} + ... \quad (8.17)$$

In the above expression hole-hole and particle-particle block of Fock matrix is treated as zeroth order and rest of the H is treated as first order. The T_1 and T_2 amplitudes for the reference state are taken as second and first order in correlation, respectively. The projection of L and R on 1h determinants (L_h and R_h) are taken as zeroth order and the projection on 2h1p determinants (L_{2h1p} and R_{2h1p}) are taken as first order in correlation. With this definition equation (8.11) can be written as

$$\left\langle L_p \middle| \bar{H}_{eff} \middle| R_p \right\rangle = \left\langle L_p \middle| \bar{H}_{pq} \left[\omega_0 - E_0 - \bar{H}^0_{qq} \right]^{-1} \bar{H}_{qq} \left[\omega_0 - E_0 - \bar{H}^0_{qq} \right]^{-1} \bar{H}_{qp} \middle| R_P \right\rangle \tag{8.18}$$

The equation (8.18) contains only terms which are fourth order and higher in correlation. Because of their negligible contribution and high computational cost associated with their evaluation, equation (8.18) has not been considered. Instead, equation (8.14), which contains terms only up to third order in perturbation, has been used for the energy correction. The elements of $\bar{H}_{pq}$ and $\bar{H}_{qp}$ are divided according to hole-particle contribution and only the terms having lowest non-vanishing contributions has been considered.

Following the above guide line, Stanton and co-workers [10] have shown that only surviving contributions are those which connect the reference determinant($|0\rangle$) to determinant generated by 3h2p operators(i.e those are obtained by excitation of two electrons and removal of the third).

The spin-orbital notation of the equation (8.15) and (8.16) as described in reference [10], are as bellow

$$D^{ijk}_{ab} l^{ijk}_{ab} = P(ijk) l^k \langle ab||ij\rangle - P(ijk) \sum_e l^{ij}_e \langle ek||ab\rangle - P(ab)P(ijk) \sum_m l^{mk}_a \langle ij||mb\rangle \tag{8.19}$$

$$\begin{aligned} D^{ab}_{ijk} r^{ab}_{ijk} &= -P(ijk) \sum_e r^e_{ij} \langle ab||ek\rangle - P(ab)P(ijk) \sum_m r^a_{mk} \langle mb||ij\rangle \\ &- P(ab)P(ijk) \sum_{me} r_m t^{ae}_{ij} \langle mb||ke\rangle + P(kji) \sum_{mn} r_m t^{ab}_{in} \langle mn||kj\rangle \end{aligned} \tag{8.20}$$

$$D_{ab}^{ijk} = D_{ijk}^{ab} = \omega_0 - E_0 + f_{ii} + f_{jj} + f_{kk} - f_{aa} - f_{bb} \tag{8.21}$$

The fT and dT correction by Manohar *et. al*. [13] for including non-iterative triples in EOMIP-CCSD were derived following a similar strategy.

8.2.2 EOM-IP-CCSD(2)*

Following the Stanton and Gauss's [7] original EOMIP-CCSD(2) scheme, the CC amplitudes can be approximated by the MBPT(2) amplitudes for a second order truncated effective Hamiltonians ($H^{[2]}$)

$$\begin{aligned} \bar{H} &= \left(H\, \mathrm{e}^{T} \right)_c \\ &\approx \left(H\, \mathrm{e}^{T'} \right)_c \end{aligned} \tag{8.23}$$

where the perturbative approximation to the T amplitudes can be written as

$$\begin{aligned} T_1' &= \frac{f_{ia}}{\varepsilon_i - \varepsilon_a} \\ T_2' &= \frac{\langle ab || ij \rangle}{\varepsilon_i + \varepsilon_j - \varepsilon_a - \varepsilon_b} \end{aligned} \tag{8.24}$$

T_1 is zero for restricted closed shell and unrestricted MBPT(2) reference. Using these T' amplitudes one can generate a modified similarity transformed Hamiltonian $\bar{H}'$, which can be used as the reference for subsequent EOMIP calculations. After solving for the right vector, one need to solve for the left vector and the correction to right and left vector is constructed in a non-iterative fashion using the equation (8.19-21). Finally, the energy correction is calculated using equation 8.14. We call this new approximation as EOMIP-CCSD(2)*

The original EOMIP-CCSD(2) method scales as iterative N^5. Now, the energy correction as described in the equation (8.20) and (8.21) scales as non-iterative N^6. So, overall the EOMIP-CCSD(2)* method is non-iterative N^6 scaling, as compared to iterative N^6

scaling of standard EOMIP-CCSD method. However, the situation is more favorable than the above statement indicates. The most expensive terms occurring due to the 3h2p corrections in our EOMIP-CCSD(2)* method scale with $n_h^3 n_p^3$ and $n_h^4 n_p^2$, where n_p and n_h represent the number of orbitals unoccupied and occupied in the reference Hartree-Fock reference state, respectively. The reference state CCSD calculation involves an iterative step that scales with $n_h^2 n_p^4$. Now for typical applications in a reasonable basis set, n_p is much greater than n_h. Therefore, the cost of a single EOMIP-CCSD*(2) calculation might be substantially less than a single iteration of the reference state CCSD equations.

Now, let us consider the storage requirements. In the EOMIP-CCSD(2)* method ,there is no four particle intermediates in the energy correction part. So, EOM-IP-CCSD(2) method has significantly less storage requirements than the standard EOMIP-CCSD method. Although, the storage requirement has increased from that in the EOMIP-CCSD(2) approximation, due to the presence of 3particle-1hole intermediates in the energy correction part, which were absent in the EOMIP-CCSD(2) approximation. So, both in terms of CPU scaling and storage requirements, the EOMIP-CCSD(2)* method lies in between EOMIP-CCSD(2) and standard EOMIP-CCSD method.

8.2.3 Computational Details:

All the EOMIP-CCSD(2)* calculations were performed using a modified public version of the quantum chemistry package Cfour [14]. The valence IP values for test molecules were calculated using a hierarchy of Dunning's correlation consistent cc-pVXZ(X=D,T and Q) basis set [15] using experimental geometry. The core-valence correlation cc-pCVXZ(X=D,T and Q) basis set [16] was used for the calculation of core IP. The structure optimization and frequency calculations of doublet radicals were performed using the numerical gradient technique. All the other EOM and single-reference coupled cluster calculations are performed using Cfour [14].

8.3 Results and Discussion

Table 8.1 presents the wall timing of EOMIP-CCSD method along with its two approximate variants for a series of water clusters (($H_2O)_n$, n=1-8). It can be seen that EOMIP-CCSD(2)* method lies in between the EOMIP-CCSD and EOMIP-CCSD(2), as expected from the theoretical foundation of the method described in the previous section. It can be seen that as the system size increases, the EOMIP-CCSD(2)* continues to become considerably cheaper compared to the standard EOMIP-CCSD method.

Table8.1 : Wall Timings for the EOMIP-CCSD(2) and EOMIP-CCSD Method[a,b] in the cc-pVDZ Basis Set

	Wall Timing (s)		
number of H_2O units	**EOMIP-CCSD**	**EOMIP-CCSD(2)**	**EOMIP-CCSD(2)***
1	1.16	1.13	1.33
2	11.54	2.89	4.84
3	108.88	9.88	29.42
4	490.52	30.67	70.61
5	1516.96	119.20	255.79
6	3795.23	289.19	1620.46
7	15129.76	673.03	4030.58
8	42946.41	1682.45	9436.54

a : All the calculations were performed using an i7 desktop with 3.40 GHz CPU speed and 16 GB of RAM. Calculations were performed using single core.

b : Calculations were performed assuming C_1 symmetry.

8.3.1 Valence Ionization Spectra

The performance of the EOMIP-CCSD(2)* method for valence ionization energies is

benchmarked for small molecules like N_2, H_2O, H_2CO, C_2H_2, and CO in a hierarchy of Dunning's correlation consistent cc-pVXZ (X = D, T, Q) basis set (Tables 8.2–8.6) and the results are compared with experimental numbers, wherever available. For the sake of comparison, we also quote the corresponding EOMIP-CCSD(2) and extrapolated EOMIP-CCSD(2) results.

Table 8.2 : Ionization Energies of N_2 (in eV)

state	EOMIP-CCSD	EOMIP-CCSD(2)	Extrapolated EOMIP-CCSD(2)	EOMIP-CCSD(2)*	EOMIP-CCSD*	Exp [17]
			cc-pVDZ Basis Set			
$3\sigma_g$	15.19	15.39	-	15.19	15.02	15.60
$1\pi_u$	16.96	17.14	-	16.59	16.45	16.98
$2\sigma_u$	18.45	18.56	-	18.44	18.35	18.78
			cc-pVTZ Basis Set			
$3\sigma_g$	15.59	15.85	15.65	15.54	15.33	15.60
$1\pi_u$	17.22	17.48	17.30	16.87	16.66	16.98
$2\sigma_u$	18.81	18.98	18.87	18.75	18.61	18.78
			cc-pVQZ Basis Set			
$3\sigma_g$	15.72	16.02	15.82	15.68	15.43	15.60
$1\pi_u$	17.34	17.64	17.46	17.00	16.75	16.98
$2\sigma_u$	18.93	19.15	19.04	18.88	18.69	18.78

The Table 8.2 presents the valence ionization energies of first three states of N_2. It can be seen that the EOMIP-CCSD(2) method overestimates the IP values compared to the

standard EOMIP-CCSD method in cc-pVDZ basis. The EOMIP-CCSD(2)* method corrects for this overestimation and gives IP values which are in superior agreement with the highly accurate EOMIP-CCSD* method. The agreement is even better than the standard EOMIP-CCSD method. The IP values in all the methods increase from cc-pVDZ to cc-pVTZ basis. The extrapolated EOMIP-CCSD(2) shows considerable improvement over the original EOMIP-CCSD(2) approximation. However, the values are inferior as compared to the EOMIP-CCSD(2)* method, which are in very good agreement with the EOMIP-CCSD* method. The IP values in all the methods increase slightly, as we go from cc-pVTZ to cc-pVQZ basis set. The EOMIP-CCSD(2)* method gives IP value which are within 0.1 eV of the experimental value [17] and the results are in even better agreement than the standard EOMIP-CCSD method.

Table 8.3 presents the vertical ionization energies corresponding to the valence orbitals of water. It can be seen that in cc-pVDZ basis set, all the EOMIP methods lead to very similar results. The IP values for all the three states increase from cc-pVDZ to cc-pVTZ basis. Here it should be noted that inclusion triples has a negligible effect on the valence ionization potentials of water. The IP values further increase as we go from cc-pVTZ to cc-pVQZ basis set. The experimental IP values corresponding to $1b_2$ and $3a_1$ are well reproduced in EOMIP-CCSD*(2)/cc-pVQZ level of theory. However, the IP value corresponding to $3a_1$ state in EOMIP-CCSD(2) method is overestimated by 0.46 eV, compared to the experiments. However, the highly accurate EOMIP-CCSD* method gives almost identical value as that of the EOMIP-CCSD(2)* method for the $3a_1$ state. It should be noted that the EOMIP-CCSD(2)* method gives slightly better agreement with experiment [17] than the EOMIP-CCSD method for all the three states, although, the values in both the methods are very close to each other.

Table 8.3 : Ionization Energies of H_2O (in eV)

state	EOMIP-CCSD	EOMIP-CCSD(2)	Extrapolated EOMIP-CCSD(2)	EOMIP-CCSD(2)*	EOMIP-CCSD*	Exp [17]
			cc-pVDZ Basis Set			
$1b_2$	11.80	11.74	-	11.85	11.91	12.62
$3a_1$	14.11	14.04	-	14.11	14.23	14.73
$1b_1$	18.47	18.37	-	18.40	18.50	18.55
			cc-pVTZ Basis Set			
$1b_2$	12.40	12.43	12.43	12.39	12.39	12.62
$3a_1$	14.63	14.63	14.63	14.60	14.62	14.73
$1b_1$	18.83	18.81	18.81	18.75	18.79	18.55
			cc-pVQZ Basis Set			
$1b_2$	12.62	12.69	12.69	12.60	12.55	12.62
$3a_1$	14.82	14.87	14.87	14.79	14.76	14.73
$3a_1$	19.00	19.01	19.01	18.91	18.92	18.55

The first four valence ionized states of formaldehyde are reported in Table 8.4. The EOMIP-CCSD(2) method gives good agreement with the EOMIP-CCSD values in cc-pVDZ basis set. The EOMIP-CCSD*(2) and EOMIP-CCSD* method give slightly lower IP values for the $1b_1$ and $1b_2$ state; however, the values are similar to the EOMIP-CCSD method for the other two states. On increasing the basis set from cc-pVDZ to cc-pVTZ, the IP values in all the methods increase by considerable amount. The EOMIP-CCSD(2)* method gives almost identical values with the EOMIP-CCSD* method, and the results are slightly lower than that in EOMIP-CCSD method in cc-pVTZ basis set. The IP values

further increase from cc-pVTZ to cc-pVQZ basis and are within 0.1 eV of experimental result in EOMIP-CCSD(2)*/cc-pVQZ level of theory, except the $1b_2$ state, which is overestimated by 0.58 eV. However, the EOMIP-CCSD* method also shows similar overestimation for the $1b_2$ state. The EOMIP-CCSD(2)* result is in much better agreement with the experimental result [17] than the EOMIP-CCSD method and EOMIP-CCSD(2) method for $1b_2$ state.

Table 8.4 : Ionization Energies of H_2CO (in eV)

state	EOMIP-CCSD	EOMIP-CCSD(2)	Extrapolated EOMIP-CCSD(2)	EOMIP-CCSD(2)*	EOMIP-CCSD*	Exp [17]
			cc-pVDZ Basis Set			
$2b_2$	10.34	10.25		10.34	10.34	10.88
$1b_1$	14.29	14.18		14.15	14.15	14.5
$5a_1$	15.71	15.63		15.66	15.66	16.0
$1b_2$	17.08	17.03		16.78	16.78	16.5
			cc-pVTZ Basis Set			
$2b_2$	10.75	10.77	10.77	10.63	10.64	10.88
$1b_1$	14.57	14.58	14.58	14.32	14.33	14.5
$5a_1$	16.05	16.07	16.07	15.87	15.87	16.0
$1b_2$	17.37	17.39	17.39	17.00	17.00	16.5
			cc-pVQZ Basis Set			
$2b_2$	10.90	10.97	10.97	10.79	10.75	10.88
$1b_1$	14.69	14.77	14.77	14.47	14.42	14.5
$5a_1$	16.19	16.28	16.28	16.03	15.97	16.0
$1b_2$	17.48	17.54	17.54	17.13	17.08	16.5

Table 8.5 : Ionization Energies of C_2H_2 (in eV)

state	EOMIP-CCSD	EOMIP-CCSD(2)	Extrapolated EOMIP-CCSD(2)	EOMIP-CCSD(2)*	EOMIP-CCSD*	Exp [18]
			cc-pVDZ Basis Set			
$^2\Pi_u$	11.33	11.35	-	11.07	11.08	11.49
$^2\Sigma^+_g$	16.98	17.01	-	16.84	16.81	16.7
$^2\Sigma^+_u$	18.88	18.86	-	18.72	18.75	18.7
			cc-pVTZ Basis Set			
$^2\Pi_u$	11.55	11.66	11.64	11.31	11.22	11.49
$^2\Sigma^+_g$	17.21	17.32	17.29	17.07	16.98	16.7
$^2\Sigma^+_u$	19.09	19.15	19.15	18.93	18.89	18.7
			cc-pVQZ Basis Set			
$^2\Pi_u$	11.63	11.80	11.78	11.41	11.27	11.49
$^2\Sigma^+_g$	17.30	17.46	17.43	17.18	17.04	16.7
$^2\Sigma^+_u$	19.17	19.27	19.27	19.03	18.94	18.7

Table 8.5 presents the IP values corresponding to $^2\Pi_u$, $^2\Sigma^+_g$ and $^2\Sigma^+_u$ states of acetylene in different EOM methods. In cc-pVDZ basis, the IP values in EOMIP-CCSD(2)* method give very good agreement with the EOMIP-CCSD* method and the values are considerably lower than the corresponding EOMIP-CCSD and EOMIP-CCSD(2) results. The IP values in all the methods undergo blue shift as we go from cc-pVDZ to cc-pVTZ basis. The EOMIP-CCSD(2)* method continue to give lower values than the EOMIP-CCSD method, however, the former gives better agreement with the highly accurate EOMIP-CCSD* method. The IP values undergo further blue shift from cc-pVTZ to cc-pVQZ basis. The EOMIP-CCSD(2)* method in cc-pVQZ basis set gives very good

agreement with the experimental value[17] for the $^2\Pi_u$ state, but it overestimates the IP values for the other two states. However, the IP values are in superior agreement with experiment, as compared to the EOMIP-CCSD method, which overestimates them by more than 0.6 eV in cc-pVQZ basis set. The EOMIP-CCSD(2) method leads to further overestimation and its extrapolated version does not provide any significant change.

Table 8.6 : Ionization Energies of O_3 (in eV)

state	EOMIP-CCSD	EOMIP-CCSD(2)	Extrapolated EOMIP-CCSD(2)	EOMIP-CCSD(2)*	EOMIP-CCSD*	EOMIP-CCSDT	Exp[17]
			cc-pVDZ Basis Set				
$1a_2$	12.35	12.76		12.26	11.93	12.20	12.73
$6a_1$	12.45	12.84		12.39	12.07	12.33	13.00
$3b_1$	13.11	13.52		12.88	12.61	13.12	13.54
			cc-pVTZ Basis Set				
$1a_2$	12.77	13.24	12.83	12.61	12.24	12.56	12.73
$6a_1$	12.85	13.30	12.91	12.72	12.36	12.67	13.00
$3b_1$	13.41	13.93	13.52	13.21	12.75	13.44	13.54
			cc-pVQZ Basis Set				
$1a_2$	12.97	13.49	13.08	12.81	12.40	12.74	12.73
$6a_1$	13.05	13.54	13.15	12.91	12.51	12.84	13.00
$3b_1$	13.58	14.15	13.74	13.39	12.88	13.60	13.54

Table 8.6 presents the ionization potential corresponding to first three states of ozone. The ozone ground state has significant multi-reference character and known to possess a significant challenge for all the EOMCC methods based on a MBPT(2) reference. In cc-

pVDZ basis set, the EOMIP-CCSD(2) values are significantly overestimated compared to the benchmark EOMIP-CCSDT values. The EOMIP-CCSD(2)* and the EOMIP-CCSD method give reasonable agreement with the EOMIP-CCSDT results. All the IP values undergo blue shift from cc-pVDZ to cc-pVTZ basis. However, the qualitative trend remains same. The IP values further increase from cc-pVTZ to cc-pVQZ basis set. The EOMIP-CCSD(2) method significantly overestimates the IP values compared to the EOMIP-CCSDT and experimental values. The extrapolated version shows improvement over the original EOMIP-CCSD(2) approximation. The EOMIP-CCSD(2)* and EOMIP-CCSD method in cc-pVQZ basis show reasonable agreement with the EOMIP-CCSDT and experimental value [17].

8.3.2 Core Ionization Spectra

The knocking of electrons from the core orbitals by ionizing radiation leads to a variety of interesting physical and chemical phenomenon and often posses a significant challenge for the conventional *ab-initio* methods. In the previous chapter, we have shown that the EOMIP-CCSD(2) method and its extrapolated version fails to model the core-excited states. Table 8.7 presents core ionization energies of H_2O, CH_4, N_2, HF and NH_3 in a hierarchy of Dunning's core valence correlation consistent cc-pCVXZ (X=D,T and Q) basis sets. The EOMIP-CCSD(2) method, in cc-pCVDZ basis set, significantly overestimates the IP values compared to the standard EOMIP-CCSD method. The EOMIP-CCSD(2)* method on the other hand gives much lower values, even compared to the EOMIP-CCSD method. The core ionization energies for all the molecules undergo blue shift from cc-pCVDZ to cc-pCVTZ basis. However, the qualitative trend remains same. The core ionization energies in all the EOM methods further increase as we go to cc-pCVQZ basis. The EOMIP-CCSD* method gives the best agreement with experiments in cc-pCVQZ basis set and the results are within 0.2 eV of experiments. The EOMIP-CCSD(2)* method gives slightly overestimated values, specially for the N_2, where the core ionization energies are over estimated by around 1 eV.

Table 8.7 : Core-ionized energies in EOMCC methods. (in eV)

Molecule	EOMIP-CCSD	EOMIP-CCSD(2)	Extrapolated EOMIP-CCSD(2)	EOMIP-CCSD(2)*	EOMIP-CCSD*	Exp
			cc-pCVDZ Basis Set			
H_2O	542.69	542.81	-	541.17	541.06	539.75[a]
CH_4	293.18	293.31	-	292.22	292.22	290.86[b]
N_2	412.61	413.27	-	412.19	411.59	409.9[b]
HF	697.24	697.19	-	696.36	695.38	693.80[b]
NH_3	408.17	408.36	-	407.06	406.89	405.52[b]
			cc-pCVTZ Basis Set			
H_2O	541.13	541.65	541.53	540.03	539.54	539.75
CH_4	291.99	292.40	292.27	291.33	290.96	290.86
N_2	411.13	412.05	411.39	410.91	410.06	409.9
HF	695.41	695.81	695.81	694.04	693.66	693.80
NH_3	406.84	407.36	407.17	406.00	405.51	405.52
			cc-pCVQZ Basis Set			
H_2O	541.35	541.92	541.80	540.13	539.62	539.75
CH_4	291.99	292.49	292.36	290.84	290.78	290.86
N_2	411.33	412.28	411.62	410.84	409.70	409.9
HF	695.74	696.19	696.19	694.27	693.83	693.80
NH_3	406.99	407.59	407.40	406.13	405.55	405.52

a : Values taken from ref [19] . b:Values taken from ref [20] .

However, the EOMIP-CCSD method itself shows higher error bar(around 1.5 eV) in cc-

pCVQZ basis set for the core ionized state of N_2. In general the EOMIP-CCSD(2)* method gives better agreement with experiment than the EOMIP-CCSD method for all the five molecules studied. The EOMIP-CCSD(2) method, on the other hand, heavily overestimates the IP values and its extrapolated version does not show any significant improvement.

8.3.3 Satellite peaks

The satellite IP peaks are characterized by ionization of one electron along with simultaneous excitation of one electron from occupied to virtual orbital. The satellite peaks are generally associated with large relaxation effects and even the standard EOMIP-CCSD method fails to provide a reasonable description. Table 8.8 provides satellite IP values for CO and N_2. It can be seen that the EOMIP-CCSD(2)* method gives much lower values compared to EOMIP-CCSD method, and the former predicts IP values, which are in very good agreement with the highly accurate EOMIP-CCSD* method for both CO and N_2.

The IP values in all the methods undergo blue shift from cc-pVDZ to cc-pVTZ. However, the qualitative trend remains the same. Except the fact that the EOMIP-CCSD(2) method grossly overestimates for the $^2\Sigma_u^+$ state of N_2 and the extrapolated version does not provide any improvement. The IP values further increase in cc-pVQZ basis set. The EOMIP-CCSD(2)* method gives very good agreement with the experimental results[17] for the satellite IP values of CO and N_2 and the agreement is even better than that in the standard EOMIP-CCSD method.

Here it should be mentioned that it is not justified to come into any conclusion about the relative accuracy of the different EOMCC methods, for satellite IP values, from the study of only two states. However, a detailed study of the satellite IP values using different truncations of EOMIP-CC method is outside the scope of this present chapter and will be followed in some future study.

Table 8.8 : Satellite IP values in EOMCC methods. (in eV)

Molecule	EOMIP-CCSD	EOMIP-CCSD(2)	Extrapolated EOMIP-CCSD(2)	EOMIP-CCSD(2)*	EOMIP-CCSD*	Exp[17]
			cc-pVDZ Basis Set			
$N_2(^2\Sigma_u^+)$	28.80	28.45	-	25.10	25.11	25.51
$CO(^2\Pi)$	26.24	26.18	-	23.07	23.16	23.4
			cc-pVTZ Basis Set			
$N_2(^2\Sigma_u^+)$	29.57	30.17	30.17	25.76	25.26	25.51
$CO(^2\Pi)$	26.76	26.80	26.80	23.26	23.25	23.4
			cc-pVQZ Basis Set			
$N_2(^2\Sigma_u^+)$	29.83	30.43	30.43	25.87	25.31	25.51
$CO(^2\Pi)$	26.96	27.06	27.06	23.36	23.28	23.4

8.3.4 Error analysis

The EOMIP-CCSD(2)* method shows significant improvement over the original EOMIP-CCSD(2) approximation for valence, core and satellite IP values. In the benchmark cc-pVQZ basis set (cc-pCVQZ for the core IP) the IP values are in very good agreement with the experimental values, and the results are even better than the standard EOMIP-CCSD method. The R_3 operator in the EOMIP-CCSD(2)* method accounts for the missing relaxation of effect caused by the absence of the T_1 operator in the reference state of EOM-CCSD(2) approximation.

Therefore, the EOMIP-CCSD(2)* method performs well even for the cases where relaxation effect is significant, like in the case of core IP or the satellite peaks. It also

works for molecules such as ozone(see Table 8.9 for the T1 diagnosis values), where

Table 8.9 : T1 Diagnosis Values in cc-pVTZ Basis Set

molecule	T1 value
N_2	0.013
H_2O	0.007
H_2CO	0.015
C_2H_4	0.011
ozone	0.028

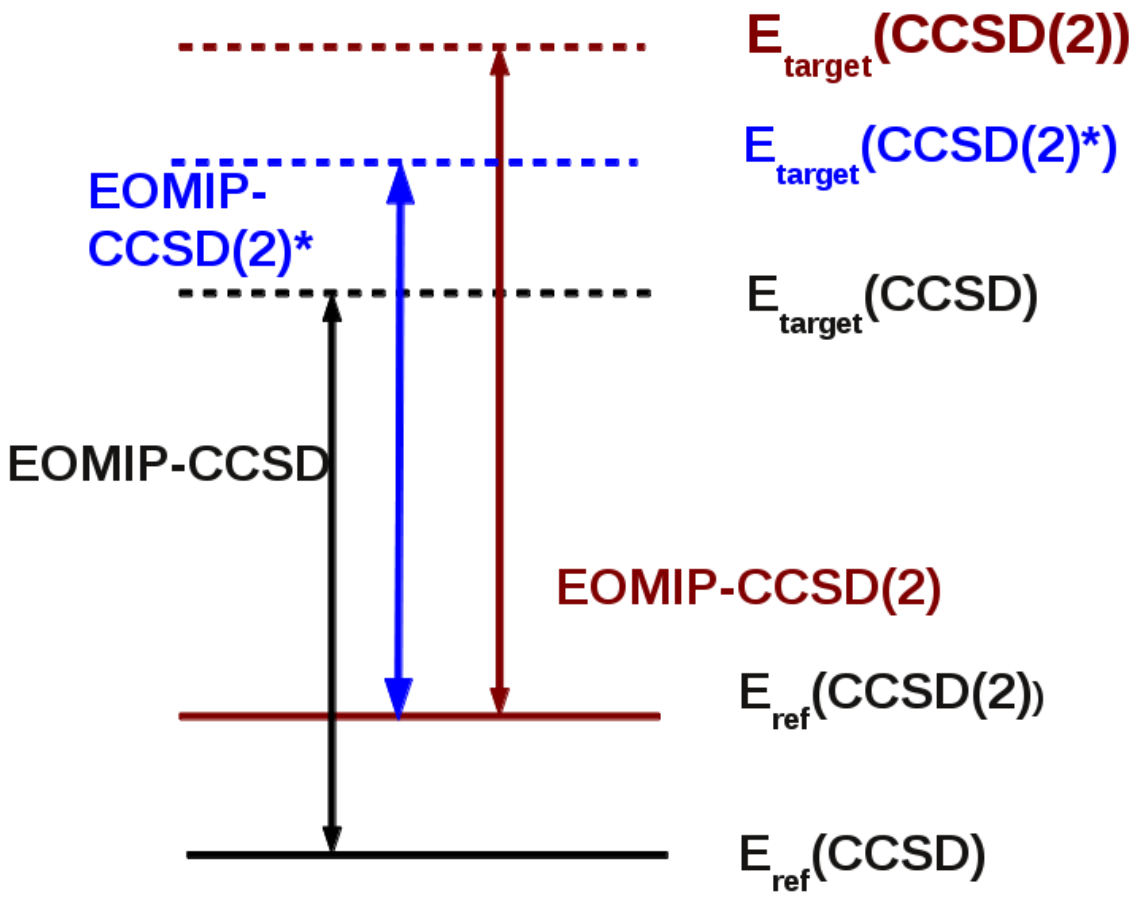

Figure 8.1: The relative ordering of reference and target state in different variants of EOM approach to IP problem

the reference state has significant multi-reference character and the original EOMIP-CCSD(2) approximation fails drastically.

Figure 8.1 provides a pictorial depiction of the relative change in the position of the target state caused by the included R_3 operator in the EOMIP-CCSD(2)* method. It can be seen that the rise in the target state energy, caused by the truncated T amplitudes in EOMIP-CCSD(2) approximation, is corrected by the R_3 operator in the EOMIP-CCSD(2)* method. This leads to a better balance between the errors in the reference state and the target state and the systematic error cancelation results in improved IP values.

8.3.5 Vertical Ionization Potential of Thymine

To show the robustness of the new method, we have calculated the valence IP values of thymine. The EOMCC investigation of IP values of thymine were extensively persuaded by Krylov and co-workers [21, 22]. Table 8.10 presents the computed and experimental vertical IP values for the first five ionized states of thymine.

It can be seen that the EOMIP-CCSD(2) method overestimates the IP values for all the five states, as compared to the standard EOMIP-CCSD method, in both cc-pVDZ and cc-pVTZ basis set. The extrapolated version shows some improvement over the original EOMIP-CCSD(2) method, but the values are still over estimated compared to the EOMIP-CCSD approximation. In cc-pVTZ basis set, the EOMIP-CCSD method overestimates the IP values compared to experiment. The EOMIP-CCSD(2)* method, on the other hand, gives a very good agreement and slightly underestimates the IP values as compared to the experimental number, except the ($3\ ^2A''$) state, where the experimental value is overestimated by 0.27 eV. In general, the EOMIP-CCSD(2)* method gives better agreement with the experimental results in cc-pVTZ basis set, than the standard EOMIP-

CCSD method.

Table 8.10 : Vertical ionization energies of thymine (in eV)

Molecule	$1\,^2A''$	$1\,^2A'$	$2\,^2A''$	$2\,^2A'$	$3\,^2A''$
			cc-pVDZ Basis Set		
EOMIP-CCSD(2)	8.98	9.77	10.26	10.67	12.47
EOMIP-CCSD	8.79	9.72	10.10	10.63	12.33
EOMIP-CCSD(2*)	8.60	9.46	9.90	10.34	12.03
			cc-pVTZ Basis Set		
EOMIP-CCSD(2)	9.44	10.31	10.78	11.20	12.88
Extrapolated EOMIP-CCSD(2)	9.25	10.26	10.62	11.16	12.74
EOMIP-CCSD	9.14	10.16	10.52	11.06	12.66
EOMIP-CCSD(2*)	8.98	9.88	10.33	10.74	12.37
Exp[23]	9.02	9.95	10.40	10.88	12.10

8.3.5 Geometry and IR frequency

The relaxation effect introduced by the R_3 operator improves the description of the total energy in EOMIP-CCSD(2)* method, over the original EOMIP-CCSD(2) approximation. Therefore, the EOMIP-CCSD(2) method can provide an improved description of the final state properties. We have investigated the geometry and IR frequencies of NO_2, NO_3 and a test set of six diatomic doublet radicals, some of them have been used for the benchmarking of the original EOMIP-CCSD(2) approximation.

8.3.5.1 NO_2

NO_2 provides significant challenges for the standard single-reference *ab-initio* methods. The UHF and ROHF based MP2 and even the CCSD method fail to provide reasonable agreement with the experiment [9] for the geometry as well as IR frequency of NO_2.

Table 8.11 provides the geometry and IR frequencies of NO_2 computed in different variants of single-reference and equation of motion coupled cluster methods in aug-cc-pVTZ basis set. The EOMIP-CCSD(2)* method shows a deviation of 0.002 Å from the experiment for the bond lengths. The results are better than the original EOMIP-CCSD(2) approximation, as well as, the standard EOMIP-CCSD method. The bond angle is however, slightly overestimated in the EOMIP-CCSD(2)* method.

Table 8.11 : ***Geometry and Harmonic Vibrational Frequency of Nitrogen Dioxide (NO_2) in aug-cc-pVTZ basis set***

Method	Bond length(Å)	Bond Angle(θ)	ω_1	ω_2	ω_3
UCCSD(T)	1.294	123.9	344	577	1134
ROCCSD(T)	1.194	134.8	761	1359	1694
EOM-IP-CCSD	1.186	133.7	795	1443	1745
EOMIP-CCSD(2)	1.186	134.9	769	1388	1784
EOM-IP-CCSD(2)*	1.192	134.7	760	1347	1560
EOM-IP-CCSD*	1.191	133.7	784	1404	1717
Experiment	1.194[a]	133.9[a]	750[b]	1325[b]	1634[b]

a : Values taken from ref [24]. b:Values taken from ref[25] .

The UCCSD(T) method fails drastically for both bond length and bond angle. The ROCCSD(T) method, on the other hand, exactly reproduces the bond length. However,

the bond angle is slightly overestimated similar to that in the case of EOMIP-CCSD(2)* method. In case of IR frequencies, the ROCCSD(T) method gives the best agreement with experiments, and the maximum deviation is observed for the asymmetric stretching mode(ω_3) which is overestimated compared to the experimental value by 64 cm^{-1}. The EOMIP-CCSD(2)* method gives a similar performance, with the difference that the asymmetric stretching mode(ω_3) gets underestimated by 74 cm^{-1}. The performance is much better than the original EOMIP-CCSD(2) approximation and even the standard EOMIP-CCSD method. The UCCSD(T) method fails for all the three modes. The EOMIP-CCSD* method gives slightly inferior performance as compared to the EOMIP-CCSD(2)* approximation.

8.3.5.2 NO_3

The equilibrium geometry of NO_3 has been a matter of long standing debate. The experimental geometry [26] of NO_3 is D_{3h} and most of the single-reference methods, even the coupled cluster method [27-29], predict a C_{2V} geometry. Multi-reference methods [9, 30, 31] like FSMRCCSD, MRCI and the EOMIP-CCSD(2) method, on the other hand, predicts a D_{3h} geometry.

Table 8.12 provides the geometry and IR frequencies of NO_3 computed in aug-cc-pVTZ basis set. Both, the UCCSD(T) and ROCCSD(T) method leads to a C_{2V} geometry with two long(L_1) and one short(L_2) bond. In ROCCSD(T) method, the long bond is in reasonable agreement with the experimental value. However, the short bond is underestimated by 0.039 Å. The UCCSD(T) method gives inferior performance for both long and short bonds. All the EOM methods lead to a D_{3h} geometry. The EOMIP-CCSD(2)* method gives the best agreement with the experimental results($|\Delta r_e|$ = 0.008 Å) among all the methods used in this study.

The UCCSD(T) and ROCCSD(T) method gives very poor agreement for all modes of vibrations of NO_3, except the umbrella and symmetric stretching mode. The EOMIP-CCSD(2)* method, on the other hand, gives very good agreement with the experimental values, except for the two asymmetric stretching modes. Specially, the asymmetric bending modes in EOMIP-CCSD(2)* method show significant improvement over the original EOMIP-CCSD(2) approximation. The two asymmetric stretching modes, however, show considerable deviation from the experimental values in all the EOM methods. Now, Stanton [34] has shown that the assignment of experimental peak at 1480 cm^{-1} is not unambiguous and detailed investigations are required for the assignment of these modes, which is outside the scope this present study.

Table 8.12 : Geometry and Harmonic Vibrational Frequency of Nitrogen Trioxide (NO3) in aug-cc-pVTZ basis

Method	**Bond length (Å) (L_1)**	**Bond length (Å) (L_2)**	**ω_1 (asym bend)**	**ω_2 (asym bend)**	**ω_3 (umbr-ella)**	**ω_4 (sym strech)**	**ω_5 (asym stretch)**	**ω_6 (asym stretch)**
UCCSD(T)	1.291	1.198	664	683	732	1031	1063	1615
ROCCSD(T)	1.252	1.201	414	506	779	896	1082	1499
EOM-IP-CCSD(2)	1.228	1.228	66	66	800	1140	1176	1176
EOMIP-CCSD	1.221	1.221	305	305	836	1170	1191	1191
EOM-IP-CCSD(2)*	1.232	1.232	172	172	785	1114	1179	1179
EOM-IP-CCSD*	1.226	122.6	349	349	822	1146	1188	1188
Experiment	1.240[a]	1.240[a]	250[b]	250[b]	762c	1060c	1480c	1480c

a : Values taken from ref [26]. b:Values taken from ref [32] . c:Values taken from ref [33] .

8.3.5.3 Diatomics

The diatomic doublet radical suffers from high degree of symmetry breaking and other typical problems associated with the theoretical treatment of open-shell molecules and

they are often used as the test cases for benchmarking the accuracy of multi-reference methods [9].

Table 8.13 : Geometry(Å) of doublet diatomic molecules in aug-cc-pVQZ basis set

Molecule	UCCSD(T)	ROCCSD(T)	EOM-IP-CCSD	EOMIP-CCSD(2)	EOM-IP-CCSD(2)*	EOM-IP-CCSD*	Exp[35]
OH	0.970	0.969	0.966	0.966	0.968	0.968	0.969
O_2^+	1.115	1.115	1.107	1.112	1.117	1.109	1.116
CN	1.167	1.173	1.161	1.164	1.173	1.167	1.172
F_2^+	1.306	1.305	1.295	1.295	1.303	1.302	1.322
CO^+	1.112	1.116	1.104	1.108	1.117	1.112	1.115
NO	1.148	1.151	1.150	1.145	1.147	1.151	1.151

The bond length and IR frequencies of six doublet radicals OH, O_2^+, CN, F_2^+, CO^+ and NO are given in Table 8.13 and 8.14, respectively. The ROCCSD(T) method gives the best agreement with the experimental bond length [35]. The EOMIP-CCSD(2)* method gives a comparable performance and it shows significant improvement over the original EOMIP-CCSD(2) approximation. Except the case of NO, the EOMIP-CCSD(2)* results are generally in better agreement with experiment than that in standard EOMIP-CCSD method. The UCCSD(T) and EOMIP-CCSD* method gives a mixed performance, while they give very good agreement in some cases, they also leads to inferior performance for others.

Table 8.14 : IR frequency(cm^{-1}) of doublet diatomic molecules in aug-cc-pVQZ basis set

Molecule	UCCSD(T)	ROCCSD(T)	EOM-IP-CCSD	EOMIP-CCSD(2)	EOM-IP-CCSD(2)*	EOM-IP-CCSD*	Exp[35]
OH	3746	3749	3802	3892	3841	3751	3738
O_2^+	1940	1942	2022	1942	1897	2002	1905
CN	2137	2068	2174	2134	2055	2119	2069
F_2^+	1126	1128	1175	1178	1137	1138	1073
CO^+	2303	2223	2331	2288	2200	2247	2212
NO	2104	1918	2004	2022	1967	1952	1904

In case of IR frequencies also, the ROCCSD(T) method gives the best agreement with experimental results [35]. The EOMIP-CCSD(2)* method gives slightly inferior performance compared to the ROCCSD(T) method. However, it shows improvement over the original EOMIP-CCSD(2) approximation for all the diatomic radicals studied, and the results are even better than the standard EOMIP-CCSD method, except for the case of OH radical, where the EOMIP-CCSD(2)* method overestimates the experimental frequency by more than hundred wave number. The UCCSD(T) and EOMIP-CCSD* method give a mixed performance with accuracy range varying from case to case.

8.4 CONCLUSION

In this chapter, we present a new method for calculation of ionization potential. Our EOMIP-CCSD(2)* method corrects for the missing relaxation effect caused by the truncated T amplitudes in the original EOMIP-CCSD(2) approximation by partial inclusion of R_3 operator in the EOM part. The EOMIP-CCSD(2)* method scales as non-iterative N^6 and has much smaller storage requirement than the standard EOMIP-CCSD method and can be applied to large systems.

The resulting EOMIP-CCSD(2)* method is free from the problem of overestimation of IP values shown by original EOMIP-CCSD(2) method and its extrapolated versions. The superiority of method is especially prominent for the ionization of core electrons and satellite peaks, where the relaxation effect plays an important role and the new method even performs better that the standard EOMIP-CCSD method for the above-mentioned cases.

The EOMIP-CCSD(2)* method also predicts geometry and IR frequencies of problematic doublet radicals and gives excellent agreement with experimental results. The results in

EOMIP-CCSD(2)* method are comparable to single-reference CCSD(T) approximation, and even better than the standard EOMIP-CCSD method for most of the cases.

However, the routine application of the EOMIP-CCSD(2)* method will require the implementation of analytic derivatives. Work is currently underway toward that direction.

References:

1. Stanton, J. F.; Bartlett, R. J., *J. Chem. Phys.* **1993,** *98*, 7029-7039.
2. Stanton, J. F.; Gauss, J., *J. Chem. Phys.* **1994,** *101*, 8938-8944.
3. Nooijen, M.; Bartlett, R. J.,. *J. Chem. Phys.* **1995,** *102*, 3629-3647.
4. Mukherjee, D.; Pal, S., Use of Cluster Expansion Methods in the Open-Shell Correlation Problem. In *Advances in Quantum Chemistry*, Per-Olov, L., Ed. Academic Press: 1989; Vol. Volume 20, pp 291-373.
5. Bartlett, R. J., MANY-BODY PERTURBATION-THEORY AND COUPLED CLUSTER THEORY FOR ELECTRON CORRELATION IN MOLECULES. *Annu. Rev. Phys. Chem.* **1981,** *32*, 359-401.
6. Nooijen, M.; Snijders, J. G., *J. Chem. Phys.* **1995,** *102*, 1681-1688.
7. Stanton, J. F.; Gauss, J., *J. Chem. Phys.* **1995,** *103*, 1064-1076.
8. (a) Dutta, A. K.; Gupta, J.; Pathak, H.; Vaval, N.; Pal, S., *J. Chem. Theor. Comp.* **2014,** *10*, 1923-1933.

   (b)Dutta, A. K.; Pal, S.; Ghosh, D., *J. Chem. Phys.* **2013,** *139*, 124116-11
9. Dutta, A. K.; Vaval, N.; Pal, S., *J. Chem. Theor. Comp.* **2013,** *9*, 4313-4331.
10. Saeh, J. C.; Stanton, J. F., *J. Chem. Phys.* **1999,** *111*, 8275-8285.
11. Musial, M.; Bartlett, R. J., *J. Chem. Phys.* **2008,** *129*, 134105-12.
12. Löwdin, P.-O., Studies in perturbation theory: Part I. *J. Mol. Spect.* **1963,** *10*, 12-33.
13. Manohar, P. U.; Stanton, J. F.; Krylov, A. I., *J. Chem. Phys.* **2009,** *131*, 114112.
14. Stanton, J. F.; Gauss, J.; Harding, M. E.; Szalay, P. G.; Auer, A. A.; Bartlett, R. J.; Benedikt, U.; Berger, C.; Bernholdt, D. E.; Bomble, Y. J., CFOUR, a quantum chemical program package. *For the current version, see http://www. cfour. de* **2009**.
15. Dunning, T. H., *J. Chem. Phys.* **1989,** *90*, 1007-1023.
16. Peterson, K. A.; Dunning, T. H., *J. Chem. Phys.* **2002,** *117*, 10548-10560.

17. Kimura, K.; Katsumata, S.; Achiba, Y.; Yamazaki, T.; Iwata, S., *Handbook of HeI Photoelectron Spectra of Fundamental Organic Molecules* Japan Scientific Societies Press: Tokyo, 1981.

18. Musial, M.; Bartlett, R. J., *Chem. Phys. Lett.* **2004,** *384*, 210-214.

19. Ohtsuka, Y.; Nakatsuji, H., *J. Chem. Phys.* **2006,** *124*, -.

20. Ehara, M.; Nakatsuji, H., G *Collect. Czek. Chem. Comm.* **2008,** *73*, 771-785.

21. Bravaya, K. B.; Kostko, O.; Dolgikh, S.; Landau, A.; Ahmed, M.; Krylov, A. I., *J. Phys. Chem. A* **2009,** *114*, 12305-12317.

22. Bravaya, K. B.; Kostko, O.; Ahmed, M.; Krylov, A. I., *Phys. Chem. Chem. Phys.* **2010,** *12*, 2292-2307.

23. Lauer, G.; SchÃ¤fer, W.; Schweig, A., *Tet. Lett.* **1975,** *16*, 3939-3942.

24. Lafferty, W. J.; Sams, R. L., *J. Mol. Spectrosc.* **1977,** *66*, 478-492.

25. Morino, Y.; Tanimoto, M.; Saito, S.; Hirota, E.; Awata, R.; Tanaka, T., *J. Mol. Spectrosc.* **1983,** *98*, 331-348.

26. Ishiwata, T.; Tanaka, I.; Kawaguchi, K.; Hirota, E., Infrared diode laser spectroscopy of the NO_3 ν_3 band. *J. Chem. Phys.* **1985,** *82*, 2196-2205.

27. Crawford, T. D.; Stanton, J. F., *J. Chem. Phys.* **2000,** *112*, 7873-7879.

28. Gauss, J.; Stanton, J. F.; Bartlett, R. J., *J. Chem. Phys.* **1991,** *95*, 2639-2645.

29. Stanton, J. F.; Gauss, J.; Bartlett, R. J., *J. Chem. Phys.* **1991,** *94*, 4084-4087.

30. Eisfeld, W.; Morokuma, K., *J. Chem. Phys.* **2000,** *113*, 5587-5597.

31. Kaldor, U., *Chem. Phys. Lett.* **1990,** *166*, 599-601.

32. Weaver, A.; Arnold, D. W.; Bradforth, S. E.; Neumark, D. M.,. *J. Chem. Phys.* **1991,** *94*, 1740-1751.

33. Friedl, R. R.; Sander, S. P., *J. Phys. Chem.* **1987,** *91*, 2721-2726.

34. Stanton, J. F., *J. Chem. Phys.* **2007,** *126*, 134309-20.

35. Huber, K. P.; Herzberg, G., Molecular Structure and Molecular Spectra. IV. Constants of Diatomic Molecules. *Van Rostrand-Reinhold, New York* **1979**.

Epilogue

"Let craft, ambition, spite,
Be quenched in reason's night,
Till weakness turns into might,
Till what is darkness is light,
Till what is wrong be right"

Lewis Carroll
Sylvie and Bruno

This thesis tries to deal with the theoretical treatment of problematic doublet radicals within the framework of coupled cluster method. The efforts were mainly directed towards the two aspects. First, the application of highly accurate FSMRCC method towards the study of the high-energy stratospheric radicals. Secondly, we went to develop low cost approximation to standard FSMRCC and EOMCC methods, which can used to study geometry and properties of large radicals in very small computational time.

In the present thesis, we have contained ourselves only in the investigation of NO_x based pathway of stratospheric ozone depiction. However, there is considerable interest in the mixed pathways where two or more species are present and reacting together. Proper understanding of the reaction pathways would require the study of dynamics, which is difficult to perform in convention multi-reference coupled cluster methods, because of the associated computational cost. Therefore, it is essential to generate low scaling approximations for them.

In this thesis, we have dealt with low cost approximation to IP, EA and spin-flip variants of EOMCC. The similar extension can be achieved in case of FSMRCC. Specially, our work on IP and EA has open the way to a new method with N^5 scaling and low storage requiring method for (1,1) sector of Fock space. The use of density fitting and Cholesky decomposition can be used to further speed the calculations. The routine use of the method would require the implementation of analytic derivatives and significant coding effort needs to be devoted towards that direction. The new developments will enable us to go beyond the small test molecules and allow the treatment of big molecules and clusters in multi-reference coupled cluster methods, which will lead to new insights into their chemistry and biology. Recent times has seen a plethora of effort towards increasing the accuracy of single- and multi-reference coupled cluster methods at the expense of substantial enhancement in the computational cost. However, there is a lot of empty space lies in the devolvement of method, which has lower computational cost than the standard coupled cluster method, without significantly compromising on its accuracy. So in Richard Feynman's word

"There's plenty of room at the bottom "...

Appendix I

Expressions for F and W intermediates for EOMEA-CCSD

$$F_{ij} = \sum_i F_i + \sum_{abk} (2t_{kj}^{ab} - t_{jk}^{ab} + 2t_k^a t_j^b - t_j^a t_k^b) \langle ki | ab \rangle + \sum_{ak} t_k^a \left(2\langle ik | ja \rangle - \langle ki | ja \rangle \right)$$

$$F_{ia} = \sum_{jb} t_j^b \left(2\langle ij | ab \rangle - \langle ij | ba \rangle \right)$$

$$F_{ab} = \sum_a f_a + \sum_{ijc} \left(-2t_{ji}^{ca} + t_{ij}^{ca} - 2t_j^c t_i^a + t_i^c t_j^a \right) \langle ji | bc \rangle + \sum_{ic} t_i^c (2\langle ai | bc \rangle - \langle ai | cb \rangle)$$

$$W_{aibj} = \langle ai | bj \rangle - \sum_{kc} \left(t_{ik}^{ba} + t_i^b t_k^a \right) \langle jk | bc \rangle - \sum_k t_k^a \left(\langle jk | ib \rangle - \langle ij | bk \rangle \right) + \sum_c t_i^c \langle aj | bc \rangle$$

$$W_{aijb} = \langle ai | jb \rangle + \sum_{kc} \left(2_{ik}^{ac} - t_{ki}^{ac} \right) \langle ik | bc \rangle - \sum_{ck} t_{ik}^{ac} \langle jk | cb \rangle + \sum_c t_i^c \langle aj | cb \rangle - \sum_k t_k^a \langle kj | ib \rangle - \sum_{kc} t_k^a t_i^c \langle kj | cb \rangle$$

$$\begin{aligned} W_{acbi} &= \langle ac | bi \rangle + \sum_{lk} \left(t_{kl}^{bc} + t_k^b t_l^c \right) \langle lk | ia \rangle + \sum_{dk} \left(2t_{ki}^{dc} - t_{ik}^{dc} - t_i^d t_k^c \right) \langle da | bk \rangle \\ &- \sum_k t_k^b \langle ck | ia \rangle + \sum_b t_i^d \langle bc | ad \rangle - \sum_k t_k^c \langle kb | ia \rangle + \sum_{kld} t_{ki}^{dc} t_l^b \langle kl | ad \rangle \\ &+ \sum_{kld} \left(t_{kl}^{cb} t_i^b + t_{li}^{bd} t_k^c \right) \langle kl | da \rangle - \sum_{kld} t_{il}^{cb} t_k^d \left(\langle kl | da \rangle - \langle lk | da \rangle \right) \\ &- \sum_{kd} \left(t_{ik}^{db} + t_i^d t_k^b \right) \langle ck | da \rangle - \sum_{kd} t_{ik}^{cd} \langle bk | da \rangle \end{aligned}$$

$$W_{aibc} = \langle ai | bc \rangle - \sum_j t_j^b \langle ji | ca \rangle$$

$$W_{acbd} = \langle ac | bd \rangle + \sum_{kl} \left(t_{kl}^{ac} + t_k^a t_l^c \right) \langle kl | bd \rangle - \sum_k \left(t_k^a \langle ck | db \rangle + t_k^c \langle ak | bd \rangle \right)$$

Expressions for F and W intermediates for P-EOMEA-MBPT(2)

$$F_{ij} = \sum_i F_i + \sum_{abk} (2t_{kj}^{ab} - t_{jk}^{ab}) \langle ki | ab \rangle$$

$$F_{ia} = 0$$

$$F_{ab} = \sum_{a} f_a + \sum_{ijc} \left(-2t_{ji}^{ca} + t_{ij}^{ca} \right) \langle ji | bc \rangle$$

$$W_{acbi} = \langle ac | bi \rangle + \sum_{lk} t_{kl}^{bc} \langle lk | ia \rangle + \sum_{dk} \left(2t_{ki}^{dc} - t_{ik}^{dc} \right) \langle da | bk \rangle$$
$$- \sum_{kd} t_{ik}^{db} \langle ck | da \rangle - \sum_{kd} t_{ik}^{cd} \langle bk | da \rangle$$

$$W_{aibc} = \langle ai | bc \rangle$$

Appendix II

Expressions for modified $\bar{H}$ intermediates for RHH and UHF bases SF-CCSD(2) and DSF-CCSD(2)[2,3]

$$F_{ia} = 0$$

$$F_{ij} = f_{ij} + \frac{1}{2}\sum_{kbc} t_{ik}^{bc} \left\langle jk \middle|\middle| bc \right\rangle$$

$$F_{ab} = f_{ab} - \frac{1}{2}\sum_{jkc} t_{jk}^{ac} \left\langle jk \middle|\middle| bc \right\rangle$$

$$l_{iajb}^{1} = \left\langle ia \middle|\middle| jb \right\rangle - \sum_{kc} t_{ik}^{bc} \left\langle jk \middle|\middle| ac \right\rangle$$

$$l_{ijka}^{2} = -\left\langle ij \middle|\middle| ka \right\rangle - \frac{1}{2}\sum_{cd} t_{ik}^{cd} \left\langle kb \middle|\middle| cd \right\rangle + \sum_{lc}\left(t_{il}^{bc} \left\langle jc \middle|\middle| kl \right\rangle + t_{jl}^{bc} \left\langle ic \middle|\middle| kl \right\rangle \right)$$

$$l_{icab}^{3} = -\left\langle ic \middle|\middle| ab \right\rangle - \frac{1}{2}\sum_{kl} t_{kl}^{ab} \left\langle ic \middle|\middle| kl \right\rangle + \sum_{kd}\left(t_{ik}^{ad} \left\langle kb \middle|\middle| cd \right\rangle + t_{ik}^{bd} \left\langle ka \middle|\middle| cd \right\rangle \right)$$

$$l_{ijkl}^{4} = \left\langle ij \middle|\middle| kl \right\rangle + \frac{1}{4}\sum_{cd} t_{ij}^{cd} \left\langle kl \middle|\middle| cd \right\rangle$$

$$l_{abcd}^{5} = \left\langle ab \middle|\middle| cd \right\rangle + \frac{1}{4}\sum_{kl} t_{kl}^{ab} \left\langle kl \middle|\middle| cd \right\rangle$$

$$l_{ijka}^{6} = \left\langle ij \middle|\middle| ka \right\rangle$$

For ROHF reference the expression for the $\bar{H}$ intermediates will be same as that given in Ref. 49 of Chapter 6.

Appendix III

Expressions for the R vectors in P-EOMIP-CCSD method

$$\left[H_{SS}R\right]_i = \sum_j F_{ij}R_j$$

$$\left[H_{SD}R\right]_i = \sum_{jb} F_{jb}\left(2R^b_{ij} - R^b_{ji}\right) + \sum_{jkb}\left(2W_{kjib} - W_{kjbi}\right)R^b_{jk}$$

$$\left[H_{DS}R\right]^a_{ij} = \sum_k W_{ijka}R_k$$

$$\left[H^{[0]}_{DD}\right]^a_{ij} = \sum_k f_{ik}R^a_{jk} + \sum_k f_{jk}R^a_{ik} + \sum_b f_{ab}R^b_{ij}$$

Erratum